

1 **Global Carbon Budget 2025**

2 Pierre Friedlingstein[1,2], Michael O'Sullivan[1], Matthew W. Jones[3], Robbie M. Andrew[4],
3 Dorothee C. E. Bakker[5], Judith Hauck[6,7], Peter Landschützer[8], Corinne Le Quéré[3], Hongmei
4 Li[9,10], Ingrid T. Lujikx[11], Glen P. Peters[4], Wouter Peters[11,12], Julia Pongratz[13,10], Clemens
5 Schwingshackl[13], Stephen Sitch[1], Josep G. Canadell[14], Philippe Ciais[15], Kjetil Aas[4], Simone
6 R. Alin[16], Peter Anthony[17], Leticia Barbero[18], Nicholas R. Bates[19,20], Nicolas Bellouin[21],
7 Alice Benoit-Cattin[22], Carla F. Berghoff[23], Raffaele Bernardello[24], Laurent Bopp[2], Ida Bagus
8 Mandhara Brasika[1,25], Matthew A. Chamberlain[26], Naveen Chandra[27], Frédéric Chevallier[15],
9 Louise P. Chini[28], Nathan O. Collier[29], Thomas H. Colligan[30], Margot Cronin[31], Laique M.
10 Djeutchouang[32,33,34], Xinyu Dou[35], Matt P. Enright[19,20], Kazutaka Enyo[36], Michael
11 Erb[37,38], Wiley Evans[39], Richard A. Feely[16], Liang Feng[40,41], Daniel J. Ford[1], Adrianna
12 Foster[42], Filippa Fransner[43,44], Thomas Gasser[45], Marion Gehlen[15], Thanos Gkritzalis[8],
13 Jefferson Goncalves De Souza[1], Giacomo Grassi[46], Luke Gregor[47,48], Nicolas Gruber[47],
14 Bertrand Guenet[49], Özgür Gürses[6], Kirsty Harrington[50], Ian Harris[51], Jens Heinke[52], George
15 C. Hurtt[28], Yosuke Iida[36], Tatiana Ilyina[53,9,10], Akihiko Ito[54], Andrew R. Jacobson[55,56],
16 Atul K. Jain[57], Tereza Jarníková[3], Annika Jersild[30], Fei Jiang[58], Steve D. Jones[8], Etsushi
17 Kato[59], Ralph F. Keeling[60], Kees Klein Goldewijk[61], Jürgen Knauer[62], Yawen Kong[63,64],
18 Jan Ivar Korsbakken[4], Charles Koven[65], Taro Kunimitsu[4], Xin Lan[55,56], Junjie Liu[66,67],
19 Zhiqiang Liu[68], Zhu Liu[69], Claire Lo Monaco[70], Lei Ma[28], Gregg Marland[37,38], Patrick C.
20 McGuire[71], Galen A. McKinley[72], Joe R. Melton[73], Natalie Monacci[74], Erwan Monier[75,76],
21 Eric J. Morgan[60], David R. Munro[55,56], Jens D. Müller[77], Shin-Ichiro Nakaoka[78], Lorna R.
22 Nayagam[78], Yosuke Niwa[78], Tobias Nutz[13], Are Olsen[43,44], Abdirahman M. Omar[79,44],
23 Naiqing Pan[80], Sudhanshu Pandey[66], Denis Pierrot[81], Zhangcai Qin[82], Pierre Regnier[83],
24 Gregor Rehder[84], Laure Resplandy[85], Alizée Roobaert[8], Thais M. Rosan[1], Christian
25 Rödenbeck[86], Jörg Schwinger[44,79], Ingunn Skjelvan[79,44], T. Luke Smallman[40,41], Victoria
26 Spada[87], Mohanan G. Sreeush[6], Qing Sun[88], Adrienne J. Sutton[16], Colm Sweeney[56], Didier
27 Swingedouw[89], Roland Séférian[90], Shintaro Takao[78], Hiroaki Tatebe[91,92], Hanqin Tian[80],
28 Xiangjun Tian[93,94], Bronte Tilbrook[26,95], Hiroyuki Tsujino[96], Francesco Tubiello[97], Erik van
29 Ooijen[26], Guido R. van der Werf[11], Sebastiaan J. van de Velde[98,99], Anthony P. Walker[100],
30 Rik Wanninkhof[81], Xiaojuan Yang[100], Wenping Yuan[101], Xu Yue[102], Jiye Zeng[78]

31

32 1: Faculty of Environment, Science and Economy, University of Exeter, Exeter, EX4 4QF, UK

33 2: Laboratoire de Météorologie Dynamique, Institut Pierre-Simon Laplace, CNRS, École Normale
34 Supérieure, Université PSL, Sorbonne Université, École Polytechnique, Paris, France

35 3: Tyndall Centre for Climate Change Research, School of Environmental Sciences, University of East
36 Anglia, Norwich Research Park, Norwich NR4 7TJ, UK

37 4: CICERO Center for International Climate Research, Oslo 0349, Norway
38 5: School of Environmental Sciences, University of East Anglia, Norwich NR4 7TJ, UK
39 6: Alfred-Wegener-Institut, Helmholtz-Zentrum für Polar- und Meeresforschung, Am Handelshafen 12,
40 27570 Bremerhaven
41 7: Universität Bremen, FB02 Biology/Chemistry Bremen, Germany
42 8: Flanders Marine Institute (VLIZ), Jacobsenstraat 1, 8400, Ostend, Belgium
43 9: Helmholtz-Zentrum Hereon, Max-Planck-Straße 1, 21502 Geesthacht, Germany
44 10: Max Planck Institute for Meteorology, Bundesstraße 53, 20146 Hamburg, Germany
45 11: Wageningen University, Environmental Sciences Group, P.O. Box 47, 6700AA, Wageningen, The
46 Netherlands
47 12: University of Groningen, Centre for Isotope Research, Groningen, The Netherlands
48 13: Ludwig-Maximilians-Universität München, Luisenstr. 37, 80333 München, Germany
49 14: CSIRO Oceans and Atmosphere, Canberra, ACT 2101, Australia
50 15: Laboratoire des Sciences du Climat et de l'Environnement, LSCE/IPSL, CEA-CNRS-UVSQ,
51 Université Paris-Saclay, F-91198 Gif-sur-Yvette, France
52 16: National Oceanic and Atmospheric Administration, Pacific Marine Environmental Laboratory
53 (NOAA/PMEL), 7600 Sand Point Way NE, Seattle, WA 98115, USA
54 17: Karlsruhe Institute of Technology, Institute of Meteorology and Climate Research/Atmospheric
55 Environmental Research, 82467 Garmisch-Partenkirchen, Germany
56 18: Rosenstiel School of Marine Atmospheric and Earth Science, Cooperative Institute for Marine and
57 Atmospheric Studies (CIMAS), University of Miami, 4600 Rickenbacker Causeway, Miami, FL, USA
58 19: Arizona State University, Tempe, Arizona, AZ 85287-5502, USA
59 20: Bermuda Institute of Ocean Sciences (BIOS), 17 Biological Lane, St. Georges, GE01, Bermuda
60 21: Department of Meteorology, University of Reading, Reading, RG6 6BB, UK
61 22: Marine and Freshwater Research Institute, Reykjavik, Iceland
62 23: Instituto Nacional de Investigación y Desarrollo Pesquero (INIDEP), Paseo Victoria Ocampo N°1,
63 B7602HSA, Mar del Plata, Argentina
64 24: Barcelona Supercomputing Center, Barcelona, Spain
65 25: Faculty of Marine Science & Fisheries, Udayana University, Denpasar, Bali, 80361, Indonesia
66 26: CSIRO Environment, Castray Esplanade, Hobart, Tasmania 7004, Australia
67 27: Research Institute for Global Change, JAMSTEC, 3173-25 Showa-machi, Kanazawa, Yokohama,
68 236-0001, Japan
69 28: Department of Geographical Sciences, University of Maryland, College Park, MD 20742, USA
70 29: Computer Science and Engineering Division, Oak Ridge National Laboratory, Oak Ridge, TN
71 37831, USA
72 30: Earth System Science Interdisciplinary Center, University of Maryland, College Park, MD 20740,
73 USA

74 31: Marine Institute, Rinville, Oranmore, Co Galway H91 R673, Ireland
75 32: School for Climate Studies, Stellenbosch University, Private Bag X1, Matieland, Stellenbosch,
76 7602, South Africa
77 33: Southern Ocean Carbon – Climate Observatory, CSIR, Rosebank, Cape Town, 7700, South Africa
78 34: Engr. Computer Science, University of California, Davis, CA 95616, USA
79 35: Department of Earth System Science, Stanford University, Stanford, CA 94305, USA
80 36: Japan Meteorological Agency, 3-6-9 Toranomon, Minato City, Tokyo, 105-8431, Japan
81 37: Research Institute for Environment, Energy, and Economics, Appalachian State University, Boone,
82 North Carolina, USA
83 38: Department of Geological and Environmental Sciences, Appalachian State University, Boone,
84 North Carolina, USA
85 39: Hakai Institute, 1713 Hyacinthe Bay Rd, Heriot Bay, BC, V0P 1H0, Canada
86 40: National Centre for Earth Observation, University of Edinburgh, Edinburgh, EH9 3FE, UK
87 41: School of Geosciences, University of Edinburgh, Edinburgh, EH9 3FE, UK
88 42: Climate and Global Dynamics Laboratory, National Center for Atmospheric Research
89 43: Geophysical Institute, University of Bergen, Allégaten 70, 5007 Bergen, Norway
90 44: Bjerknes Centre for Climate Research, Bergen, Norway
91 45: International Institute for Applied Systems Analysis (IIASA), Schlossplatz 1 A-2361 Laxenburg,
92 Austria
93 46: European Commission, Joint Research Centre (JRC), Ispra, Italy
94 47: Environmental Physics Group, Institute of Biogeochemistry and Pollutant Dynamics and Center for
95 Climate Systems Modeling (C2SM), ETH Zürich, Zurich, Switzerland
96 48: Swiss Data Science Center, 8050 Zurich, Switzerland
97 49: Laboratoire de Géologie, Ecole Normale Supérieure, CNRS UMR 8538, Institut Pierre-Simon
98 Laplace, PSL Research University, Paris, France
99 50: Smith School for Enterprise and the Environment, University of Oxford, Oxford, UK
100 51: NCAS-Climate, Climatic Research Unit, School of Environmental Sciences, University of East
101 Anglia, Norwich Research Park, Norwich, NR4 7TJ, UK
102 52: Potsdam Institute for Climate Impact Research (PIK), member of the Leibniz Association, P.O. Box
103 60 12 03, 14412 Potsdam, Germany
104 53: Universität Hamburg, Bundesstraße 55, 20146 Hamburg, Germany
105 54: Graduate School of Agricultural and Life Sciences, University of Tokyo, Tokyo, Japan
106 55: Cooperative Institute for Research in Environmental Sciences (CIRES), University of Colorado
107 Boulder, Boulder, CO 80305, USA
108 56: National Oceanic and Atmospheric Administration Global Monitoring Laboratory (NOAA/GML),
109 325 Broadway R/GML, Boulder, CO 80305, USA

110 57: Department of Climate, Meteorology and Atmospheric Sciences, University of Illinois, Urbana, IL
111 61801, USA
112 58: Jiangsu Provincial Key Laboratory for Advanced Remote Sensing and Geographic Information
113 Technology, International Institute for Earth System Science, Nanjing University, Nanjing, 210023,
114 China.
115 59: Institute of Applied Energy (IAE), Minato-ku, Tokyo 105-0003, Japan
116 60: University of California, San Diego, Scripps Institution of Oceanography, La Jolla, CA 92093-
117 0244, USA
118 61: Utrecht University, Faculty of Geosciences, Department IMEW, Copernicus Institute of Sustainable
119 Development, Heidelberglaan 2, P.O. Box 80115, 3508 TC, Utrecht, the Netherlands
120 62: School of Life Sciences, Faculty of Science, University of Technology Sydney, Ultimo, NSW 2007,
121 Australia
122 63: State Key Laboratory of Remote Sensing and Digital Earth, Aerospace Information Research
123 Institute, Chinese Academy of Sciences, Beijing 100101, China
124 64: Ministry of Education Key Laboratory for Earth System Modeling, Department of Earth System
125 Science, Tsinghua University, Beijing 100084, China
126 65: Lawrence Berkeley National Laboratory, USA
127 66: Jet Propulsion Laboratory, California Institute of Technology, Pasadena, CA, USA
128 67: Division of Geological and Planetary Sciences, California Institute of Technology, Pasadena, CA,
129 USA
130 68: CMA Key Open Laboratory of Transforming Climate Resources to Economy, Chongqing Institute
131 of Meteorological Sciences, Chongqing 401147, China
132 69: Department of Earth System Science, Tsinghua University, Beijing, China
133 70: LOCEAN Laboratory (Sorbonne Université, CNRS, IRD, MNHN), 4 Place Jussieu, F-75005 Paris,
134 France
135 71: Department of Meteorology and National Centre for Atmospheric Science, University of Reading,
136 Reading, UK
137 72: Lamont-Doherty Earth Observatory, Columbia University, New York, NY, USA
138 73: Climate Research Division, Environment and Climate Change Canada, Victoria, BC, Canada
139 74: College of Fisheries and Ocean Sciences, University of Alaska Fairbanks, Fairbanks, Alaska 99775-
140 7220, USA
141 75: Department of Land, Air and Water Resources, University of California, Davis, CA 95616, USA
142 76: Climate Adaptation Research Center, University of California, Davis, CA 95616, USA
143 77: Carbon to Sea Initiative, Washington D.C., USA
144 78: Earth System Division, National Institute for Environmental Studies (NIES), 16-2 Onogawa,
145 Tsukuba Ibaraki, 305-8506, Japan
146 79: NORCE Research, Jahnebakken 5, 5007 Bergen, Norway

147 80: Schiller Institute of Integrated Science and Society, Department of Earth and Environmental
148 Sciences, Boston College, Chestnut Hill, MA 02467, USA
149 81: National Oceanic and Atmospheric Administration, Atlantic Oceanographic & Meteorological
150 Laboratory (NOAA/AOML), 4301 Rickenbacker Causeway, Miami, FL 33149, USA
151 82: School of Atmospheric Sciences, Sun Yat-sen University, Zhuhai 519000, China
152 83: Department of Geoscience, Environment & Society-BGEOSYS, Université Libre de Bruxelles,
153 1050 Brussels, Belgium
154 84: Leibniz Institute for Baltic Sea Research Warnemünde (IOW), Seestrasse 15, 18119 Rostock,
155 Germany
156 85: Princeton University, Department of Geosciences and Princeton Environmental Institute, Princeton,
157 NJ, USA
158 86: Max Planck Institute for Biogeochemistry, P.O. Box 600164, Hans-Knöll-Str. 10, 07745 Jena,
159 Germany
160 87: Canadian Centre for Climate Modelling and Analysis, Environment and Climate Change Canada,
161 Victoria, BC, Canada
162 88: Institute for Climate and Environmental Physics, University of Bern, Bern, Switzerland
163 89: Environnements et Paléoenvironnements Océaniques et Continentaux (EPOC) UMR CNRS 5805
164 EPOC - OASU, Université de Bordeaux, Allée Geoffroy Saint Hilaire, 33615 Pessac, France
165 90: Centre National de Recherches Météorologiques, Université de Toulouse, Météo-France, CNRS,
166 UMR 3589, Toulouse, France
167 91: Research Center for Environmental Modeling and Application, Japan Agency for Marine-Earth
168 Science and Technology, Yokohama, Japan
169 92: Advanced Institute for Marine Ecosystem Change, Japan Agency for Marine-Earth Science and
170 Technology, Yokohama, Japan
171 93: State Key Laboratory of Tibetan Plateau Earth System and Resource Environment, Institute of
172 Tibetan Plateau Research, Chinese Academy of Sciences, Beijing 100101, China
173 94: University of Chinese Academy of Sciences, Beijing 101408, China
174 95: Australian Antarctic Partnership Program, University of Tasmania, Hobart, Australia
175 96: JMA Meteorological Research Institute, Tsukuba, Ibaraki, Japan
176 97: Statistics Division, Food and Agriculture Organization of the United Nations, Via Terme di
177 Caracalla, Rome 00153, Italy
178 98: Earth Sciences New Zealand, Wellington, New Zealand
179 99: Department of Marine Science, University of Otago, Dunedin, New Zealand
180 100: Climate Change Science Institute and Environmental Sciences Division, Oak Ridge National
181 Laboratory, Oak Ridge, TN 37831, USA
182 101: Institute of Carbon Neutrality, College of Urban and Environmental Sciences, Peking University,
183 Beijing 100091, China

184 102: School of Environmental Science and Engineering, Nanjing University of Information Science and
185 Technology (NUIST), Nanjing, 210044, China

186

187 *Correspondence to:* Pierre Friedlingstein (p.friedlingstein@exeter.ac.uk)

188 **Abstract**

189 Accurate assessment of anthropogenic carbon dioxide (CO₂) emissions and their redistribution among
190 the atmosphere, ocean, and terrestrial biosphere in a changing climate is critical to better understand
191 the global carbon cycle, support the development of climate policies, and project future climate
192 change. Here we describe and synthesise datasets and methodologies to quantify the five major
193 components of the global carbon budget and their uncertainties. Fossil CO₂ emissions (E_{FOS}) are based
194 on energy and cement production data. Emissions from land-use change (E_{LUC}) are estimated by
195 bookkeeping models based on land-use data. The global atmospheric CO₂ growth rate (G_{ATM}) is
196 computed from changes in concentration measured at surface stations. The global net uptake of CO₂
197 by the ocean (S_{OCEAN}) is estimated with global ocean biogeochemistry models and observation-based
198 fCO₂-products. The global net uptake of CO₂ by the land (S_{LAND}) is estimated with dynamic global
199 vegetation models. Additional lines of evidence are provided by atmospheric inversions, atmospheric
200 oxygen measurements, ocean interior observation-based estimates, and Earth System Models. This
201 year, we introduced corrections on the E_{LUC}, S_{OCEAN} and S_{LAND} estimates. The sum of all sources and
202 sinks results in the carbon budget imbalance (B_{IM}), a measure of imperfect data and incomplete
203 understanding of the contemporary carbon cycle. All uncertainties are reported as $\pm 1\sigma$.

204 For the year 2024, E_{FOS} increased by 1.1% relative to 2023, with fossil emissions at 10.3 ± 0.5 GtC yr⁻¹
205 (including the cement carbonation sink, 0.2 GtC yr⁻¹), E_{LUC} was 1.3 ± 0.7 GtC yr⁻¹, for total
206 anthropogenic CO₂ emissions of 11.6 ± 0.9 GtC yr⁻¹ (42.4 ± 3.2 GtCO₂ yr⁻¹). Also, for 2024, G_{ATM} was
207 7.9 ± 0.2 GtC yr⁻¹ (3.73 ± 0.1 ppm yr⁻¹), 2.2 GtC above the 2023 growth rate. S_{OCEAN} was 3.4 ± 0.4
208 GtC yr⁻¹ and S_{LAND} was 1.9 ± 1.1 GtC yr⁻¹, leaving a large negative B_{IM} (-1.7 GtC yr⁻¹), suggesting that
209 the total sink or G_{ATM} is strongly overestimated in 2024. The global atmospheric CO₂ concentration
210 averaged over 2024 reached 422.8 ± 0.1 ppm. Preliminary data for 2025 suggest an increase in E_{FOS}
211 relative to 2024 of +1.0% (0.2% to 1.7%) globally, and atmospheric CO₂ concentration increasing by
212 2.1 ppm reaching 425.6 ppm, 53% above the pre-industrial level (around 278 ppm in 1750). Overall,
213 the mean and trend in the components of the global carbon budget are consistently estimated over the
214 period 1959-2024, with a near-zero overall budget imbalance, although discrepancies of up to around
215 1 GtC yr⁻¹ persist for the representation of annual to decadal variability in CO₂ fluxes. Comparison of
216 estimates from multiple approaches and observations shows: (1) a persistent large uncertainty in the
217 estimate of land-use change emissions, (2) a low agreement between the different methods on the

218 magnitude of the land CO₂ flux in the northern extra-tropics, and (3) a discrepancy between the
219 different methods on the mean ocean sink.

220 This living data update documents changes in methods and datasets applied to this most-recent global
221 carbon budget as well as evolving community understanding of the global carbon cycle. The data
222 presented in this work are available at <https://doi.org/10.18160/GCP-2025> (Friedlingstein et al.,
223 2025c).

224

225 **Executive Summary**

226 **Global fossil CO₂ emissions (including cement carbonation) are expected to further increase in**
227 **2025 by 1.0% relative to 2024** (range 0.2% to 1.7%), bringing fossil emissions to an expected 10.4
228 GtC yr⁻¹ (38.1 GtCO₂ yr⁻¹)¹. Emissions from coal, oil and gas in 2025 are all expected to be above their
229 2024 levels (by 1.0%, 1.1% and 1.3% respectively). These preliminary estimates are based on available
230 data for 2025. Consolidated data confirm a growth of 1.1% in 2024 relative to 2023, with fossil CO₂
231 emissions of 10.3 ± 0.5 GtC yr⁻¹ (37.8 ± 1.8 GtCO₂ yr⁻¹) in 2024.

232 **Regionally, fossil emissions are projected to grow in 2025 in the USA and be nearly flat in the**
233 **European Union, reversing long-term decreases, and also in China and India, albeit more slowly**
234 **compared to recent trends.** The increase in fossil emissions in 2025 relative to 2024 is projected to be
235 0.4% (-0.1% to 0.9%) for China, 2.5% (2.2% to 2.8%) for the United States, 1.1% for India. 2025
236 emissions for the European Union are projected to decrease by -0.1%. Projected emissions in Japan,
237 provided this year for the first time, are for a decrease of -0.9%. Emissions are also projected to
238 increase by 6.7% for international aviation and by 2.0% for international shipping, and to increase by
239 0.9% (-1.0% to 3.0%) for the rest of the world in aggregate. The global carbon intensity of energy has
240 consistently decreased over the past decade (-0.7% yr⁻¹), indicating decarbonisation of the energy
241 system in China (-1.4% yr⁻¹), the European Union (-1.5% yr⁻¹), and the USA (-1.3% yr⁻¹), but no decline
242 in India and an increase in the rest of the world in aggregate. These trends are not sufficient to offset the
243 growth in global energy demand, which is driven by growing GDP globally and a weakening decline in
244 energy per GDP, particularly in China and the US.

245 **Fossil CO₂ emissions decreased (p<0.05) in 35 economies with growing GDP (p<0.05) during the**
246 **decade 2015-2024.** The list of decarbonising economies nearly doubled since the previous decade
247 (2005-2014; 18 countries). These 35 decarbonising economies contribute 2.7 GtC yr⁻¹ (9.7 GtCO₂)
248 fossil fuel CO₂ emissions over the last decade in aggregate, representing 27% of the world CO₂ fossil

¹ All growth rates use a leap year adjustment that corrects for the extra day in 2024.

249 emissions.

250 **Global net CO₂ emissions from land use averaged 1.4 ± 0.7 GtC yr⁻¹ (5.0 ± 2.6 GtCO₂ yr⁻¹) for the**
251 **2015-2024 period.** Emissions from deforestation, the main driver of global gross emissions, remain
252 high at around 1.9 GtC yr⁻¹ over the 2015-2024 period, highlighting the strong potential of halting
253 deforestation for emissions reductions. Sequestration of 1.3 GtC yr⁻¹ through re-/afforestation and forest
254 regrowth in shifting cultivation cycles offsets two third of the deforestation emissions. In addition,
255 smaller net emissions are due to wood harvest & forest management, peat drainage and peat fire.
256 Regionally, the highest net emitters during 2015-2024 were Brazil, Indonesia, and the Democratic
257 Republic of the Congo, with these 3 countries contributing more than half of global land-use CO₂
258 emissions. Net carbon dioxide removals (CDR) from re-/afforestation were highest in China, the USA,
259 and the EU27, with combined removals of 0.3 GtC yr⁻¹ during 2015-2024.

260 **Since the late-1990s, emissions from land use show a statistically significant decrease at a rate of**
261 **around 0.2 GtC per decade, with a larger drop within the most recent decade. Preliminary data**
262 **for 2025 suggest emissions decreased to around 1.1 GtC (4.1 GtCO₂ yr⁻¹), mainly attributable to**
263 **the end of the El Niño conditions.**

264 **Total anthropogenic emissions (fossil and land use, including the carbonation sink) were 11.6 GtC**
265 **yr⁻¹ (42.4 GtCO₂ yr⁻¹) in 2024, with a slightly lower preliminary estimate of 11.5 GtC yr⁻¹ (42.2**
266 **GtCO₂ yr⁻¹) for 2025.** Total anthropogenic emissions have grown more slowly over the last decade
267 (0.3% yr⁻¹ over the 2015-2024 period) compared to the previous decade (1.9% yr⁻¹ over 2005-2014).

268 **The remaining carbon budget from the beginning of 2026 for a 50% likelihood to limit warming**
269 **to 1.5°C is nearly exhausted (50 GtC, 170 GtCO₂ left, equivalent to around 4 years at the 2025**
270 **emissions levels), consistent with the warming of the planet attributed to human activities, which**
271 **reached 1.36°C in 2024.** Each additional cumulative emission of about 180 GtCO₂ will lead to
272 approximately 0.1°C of warming. The remaining carbon budgets to limit warming to 1.7°C and 2°C
273 above the 1850-1900 level have been reduced to 145 GtC (525 GtCO₂, 12 years) and 290 GtC (1055
274 GtCO₂, 25 years) respectively.

275 **The concentration of CO₂ in the atmosphere is set to reach 425.6 ppm in 2025, 53% above pre-**
276 **industrial levels.** The atmospheric CO₂ growth rate was 5.6 ± 0.02 GtC yr⁻¹ (2.6 ppm) during the
277 decade 2015-2024 (50% of total CO₂ emissions). 2024 had a record-high growth rate of 7.9 ± 0.02 GtC
278 yr⁻¹ (3.7 ppm) mainly due to the 2023/2024 El Niño conditions. The preliminary 2025 growth rate
279 estimate is 4.4 GtC (2.1 ppm).

280 **The ocean sink, the global net uptake of CO₂ by the ocean, has taken up 29% of the total**
281 **emissions in the past decade, after being re-evaluated upwards based on new evidence and**
282 **process understanding. The ocean sink has been stagnant since 2016, largely in response to**
283 **climate variability modulating the growing sink trend, but further affected by the ocean heatwave**

284 **of 2023-2024 in the Northern Hemisphere.** The ocean CO₂ sink was 3.2 ± 0.4 GtC yr⁻¹ during the
285 decade 2015-2024, with a preliminary estimate of 3.2 GtC yr⁻¹ for 2025, slightly below 2024 levels, due
286 to the end of the El Niño conditions in 2024 and associated reduced atmospheric CO₂ growth rate.

287 **The land sink, which is the global net uptake of CO₂ by the land excluding land use, has taken up**
288 **21% of the total emissions in the past decade, after being re-evaluated downwards based on**
289 **improved process representation. The land sink has been relatively stagnant since 2000, largely in**
290 **response to climate variability and climate change offsetting the CO₂ induced growth.** The land
291 CO₂ sink was 2.4 ± 0.8 GtC yr⁻¹ during the 2015-2024 decade, but was reduced to $1.9 \text{ GtC} \pm 0.8 \text{ GtC yr}^{-1}$
292 ¹ in 2024. The preliminary estimate for the land sink in 2025 is an increase to 3.1 GtC, recovering
293 entirely from its strong drop during the 2023-2024 El Niño conditions.

294 **The effects of climate change and climate variability act to reduce the land and ocean CO₂ sinks**
295 **by 25% and 7.1% respectively, on average for the 2015-2024 period.** The land sink is negatively
296 affected by warming with decreased tropical plant productivity and enhanced ecosystem respiration
297 globally. The ocean sink is negatively affected by altered oceanic circulation and surface warming
298 which decreases CO₂ solubility.

299 **So far in 2025, global fire CO₂ emissions have been approximately 20% lower than the 2015-2024**
300 **average due to low fire activity in Africa and the tropics, reaching 1.2-1.4 GtC globally during**
301 **January-September.** This contrasts with the above average fire emissions in 2023 ($1.7\text{-}2.1 \text{ GtC yr}^{-1}$)
302 and 2024 ($1.6\text{-}2.2 \text{ GtC yr}^{-1}$) due to extensive fires in Canada (2023) and Brazil and Bolivia (2024).
303 These fire emissions estimates should not be directly compared with the land-use emissions or the land
304 sink, because they represent a gross carbon flux to the atmosphere and do not account for post-fire
305 recovery. They also do not distinguish between natural, climate-driven, and land-use-related fires.

306

307

308 **1 Introduction**

309 The concentration of carbon dioxide (CO₂) in the atmosphere has increased from approximately 278
310 parts per million (ppm) in 1750 (Gulev et al., 2021), the beginning of the Industrial Era, to 422.8 ± 0.1
311 ppm in 2024 (Lan et al., 2025; Figure 1). The atmospheric CO₂ increase above pre-industrial levels was,
312 initially, primarily caused by the release of carbon to the atmosphere from deforestation and other land-
313 use change activities (Canadell et al., 2021). While emissions from fossil fuels started before the
314 Industrial Era, they became the dominant source of anthropogenic emissions to the atmosphere from
315 around 1950 and their relative share has continued to increase until present. Anthropogenic emissions
316 occur on top of an active natural carbon cycle that circulates carbon between the reservoirs of the
317 atmosphere, ocean, and terrestrial biosphere on time scales from sub-daily to millennial, while
318 exchanges with geologic reservoirs occur on longer timescales (Archer et al., 2009).

319 The global carbon budget (GCB) presented here refers to the mean, variations, and trends in the
320 perturbation of CO₂ in the environment, referenced to the beginning of the Industrial Era (defined here
321 as 1750). This paper describes the components of the global carbon cycle over the historical period with
322 a stronger focus on the recent period (since 1959, onset of robust atmospheric CO₂ measurements), the
323 last decade (2015-2024), the last year (2024) and the current year (2025). Finally, it provides
324 cumulative emissions from fossil fuels and land-use change since the year 1750, and since the year
325 1850 (the reference year for historical simulations in IPCC).

326 We quantify the input of CO₂ to the atmosphere by emissions from human activities, the growth rate of
327 atmospheric CO₂ concentration, and the resulting changes in the storage of carbon in the land and ocean
328 reservoirs in response to increasing atmospheric CO₂ levels, climate change and variability, and other
329 anthropogenic and natural changes (Figure 2). An understanding of this perturbation budget over time
330 and the underlying variability and trends of the natural carbon cycle is necessary to understand the
331 response of natural sinks to changes in climate, CO₂ and land-use change drivers, and to quantify
332 emissions compatible with a given climate stabilisation target.

333 The components of the CO₂ budget that are reported annually in this paper include separate and
334 independent estimates for the CO₂ emissions from (1) fossil fuel combustion and oxidation from all
335 energy and industrial processes; also including cement production and carbonation (E_{FOS} ; GtC yr⁻¹) and
336 (2) the emissions resulting from deliberate human activities on land, including those leading to land-use
337 change (E_{LUC} ; GtC yr⁻¹); and their partitioning among (3) the growth rate of atmospheric CO₂
338 concentration (G_{ATM} ; GtC yr⁻¹), and the uptake of CO₂ (the ‘CO₂ sinks’) in (4) the ocean (S_{OCEAN} ; GtC
339 yr⁻¹) and (5) on land (S_{LAND} ; GtC yr⁻¹). The CO₂ sinks as defined here conceptually include the response
340 of the land (including inland waters and estuaries) and ocean (including coastal and marginal seas) to

341 elevated CO₂ and changes in climate and other environmental conditions, although in practice not all
342 processes are fully accounted for (see Section 2.10). Note that the term sink means that the net transfer
343 of carbon is from the atmosphere to land or the ocean, but it does not imply any permanence of that sink
344 in the future.

345 Global emissions and their partitioning among the atmosphere, ocean and land are in mass balance in
346 the real world. Due to the combination of imperfect spatial and/or temporal data coverage, errors in
347 each estimate, and smaller terms not included in our budget estimate (discussed in Section 2.10), the
348 GCB independent estimates (1) to (5) above do not necessarily add up to zero. We hence estimate a
349 budget imbalance (B_{IM}), which is a measure of the mismatch between the estimated emissions and the
350 estimated changes in the atmosphere, land and ocean, as follows:

$$351 \quad B_{IM} = E_{FOS} + E_{LUC} - (G_{ATM} + S_{OCEAN} + S_{LAND}) \quad (1)$$

352 G_{ATM} is usually reported in ppm yr⁻¹, which we convert to units of carbon mass per year, GtC yr⁻¹, using
353 1 ppm = 2.124 GtC (Ballantyne et al., 2012; Table 1). Units of gigatonnes of CO₂ (or billion tonnes of
354 CO₂) used in policy are equal to 3.664 multiplied by the value in units of GtC.

355 We also assess a set of additional lines of evidence derived from global atmospheric inversion system
356 results (Section 2.7), observed changes in oxygen concentration (Section 2.8) and Earth System Models
357 (ESMs) simulations (Section 2.9), all of these methods closing the global carbon balance (zero B_{IM}).

358 We further quantify E_{FOS} and E_{LUC} by country, including both territorial and consumption-based
359 accounting for E_{FOS} (see Section 2), and discuss missing terms from sources other than the combustion
360 of fossil fuels (see Section 2.10). We also assess carbon dioxide removal (CDR) (see Sect. 2.2 and 2.3).
361 Land-based CDR is significant, but already accounted for in E_{LUC} in equation (1) (Sect 3.2.2). Other
362 CDR methods, not based on vegetation, are currently several orders of magnitude smaller than the other
363 components of the budget (Sect. 3.3), hence these are not included in equation (1), or in the global
364 carbon budget tables or figures (with the exception of Figure 2 where CDR is shown primarily for
365 illustrative purpose).

366 The global CO₂ budget has been assessed by the Intergovernmental Panel on Climate Change (IPCC) in
367 all assessment reports (Watson et al., 1990; Schimel et al., 1995; Prentice et al., 2001; Denman et al.,
368 2007; Ciais et al., 2013; Canadell et al., 2021), and by others (e.g. Ballantyne et al., 2012). The Global
369 Carbon Project (GCP, www.globalcarbonproject.org, last access: 23 October 2025) has coordinated this
370 cooperative community effort for the annual publication of global carbon budgets for the year 2005
371 (Raupach et al., 2007; including fossil emissions only), year 2006 (Canadell et al., 2007), year 2007
372 (GCP, 2008), year 2008 (Le Quéré et al., 2009), year 2009 (Friedlingstein et al., 2010), year 2010
373 (Peters et al., 2012a), year 2012 (Le Quéré et al., 2013; Peters et al., 2013), year 2013 (Le Quéré et al.,
374 2014), year 2014 (Le Quéré et al., 2015a; Friedlingstein et al., 2014), year 2015 (Jackson et al., 2016;

375 Le Quéré et al., 2015b), year 2016 (Le Quéré et al., 2016), year 2017 (Le Quéré et al., 2018a; Peters et
376 al., 2017a), year 2018 (Le Quéré et al., 2018b; Jackson et al., 2018), year 2019 (Friedlingstein et al.,
377 2019; Jackson et al., 2019; Peters et al., 2020), year 2020 (Friedlingstein et al., 2020; Le Quéré et al.,
378 2021), year 2021 (Friedlingstein et al., 2022a; Jackson et al., 2022), year 2022 (Friedlingstein et al.,
379 2022b), the year 2023 (Friedlingstein et al., 2023), and most recently the year 2024 (Friedlingstein et
380 al., 2025a). Each of these papers updated previous estimates with the latest available information for the
381 entire time series.

382 We adopt a range of ± 1 standard deviation (σ) to report the uncertainties in our global estimates,
383 representing a likelihood of 68% that the true value will be within the provided range if the errors have
384 a gaussian distribution, and no bias is assumed. Note that when less than 10 individual data are
385 available for an estimate (e.g. atmospheric inversions, f -CO₂ products), we provide the full range, as
386 opposed to the standard deviation. The choice of reporting a $\pm 1 \sigma$ reflects the difficulty of
387 characterising the uncertainty in the CO₂ fluxes between the atmosphere and the ocean and land
388 reservoirs individually, particularly on an annual basis, as well as the difficulty of updating the CO₂
389 emissions from land-use change. A likelihood of 68% provides an indication of our current capability to
390 quantify each term and its uncertainty given the available information. The uncertainties reported here
391 combine statistical analysis of the underlying data, assessments of uncertainties in the generation of the
392 datasets, and expert judgement of the likelihood of results lying outside this range. The limitations of
393 current information are discussed in the paper and have been examined in detail elsewhere (Ballantyne
394 et al., 2015; Zscheischler et al., 2017). We also use a qualitative assessment of confidence level to
395 characterise the annual estimates from each term based on the type, amount, quality, and consistency of
396 the different lines of evidence as defined by the IPCC (Stocker et al., 2013).

397 This paper provides a detailed description of the datasets and methodology used to compute the global
398 carbon budget estimates for the industrial period, from 1750 to 2025, and in more detail for the recent
399 period since 1959. This paper is updated every year using the format of ‘living data’ to keep a record of
400 budget versions and the changes in new data, revision of data, and changes in methodology that lead to
401 changes in estimates of the carbon budget. All underlying data used to produce the budget and
402 additional materials associated with the release of each new version are available via the Global Carbon
403 Budget website (<https://globalcarbonbudget.org/>, last access: 23 October 2025), with emissions also
404 available through the Global Carbon Atlas (<http://www.globalcarbonatlas.org>, last access: 23 October
405 2025). With this approach, we aim to provide the highest transparency and traceability in the reporting
406 of CO₂, the key driver of climate change.

407 **2 Methods**

408 Multiple organisations and research groups around the world generated the original measurements and
409 data used to complete the global carbon budget. The effort presented here is thus mainly one of

410 synthesis, where results from individual groups are collated, analysed, and evaluated for consistency.
411 We facilitate access to original data with the understanding that primary datasets will be referenced in
412 future work (see Table 2 for how to cite the datasets, and Section on data availability). Descriptions of
413 the measurements, models, and methodologies follow below, with more detailed descriptions of each
414 component provided as Supplementary Information (Supplement Tables S1 to S5). In the GCB, when
415 possible, we account for adjustments and corrections to the components estimates. We refer to
416 ‘adjustments’ when accounting for known processes not included in one estimate (ex. river
417 correction for fCO₂ products), while we refer to ‘corrections’ when addressing known biases in
418 one estimate (ex. replaced sinks and sources for DGVMs).

419 This is the 20th version of the global carbon budget and the 14th revised version in the format of a living
420 data update in Earth System Science Data. It builds on the latest published global carbon budget of
421 Friedlingstein et al. (2025a). The main changes this year are: the inclusion of (1) data to year 2024 and
422 a projection for the global carbon budget for year 2025; (2) transient carbon densities in the estimate of
423 ELUC, (3) a correction on S_{LAND} to account for the historical changes in forest cover, (4) a correction on
424 S_{OCEAN} to account for the underestimation of the sink by GOBMs and for the ocean temperature
425 gradients in the fCO₂-products estimate, (5) an estimate of the atmospheric CO₂ growth rate derived
426 from satellite observations, and (6) decadal estimates of change in the dissolved inorganic carbon
427 inventory in the interior ocean. Other methodological differences are summarised in Table 3 and
428 previous changes since 2006 are provided in Table S10.

429 **2.1 Fossil CO₂ emissions (E_{FOS})**

430 **2.1.1 Historical period 1850-2024**

431 The estimates of global and national fossil CO₂ emissions (E_{FOS}) include the oxidation of fossil fuels
432 through both combustion (e.g., transport, heating) and chemical oxidation (e.g. carbon anode
433 decomposition in aluminium refining) activities, and the decomposition of carbonates in industrial
434 processes (e.g. the production of cement). We also include CO₂ uptake from the cement carbonation
435 process. Several emissions sources are not estimated or not fully covered: coverage of emissions from
436 lime production are not global, and decomposition of carbonates in glass and ceramic production are
437 included only for the “Annex 1” countries of the United Nations Framework Convention on Climate
438 Change (UNFCCC) for lack of activity data. These omissions are considered to be minor. Short-cycle
439 carbon emissions - for example from combustion of biomass - are not included here but are accounted
440 for in the CO₂ emissions from land use (see Section 2.2).

441 Our estimates of fossil CO₂ emissions rely on data collection by many other parties. Our goal is to
442 produce the best estimate of this flux, and we therefore use a prioritisation framework to combine data
443 from different sources that have used different methods, while being careful to avoid double counting

444 and undercounting of emissions sources. The CDIAC-FF emissions dataset, derived largely from UN
445 energy data, forms the foundation, and we extend emissions to 2024 using energy growth rates reported
446 by the Energy Institute (a dataset formerly produced by BP). We then proceed to replace estimates
447 using data from what we consider to be superior sources, for example Annex 1 countries' official
448 submissions to the UNFCCC. All data points are potentially subject to revision, not just the latest year.
449 For full details see Andrew and Peters (2025).

450 Other estimates of global fossil CO₂ emissions exist, and these are compared by Andrew (2020a). The
451 most common reason for differences in estimates of global fossil CO₂ emissions is a difference in which
452 emissions sources are included in the datasets. Datasets such as those published by the Energy Institute,
453 the US Energy Information Administration, and the International Energy Agency's 'CO₂ emissions
454 from fuel combustion' are all generally limited to emissions from combustion of fossil fuels. In
455 contrast, datasets such as PRIMAP-hist, CEDS, EDGAR, and GCP's dataset aim to include all sources
456 of fossil CO₂ emissions. See Andrew (2020a) for detailed comparisons and discussion.

457 Cement products absorb CO₂ from the atmosphere over their lifetimes, a process known as 'cement
458 carbonation'. We estimate this CO₂ sink, from 1931 onwards, as the average of two studies in the
459 literature (Cao et al., 2020; Guo et al., 2021). Both studies use the same model, developed by Xi et al.
460 (2016), with different parameterisations and input data, with the estimate of Guo and colleagues being a
461 revision of Xi et al. (2016). The trends of the two studies are very similar. Since carbonation is a
462 function of both current and previous cement production, we extend these estimates to 2024 by using
463 the growth rate derived from the smoothed cement emissions (10-year smoothing) fitted to the
464 carbonation data. In the present budget, we always include the cement carbonation carbon sink in the
465 fossil CO₂ emission component (E_{FOS}) unless explicitly stated otherwise.

466 We use the Kaya Identity for a simple decomposition of CO₂ emissions into the key drivers (Raupach et
467 al., 2007). While there are variants (Peters et al., 2017b), we focus here on a decomposition of CO₂
468 emissions into population, GDP per person, energy use per GDP, and CO₂ emissions per energy.
469 Multiplying these individual components together returns the CO₂ emissions. Using the decomposition,
470 it is possible to attribute the change in CO₂ emissions to the change in each of the drivers. This method
471 gives a first-order understanding of what causes CO₂ emissions to change each year.

472 **2.1.2 2025 projection**

473 We provide a projection of global fossil CO₂ emissions in 2025 by combining separate projections for
474 China, USA, EU, India, Japan, and for all other countries combined. The methods are different for each
475 of these. For China we use growth rates from the 2026 edition of the National Bureau of Statistics'
476 Statistical Communique along with cement clinker trade data and estimated changes in lime production.
477 For the USA our projection is taken directly from the Energy Information Administration's (EIA)

478 Short-Term Energy Outlook (EIA, 2026), combined with the year-to-date growth rate of cement clinker
479 production. For the EU we use monthly energy data from Eurostat to derive estimates of monthly CO₂
480 emissions through December (Andrew, 2021). EU cement emissions are based on available production
481 data through December from three of the largest producers, Germany, Poland, and Spain as well as
482 production indices for Italy and France. India’s projected emissions are derived from monthly estimates
483 through December using the methods of Andrew (2020b). Japan’s emissions are based on monthly
484 estimates through December. Emissions from international transportation (bunkers) are estimated
485 separately for aviation and shipping. Changes in aviation emissions are derived primarily from OECD
486 monthly estimates, extrapolated using the growth rates of global flight miles from Airportia. Shipping
487 emissions are derived from estimates of sales of bunker fuels provided by Ship and Bunker (Ship and
488 Bunker, 2026). Emissions for the rest of the world are derived for coal and cement using projected
489 growth in economic production from the IMF (2025) combined with extrapolated changes in emissions
490 intensity of economic production; for oil using a global constraint from EIA; and for natural gas using a
491 global constraint from IEA. More details on the EFOS methodology and its 2025 projection can be found
492 in Supplement S.1.

493 We compare our 2025 projection with the Carbon Monitor (2025). Carbon Monitor is a dataset of daily
494 emissions constructed using hourly to daily proxy data (e.g., electricity consumption, travel patterns,
495 etc) instead of energy use data (Liu et al., 2020a; Liu et al., 2020b). Emissions estimates from January
496 to December are combined to give a full-year 2025 estimate.

497 **2.2 CO₂ emissions from land-use, land-use change and forestry (E_{LUC})**

498 **2.2.1 Historical period 1850-2024**

499 The net CO₂ flux from land-use, land-use change and forestry (E_{LUC}, called land-use change emissions
500 in the rest of the text) includes CO₂ fluxes from deforestation, afforestation, logging and forest
501 degradation (including harvest activity), shifting cultivation (cycle of cutting forest for agriculture, then
502 abandoning), regrowth of forests (following wood harvest or agriculture abandonment), peat burning,
503 and peat drainage.

504 Updated estimates from three bookkeeping models are used to quantify gross emissions, gross removals
505 and the resulting net E_{LUC}: BLUE (Hansis et al., 2015), LUCE (Qin et al. 2024), and OSCAR (Gasser et
506 al., 2020). An important improvement compared to previous GCBs is the use of transient carbon
507 densities by all three bookkeeping models, i.e., they consider the effects of environmental changes, such
508 as atmospheric CO₂ increase, on vegetation and soil carbon densities, to estimate E_{LUC} (Gasser et al.,
509 2020; Dorgeist et al., 2024). The GCB assessments have for a long time also (and initially exclusively)
510 used estimates from the bookkeeping model H&C2023 (Houghton and Castanho, 2023), its predecessor
511 H&N2017 (Houghton and Nassikas, 2017), and earlier versions. However, H&C2023 does not consider

512 transient carbon densities and only provides data up to 2020, which implies the need to extrapolate its
513 data to the time after 2020. As the model does thus not incorporate the most recent developments in
514 bookkeeping modeling, it is not used anymore in GCB2025.

515 Emissions from peat burning and peat drainage are added from external datasets (see Supplement
516 S.2.2): peat fire emissions from the Global Fire Emission Database (GFED4s; van der Werf et al.,
517 2017) and peat drainage emissions averaged from estimates of the Food Agriculture Organization
518 (Conchedda and Tubiello, 2020; FAO, 2025a) and from simulations with the DGVM ORCHIDEE-
519 PEAT (Qiu et al., 2021) and the DGVM LPX-Bern (Lienert and Joos, 2018; Müller and Joos, 2021).

520 Uncertainty estimates were derived from the Dynamic Global Vegetation Models (DGVMs) ensemble
521 for the time period prior to 1960, and using for the recent decades an uncertainty range of ± 0.7 GtC yr⁻¹,
522 which is a semi-quantitative measure for annual and decadal emissions and reflects our best value
523 judgement that there is at least 68% chance ($\pm 1\sigma$) that the true land-use change emission lies within the
524 given range, for the range of processes considered here.

525 The GCB E_{LUC} estimates follow the CO₂ flux definition of global carbon cycle models and differ from
526 IPCC definitions adopted in National GHG Inventories (NGHGI) for reporting under the UNFCCC.
527 The latter typically include terrestrial fluxes occurring on all land that countries define as managed,
528 following the IPCC managed land proxy approach (Grassi et al., 2018). This partly includes fluxes due
529 to environmental change (e.g. atmospheric CO₂ increase), which are part of S_{LAND} in our definition. As
530 a result, global emission estimates are smaller for NGHGI than for the global carbon budget definition
531 (Grassi et al., 2023). The same is the case for the FAO estimates of carbon fluxes on forest land, which
532 include both anthropogenic and natural fluxes on managed land (Tubiello et al., 2025; FAO, 2025b).
533 Using the NGHGI data collected and processed in the LULUCF data hub V3.1 (Melo et al. 2025), we
534 translate the GCB and NGHGI definitions to each other, to provide a comparison of the anthropogenic
535 carbon budget as reported in GCB to the official country reporting to the UNFCCC convention. We
536 further compare these estimates with the net atmosphere-to-land flux from atmospheric inversion
537 systems (see Section 2.7), averaged over managed land only.

538 E_{LUC} contains a range of fluxes that are related to Carbon Dioxide Removal (CDR). CDR is defined as
539 the set of anthropogenic activities that remove CO₂ from the atmosphere, in addition to the Earth's
540 natural processes (such as carbon uptake in response to atmospheric CO₂ increase), and store it in
541 durable form, such as in forest biomass, soils, long-lived products, oceans or geological reservoirs.
542 Here, we quantify vegetation-based CDR that is implicitly or explicitly captured by land-use fluxes
543 (CDR not based on vegetation is discussed in Section 2.3). We quantify CDR through re/afforestation
544 from the three bookkeeping estimates by separating permanent increases in forest cover, which counts
545 as CDR, from forest regrowth in shifting cultivation cycles (not part of CDR; see Supplement S.2.2). It
546 should be noted that the permanence of the storage under climate risks such as fire is increasingly

547 questioned. Other CDR activities related to land use but not fully accounted for in our E_{LUC} estimate
548 include the transfer of carbon to harvested wood products (HWP), bioenergy with carbon capture and
549 storage (BECCS), and biochar production (Babiker et al., 2022; Smith et al., 2024). The different
550 bookkeeping models all represent HWP but with varying details concerning product usage and their
551 lifetimes. BECCS and biochar are currently only represented in bookkeeping and DGVM models with
552 regard to the CO_2 removal through photosynthesis, without accounting for the durable storage. HWP,
553 BECCS, and biochar are typically counted as CDR once the transfer to the durable storage site occurs
554 and not when the CO_2 is removed from the atmosphere, which complicates a direct comparison to the
555 GCB approach to quantify annual fluxes to and from the atmosphere. We provide estimates for CDR
556 through HWP, BECCS, and biochar based on independent studies in Section 3.2.2. HWP and BECCS
557 estimates reflect updated 2024 data of the State of CDR report (Smith et al., 2024), while biochar
558 estimates correspond to 2023 due to unavailability of newer data. We do not add them to our E_{LUC}
559 estimate to avoid potential double-counting that arises from the partial consideration of HWP, BECCS,
560 and biochar in the bookkeeping and DGVM models and to avoid inconsistencies from the temporal
561 discrepancy between transfer to storage and removal from the atmosphere. More details on the E_{LUC}
562 methodology can be found in Supplement S.2.

563 **2.2.2 2025 Projection**

564 We project the 2025 land-use emissions for BLUE, OSCAR, and LUCE based on their E_{LUC} estimates
565 for 2023 and adding the anomalies in carbon emissions from peat fires in equatorial Asia and tropical
566 deforestation and degradation fires (2025 emissions relative to 2023 emissions) from GFED4s (van der
567 Werf et al., 2017) estimated using active fire data (MCD14ML; Giglio et al., 2016). 2023 is used as
568 base year since the E_{LUC} estimate for the year 2024 is informed by extrapolated land-use data
569 (Supplement S.2.1). Peat drainage is assumed to be unaltered as it has low interannual variability.

570 **2.3 Carbon Dioxide Removal (CDR) not based on vegetation**

571 Some CDR involves CO_2 fluxes via land use, which is included in our estimate of E_{LUC}
572 (re/afforestation) or provided separately in Section 3.2.2 (biochar, HWP, and BECCS). Other CDR
573 occurs through CO_2 fluxes directly from the air to the geosphere, which is reported in Section 3.3. The
574 majority of this derives from bio-oil storage in geological reservoirs, enhanced weathering through the
575 application of crushed rock to soils, and the production of solid mineral products with CO_2 captured
576 from the atmosphere, with smaller contributions from Direct Air Carbon Capture and Storage
577 (DACCS), sinking of terrestrial (e.g., straw) or marine (e.g., macroalgae) biomass into the deep ocean
578 through human intervention, and others like intentional ocean or river alkalinity enhancement. For these
579 methods, we use updated 2024 data (Smith et al., 2024), which compiles and harmonises reported CDR
580 from a combination of existing databases, surveys, and novel research. Currently, there are no
581 internationally agreed methods for reporting these types of CDR, implying that estimates are based on

582 self-disclosure by projects following their own protocols or protocols produced by third party registries.
583 As such, the fractional uncertainty on these numbers should be viewed as substantial, and numbers are
584 liable to change in future years as protocols are harmonised and improved.

585 **2.4 Growth rate in atmospheric CO₂ concentration (G_{ATM})**

586 **2.4.1 Historical period 1850-2024**

587 The rate of growth of the atmospheric CO₂ concentration is provided for years 1959-2024 by the US
588 National Oceanic and Atmospheric Administration Global Monitoring Laboratory (NOAA/GML; Lan
589 et al., 2025), which includes recent revisions to the calibration scale of atmospheric CO₂ measurements
590 (WMO-CO₂-X2019; Hall et al., 2021). For the 1959-1979 period, the global growth rate is based on
591 measurements of atmospheric CO₂ concentration averaged from the Mauna Loa and South Pole
592 stations, as observed by the CO₂ Program at Scripps Institution of Oceanography (SIO, Keeling et al.,
593 1976). For the 1980-2024 time period, the global growth rate is based on the average of multiple
594 stations selected from the marine boundary layer sites with well-mixed background air (Lan et al.,
595 2024), after fitting a smooth curve through the data for each station as a function of time, and averaging
596 by latitude band (Masarie and Tans, 1995). The annual growth rate is estimated by Lan et al. (2025)
597 from atmospheric CO₂ concentration by taking the average of the most recent December-January
598 months corrected for the average seasonal cycle and subtracting this same average one year earlier. To
599 obtain G_{ATM}, the observation-based growth rate in units of ppm yr⁻¹ is converted to units of GtC yr⁻¹ by
600 multiplying by a factor of 2.124 GtC per ppm, assuming instantaneous mixing of CO₂ throughout the
601 atmosphere (Ballantyne et al., 2012; Table 1). There is high confidence in the observations because
602 they are based on direct measurements from stations distributed around the world (Lan et al., 2024)
603 with all CO₂ measurements consistently measured against the same CO₂ standard scale (WMO X2019)
604 defined by a suite of gas standards (Hall et al., 2021). However, the conversion to estimates of G_{ATM} in
605 GtC yr⁻¹ incurs large uncertainty on annual time scale as discussed next.

606 The uncertainty around G_{ATM} is due to three main factors. First, the network composition of the marine
607 boundary layer sites with some sites coming or going, gaps in the time series at each site, etc. This
608 uncertainty was estimated with a bootstrap method by constructing 100 "alternative" networks (Steele
609 et al., 1992; Masarie and Tans, 1995; Lan et al., 2025). Second, the analytical uncertainty that describes
610 the short- and long-term uncertainties associated with the CO₂ analyzers. A Monte Carlo method was
611 used to estimate the total analytical uncertainty by randomly selecting errors to add to each observation
612 from a normal distribution of combined short- and long-term uncertainties. Prior to the 1980s when
613 analyzers were less precise and CO₂ measurement scale was slightly less well defined, larger analytical
614 errors were assigned to account for these factors. However, the network uncertainty remains the larger
615 term of uncertainty. The first and second uncertainties are reported as 1-sigma standard deviations (i.e.,
616 68% confidence interval), and summed in quadrature to determine the global surface growth rate

617 uncertainty, which averaged to 0.085 ppm (Lan et al., 2024). Third, the uncertainty associated with
618 using the average CO₂ concentration from a surface network to approximate the true atmospheric
619 average CO₂ concentration (mass-weighted, in 3 dimensions) as needed to assess the total atmospheric
620 CO₂ burden. In reality, CO₂ variations measured at the stations will not exactly track changes in total
621 atmospheric burden, with offsets in magnitude and phasing due to vertical and horizontal mixing
622 (Pandey et al., 2025). This effect must be very small on decadal and longer time scales, when the
623 atmosphere can be considered well mixed. The long-term CO₂ increase in the stratosphere lags the
624 increase (meaning lower concentrations) that we observe in the marine boundary layer, while the
625 continental boundary layer (where most of the emissions take place) leads the marine boundary layer
626 with higher concentrations. These effects nearly cancel each other on decadal time scales, when the
627 growth rate is nearly the same everywhere (Ballantyne et al., 2012). We therefore maintain an
628 uncertainty around the annual growth rate based on the multiple stations dataset ranges between 0.11
629 and 0.72 GtC yr⁻¹, with a mean of 0.61 GtC yr⁻¹ for 1959-1979 and 0.17 GtC yr⁻¹ for 1980-2024, when
630 more measurement sites were available (Lan et al., 2025). We estimate the uncertainty of the decadal
631 averaged growth rate after 1980 at 0.02 GtC yr⁻¹ based on the annual growth rate uncertainty but
632 stretched over a 10-year interval. For years prior to 1980, we estimate the decadal averaged uncertainty
633 to be 0.07 GtC yr⁻¹ based on a factor proportional to the annual uncertainty prior and after 1980 (0.02 *
634 [0.61/0.17] GtC yr⁻¹).

635 To estimate the total carbon accumulated in the atmosphere since 1750 or 1850, we use an atmospheric
636 CO₂ concentration of 278.0 ± 3 ppm or 287.7 ± 3 ppm, respectively (Gulev et al., 2021). For the
637 construction of the historical budget shown in Figure 3, we use the fitted estimates of CO₂
638 concentration from Joos and Spahni (2008) to estimate the annual atmospheric growth rate (see
639 Supplement S.7). The uncertainty of ±3 ppm (converted to ±1σ) is taken directly from the IPCC's AR5
640 assessment (Ciais et al., 2013). Typical uncertainties in the growth rate in atmospheric CO₂
641 concentration from ice core data are equivalent to ±0.1-0.15 GtC yr⁻¹ as evaluated from the Law Dome
642 data (Etheridge et al., 1996) for individual 20-year intervals over the period from 1850 to 1960 (Bruno
643 and Joos, 1997).

644 **2.4.2 Satellite-based (2015-present)**

645 Further opportunities to estimate global CO₂ growth rates are offered by space-based platforms such as
646 GOSAT (since 2010) and OCO-2 (since 2015). Their recorded short-wave infrared spectra allow
647 retrieval of column CO₂ abundances (XCO₂) over cloud-free scenes over land and ocean with footprints
648 of 80 (GOSAT) and 3 (OCO-2) km² respectively. The columns are not full integrals; the sensitivity to
649 surface and lower-tropospheric CO₂ mole fractions is much higher than to upper tropospheric and
650 stratospheric CO₂. However, for the purpose of calculating atmospheric growth rates, the sensitivity is
651 not limiting, as the pressure-weighted sensitivity is still above 0.5 in the stratosphere (Pandey et al.

652 2024) and priors used in OCO-2 account for the slow stratospheric-tropospheric exchanges using the
653 age of air (Laughner et al. 2023). Here, we use OCO-2 based whole atmosphere growth rates using the
654 Growth Rate from Satellite Observations (GRESO) approach (Pandey et al., 2024). We specifically
655 note that their retrievals are evaluated against surface-based remote sensing (Total Column Carbon
656 Observing Network) data, which in turn are tied to atmospheric observations (from aircraft and using
657 aircore) (Wunch et al., 2017). Furthermore, OCO-2 retrievals use a priori CO₂ mole fraction profiles
658 tied to NOAA GML in-situ flask records at Mauna Loa (MLO) and American Samoa (SMO)
659 measurement stations (Laughner et al., 2023). For details on evaluation, bias-correction, and
660 spatiotemporal coverage of OCO-2 we refer to O'Dell et al (2018).

661 Relative to surface observations, the GRESO product typically reflects tropical growth rate anomalies
662 earlier and sees whole atmosphere carbon stock changes with a lower latency. The GRESO growth
663 rates presented here use both land and ocean observations of OCO-2 providing global sampling of the
664 atmosphere. We used GRESO post 2015 to present an alternative quantification of the atmospheric
665 carbon stock changes in G_{ATM} , using the reported 1-sigma uncertainty of 0.08 ppm yr⁻¹. The mean
666 differences between GRESO and surface-data derived G_{ATM} is 0.05±0.26 ppm yr⁻¹ over the 2015-2024
667 (n=10 years) period.

668 **2.4.3 2025 projection**

669 We provide an assessment of G_{ATM} for 2025 as the average of two methods. First, the GCB regression
670 method models monthly global-average atmospheric CO₂ concentrations and derives the increment and
671 annual average from these. The model uses lagged observations of concentration (Lan et al., 2025):
672 both a 12-month lag, and the lowest lag that will allow model prediction to produce an estimate for the
673 following January, recalling that the G_{ATM} increment is derived from December/January pairs. The
674 largest driver of interannual changes is the ENSO signal (Betts et al., 2016), so the monthly ENSO 3.4
675 index (Huang et al., 2023) is included in the model. Given the natural lag between sea-surface
676 temperatures and effects on the biosphere, and in turn effects on globally mixed atmospheric CO₂
677 concentration, a lagged ENSO index is used, and we use both a 5-month and a 6-month lag. The
678 combination of the two lagged ENSO values helps reduce possible effects of noise in a single month.
679 To help characterise the seasonal variation, we add month as a categorical variable. Finally, we flag the
680 period affected by the Pinatubo eruption (August 1991 - November 1993) as a categorical variable.

681 The second method uses the multi-model mean and uncertainty of the 2025 G_{ATM} estimated by the
682 ESMs prediction system (see Section 2.9). We then take the average of the GCB regression and ESMs
683 G_{ATM} estimates, with their respective uncertainty combined quadratically.

684 Similarly, the projection of the 2025 global average CO₂ concentration (in ppm), is calculated as the
685 average of the estimates from the two methods. For the GCB regression method, it is the annual average

686 of global concentration over the 12 months of 2025; for the ESMs, it is the observed global average
687 CO₂ concentration for 2024 plus the annual increase in 2025 of the global average CO₂ concentration,
688 which is an average of NOAA/GML measurements from January to June (Lan et al., 2025) and
689 predictions of the ESMs multi-model mean from July to December (see Section 2.9).

690 **2.5 Ocean CO₂ sink**

691 **2.5.1 Historical period 1850-2024**

692 The reported estimate of the global ocean anthropogenic CO₂ sink S_{OCEAN} is derived as the average of
693 two estimates. The first estimate is derived as the mean over an ensemble of ten global ocean
694 biogeochemistry models (GOBMs, Table 4 and Table S2). The second estimate is obtained as the mean
695 over an ensemble of nine surface ocean $f\text{CO}_2$ -observation-based data-products (Table 4 and Table S3).

696 The GOBMs simulate both the natural and anthropogenic CO₂ cycles in the ocean. They constrain the
697 anthropogenic air-sea CO₂ flux (the dominant component of S_{OCEAN}) by the transport of carbon into the
698 ocean interior, which is also the controlling factor of present-day ocean carbon uptake in the real world.
699 They cover the full globe and all seasons and were evaluated against surface ocean carbon observations,
700 suggesting they are suitable to estimate the annual ocean carbon sink (Hauck et al., 2020). We derive
701 S_{OCEAN} from GOBMs by using a simulation (sim A) with historical forcing of climate and atmospheric
702 CO₂ from GCB (Section 2.4), accounting for model biases and drift from a control simulation (sim B)
703 with constant atmospheric CO₂ and normal year climate forcing. A third simulation (sim C) with
704 historical atmospheric CO₂ increase and normal year climate forcing is used to attribute the ocean sink
705 to CO₂ (sim C minus sim B) and climate (sim A minus sim C) effects. A fourth simulation (sim D;
706 historical climate forcing and constant atmospheric CO₂) is used to compare the change in
707 anthropogenic carbon inventory in the interior ocean (sim A minus sim D) to the observation-based
708 estimates of Gruber et al. (2019) and Müller et al. (2023) with the same flux components (steady state
709 and non-steady state anthropogenic carbon flux).

710 As there is accumulating evidence for a 10-20% underestimation of S_{OCEAN} by the GOBMs based on
711 ocean interior data (section 3.6.5), atmospheric oxygen (section 3.6.2), atmospheric inversions (section
712 3.8) and supported by eddy-covariance measurements (Dong et al., 2024), we scale up the global
713 GOBM multi-model mean estimates by 10% when estimating S_{OCEAN} (Friedlingstein et al., 2025b) (see
714 Supplement S3.3). Analysis of Earth System Models and GOBMs indicate that an underestimation by
715 about 10% may be due to biases in ocean carbon transport and mixing from the surface mixed layer to
716 the ocean interior (Goris et al., 2018, Terhaar et al., 2021, Bourgeois et al., 2022, Terhaar et al., 2022),
717 biases in the chemical buffer capacity (Revelle factor) of the ocean (Vaittinada Ayar et al., 2022;
718 Terhaar et al., 2022) and partly due to a late starting date of the simulations (mirrored in atmospheric
719 CO₂ chosen for the pre-industrial control simulation, Table S2, Bronselaer et al., 2017, Terhaar et al.,

720 2022; 2024). GOBMs are evaluated against key metrics and their capability to reproduce various
721 statistical measures of physical and biogeochemical fields using the International Ocean Model
722 Benchmarking (IOMB) Scheme (Fu et al., 2022, Text S3.3).

723 The $f\text{CO}_2$ -products are tightly linked to observations of $f\text{CO}_2$ (fugacity of CO_2 , which equals $p\text{CO}_2$
724 corrected for the non-ideal behaviour of the gas; Pfeil et al., 2013), which carry imprints of temporal
725 and spatial variability, but are also sensitive to uncertainties in gas-exchange parameterizations and
726 data-sparsity (Fay et al., 2021, Gloege et al., 2021, Hauck et al., 2023a). Their asset is the assessment of
727 the mean spatial pattern of variability and its seasonality (Hauck et al., 2020, Gloege et al. 2021, Hauck
728 et al., 2023a). To benchmark biases and trends derived from the $f\text{CO}_2$ -products, we update a model
729 subsampling exercise following Hauck et al. (2023a, see section S3) and use independent measurements
730 from the SOCAT (Surface Ocean CO_2 Atlas) flag E dataset (uncertainty less than $10 \mu\text{atm}$) (Bakker et
731 al., 2016) and calculated $f\text{CO}_2$ from the Global Ocean Data Analysis Project GLODAP (Lauvset et al.,
732 2024). New in GCB2025, we now also include the UExp-FNN-U product in the ensemble mean, which
733 was previously shown but not included. We include it since new evidence emerged from field and
734 modelling studies, recommending to adopt a temperature correction to the $f\text{CO}_2$ from measurement
735 depth to the surface skin layer where the gas exchange takes place (Dong et al., 2024, Ford et al.,
736 2024a, Bellenger et al., 2022). Furthermore, a second $f\text{CO}_2$ -product submitted temperature corrected
737 $f\text{CO}_2$ (JMA-MLR) this year, so we now include these corrected estimates in the ensemble mean.
738 Additionally, following Friedlingstein et al (2025b), we now also add 0.18 PgC yr^{-1} (multiplied by $7/9$
739 as two products already include a temperature correction) to the multi $f\text{CO}_2$ -product average when
740 calculating So_{OCEAN} to account for the warm layer and cool skin effect (See Supplement S3.1). This
741 correction is based on a recent field study (Ford et al., 2024a) and broadly consistent in magnitude with
742 a GOBM study (Bellenger et al 2022) .

743 The global $f\text{CO}_2$ -based flux estimates were adjusted to remove the pre-industrial natural ocean source of
744 CO_2 to the atmosphere of $0.65 \pm 0.3 \text{ GtC yr}^{-1}$, arising from the transfer of carbon from land to ocean via
745 rivers (Regnier et al., 2022), to satisfy our definition of So_{OCEAN} (Hauck et al., 2020). This CO_2
746 outgassing adjustment was distributed over the latitudinal bands using the regional distribution of
747 Lacroix et al. (2020; North: 0.14 GtC yr^{-1} , Tropics: 0.42 GtC yr^{-1} , South: 0.09 GtC yr^{-1}).
748 Acknowledging that this distribution is based on only one model, the advantage is that a gridded field is
749 available, and the adjustment can be calculated for the three latitudinal bands and the RECCAP regions
750 (REgional Carbon Cycle Assessment and Processes (RECCAP2; Ciais et al., 2020, Poulter et al., 2022,
751 DeVries et al., 2023). This dataset suggests that more of the river-induced outgassing is located in the
752 tropics than in the Southern Ocean and is thus opposed to the previously used dataset of Aumont et al.
753 (2001). Accordingly, the regional distribution is associated with an additional uncertainty in addition to
754 the large uncertainty around the global estimate (Crisp et al., 2022; Gruber et al., 2023). Anthropogenic
755 perturbations of river carbon and nutrient transport to the ocean are not represented in the process

756 models used to quantify S_{OCEAN} , but an a-posteriori correction is applied to the global S_{OCEAN} estimate
757 (see Section 2.10 and Supplement S.8.3). We calculate S_{OCEAN} as the average of the GOBM ensemble
758 mean and the $f\text{CO}_2$ -product ensemble mean from 1990 onwards, including the corrections on the
759 GOBM and $f\text{CO}_2$ -product ensemble means as described above. For the 1959-1989 period, it is
760 calculated as the GOBM ensemble mean plus half of the offset between GOBMs and $f\text{CO}_2$ -products
761 ensemble means over 1990-2001, also including the above corrections. In addition, two diagnostic
762 ocean models are used to estimate S_{OCEAN} over the industrial era (1781-1958, Khatiwala et al. (2013)
763 and DeVries (2014)).

764 S_{OCEAN} is evaluated against the change in the total dissolved inorganic carbon inventory in the interior
765 ocean from the observation-based estimates of Keppler et al. (2023) with the same flux components.

766 We assign an uncertainty of $\pm 0.4 \text{ GtC yr}^{-1}$ to the ocean sink based on a combination of random
767 (ensemble standard deviation) and systematic uncertainties (GOBMs bias in anthropogenic carbon
768 accumulation, previously reported uncertainties in $f\text{CO}_2$ -products; see Supplement S.3.4). While this
769 approach is consistent within the GCB, an independent uncertainty assessment of the $f\text{CO}_2$ -products
770 alone suggests a somewhat larger uncertainty of up to 0.7 GtC yr^{-1} (Ford et al. 2024). We assess a
771 medium confidence level to the annual ocean CO_2 sink and its uncertainty because it is based on
772 multiple lines of evidence, it is consistent with ocean interior carbon estimates (see Section 3.6.5) and
773 the interannual variability in the GOBMs and data-based estimates is largely consistent and can be
774 explained by climate variability. We refrain from assigning a high confidence because of the deviation
775 between the GOBM and $f\text{CO}_2$ -product trends between around 2002 and 2020 and the higher S_{OCEAN}
776 estimate from $\text{O}_2:\text{N}_2$ (section 2.8). More details on the S_{OCEAN} methodology can be found in Supplement
777 S.3.

778 **2.5.2 2025 Projection**

779 The S_{OCEAN} forecast for the year 2025 is based on (a) the historical (Lan et al., 2025) and our 2025
780 estimate of atmospheric CO_2 concentration, (b) the historical and our 2025 estimate of global fossil
781 emissions, and (c) the boreal spring (March, April, May) Oceanic Niño Index (ONI) (NCEP, 2025).
782 Using a non-linear regression approach, i.e., a feed-forward neural network, atmospheric CO_2 , ONI, and
783 the fossil emissions are used as training data to best match the corrected S_{OCEAN} from 1959 through
784 2024 from this year's carbon budget. Using this relationship, the 2025 S_{OCEAN} can then be estimated
785 from the projected 2025 input data using the non-linear relationship established during the network
786 training. To avoid overfitting, the neural network training was done using a Monte Carlo approach, with
787 a variable number of artificial neurons (varying between 2-5) and 20% of the randomly selected
788 training data were withheld for independent internal testing.

789 Based on the best output performance (tested using the 20% withheld input data), the best performing
790 number of neurons was selected. In a second step, we trained the network 10 times using the best
791 number of neurons identified in step 1 and different sets of randomly selected training data. The mean
792 of the 10 trainings is considered our best forecast, whereas the standard deviation of the 10 ensembles
793 provides a first order estimate of the forecast uncertainty. This uncertainty is then combined with the
794 S_{OCEAN} uncertainty (0.4 GtC yr^{-1}) to estimate the overall uncertainty of the 2025 projection. As an
795 additional line of evidence, we also assess the 2025 atmosphere-ocean carbon flux from the ESM
796 prediction system (see Section 2.9).

797 **2.6 Land CO₂ sink**

798 **2.6.1 Historical Period 1850-2024**

799 The terrestrial land sink (S_{LAND}) is thought to be due to the combined effects of rising atmospheric CO₂,
800 increasing N inputs, and climate change, on plant growth and terrestrial carbon storage. S_{LAND} does not
801 include land sinks directly resulting from land-use and land-use change (e.g., regrowth of vegetation) as
802 these are part of the land-use change emissions (E_{LUC}), although system boundaries make it difficult to
803 attribute exactly CO₂ fluxes on land between S_{LAND} and E_{LUC} (Erb et al., 2013).

804 S_{LAND} is derived from the multi-model mean of 22 DGVMs (Table 4 and Table S1). DGVMs
805 simulations include all climate variability and CO₂ effects over land. In addition to the carbon cycle
806 represented in all DGVMs, 15 models also account for the nitrogen cycle and hence can include the
807 effect of N inputs on S_{LAND} . The DGVMs estimates of S_{LAND} do not explicitly include the export of
808 carbon to aquatic systems or its historical perturbation, which is discussed in Supplement S.8.3.
809 DGVMs need to meet several criteria to be included in this assessment (see Supplement S.4.2). In
810 addition, we use the International Land Model Benchmarking system (ILAMB; Collier et al., 2018) for
811 the DGVMs evaluation (see Supplement S.4.2), with an additional comparison of DGVMs with a data-
812 informed, Bayesian model-data fusion framework (CARDAMOM) (Bloom and Williams, 2015; Bloom
813 et al., 2016). The uncertainty on S_{LAND} is taken from the DGVMs standard deviation.

814 New to GCB2025 is a correction applied to the S_{LAND} estimate to account for its overestimation
815 resulting from the assumption of pre-industrial land-use in the DGVM simulations, when in reality a
816 large portion of the land surface has been converted to pasture and cropland, with a lower sink capacity.
817 This bias is termed the Replaced Sinks and Sources (RSS) (Gitz and Ciais, 2003; Sitch et al., 2005,
818 Pongratz et al., 2009; Gasser et al., 2021; Obermeier et al. 2021; Dorgeist et al., 2024). The correction
819 which is only applied when estimating the global S_{LAND} , utilises results from a subset of DGVMs that
820 were able to supply Net Biome Productivity estimates at a Plant Functional Type basis combined with
821 time-varying PFT area fractions from the simulation with land use and land use change considered
822 (O’Sullivan et al., 2025; Friedlingstein et al. 2025b), see S.4.1 for details on methodology. The

823 corrected S_{LAND} is reduced by 19% globally when accounting for the RSS. More details on the S_{LAND}
824 methodology can be found in Supplement S.4.

825 **2.6.2 2025 Projection**

826 In previous versions of the GCB, the land sink projection was similar to the ocean sink forecast, based
827 on a non-linear regression approach with a feed-forward neural network. This approach, however,
828 resulted in a large uncertainty and underestimated the land sink variability in the past. This year, we
829 update the projection and simply calculate the land sink for 2025 as the residual of the projection of the
830 other components of the carbon cycle ($S_{\text{LAND}}=E_{\text{FOS}}+E_{\text{LUC}}-G_{\text{ATM}}-S_{\text{OCEAN}}$). Hence, by construction the
831 2025 B_{IM} is set to zero.

832

833 **2.7 Atmospheric inversion estimate**

834 The world-wide network of in-situ atmospheric measurements and satellite derived atmospheric CO_2
835 column ($X\text{CO}_2$) observations put a strong constraint on changes in the atmospheric abundance of CO_2 .
836 This allows atmospheric inversion methods to constrain the magnitude and location of the combined
837 total surface CO_2 fluxes from all sources, including fossil and land-use change emissions and land and
838 ocean CO_2 fluxes. The inversions assume E_{FOS} to be well known, and they solve for the spatial and
839 temporal distribution of land and ocean fluxes from the residual gradients of CO_2 between stations that
840 are not explained by fossil fuel emissions. By design, such systems thus close the carbon balance ($B_{\text{IM}} =$
841 0) and provide an additional perspective on the independent estimates of the ocean and land fluxes.

842 This year's release includes fourteen inversion systems that are described in Table S4. Each system is
843 rooted in Bayesian inversion principles but uses different methodologies. These differences concern the
844 selection of atmospheric CO_2 data or $X\text{CO}_2$, and the choice of a-priori fluxes to refine. They also differ
845 in spatial and temporal resolution, assumed correlation structures, and mathematical approach of the
846 models (see references in Table S4 for details). Importantly, the systems use a variety of transport
847 models, which was demonstrated to be a driving factor behind differences in atmospheric inversion-
848 based flux estimates, and specifically their distribution across latitudinal bands (Gaubert et al., 2019;
849 Schuh et al., 2019). Six inversion systems used surface observations from the global measurement
850 network (Schuldt et al., 2024, 2025). Eight inversion systems used satellite $X\text{CO}_2$ retrievals from
851 GOSAT and/or OCO-2, scaled to the WMO 2019 calibration scale, of which three inversions this year
852 used these $X\text{CO}_2$ datasets in addition to the in-situ observational CO_2 mole fraction records.

853 The original products delivered by the inverse modellers were modified to facilitate the comparison to
854 the other elements of the budget, specifically on two accounts: (1) global total fossil emissions
855 including cement carbonation CO_2 uptake, and (2) riverine CO_2 transport. We note that with these

856 adjustments the inverse results no longer represent the net atmosphere-surface exchange over
857 land/ocean areas as sensed by atmospheric observations. Instead, for land, they become the net uptake
858 of CO₂ by vegetation and soils that is not exported by fluvial systems, similar to the DGVMs estimates.
859 For oceans, they become the net uptake of anthropogenic CO₂, similar to the GOBMs estimates.

860 The inversion systems prescribe global fossil emissions based on e.g. the GCP's Gridded Fossil
861 Emissions Dataset versions 2025.1 (GCP-GridFED; Jones et al., 2025), which are updates to GCP-
862 GridFEDv2021 presented by Jones et al. (2021b). GCP-GridFEDv2025.1 scales gridded estimates of
863 CO₂ emissions from EDGARv4.3.2 (Janssens-Maenhout et al., 2019) within national territories to
864 match national emissions estimates provided by the GCB for the years 1959-2024, which were
865 compiled following the methodology described in Section 2.1. Small differences between the systems
866 due to for instance regridding to the transport model resolution, or use of different fossil fuel emissions
867 than GCP-GridFEDv2025.1, are adjusted in the latitudinal partitioning we present, to ensure agreement
868 with the estimate of E_{FOS} in this budget. We also note that the ocean fluxes used as prior by 8 out of 14
869 inversions are part of the suite of the ocean process model or *f*CO₂-products listed in Section 2.5.
870 Although these fluxes are further adjusted by the atmospheric inversions (except for Jena CarboScope),
871 it makes the inversion estimates of the ocean fluxes not completely independent of S_{OCEAN} assessed
872 here.

873 To facilitate comparisons to the independent S_{OCEAN} and S_{LAND}, we used the same adjustments for
874 transport and outgassing of carbon transported from land to ocean, as done for the observation-based
875 estimates of S_{OCEAN} (see Supplement S.5.1).

876 The atmospheric inversions are evaluated using vertical profiles of atmospheric CO₂ concentrations
877 (Figure S13). More than 50 aircraft programs over the globe, either regular programs or repeated
878 surveys over at least 9 months (except for SH programs), have been used to assess system performance
879 (with space-time observational coverage sparse in the SH and tropics, and denser in NH mid-latitudes;
880 Table S9). The fourteen systems are compared to the independent aircraft CO₂ measurements between 2
881 and 7 km above sea level between 2001 and 2024. Results are shown in Figure S13 and discussed in
882 Supplement S.5.2.

883 We note that as of GCB2025, the ensemble of inverse models covering a full decade is deemed
884 sufficiently large to report the 1-sigma standard deviation as uncertainty, following the convention of
885 the other components in GCB. More details on the atmospheric inversion methodology can be found in
886 Supplement S.5.

887 **2.8 Atmospheric oxygen based estimate**

888 Long-term atmospheric O₂ and CO₂ observations allow estimation of the global ocean and land carbon
889 sinks, due to the coupling of O₂ and CO₂ with distinct exchange ratios for fossil fuel emissions and land

890 uptake, and uncoupled O₂ and CO₂ ocean exchange (Keeling and Manning, 2014). The global ocean
891 and net land carbon sinks were calculated following methods and constants used in Keeling and
892 Manning (2014) but modified to also include the effective O₂ source from metal refining (Battle et al.,
893 2023). For the exchange ratio of the net land sink at value of 1.05 is used, following Resplandy et al.
894 (2019). For fossil fuels, the following values are used: gas: 1.95 (+/-) 0.04, liquid: 1.44, (+/-) 0.03,
895 solid: 1.17 (+/-) 0.03, cement: 0 (+/-) 0, gas flaring: 1.98 (+/-) 0.07 (Keeling, 1988). Atmospheric O₂ is
896 observed as $\delta(\text{O}_2/\text{N}_2)$ and combined with CO₂ mole fraction observations into Atmospheric Potential
897 Oxygen (APO, Stephens et al., 1998). The APO observations from 1990 to 2024 were taken from a
898 weighted average of flask records from three stations in the Scripps O₂ program network (Alert, Canada
899 (ALT), La Jolla, California (LJO), and Cape Grim, Australia (CGO), weighted per Keeling and
900 Manning (2014). Observed CO₂ was taken from the globally averaged marine surface annual mean
901 growth rate from the NOAA/GML Global Greenhouse Gas Reference Network (Lan et al., 2025). The
902 O₂ source from ocean warming is based on ocean heat content from updated data from NOAA/NCEI
903 (Levitus et al., 2012). The effective O₂ source from metal refining is based on production data from
904 Bray (2020), Flanagan (2021), and Tuck (2022). Uncertainty was determined through a Monte Carlo
905 approach with 20,000 iterations, using uncertainties prescribed in Keeling and Manning (2014),
906 including observational uncertainties from Keeling et al. (2007) and autoregressive errors in fossil fuel
907 emissions (Ballantyne et al., 2015). The reported uncertainty is 1 standard deviation of the ensemble.
908 As for the atmospheric inversions, the O₂ based estimates also closes the carbon balance ($B_{\text{IM}} = 0$) by
909 design and provides another independent estimate of the ocean and land fluxes. Note that the O₂ method
910 requires a correction for global air-sea O₂ flux, which has the largest uncertainty at annual time scales,
911 but which is still non-negligible for decadal estimates (Nevison et al., 2008).

912 **2.9 Earth System Models estimate**

913 Reconstructions and predictions from decadal prediction systems based on Earth system models
914 (ESMs) provide a novel line of evidence in assessing the atmosphere-land and atmosphere-ocean
915 carbon fluxes in the past decades and predicting their changes for the current year and years to come.
916 By assimilating physical atmospheric and oceanic data products into the ESMs, the models are able to
917 reproduce the historical variations of the atmosphere-sea CO₂ fluxes, atmosphere-land CO₂ fluxes, and
918 atmospheric CO₂ growth rate (Li et al., 2016, 2019; Lovenduski et al., 2019a,b; Ilyina et al., 2021; Li et
919 al., 2023). Furthermore, the ESM-based predictions have proven their skill in predicting the air-sea CO₂
920 fluxes for up to 6 years, the air-land CO₂ fluxes and atmospheric CO₂ growth for 2 years (Lovenduski et
921 al., 2019a,b; Ilyina et al., 2021; Li et al., 2023). The reconstructions from the fully coupled model
922 simulations ensure a closed budget within the Earth system, i.e., no budget imbalance term.

923 Six ESMs have performed the set of prediction simulations. The ensemble size of initialized prediction
924 simulations is 10, and the ensemble mean for each individual model is used here. Each ESM uses a

925 different assimilation method and combination of data products incorporated in the system, more details
926 on the models configuration can be found in Table 4 and Supplement Table S5. Reconstructions of
927 atmosphere-ocean CO₂ fluxes (S_{OCEAN}) and atmosphere-land CO₂ fluxes ($S_{\text{LAND}} - E_{\text{LUC}}$) for the time period
928 from 1960-2024 are assessed here. Predictions of the atmosphere-ocean CO₂ flux, atmosphere-land CO₂
929 flux, and atmospheric CO₂ growth for 2025 are calculated based on the predictions at lead year 1. The
930 predictions of atmosphere-ocean CO₂ flux and atmosphere-land CO₂ flux are bias corrected by removing
931 the climatological mean and linear trend biases from 1981-2021 referring to GCB2022 (Friedlingstein et
932 al., 2022), the atmospheric CO₂ growth (G_{ATM}) is then calculated as the residual of the CO₂ emissions
933 subtracting the carbon sinks into the ocean and the land. With the ESMs simulations, we also compute
934 the G_{ATM} in another way based on monthly atmospheric CO₂ concentrations at 1000hPa level over the
935 oceans to be comparable to the NOAA/GML global measurements of atmospheric CO₂ concentrations
936 (Lan et al., 2025). The bias correction is done referring to NOAA/GML monthly CO₂ concentrations in
937 recent 10 years from 2015-2024 regarding mean state and linear trend, a shorter period is used because a
938 non-linear trend for the whole period is observed from both NOAA/GML measurements and model
939 simulations. The 2025 G_{ATM} is then calculated by the increment of atmospheric CO₂ concentration in
940 December 2025 minus that in December 2024 multiplied by 2.124 to convert the unit from ppm to GtC.
941 The prediction of 2025 atmospheric CO₂ concentration is an average of the available NOAA/GML
942 measurements from January to June (Lan et al., 2025) and ESMs' predictions from July to December.
943 Note that the two methods, i.e., one based on the residual of carbon sources and sinks and another based
944 on atmospheric concentration increment, of calculation of G_{ATM} result in different magnitudes, which
945 suggests the consideration of variable ratio rather than a constant value in converting CO₂ concentration
946 to mass. More details on methods of bias correction of decadal predictions can be found in Kharin et al.
947 (2012), Boer et al. (2016) and Li et al. (2023). The ESMs are used here to support the assessment of
948 S_{OCEAN} and net atmosphere-land CO₂ flux ($S_{\text{LAND}} - E_{\text{LUC}}$) over the 1960-2024 period, and to provide an
949 estimate of the 2025 prediction of G_{ATM} and atmospheric CO₂ concentration.

950 **2.10 Processes not fully included in the global carbon budget**

951 The contribution of anthropogenic CO and CH₄ to the global carbon budget is not fully accounted for in
952 Eq. (1) and is described in Supplement S.8.1. The contributions to CO₂ emissions of decomposition of
953 carbonates not accounted for is described in Supplement S.8.2. The contribution of anthropogenic
954 changes in river fluxes is conceptually included in Eq. (1) in S_{OCEAN} and in S_{LAND} , but it is not
955 represented in the process models used to quantify these fluxes. However, a correction of $-0.07 \text{ GtC yr}^{-1}$
956 is applied a posteriori to the S_{LAND} estimate for the 2015-2024 period, as proposed in Friedlingstein et
957 al. (2025b). This effect is discussed in Supplement S.8.3. Similarly, the Replaced Sinks and Sources
958 effect from reduced forest cover over the historical period is missing from the DGVMs used here to
959 estimate S_{LAND} . However, a correction (-19%) is applied a posteriori to the S_{LAND} estimate from
960 DGVMs, based on O'Sullivan et al. (2025; see Section 2.6 and Supplement S.4.1).

961 **3 Results**

962 For each component of the global carbon budget, we present results for three different time periods: the
963 full historical period, from 1850 to 2024, the decades in which we have atmospheric concentration
964 records from Mauna Loa (1959-2024), a specific focus on last year (2024), and the projection for the
965 current year (2025). Subsequently, we assess the estimates of the budget components of the last decades
966 against the top-down constraints from inverse modelling of atmospheric observations and the
967 land/ocean partitioning derived from the atmospheric O₂ measurements. Atmospheric inversions further
968 allow for an assessment of the budget components with a regional breakdown of land and ocean sinks.
969

970 **3.1 Fossil CO₂ Emissions**

971 **3.1.1 Historical period 1850-2024**

972 Cumulative fossil CO₂ emissions for 1850-2024 were 495 ± 25 GtC, including the cement carbonation
973 sink (Table 8, with all cumulative numbers rounded to the nearest 5GtC). In this period, 46% of global
974 fossil CO₂ emissions came from coal, 35% from oil, 15% from natural gas, 3% from decomposition of
975 carbonates for cement production, and 1% from flaring. In 1850, the UK stood for 62% of global fossil
976 CO₂ emissions. In 1893 the combined cumulative emissions of the current members of the European
977 Union reached and subsequently surpassed the level of the UK. Since 1917 US cumulative emissions
978 have been the largest. Over the entire period 1850-2024, US cumulative emissions amounted to 120
979 GtC (24% of world total), the EU's to 80 GtC (16%), China's to 80 GtC (15%), and India's to 18 GtC
980 (4%).

981 In addition to the estimates of fossil CO₂ emissions that we provide here (see Section 2.1), there are
982 three global datasets with long time series that include all sources of fossil CO₂ emissions: CDIAC-FF
983 (Erb and Marland, 2025), CEDS version 2024_07_08 (Hoesly et al., 2024) and PRIMAP-hist version
984 2.6 (Gütschow et al., 2016; Gütschow et al., 2024), although these datasets are not entirely independent
985 from each other (Andrew, 2020a). CEDS has cumulative emissions over 1750-2022 at 480 GtC,
986 CDIAC-FF has 481 GtC, GCP 484 GtC, PRIMAP-hist CR 490 GtC, and PRIMAP-hist TR 492 GtC.
987 CDIAC-FF excludes emissions from lime production. CEDS estimates higher emissions from
988 international shipping in recent years, while PRIMAP-hist has higher fugitive emissions than the other
989 datasets. However, in general these four datasets are in relative agreement as to total historical global
990 emissions of fossil CO₂.

991 **3.1.2 Recent period 1959-2024**

992 Global fossil CO₂ emissions, E_{FOS} (including the cement carbonation sink), have increased every decade
993 from an average of 3.0 ± 0.2 GtC yr⁻¹ for the decade of the 1960s to an average of 9.8 ± 0.5 GtC yr⁻¹

994 during 2015-2024 (Table 7, Figure 2 and Figure 4). The growth rate in these emissions decreased
995 between the 1960s and the 1990s, from 4.3% yr⁻¹ in the 1960s (1960-1969), 3.1% yr⁻¹ in the 1970s
996 (1970-1979), 1.5% yr⁻¹ in the 1980s (1980-1989), to 1.0% yr⁻¹ in the 1990s (1990-1999). After this
997 period, the growth rate began increasing again in the 2000s at an average growth rate of 2.8% yr⁻¹,
998 decreasing to 1.2% yr⁻¹ in the 2010s, and 0.8% yr⁻¹ for the last decade (2015-2024). China's emissions
999 increased by 2.5% yr⁻¹ on average over the last 10 years dominating the global trend, and India's
1000 emissions increased by 3.6% yr⁻¹, while emissions decreased in EU27 (-2.5% yr⁻¹), and in the USA (-
1001 1.2% yr⁻¹) (Figure 5a). Figure 6 illustrates the spatial distribution of fossil fuel emissions for the 2015-
1002 2024 period.

1003 E_{FOS} reported here includes the uptake of CO₂ by cement via carbonation which has increased with
1004 increasing stocks of cement products, from an average of 20 MtC yr⁻¹ (0.02 GtC yr⁻¹) in the 1960s to an
1005 average of 210MtC yr⁻¹ (0.21 GtC yr⁻¹) during 2015-2024 (Figure 5b).

1006 **3.1.3 Final year 2024**

1007 Global fossil CO₂ emissions were slightly higher, 1.1%, in 2024 than in 2023, with an increase of 0.11
1008 GtC to reach 10.3 ± 0.5 GtC (including the 0.22 GtC cement carbonation sink) in 2024 (Figure 4),
1009 distributed among coal (41%), oil (32%), natural gas (21%), cement (4%), flaring (1%), and others
1010 (1%). Compared to 2023, the 2024 emissions from coal, oil, and gas increased by 0.8%, 1.3%, and
1011 2.4% respectively, while emissions from cement decreased by 4.6%. All annual growth rates presented
1012 are adjusted for the leap year, unless stated otherwise.

1013 In 2024, the largest absolute contributions to global fossil CO₂ emissions were from China (32%), the
1014 USA (13%), India (8%), and the EU27 (6%). These four regions account for 59% of global fossil CO₂
1015 emissions, while the rest of the world contributed 41%, including international aviation and marine
1016 bunker fuels (3% of the total). Growth rates for these countries from 2023 to 2024 were 0.7% (China), -
1017 0.6% (USA), -2.6% (EU27), and 4.0% (India), with +1.3% for the rest of the world, including
1018 international aviation and marine bunker fuels (9.8%). The per-capita fossil CO₂ emissions in 2024
1019 were 1.3 tC person⁻¹ yr⁻¹ for the globe, and were 3.9 (USA), 2.4 (China), 1.5 (EU27) and 0.6 (India) tC
1020 person⁻¹ yr⁻¹ for the four highest emitters (Figure 5c).

1021 **3.1.4 Year 2025 Projection**

1022 Globally, we estimate that global fossil CO₂ emissions (including cement carbonation, -0.21 GtC) grew
1023 by 1.0% in 2025 (0.2% to 1.7%) to 10.4 GtC (38.1 GtCO₂), an historical record high². The estimates of
1024 changes in 2025 emissions per fuel types, relative to 2024, are projected to be 1.0% (range 0.2% to

² Growth rates in this section use a leap year adjustment that corrects for the extra day in 2024.

1025 1.7%) for coal, 1.1% (range 0.7% to 1.5%) for oil, 1.3% (range 0.1% to 2.4%) for natural gas, and -
1026 0.9% (range -2.5% to 0.8%) for cement (Figure 5b).

1027 The uncertainty presented for projections relates only to the estimated growth rate, and excludes the
1028 uncertainty of the baseline (i.e. 2024) level. Given that our projection is effectively of what the data will
1029 show when observations are first available, the uncertainty drops to zero for any country where we
1030 already have data reported for all of 2025. This is the case below for both India and Japan, and also for
1031 Carbon Monitor's estimates of growth in 2025, since they report data through December 2025.

1032 For China, projected fossil emissions in 2025 are expected to have increased slightly by 0.4% (range -
1033 0.1% to 0.9%) compared with 2024 emissions, bringing 2024 emissions for China around 3.4 GtC yr⁻¹
1034 (12.3 GtCO₂ yr⁻¹). Our projected changes by fuel for China are 0.3% for coal, 3.8% for oil, 2.3% for
1035 natural gas, and -7.3% for cement.

1036 For the USA, using the Energy Information Administration (EIA) emissions estimate for 2025
1037 combined with cement clinker data from USGS, we estimate an increase of 2.5% (range 2.2% to 2.8%)
1038 compared to 2024, bringing USA 2025 emissions to around 1.4 GtC yr⁻¹ (5.0 GtCO₂ yr⁻¹). Our
1039 estimated changes by fuel are 10.4% for coal, 1.1% for oil, 1.4% for natural gas, and -3.1% for cement.

1040 For India, our estimate for 2025 is an increase of 1.1% over 2024, with 2025 emissions around 0.9 GtC
1041 yr⁻¹ (3.2 GtCO₂ yr⁻¹). Our projected changes by fuel are 1.3% for coal, -0.5% for oil, -5.7% for natural
1042 gas, and 10.5% for cement.

1043 For the European Union, our projection for 2025 is for a decrease of -0.1% (range -2.6% to 2.3%)
1044 relative to 2024, with 2025 emissions around 0.7 GtC yr⁻¹ (2.4 GtCO₂ yr⁻¹). Our projected changes by
1045 fuel are -2.6% for coal, -0.7% for oil, 2.8% for natural gas, and -0.8% for cement.

1046 New this year, we provide a projection for Japan, with a 2025 decrease of 0.9%, with 2025 emissions
1047 around 0.3 GtC yr⁻¹ (0.9 GtCO₂ yr⁻¹). Our projected changes by fuel are -0.7% for coal, -0.8% for oil, -
1048 1.2% for natural gas, and -2.9% for cement.

1049 International aviation and shipping are expected to have increased by 4.3% in 2025, reaching 0.3 GtC
1050 yr⁻¹ (1.2 GtCO₂ yr⁻¹), with international aviation and international shipping projected to be respectively
1051 6.7% and 2.0% over 2024. For the rest of the world, the expected change for 2025 is an increase of
1052 0.9% (range -1.1% to 3.0%) with 2025 emissions around 3.7 GtC yr⁻¹ (13.7 GtCO₂ yr⁻¹). The fuel-
1053 specific projected 2025 growth rates for the rest of the world are: 1.3% for coal, 0.3% for oil, 1.2% for
1054 natural gas, 2.6% for cement.

1055 Compared to the GCB estimate, Carbon Monitor estimates an increase in global fossil CO₂ emissions of
1056 0.7% for 2025, lower than GCB but with overlapping uncertainties. In contrast to GCB, Carbon
1057 Monitor projects the 2025 emissions from China to decline by -0.6%. Conversely, Carbon Monitor

1058 projects the 2025 emissions to increase by 1.4% for the USA, by 0.7% for India, by 0.8% for the EU27,
1059 but to decrease by -0.3% for Japan. The Carbon Monitor estimates that international aviation and
1060 shipping increased by 3.4% in 2025. For the rest of the world, the estimated change is an increase of
1061 1.3%.

1062 For traceability, Table S6 provides a comparison of annual projections from GCB since 2015 with the
1063 actual emissions assessed in the subsequent GCB annual report.

1064 **3.2 Emissions from Land-Use Change**

1065 **3.2.1 Historical period 1850-2024**

1066 Cumulative net CO₂ emissions from land-use change (ELUC) for 1850-2024 are 250 ± 60 GtC (Table 8)
1067 with a large spread among individual bookkeeping estimates of 210 GtC (OSCAR), 240 GtC (LUCE)
1068 and 290 GtC (BLUE). DGVMs show a lower estimate of 160 ± 60 GtC. Vegetation biomass
1069 observations provide independent constraints on the ELUC estimates over the 1901-2012 period (Li et
1070 al., 2017). Over that period, the GCB bookkeeping models' cumulative ELUC amounts to 180 GtC [155
1071 to 210 GtC] and the DGVM cumulative ELUC to 121 ± 45 GtC, both not significantly different from the
1072 observation-based estimate of 155 ± 50 GtC (Li et al., 2017). The substantially lower cumulative ELUC
1073 estimates from DGVMs compared to GCB2024 are due to the correction for the RSS bias, which is
1074 implemented in this assessment (see Section 2.6.1; O'Sullivan et al., 2025).

1075 **3.2.2 Recent period 1959-2024**

1076 In contrast to growing fossil emissions, net CO₂ emissions from land use, land-use change, and forestry
1077 remained relatively constant (around 1.8 GtC yr⁻¹) over the 1959-1999 period. Since then, they have
1078 shown a statistically significant decrease of about 0.2 GtC per decade (p<0.001), reaching 1.4 ± 0.7 GtC
1079 yr⁻¹ for the 2015-2024 period (Table 7), with a spread from 1.3 to 1.6 GtC yr⁻¹ across the three
1080 bookkeeping estimates (Table 5, Figure 4b). Different from the bookkeeping average, the DGVM
1081 average grows slightly larger over the 1980-2010 period, but as bookkeeping models, DGVMs show
1082 decreasing emissions in the most recent decade, 2015-2024 (Table 5).

1083 Compared to GCB2024, the overall trends in ELUC remained similar but the ELUC estimates increased.
1084 The main reason for the larger estimates in this assessment is that the H&C2023 model, included up to
1085 GCB2024, is not included anymore (see Section 2.2). H&C2023 had the lowest ELUC estimates among
1086 all bookkeeping models (Figure S3). Larger ELUC estimates in the last few decades (compared to
1087 GCB2024) are also due to the consideration of transient, instead of constant, carbon densities by all
1088 three bookkeeping models (Section 2.2.1). The inclusion of transient carbon densities increases gross
1089 fluxes for all ELUC components in the last few decades (Figure S3). Net ELUC increases because
1090 emissions from deforestation are still the dominating term.

1091 We separate E_{LUC} into five component fluxes to gain further insight into the drivers of net emissions:
1092 deforestation, forest (re-)growth, wood harvest and other forest management, peat drainage and peat
1093 fires, and all other transitions, with CO_2 emissions to the atmosphere being positive and CO_2 removals
1094 from the atmosphere being negative (Figure 7b; Supplement S.2.2). We further decompose the
1095 deforestation and the forest (re-)growth term into contributions from shifting cultivation vs permanent
1096 forest cover changes (Figure 7c). Averaged over the 2015-2024 period and over the three bookkeeping
1097 estimates, fluxes from deforestation amount to an emission of 1.9 [1.5 to 2.3] $GtC\ yr^{-1}$ (Table 5), of
1098 which 1.1 [0.9, 1.2] $GtC\ yr^{-1}$ are from permanent deforestation. Fluxes from forest (re-)growth amount
1099 to a removal of -1.3 [-1.5, -1.0] $GtC\ yr^{-1}$ (Table 5), of which -0.6 [-0.7, -0.5] $GtC\ yr^{-1}$ is from
1100 re/afforestation and the remainder from forest regrowth in shifting cultivation cycles. Wood harvest and
1101 other forest management causes net emissions of 0.4 [0.1, 0.7] $GtC\ yr^{-1}$ (with substantial gross fluxes
1102 largely compensating each other; see Figure S2). Emissions from peat drainage and peat fires (0.2 [0.2,
1103 0.3] $GtC\ yr^{-1}$) and the net flux from other transitions (0.1 [0.1, 0.1] $GtC\ yr^{-1}$) are of smaller magnitude
1104 globally (Table 5).

1105 The split into component fluxes clarifies the potentials for emission reduction and carbon dioxide
1106 removal: emissions from permanent deforestation - the largest of our component fluxes - could be
1107 halted (largely) without compromising carbon uptake by forests, contributing substantially to emissions
1108 reduction. By contrast, reducing wood harvesting would have limited potential to reduce net emissions
1109 as it would be associated with less forest regrowth; removals and emissions cannot be decoupled here
1110 on long timescales. A similar conclusion applies to removals and emissions from shifting cultivation,
1111 which we have therefore separated out. Carbon Dioxide Removal (CDR) in forests could instead be
1112 increased by permanently increasing the forest cover through re/afforestation. Currently,
1113 re/afforestation creates a removal of -0.6 $GtC\ yr^{-1}$ from the atmosphere averaged over 2015-2024. This
1114 value is similar to independent estimates derived from NGHGs for CDR in managed forests (through
1115 re/afforestation plus forest management) for 2013-2022 (-0.5 $GtC\ yr^{-1}$, Pongratz et al., 2024). In
1116 contrast to NGHGs, bookkeeping estimates do not consider the impacts from natural disturbances (like
1117 fires, windthrow, insect outbreaks), which may lead to an overestimation of removals from
1118 re/afforestation. Re/afforestation constitutes the vast majority of all current CDR (Pongratz et al., 2024).
1119 Though they cannot be compared directly to annual fluxes from the atmosphere and are thus not
1120 included in our estimate of E_{LUC} , CDR through transfers between non-atmospheric reservoirs such as in
1121 durable HWPs, biochar, or BECCS comprise much smaller amounts of carbon. 218 $MtC\ yr^{-1}$ have been
1122 estimated to be transferred to HWPs, averaged over 2013-2022 (Pongratz et al., 2024). The net flux of
1123 HWPs, considering the re-release of CO_2 through their decay, amounts to 91 $MtC\ yr^{-1}$ over that period
1124 (Pongratz et al., 2024). Note that some double-accounting between the CDR through HWPs and the
1125 CDR through re/afforestation exists if the HWPs are derived from newly forested areas. CDR from
1126 Biochar and BECCS in 2024 amount to 0.31 $MtC\ yr^{-1}$ and 0.18 $MtC\ yr^{-1}$ respectively. “Blue carbon”,
1127 i.e. coastal wetland management such as restoration of mangrove forests, saltmarshes and seagrass

1128 meadows, though at the interface of land and ocean carbon fluxes, are counted towards the land-use
1129 sector as well. Currently, bookkeeping models do not include blue carbon; however, current CDR
1130 deployment in coastal wetlands is small globally, less than 0.003 MtC yr⁻¹ (Powis et al., 2023).

1131 The statistically significant decrease in E_{LUC} since the late-1990s, including the larger drop within the
1132 most recent decade, is due to the combination of decreasing emissions from deforestation (in particular
1133 permanent deforestation) and increasing removals from forest regrowth (with those from
1134 re/afforestation stagnating globally in the last decade). Net emissions in 2015-2024 are 23% lower than
1135 in the late-1990s (1995-2004) and 19% lower than in 2005-2014. The steep drop in E_{LUC} after 2015 is
1136 due to the combined effect from a peak in peat fire emissions in 2015 and a long-term decline in
1137 deforestation emissions in many countries over the 2010-2020 period. The processes behind gross
1138 removals, foremost forest regrowth and soil recovery, are all slow, while gross emissions include a
1139 large instantaneous component. Short-term changes in gross emissions dynamics, such as a temporary
1140 decrease in deforestation, influences E_{LUC} faster than a change in gross removals, which rather act on
1141 longer-term timescales. Component fluxes often differ more across the bookkeeping estimates than the
1142 net flux (Figure 7b), which is expected due to different process representation; in particular, the
1143 treatment of shifting cultivation, which increases both gross emissions and gross removals, differs
1144 across models, but also net and gross wood harvest fluxes show high model spread (Figure S2). By
1145 contrast, models agree relatively well for emissions from permanent deforestation.

1146 Overall, highest net land-use emissions occur in the tropical regions of all three continents. The top
1147 three emitters over 2015-2024 are Brazil (in particular the Amazon Arc of Deforestation), Indonesia,
1148 and the Democratic Republic of the Congo, with these 3 countries contributing 0.8 GtC yr⁻¹ or 57% of
1149 the global net land-use emissions (average over 2015-2024; Figure 6b, Figure 7a). This is related to
1150 massive expansion of cropland (FAO, 2025c), particularly in the last few decades in Latin America,
1151 Southeast Asia, and sub-Saharan Africa (Hong et al., 2021), to a substantial part for export of
1152 agricultural products (Pendrill et al., 2019). Emission intensity is high in many tropical countries,
1153 particularly of Southeast Asia, due to high rates of land conversion in regions of carbon-dense and often
1154 still pristine, undegraded natural forests (Hong et al., 2021). Emissions are further increased by peat
1155 fires in equatorial Asia (GFED4s, van der Werf et al., 2017), contributing substantially to emissions in
1156 individual years, typically related to dry conditions during El Niño (0.2 GtC in 2015; 0.03 GtC yr⁻¹
1157 averaged over 2015-2024). Uptake due to land-use change occurs in several regions of the world
1158 (Figure 6b) particularly due to re/afforestation. Highest nature-based CDR in the last decade is seen in
1159 China, the USA, and the EU27, partly related to expanding forest area as a consequence of the forest
1160 transition in the 19th and 20th century and subsequent regrowth of forest (Mather 2001; McGrath et al.,
1161 2015). Substantial uptake through re/afforestation also exists in other regions such as Brazil, Russia, or
1162 Indonesia, where, however, emissions from deforestation and other land-use changes dominate the net
1163 land-use flux. While the mentioned patterns are robust and supported by independent literature, we

1164 acknowledge that model spread is substantially larger on regional than global levels, as has been shown
1165 for bookkeeping models (Bastos et al., 2021) as well as DGVMs (Obermeier et al., 2021). Independent
1166 assessments exist for selected regions (e.g., for Europe by Petrescu et al., 2020; for Brazil by Rosan et
1167 al., 2021; for China by Zhu et al., 2025; and for 8 selected countries/regions in comparison to inventory
1168 data by Schwingshackl et al., 2022).

1169 The NGHGI data under the land-use, land-use change, and forestry (LULUCF) sector (Melo et al.
1170 2025) and the LULUCF estimates from FAOSTAT (FAO, 2025d) differ from the global models'
1171 definition of E_{LUC} (see Section 2.2.1). In the NGHGI reporting, natural land fluxes (S_{LAND}) are counted
1172 towards E_{LUC} when they occur on managed land (Grassi et al., 2018) whereas FAOSTAT LULUCF
1173 estimates generally include natural fluxes in managed and unmanaged forests (Tubiello et al., 2021). To
1174 compare our results to the NGHGI approach, we perform a translation of our E_{LUC} estimates by adding
1175 S_{LAND} in managed forest from the DGVMs simulations (1.9 GtC yr⁻¹ in 2015-2024) to the bookkeeping
1176 E_{LUC} estimate (following the methodology described in Grassi et al., 2023; see Supplement S.2.4).
1177 Adding this sink changes E_{LUC} from being a source of 1.4 GtC yr⁻¹ to a sink of 0.5 GtC yr⁻¹, much
1178 closer to the NGHGI estimate reporting a sink of 1.0 GtC yr⁻¹ (Figure 8a, Table S11). Remaining
1179 differences in the bookkeeping and NGHGI estimates are mainly stemming from fluxes due to other
1180 transitions and permanent deforestation, whereas peat emissions and the net flux in managed forests
1181 agree well (Figure 8b,c). We further apply a mask of managed land to the net atmosphere-to-land flux
1182 estimate from atmospheric inversions to obtain inverse estimates that are comparable to the NGHGI
1183 estimates and to the translated E_{LUC} estimates from bookkeeping models (see Supplement S.2.4). The
1184 inversion-based net flux in managed land indicates a sink of 0.7 GtC yr⁻¹ for 2015-2024, which is in
1185 broad agreement with the NGHGI and the translated E_{LUC} estimates (Figure 8, Table S11).
1186 Additionally, the interannual variability of the inversion estimates and the translated E_{LUC} estimates
1187 show a remarkable agreement (Pearson correlation of 0.71 in 2000-2024), which supports the suggested
1188 translation approach. Though estimates of NGHGI, FAOSTAT, and atmospheric inversions and the
1189 translated bookkeeping estimates still differ in value and need further analysis, the approach suggested
1190 by Grassi et al. (2023), which we adopt here, provides a feasible way to relate the global models' and
1191 NGHGI approach to each other and thus link the anthropogenic carbon budget estimates of land-use
1192 CO₂ fluxes directly to the Global Stocktake, as part of the UNFCCC Paris Agreement. The translation
1193 approach has been shown to be generally applicable also at the country-level (Grassi et al., 2023;
1194 Schwingshackl et al., 2022).

1195 **3.2.3 Final year 2024**

1196 The global CO₂ emissions from land-use change are estimated as 1.3 ± 0.7 GtC in 2024, similar to the
1197 2023 estimate. However, confidence in the annual change remains low, as the land-use forcing
1198 underlying the E_{LUC} estimates was informed directly by data only up to and including 2023, with a trend

1199 extrapolation to 2024 (see Supplement Section S.2.1). The impacts of the 2023/2024 droughts linked to
1200 El Niño on the 2024 E_{LUC} estimate are thus not captured - while natural fires are not counted towards
1201 E_{LUC} , deforestation fires spreading further or drained peatlands burning more vastly because of dry
1202 conditions would be part of E_{LUC} . The extent of degradation was anomalously high in the Amazon in
1203 2024 and partly masked relatively low deforestation rates (<https://terrabrasilis.dpi.inpe.br>). However,
1204 this is not captured by our approach that is based on forest cover changes. For degradation it is currently
1205 impossible to be separated into effects of land-use activity versus effects of climate variability.

1206 **3.2.4 Year 2025 Projection**

1207 In equatorial Asia, peat fire emissions remained low (1 TgC in 2025 through October 15 2025, after 2
1208 TgC in 2024; GFED4.1s, van der Werf et al., 2017), as did deforestation and degradation fires (4 TgC
1209 in 2025; 8 TgC in 2024). South America saw a big reduction in emissions from deforestation and
1210 degradation fires, from 334 TgC in 2024 to 35 TgC until October 15 2025. Pantropical 2025 fire
1211 emission estimates from deforestation and degradation through October 15 are 105 TgC, which is not
1212 just a massive drop compared to the anomalously high 2024 emissions, but also only about one third of
1213 the long-term average (1997-2024). The reduction in emissions is mainly attributable to anomalously
1214 low deforestation and degradation fire emissions in South America, likely connected to the ceasing of
1215 the El Niño conditions and their impacts on ecosystems.

1216 Since the E_{LUC} estimate for the year 2024 is not informed directly by data on land-use dynamics
1217 (Section 3.2.3), we estimate the 2025 projection based on fire anomalies over the year 2023. We expect
1218 E_{LUC} emissions of around 1.1 GtC (4.1 GtCO₂) in 2025, 0.1 GtC below the 2024 level (0.3 GtC below
1219 the 2015-2024 average). Note that the confidence in the 2025 E_{LUC} projection remains low, as it is
1220 based on deforestation, degradation and peat fire emissions, which are only a proxy for land-use
1221 change. Projections in past GCB assessments are only partially confirmed by updated E_{LUC} estimates
1222 based on bookkeeping models in the following GCB assessments (Figure S4). Although our
1223 extrapolation includes tropical deforestation and degradation fires, the degradation attributable to
1224 selective logging, edge-effects or fragmentation is not captured. Further, deforestation and fires in
1225 deforestation zones may become more disconnected, partly due to changes in legislation in some
1226 regions. For example, Van Wees et al. (2021) found that the contribution from fires to forest loss
1227 decreased in the Amazon and in Indonesia over the period of 2003-2018.

1228 **3.3 CDR not based on vegetation**

1229 Besides the CDR through land use (Sec. 3.2), the atmosphere-to-geosphere flux of carbon resulting
1230 from carbon dioxide removal (CDR) activities in 2024 is estimated at 0.011 MtC yr⁻¹. This results
1231 primarily from 0.0048 MtC yr⁻¹ of biomass direct storage (compressing waste biomass to store
1232 underground), 0.003 MtC yr⁻¹ and 0.002 MtC yr⁻¹ of mineralisation and enhanced weathering projects

1233 respectively, and $0.0004 \text{ MtC yr}^{-1}$ of DACCS (Pongratz et al., 2024). This represents an increase
1234 (267%) in the anthropogenic sink compared to revised estimates for 2023 ($0.003 \text{ MtC yr}^{-1}$), although it
1235 remains roughly a million times smaller than current fossil CO_2 emissions. Note that the lower DACCS
1236 estimates, as well as revised 2023 values, reflect updated CDR tracking methodologies which include
1237 drawing on more accurate annual data from registries, indicating that operational projects are currently
1238 removing less CO_2 than their expected capacities. Similarly, reported CDR via Enhanced Rock
1239 Weathering decreased in 2024; however, this may not indicate a real decline in activity. The decline
1240 likely reflects a transition toward third party verification, with some removals not yet appearing on
1241 registries. Other novel CDR methods, including ocean and river alkalinity enhancement (0.0003 MtC
1242 yr^{-1} and $0.00001 \text{ MtC yr}^{-1}$ in 2024 respectively), and bio-oil geological storage ($0.0002 \text{ MtC yr}^{-1}$, jointly
1243 contributed just over $0.0005 \text{ MtC yr}^{-1}$ according to updated 2024 estimates of the State of CDR report
1244 (Smith et al., 2024). CDR through intentional biomass sinking into the deep ocean was reported at
1245 $0.001 \text{ MtC yr}^{-1}$ for 2023, but no activities have been identified for 2024.

1246 **3.4 Total anthropogenic emissions**

1247 Cumulative anthropogenic CO_2 emissions (fossil, including cement carbonation, and land-use change)
1248 for 1850-2024 totalled $745 \pm 65 \text{ GtC}$ ($2730 \pm 240 \text{ GtCO}_2$), of which 71% (530 GtC) occurred since
1249 1959 and 35% (260GtC) since 2000 (Table 7 and 8). Total anthropogenic emissions more than doubled
1250 since the 1960s, from $4.9 \pm 0.7 \text{ GtC yr}^{-1}$ for the decade of the 1960s to an average of $11.2 \pm 0.9 \text{ GtC yr}^{-1}$
1251 during 2015-2024, and reaching $11.6 \pm 0.9 \text{ GtC}$ ($42.4 \pm 3.2 \text{ GtCO}_2$) in 2024. However, total
1252 anthropogenic CO_2 emissions have been almost stable over the last decade ($0.3\% \text{ yr}^{-1}$ average growth
1253 rate over the 2015-2024 period), much lower than the 1.9% growth rate over the previous decade
1254 (2005-2014). This slower growth is due both to the reduced growth in E_{FOS} between the two decades,
1255 and to the decrease in emissions from E_{LUC} over the past decade.

1256 During the historical period 1850-2024, 67% of historical emissions were from fossil emissions and
1257 33% from land-use change. However, fossil emissions have grown significantly since the 1960s while
1258 net land-use change emissions have not, and consequently the contributions of land-use change to total
1259 anthropogenic emissions were smaller during recent periods, 21% during the period 1959-2024 and
1260 down to 12% over the last decade (2015-2024).

1261 For 2025 we project global total anthropogenic CO_2 emissions from fossil and land-use changes to be
1262 around 11.5 GtC (42.2 GtCO_2), marginally below the 2024 level due to lower net land-use emissions (-
1263 0.13 GtC) compensating the growth in fossil emission ($+0.09 \text{ GtC}$).

1264 **3.5 Atmospheric CO₂**

1265 **3.5.1 Historical period 1850-2024**

1266 Atmospheric CO₂ concentration was approximately 278 parts per million (ppm) in 1750, reaching 300
1267 ppm in the late 1900s, 350 ppm in the late 1980s, and reaching 422.80 ± 0.1 ppm in 2024 (Lan et al.,
1268 2025; Figure 1). The mass of carbon in the atmosphere increased by 52% from 590 GtC in 1750 to 898
1269 GtC in 2024. Current CO₂ concentrations in the atmosphere are unprecedented in the last 2 million
1270 years and the current rate of atmospheric CO₂ increase is at least 10 times faster than at any other time
1271 during the last 800,000 years (Canadell et al., 2021).

1272 **3.5.2 Recent period 1959-2024**

1273 The growth rate in atmospheric CO₂ level increased from 1.7 ± 0.07 GtC yr⁻¹ in the 1960s to 5.6 ± 0.02
1274 GtC yr⁻¹ during 2015-2024 with important decadal variations (Table 7, Figure 3 and Figure 4c). During
1275 the last decade (2015-2024), the growth rate in atmospheric CO₂ concentration continued to increase,
1276 albeit with large interannual variability (Figure 9). This interannual variability is highly consistent
1277 between the surface-based CO₂ growth rate and GRESO, the XCO₂-based growth rate (Pearson
1278 correlation of 0.84), but substantial differences are seen in 2019 and 2022-2024. These reflect
1279 differences in the total atmospheric carbon stock seen within the set boundaries of Jan-1 and Dec-31
1280 used to create an annual growth rate, as discussed in Section 2.4.2. Especially with large anomalies in
1281 tropical regions and close to January 1st, the calculation becomes sensitive to when the change is
1282 detected. This affected the 2023 and 2024 growth rates most strongly as they originated from tropical
1283 regions, and late in the calendar year (see next section). Figure 9 also shows the total annual fluxes (in
1284 GtC yr⁻¹) from the inverse models, which are derived to match the observed atmospheric increase while
1285 numerically accounting for the atmospheric transport-related delay in detection. The inversely modeled
1286 values generally match the GRESO growth rate better than the surface observations-based growth rate,
1287 indicating that the latter is more strongly influenced by the delay between the fluxes occurring and the
1288 actual observation of these signals. Note that this effect is mainly important on the annual timescale,
1289 and not over longer periods.

1290 **3.5.3 Final year 2024**

1291 The growth rate in the surface based atmospheric CO₂ concentration was 7.9 ± 0.2 GtC (3.73 ± 0.08
1292 ppm) in 2024 (Figure 4c; Lan et al., 2025), well above the 2023 growth rate (5.7 ± 0.2 GtC, 2.7 ± 0.08
1293 ppm) or the 2015-2024 average (5.6 ± 0.02 GtC, 2.6 ± 0.008 ppm), as to be expected during an El Niño
1294 year. The 2024 atmospheric CO₂ growth rate was the largest over the 1959-2024 atmospheric
1295 observational record, more than 1.5 GtC above the growth rates of 1998, 2015, and 2016 and 1998, all
1296 strong El Niño years.

1297 In contrast, the satellite-based GRESO growth rate was $6.8 \pm 0.2 \text{ GtC yr}^{-1}$ ($3.20 \pm 0.09 \text{ ppm yr}^{-1}$) for 2024
1298 which was also above its 2023 growth rate ($6.5 \pm 0.2 \text{ GtC yr}^{-1}$, $3.06 \pm 0.07 \text{ ppm yr}^{-1}$) and the highest on its
1299 10-year record. But it shows a more equal split of the anomaly between both years (2023-2024). This
1300 likely reflects more accurately that a substantial fraction of the flux anomaly occurred in 2023, but this
1301 was only detected by the surface network in 2024. For the interpretation of the annual global budget
1302 this has strong implications, as 2024 surface fluxes would need to add up to a smaller anomaly (by 1.1
1303 GtC yr^{-1}) than when using the surface-based annual growth rate. Hence the budget imbalance in 2024
1304 (Table 7) would be reduced from -1.7 GtC to -0.6 GtC if the GRESO growth rate was used for the
1305 budget estimate.

1306 As the the satellite-based GRESO growth rate is more evenly split between 2023 and 2024, so would be
1307 the B_{IM} , -0.3 GtC in 2023 and -0.6 GtC in 2024 with GRESO, compared to $+0.4 \text{ GtC}$ in 2023 and -1.7
1308 GtC in 2024 with the G_{ATM} from the surface based network.

1309 **3.5.4 Year 2025 Projection**

1310 The 2025 atmospheric CO_2 concentration, averaged over the year reached the level of 425.64 ppm ,
1311 53% over the pre-industrial level (Lan et al., 2025). We estimate the annual growth in atmospheric CO_2
1312 (G_{ATM}) to be about 4.4 GtC (equivalent to a 2.1 ppm increase in the global mean concentration), in line
1313 with a neutral ENSO year (ENSO 3.4 Index between -0.5 and 0.5). The projected growth rate estimated
1314 by the ESMs multi-model mean is slightly larger (5.5 GtC , 2.6 ppm).

1315 For traceability, Table S7 provides a comparison of annual projections of the G_{ATM} , S_{OCEAN} and S_{LAND}
1316 from GCB since 2021 with the actual estimate assessed in the subsequent GCB annual report.

1317 **3.6 Ocean Sink**

1318 **3.6.1 Historical period 1850-2024**

1319 Cumulated since 1850, the ocean sink S_{OCEAN} adds up to $200 \pm 35 \text{ GtC}$, with more than 70% of this
1320 amount ($145 \pm 25 \text{ GtC}$) being taken up by the global ocean since 1959. Over the historical period, the
1321 ocean sink increased in pace with the anthropogenic emissions exponential increase (Figure 3). Since
1322 1850, the ocean has removed 27% of total anthropogenic emissions.

1323 **3.6.2 Recent period 1959-2024**

1324 S_{OCEAN} increased from $1.3 \pm 0.4 \text{ GtC yr}^{-1}$ in the 1960s to $3.2 \pm 0.4 \text{ GtC yr}^{-1}$ during 2015-2024 (Table 7),
1325 with interannual variations of the order of a few tenths of GtC yr^{-1} (Figure 4d, Figure 10b). As
1326 described in section 2.5.1, S_{OCEAN} is now corrected for identified biases in the G_{OBMs} and $f\text{CO}_2$

1327 products estimates. Compared to the uncorrected estimate, S_{OCEAN} is increased by 0.2 GtC yr^{-1} for the
1328 2015-2024 period.

1329 The ocean-borne fraction ($S_{OCEAN}/(E_{FOS}+E_{LUC})$) has been remarkably constant around 27% on average,
1330 with variations around this mean illustrating the decadal variability of the ocean carbon sink. So far,
1331 there is no evidence of a sustained decrease in the ocean-borne fraction from 1959 to 2024 (Figure
1332 S16).

1333 The increase of the ocean sink is primarily driven by the increased atmospheric CO_2 concentration, with
1334 the strongest CO_2 induced signal in the North Atlantic and the Southern Ocean (Figure 12a, Figure
1335 S10). The effect of climate change is much weaker, reducing the ocean sink globally by 0.20 ± 0.05
1336 GtC yr^{-1} (-7.1% relative to the simulation that only accounts for the effect of atmospheric CO_2 increase)
1337 during 2015-2024 (all models simulate a weakening of the ocean sink by climate change, range -4.2 to -
1338 10.7%). The climate change effect leading to a reduced ocean sink is evident in all large-scale
1339 latitudinal bands (north, tropics, south, Figure 12b, Figure S10). This is the combined effect of change
1340 and variability in all atmospheric forcing fields, previously attributed to wind and temperature changes
1341 (Le Quéré et al., 2010, Bunsen et al., 2024). The effect of warming is smaller than expected from
1342 offline calculation due to a stabilising feedback from limited exchange between surface and deep waters
1343 (Bunsen et al., 2024; Müller et al., 2025).

1344 The global net air-sea CO_2 flux is a residual of large natural and anthropogenic CO_2 fluxes into and out
1345 of the ocean with distinct regional and seasonal variations (Figure 6c and Figure S5). Natural fluxes
1346 dominate on regional scales, but largely cancel out when integrated globally (Gruber et al., 2009;
1347 DeVries et al., 2023). Mid-latitudes in all basins and the high-latitude North Atlantic dominate the
1348 ocean CO_2 uptake where low temperatures and high wind speeds facilitate CO_2 uptake at the surface
1349 (Takahashi et al., 2009). In these regions, formation of mode, intermediate and deep-water masses
1350 transport anthropogenic carbon into the ocean interior, thus allowing for continued CO_2 uptake at the
1351 surface. Outgassing of natural CO_2 occurs mostly in the tropics, especially in the equatorial upwelling
1352 region, and to a lesser extent in the North Pacific and polar Southern Ocean, mirroring a well-
1353 established understanding of regional patterns of air-sea CO_2 exchange (e.g., Takahashi et al., 2009,
1354 Gruber et al., 2009; DeVries et al., 2023). These patterns are also noticeable in the Surface Ocean CO_2
1355 Atlas dataset, where an ocean $f\text{CO}_2$ value above the atmospheric level indicates outgassing (Figure S5).
1356 This map further illustrates the data-sparsity in the Indian Ocean and the Southern Hemisphere in
1357 general.

1358 The largest variability in the ocean sink occurs on decadal time-scales (Figure 10b). The ensemble
1359 means of GOBMs and $f\text{CO}_2$ -products show the same patterns of decadal variability, although with a
1360 larger amplitude of variability in the $f\text{CO}_2$ -products than in the GOBMs. The ocean sink stagnated in
1361 the 1990s and strengthened between the early 2000s and the mid-2010s (Figure 10b; Le Quéré et al.,

1362 2007; Landschützer et al., 2015, 2016; DeVries et al., 2017; Hauck et al., 2020; McKinley et al., 2020,
1363 Gruber et al., 2023). Different explanations have been proposed for the decadal variability in the 1990s
1364 and 2000s, ranging from the ocean's response to changes in atmospheric wind systems (e.g., Le Quéré
1365 et al., 2007, Keppler and Landschützer, 2019), including variations in upper ocean overturning
1366 circulation (DeVries et al., 2017) to the eruption of Mount Pinatubo in the 1990s (McKinley et al.,
1367 2020, Fay et al., 2023). The main origin of the decadal variability is a matter of debate with a number of
1368 studies initially pointing to the Southern Ocean (see review in Canadell et al., 2021 and Gruber et al.,
1369 2023), but also contributions from the North Atlantic and North Pacific (Landschützer et al., 2016,
1370 DeVries et al., 2019), or a global signal (McKinley et al., 2020) were proposed. The GOBM
1371 decomposition into climate and CO₂ effects emphasizes the role of the climate effect (that would
1372 include cooling signals from volcanic eruptions) for the stagnation in the 1990s until 2002, which are
1373 seemingly more pronounced in the tropics and north than in the south (Figure S10). The atmospheric
1374 *p*CO₂ growth rate is a spatially uniform driver that amplifies with large-scale averaging, while climate
1375 exerts spatially heterogeneous effects that cancel with averaging. Thus, climate dominates small-scale
1376 flux variability, but is matched on the global mean by the impact of the *p*CO₂ growth rate (Fay et al.,
1377 2024).

1378 More recently, the sink seems to have entered a phase of stagnation 2016 - 2022, largely in response to
1379 large inter-annual climate variability. The first-order effect of interannual variability stems from a
1380 stronger ocean sink during large El Niño events leading to a reduction in CO₂ outgassing from the
1381 Tropical Pacific (e.g., 1997/98, 2015/16) and a weaker sink in neutral years following El Niño (2017)
1382 and during La Niña events (2020-2022, Figure 10b; Rödenbeck et al., 2014, Hauck et al., 2020;
1383 McKinley et al. 2017). After the triple La Niña event 2020-2022, the ocean sink rebound in 2023 linked
1384 to the onset of an El Niño event. Warming in the extratropics, in particular in the Northern Hemisphere,
1385 however, weakened the overall increase in the ocean carbon sink (Müller et al., 2025). In the GOBMs,
1386 the ocean sink stagnation 2016-2022 is associated with a period of a stronger climate effect reducing
1387 the ocean sink, mostly stemming from the tropics, in line with the expected patterns from El Niño and
1388 La Niña (Figure S10). The CO₂ effect has also shown a lower growth rate since around 2016.

1389 The ensemble means of GOBMs, and *f*CO₂-products (adjusted for the riverine flux) show a mean offset
1390 increasing from 0.28 GtC yr⁻¹ in the 1990s (first decade available) to 0.59 GtC yr⁻¹ in the decade 2015-
1391 2024. The offset is larger than in previous GCB versions, because two *f*CO₂-products (UEXP-FNN-U,
1392 JMA-MLR), that use an adjusted version of the Surface Ocean CO₂ Atlas data to represent the sea
1393 surface *f*CO₂ within the surface skin layer where gas exchange takes place (Ford et al., 2025), are now
1394 included in the *f*CO₂-product mean. Additionally, an update in the SOCAT dataset with regards to
1395 Southern Ocean data led to an increase in the sink strength in three of the *f*CO₂-products (VLIZ-
1396 SOMFFN, LDEO-HPD, CMEMS-LSCE-FFNN - see section S3.1, Fay et al., 2025). In this version of
1397 the GCB, the positive trends in the ocean sink estimated by the GOBMs and the *f*CO₂-products diverges

1398 over time by a factor of 1.6 since 2002 (GOBMs: 0.27 ± 0.05 GtC yr⁻¹ per decade, *f*CO₂-products: 0.46
1399 GtC yr⁻¹ per decade [0.22 to 0.81 GtC yr⁻¹ per decade], corrected *S*_{ocean}: 0.38 GtC yr⁻¹ per decade), but
1400 the uncertainty ranges overlap. A hybrid approach recently constrained the trend for 2000 to 2022 to
1401 0.42 ± 0.06 GtC yr⁻¹ decade⁻¹ (Mayot et al., 2024), which aligns with the updated trend of *S*_{ocean}
1402 (0.46 GtC yr⁻¹ decade⁻¹), while the *f*CO₂-products exhibit a larger (0.54 [0.29, 0.85] GtC yr⁻¹
1403 decade⁻¹) and the GOBMs a lower trend (0.34 ± 0.05 GtC yr⁻¹ per decade) over the same period.

1404 In the current budget, the discrepancy between the two types of estimates stems from a persistently
1405 larger ocean sink in the *f*CO₂-products in the northern and southern extra-tropics since around 2002
1406 (Figure 14). Note that the discrepancy in the mean flux, which was located in the Southern Ocean in
1407 GCB2022 and earlier, was reduced due to the choice of the regional river flux adjustment (Lacroix et
1408 al., 2020 instead of Aumont et al., 2001). This comes at the expense of a discrepancy in the mean
1409 *S*_{ocean} of about 0.2-0.3 GtC yr⁻¹ in the tropics. Likely explanations for the discrepancy in the trends and
1410 decadal variability in the high latitudes are data sparsity and uneven data distribution (Bushinsky et al.,
1411 2019, Gloege et al., 2021, Hauck et al., 2023a, Mayot et al., 2024). In particular, two *f*CO₂-products
1412 were shown to overestimate the Southern Ocean CO₂ flux trend by 50 and 130% based on current
1413 sampling in a model subsampling experiment (Hauck et al., 2023a) and the largest trends in the *f*CO₂-
1414 products occurred in a data devoid region in the North Pacific (Mayot et al., 2024). In Supplement S3
1415 we show that the strength of the trends in *f*CO₂ products may be linked to reconstruction biases of the
1416 true trend signal. In this respect it is highly worrisome that the coverage of *f*CO₂ observations has
1417 declined since 2016/17 (Dong et al., 2022, 2024; Bakker et al., 2025b) and is now down to that of the
1418 mid-2000s (Figure 10b). The temperature correction applied in two products further worsens the
1419 agreement in trends between GOBMs and *f*CO₂-products. Similarly, model biases likely contribute to
1420 the discrepancy between GOBMs and *f*CO₂-products (as indicated by the comparison with Mayot et al.,
1421 2024, and by the large model spread in the South, Figure 14).

1422 The *S*_{ocean} estimate is 2.9 ± 0.4 GtC yr⁻¹ over the period 2004 to 2019, which agrees within the ranges
1423 of uncertainty with the ocean interior estimate of 3.2 ± 0.7 GtC yr⁻¹ obtained with the MOBO-DIC
1424 approach (Keppler et al., 2023). The carbon flux components of the observation-based ocean interior
1425 estimate match the definition of *S*_{ocean} used here (Hauck et al., 2020). Furthermore, the decadal *S*_{ocean}
1426 estimates agree well with the corresponding ocean interior estimates for all decades from the 1960s to
1427 the 2010s, which represent a composite estimate of three observation-based products (Table 6).

1428 The *S*_{ocean} estimate agrees within uncertainties with other lines of evidence from atmospheric oxygen
1429 based estimates, atmospheric inversions, and ocean interior observation-based constraints (Table 6).
1430 The atmospheric oxygen-based estimate shows a lower estimate than *S*_{ocean} in the 1990s, but a larger
1431 estimate over the 2015-2024 period, indicating a strong growth of >1.5 GtC yr⁻¹ over that period. ESMs
1432 with data assimilation result in lower estimates of the ocean sink than all other estimates (Table 6).

1433 Also, the atmospheric inversion estimates of the ocean sink are generally lower than S_{OCEAN} on average,
1434 but are within the uncertainties of the GOBMs and $f\text{CO}_2$ products.

1435 **3.6.3 Final year 2024**

1436 The estimated ocean CO_2 sink is 3.4 ± 0.4 GtC for 2024. This is an increase of 0.1 GtC compared to
1437 2023 (Figure 4d). The sink strengthening was expected from the atmospheric CO_2 growth and El Niño
1438 conditions in the beginning of the year (January to April). However, the continuation of the anomalous
1439 warm conditions in the extratropics, especially of the Atlantic Ocean, led to a weaker than expected
1440 increase in the sink (Figure 11c). The GOBMs suggest that the increase is driven by the anomalously
1441 high atmospheric CO_2 growth rate and dampened by climate effects, thus suggesting that warming
1442 overcompensated the effect from El Niño (Figure S10). GOBMs and $f\text{CO}_2$ -products largely agree on
1443 patterns of ocean sink anomalies with a reduced sink in parts of the subtropical and subpolar North
1444 Atlantic and North Pacific that coincides with regions of anomalously warm sea surface temperatures
1445 (Figure S9). GOBM and $f\text{CO}_2$ -product ensemble mean estimates consistently result in an ocean sink
1446 increase in 2024 (GOBMs: 0.13 ± 0.14 GtC, $f\text{CO}_2$ -products: $0.08 [-0.34, 0.43]$ GtC). Eight GOBMs and
1447 six $f\text{CO}_2$ -products show an increase in S_{OCEAN} , while only two GOBMs and three $f\text{CO}_2$ -products show a
1448 decrease in S_{OCEAN} . The $f\text{CO}_2$ -products have a larger uncertainty at the end of the reconstructed time
1449 series, potentially linked to uncertainties related to fewer available observations in the final year (see
1450 e.g. Watson et al 2020, Pérez et al 2024). Specifically, the $f\text{CO}_2$ -products' estimate of the last year is
1451 regularly adjusted in the following release owing to the tail effect and an incrementally increasing data
1452 availability. While the monthly grid cells covered may have a lag of only about a year (Figure 10b
1453 inset), the values within grid cells may change with 1-5 years lag (see absolute number of observations
1454 plotted in previous GCB releases), potentially resulting in annual changes in the flux magnitude from
1455 $f\text{CO}_2$ -products.

1456 **3.6.4 Year 2025 projection**

1457 Using a feed-forward neural network method (see Section 2.5.2) we project an ocean sink of 3.3 ± 0.4
1458 GtC for 2025, which is a declining sink of -0.1 GtC compared to 2024 and can be explained by the
1459 generally lower ocean CO_2 uptake following the El Niño event ending in 2024, consistent with the
1460 projected recovery of the atmospheric CO_2 growth rate after a record high in 2024. The set of ESMs
1461 predictions support this estimate with a 2025 ocean sink of around 3.1 [3.0, 3.2] GtC. Taking the
1462 average of both estimates, we project an ocean sink of 3.2 ± 0.4 GtC for 2025.

1463 **3.6.5 Evaluation of ocean models and $f\text{CO}_2$ -products**

1464 The process-based model evaluation draws a generally positive picture with GOBMs scattered around
1465 the observational values for Southern Ocean sea-surface salinity, Southern Ocean stratification index,

1466 albeit outliers exist (Section S3.3 and Table S12). The Revelle factor is high in most GOBMs when
1467 compared to GLODAP, but appears less biased when compared to OceanSODA. However, the Atlantic
1468 Meridional Overturning Circulation at 26°N is underestimated by 8 out of 10 GOBMs and
1469 overestimated by one GOBM. IOMB summarizes the GOBMs' performance across physical and
1470 biogeochemical data sets and various statistics relative to the GOBM ensemble (Figure S6). All
1471 GOBMs perform better in some variables compared to the other models, and worse in other variables.
1472 Despite the indication that GOBMs underestimate the ocean sink, low sink models do not perform
1473 generally worse than the other models; and similarly, high sink models do not perform better than the
1474 others.

1475 The model simulations allow to separate the anthropogenic carbon component and to compare the
1476 GOBMs DIC inventory change directly to the interior ocean estimates of Gruber et al. (2019), Müller et
1477 al. (2023) and the GOBM anthropogenic surface fluxes to DeVries (2022) without further assumptions
1478 (Table S12). The GOBMs ensemble average of anthropogenic carbon inventory changes 1994-2007
1479 amounts to 2.3 GtC yr^{-1} and is thus 10.5% lower than the $2.6 \pm 0.3 \text{ GtC yr}^{-1}$ estimated by Gruber et al.
1480 (2019) although within the uncertainty. Five models fall within the range reported by Gruber et al.
1481 (2019). Comparison to the decadal estimates of anthropogenic carbon accumulation (Müller et al.,
1482 2023) are close to the interior ocean data based estimate for the decade 2004-2014 (GOBMs sim D
1483 minus sim A, $2.6 \pm 0.4 \text{ GtC yr}^{-1}$, Müller et al. $2.7 \pm 0.3 \text{ GtC yr}^{-1}$), but do not reproduce the supposedly
1484 higher anthropogenic carbon accumulation in the earlier period 1994-2004 (GOBMs sim D minus sim
1485 A, $2.2 \pm 0.3 \text{ GtC yr}^{-1}$, Müller et al. $2.9 \pm 0.3 \text{ GtC yr}^{-1}$). Finally, the mean anthropogenic carbon uptake
1486 in GOBMs from 1985 to 2018 amounts to 2.3 GtC yr^{-1} , slightly lower than the corresponding
1487 observation-based uptake rate of $2.4 \pm 0.2 \text{ Gt yr}^{-1}$ based on OCIM (DeVries, 2022; DeVries et al.,
1488 2023). The underestimation of anthropogenic carbon accumulation by 10% in the period 1994 to 2007,
1489 in the 1990s and 2000s (Table 6) and by 15% in the 2010s (Table 6) justifies the correction of GOBMs
1490 by 10% (Friedlingstein et al., 2025a, section 2.5.1). Interestingly, and in contrast to the uncertainties in
1491 the surface CO₂ flux, we find the largest mismatch in interior ocean carbon accumulation in the tropics,
1492 with smaller contributions from the north and the south (Table S12). The large discrepancy in
1493 accumulation in the tropics highlights the role of interior ocean carbon redistribution for those
1494 inventories (Khatiwala et al., 2009, DeVries et al., 2023).

1495 Additional benchmarking of the $f\text{CO}_2$ -products with independent data generally shows low and
1496 consistent biases and RMSEs, with the exception of the comparison with SOCAT flag E data in the
1497 tropics where the biases range from $-6.6 \mu\text{atm}$ in JMA-MLR to $-10.29 \mu\text{atm}$ in OceanSODA_ETHv2 ,
1498 (Figure S7) and the Northern Hemisphere, where biases range from $-2.68 \mu\text{atm}$ in VLIZ-SOMFFN to -
1499 $40.47 \mu\text{atm}$ in UExp-FNN-U (Figure S7), although with few measurements covering the latter area.
1500 Furthermore, we evaluate the trends derived from a subset of $f\text{CO}_2$ -products by subsampling five
1501 GOBMs used in Friedlingstein et al. (2023; covering the period up to the year 2022) following the

1502 approach of Hauck et al. (2023a) and evaluating the air-sea CO₂ flux trend for the 2001-2021 period,
1503 i.e. the period of strong divergence in the air-sea CO₂ exchange excluding the tail effect, against trend
1504 biases identified by the GOBM reconstruction. The results indicate a relationship between
1505 reconstruction bias and strength of the decadal trends (Figure S8), indicating a tendency of the f_{CO_2} -
1506 products ensemble to overestimate the air-sea CO₂ flux trends in agreement with Mayot et al. (2024).
1507 This relationship, however, remains uncertain and its sensitivity to the GOBM used needs further
1508 investigation.

1509 **3.7 Land Sink**

1510 **3.7.1 Historical period 1850-2024**

1511 Cumulated since 1850, the terrestrial carbon sink S_{LAND} amounts to 175 ± 50 GtC, 24% of total
1512 anthropogenic emissions, with more than two thirds of this amount (120 ± 40 GtC) being taken up by
1513 the terrestrial ecosystems since 1959. Over the historical period, the land sink increased in pace with the
1514 anthropogenic emissions exponential increase (Figure 3). As described in section 2, S_{LAND} estimate now
1515 includes the RSS correction.

1516 **3.7.2 Recent period 1959-2024**

1517 S_{LAND} increased from 0.9 ± 0.3 GtC yr⁻¹ in the 1960s to 2.4 ± 0.8 GtC yr⁻¹ during 2015-2024, with
1518 important interannual variations of up to 2 GtC yr⁻¹ generally showing a decreased land sink during El
1519 Niño events (Figure 10a), responsible for the corresponding enhanced growth rate in atmospheric CO₂
1520 concentration. The larger land CO₂ sink during 2015-2024 compared to the 1960s is reproduced by all
1521 the DGVMs in response to the increase in both atmospheric CO₂, nitrogen deposition, and the changes
1522 in climate, and is broadly consistent with the residual estimated from the other budget terms, that is
1523 $E_{\text{FOS}} + E_{\text{LUC}} - G_{\text{ATM}} - S_{\text{OCEAN}}$ which amounts to 2.4 GtC for the last decade (See Table 5). As described in
1524 section 2.6.1, S_{LAND} is now corrected for the Replaced Sinks and Sources (RSS) bias. Compared to the
1525 uncorrected estimate, S_{LAND} is reduced by 0.6 GtC yr⁻¹ for the 2015-2024 period.

1526 Over the historical period, the increase in the global terrestrial CO₂ sink is largely attributed to the CO₂
1527 fertilisation effect (Prentice et al., 2001, Piao et al., 2009, Schimel et al., 2015) and increased nitrogen
1528 deposition (Huntzinger et al., 2017, O’Sullivan et al., 2019), directly stimulating plant photosynthesis
1529 and increased plant water use in water limited systems, with a smaller negative contribution of climate
1530 change (Figure 12). There is a range of evidence to support a positive terrestrial carbon sink in response
1531 to increasing atmospheric CO₂ (Walker et al., 2021), including a new synthesis of free-air CO₂-
1532 enrichment experiments across forests and ages, which concluded that Net Primary Productivity
1533 increased by 22% for a common 41% CO₂ enrichment (Norby 2025). As expected from theory, the
1534 greatest CO₂ effect is simulated in the tropical forest regions, associated with warm temperatures and

1535 long growing seasons (Hickler et al., 2008) (Figure 12a). However, evidence from tropical intact forest
1536 plots indicate an overall decline in the land sink across Amazonia (1985-2011), attributed to enhanced
1537 mortality offsetting productivity gains (Brienen et al., 2015, Hubau et al., 2020). During 2015-2024 the
1538 land sink is positive in all regions (Figure 6d) with the exception of eastern Brazil, Bolivia, northern
1539 Venezuela, Southwest USA, central Europe and Central Asia, North and South Africa, and eastern
1540 Australia, where the negative effects of climate variability and change (i.e. reduced rainfall and/or
1541 increased temperature) counterbalance CO₂ effects. This is clearly visible in Figure 12 where the effects
1542 of CO₂ (Figure 12a) and climate (Figure 12b) as simulated by the DGVMs are isolated (see also Figure
1543 S12). The negative effect of climate can be seen across the globe, and is particularly strong in most of
1544 South America, Central America, Southwest US, Central Europe, western Sahel, southern Africa,
1545 Southeast Asia and southern China, and eastern Australia (Figure 12b, Figure S12). Globally, over the
1546 2015-2024 period, climate change reduces the land sink by 0.8 ± 0.7 GtC yr⁻¹ (25% of the CO₂ effect,
1547 which is 3.2 ± 1.1 GtC yr⁻¹ for the corresponding period, see Supplement S4.1).

1548 Most DGVMs have similar S_{LAND} averaged over 2015-2024, and 14/22 models fall within the 1σ range
1549 of the residual land sink [1.4 to 3.3 GtC yr⁻¹] (see Table 5), and all models but one are within the 2σ
1550 range [0.5 to 4.3 GtC yr⁻¹]. The ED model is an outlier, with a land sink estimate of 4.9 GtC yr⁻¹ for the
1551 2015-2024 period (accounting for the RSS correction), driven by a strong CO₂ fertilisation effect (6.4
1552 GtC yr⁻¹ in the CO₂ only (S1) simulation). There are no direct global observations of the land sink
1553 (S_{LAND}), or the CO₂ fertilisation effect, and so we are not yet in a position to rule out models based on
1554 component fluxes if their net land sink (S_{LAND}-E_{LUC}) is within the observational uncertainty provided by
1555 O₂ measurements. The important role of non-living carbon pools in carbon budgets has also been
1556 recently highlighted from an Earth-observation (EO) perspective, where contrary to DGVMs, EO
1557 products do not show an increase in biomass, thus inferring a larger role of dead carbon in land carbon
1558 cycle dynamics (Bar-On et al., 2025).

1559 Since 2020 the globe has experienced La Niña conditions which would be expected to lead to an
1560 increased land carbon sink. This 3-year long period of La Niña conditions came to an end by the second
1561 half of 2023 and transitioned to an El Niño which lasted until mid-2024. A clear transition from
1562 maximum to a minimum in the global land sink is evident in S_{LAND}, from 2022 to 2023 and we find that
1563 an El Niño-driven decrease in tropical land sink is offset by a smaller increase in the high-latitude land
1564 sink. In the past years several regions experienced record-setting fire events (see also section 3.8.3).
1565 While global burned area has declined over the past decades mostly due to declining fire activity in
1566 savannas (Andela et al., 2017), forest fire emissions are rising and have the potential to counter the
1567 negative fire trend in savannas (Zheng et al., 2021). Noteworthy extreme fire events include the 2019-
1568 2020 Black Summer event in Australia (emissions of roughly 0.2 GtC; van der Velde et al., 2021),
1569 Siberia in 2021, where emissions approached 0.4 GtC or three times the 1997-2020 average according
1570 to GFED4s, Canada in 2023 and 2024 (Byrne et al., 2024), and unprecedented wildfires in Brazil and

1571 Bolivia in 2024 (partly related to land-use activity, see Sec. 3.2.3 and 3.2.4) (Bourgoin et al., 2025),
1572 partially offset by a negative trend in wildfire over Northern Hemisphere Africa. While other regions,
1573 including Western US and Mediterranean Europe, also experienced intense fire seasons in 2021 their
1574 emissions are substantially lower.

1575 Despite these regional negative effects of climate change on S_{LAND} , the efficiency of land to remove
1576 anthropogenic CO_2 emissions has remained broadly constant over the last six decades at around 23%
1577 (including the RSS correction) (Figure S16).

1578 **3.7.3 Final year 2024**

1579 The terrestrial CO_2 sink from the DGVMs ensemble S_{LAND} was 1.9 ± 0.9 GtC in 2024, 37% below the
1580 2022 La Niña induced strong sink of 3.1 ± 1.0 GtC, and also below the 2015-2024 average of 2.4 ± 0.8
1581 GtC yr^{-1} (Figure 4e, Table 7). We estimate that the 2024 land sink was the lowest since 2015. The
1582 severe reduction in the land sink in 2024 is likely driven by the El Niño conditions, leading to a 66%
1583 reduction in S_{LAND} in the tropics (30N-30S) from 2.8 GtC in 2022 to 1.0 GtC in 2024. This is combined
1584 with intense wildfires in Canada, Bolivia and Brazil that led to a significant CO_2 source (see also
1585 Section 3.8.3). We note that the S_{LAND} estimate for 2024 of 1.9 ± 0.9 GtC is much larger than the $0.3 \pm$
1586 1.0 GtC yr^{-1} estimate from the residual sink from the global budget ($E_{\text{FOS}}+E_{\text{LUC}}-G_{\text{ATM}}-S_{\text{OCEAN}}$, Table 5),
1587 although the residual sink would be substantially larger (at around 1.4 GtC yr^{-1}) if using the satellite-
1588 based GRESO in this equation. A large budget imbalance is often associated with El Niño years (e.g.
1589 1986/87, 1997/98, 2005/06, 2023/24), and the possible underestimation in DGVMs of the tropical land
1590 carbon losses in response to drought, high temperature extremes, and fires. Few DGVMs have explicit
1591 representation of drought-mortality and only 8 from 22 include some form of forest demography,
1592 although recent efforts are underway to fill these critical research gaps (Eckes-Shephard et al., 2025
1593 Yao et al., 2022, 2023).

1594 An overestimate in S_{LAND} in 2024 can in part be attributed to the inability in DGVMs to reproduce
1595 extreme fire emissions in 2024. Globally fire emissions as calculated by GFED were 0.43 GtC yr^{-1}
1596 higher in 2024 compared to the decadal average (2015-2024), similar to the anomaly in 2023 (0.44 GtC
1597 yr^{-1}). This was mainly due to an increase in fire over forests in Boreal North America (0.16 GtC yr^{-1})
1598 and forests, savannahs and grasslands over Southern Hemisphere South America (0.35 GtC yr^{-1}) in
1599 2024, partly offset by a negative trend in fires over Northern Hemisphere Africa (-0.05 GtC yr^{-1}
1600 anomaly). In fact, across the Amazon basin emissions from degradation fires (two thirds Brazil, one
1601 third Bolivia) surpassed those from deforestation fires in 2024 (Bourgoin et al., 2025). In contrast
1602 DGVMs simulate an anomaly of 0.2 GtC yr^{-1} in 2024, i.e. an underestimate of 0.23 GtC yr^{-1} in fire
1603 emissions for 2024. Fire enabled DGVMs do simulate a larger reduction in S_{LAND} in 2024 compared to
1604 non-fire models (0.6 vs 0.3 GtC), indicating the importance of representing fire extremes when
1605 explaining reductions in the land sink.

1606 Finally, a large uncertainty relates to climate forcing datasets, particularly over the critical carbon-rich
1607 tropical forest regions with poor coverage of meteorological stations. For example, there are large
1608 differences in climate forcing (e.g. CRUJRA-3Q and ERA5) and downstream DGVM carbon
1609 simulations over the Congo basin and tropical central and northern Africa in 2024 (Ke et al., 2025).

1610 **3.7.4 Year 2025 projection**

1611 Calculating the land sink as the residual of the other projections for 2025, we project a land sink of 3.1
1612 GtC for 2025, 1.1 GtC larger than the 2024 estimate, consistent with an expected recovery of the land
1613 sink after an El Niño event. The ESMs do not provide an additional estimate of S_{LAND} as they only
1614 simulate the net atmosphere-land carbon flux ($S_{\text{LAND}} - E_{\text{LUC}}$).

1615 **3.7.5 Evaluation of land models**

1616 The evaluation of the DGVMs shows generally higher agreement across models for runoff, and to a
1617 lesser extent for GPP, and ecosystem respiration. These conclusions are supported by a more
1618 comprehensive analysis of DGVM performance in comparison with benchmark data (Sitch et al.,
1619 2024). A relative comparison of DGVM performance (Figure S11) suggests several DGVMs (CABLE-
1620 POP, CLASSIC, OCN, ORCHIDEE) may outperform others at multiple carbon and water cycle
1621 benchmarks. However, results from Seiler et al., 2022, also show how DGVM differences are often of
1622 similar magnitude compared with the range across observational datasets. All models score high
1623 enough over the metrics tests to support their use here. There are a few anomalously low scores for
1624 individual metrics from a single model, and these can direct the effort to improve models for use in
1625 future budgets (See also Supplement S.4.2).

1626 **3.8 Partitioning the carbon sinks**

1627 **3.8.1 Global sinks and spread of estimates**

1628 In the period 2015-2024, the bottom-up view of global net ocean and land carbon sinks provided by the
1629 GCB, S_{OCEAN} for the ocean and $S_{\text{LAND}} - E_{\text{LUC}}$ for the land, agrees closely with the top-down global
1630 carbon sinks delivered by the atmospheric inversions. This is shown in Figure 13, which visualises the
1631 individual decadal mean atmosphere-land and atmosphere-ocean fluxes from each, along with the
1632 constraints on their sum offered by the global fossil CO_2 emissions flux minus the atmospheric growth
1633 rate ($E_{\text{FOS}} - G_{\text{ATM}}$, $4.2 \pm 0.5 \text{ Gt C yr}^{-1}$, Table 7, shown as diagonal line in Figure 13). The GCB estimate
1634 for net atmosphere-to-surface flux ($S_{\text{OCEAN}} + S_{\text{LAND}} - E_{\text{LUC}}$) during 2015-2024 is $4.2 \pm 1.1 \text{ Gt C yr}^{-1}$
1635 (Table 7), implying a zero budget imbalance (B_{IM}) (see Section 3.9). The atmospheric inversions
1636 estimate of the net atmosphere-to-surface flux during 2015-2024 is 4.3 Gt C yr^{-1} , with a $< 0.1 \text{ Gt C yr}^{-1}$
1637 imbalance, and thus scatter across the diagonal, with inverse models trading land for ocean fluxes in

1638 their solution. The independent constraint on the net atmosphere-to-surface flux based on atmospheric
1639 O₂ by design also closes the balance and is 4.2 ± 0.9 GtC yr⁻¹ over the 2015-2024 period (orange
1640 symbol on Figure 13), while the ESMs estimate for the net atmosphere-to-surface flux over that period
1641 is $4.8 [2.4, 6.0]$ GtC yr⁻¹ (Tables 5 and 6).

1642 The distributions based on the individual models and f CO₂-products reveal substantial spread but
1643 converge near the decadal means quoted in Tables 5 to 7. Sink estimates for S_{ocean} are mostly non-
1644 Gaussian, while the ensemble of DGVMs and inverse models appears more normally distributed
1645 justifying the use of a multi-model mean and standard deviation for their errors in the budget.
1646 Noteworthy is that the tails of the distributions provided by the land and ocean bottom-up estimates
1647 would not agree with the global constraint provided by the fossil fuel emissions and the observed
1648 atmospheric CO₂ growth rate. This illustrates the power of the atmospheric joint constraint from the
1649 global CO₂ observation capacity.

1650 **3.8.1.1 Net atmosphere-to-land flux**

1651 The GCB estimate of the net atmosphere-to-land flux (S_{land} – E_{luc}), calculated as the difference
1652 between S_{land} from the DGVMs and E_{luc} from the bookkeeping models, amounts to a 1.0 ± 1.0 GtC
1653 yr⁻¹ sink during 2015-2024 (Table 5). The estimate of net atmosphere-to-land flux (S_{land} – E_{luc}) from
1654 the DGVMs alone (1.4 ± 0.7 GtC yr⁻¹, Table 5, green symbols on Figure 13) is slightly larger, although
1655 within the uncertainty of the GCB estimate and also within uncertainty of the global carbon budget
1656 constraint (E_{fos} – G_{atm} – S_{ocean}, 1.0 ± 0.6 GtC yr⁻¹; Table 7). Also, for 2015-2024, the inversions
1657 estimate the net atmosphere-to-land flux is a 1.3 ± 0.3 GtC yr⁻¹ sink, similar to the mean of the DGVMs
1658 estimates (purple versus grey symbols on Figure 13). The independent constraint based on atmospheric
1659 O₂ is slightly lower, 0.7 ± 0.8 GtC yr⁻¹ (orange symbol in Figure 13), although its uncertainty overlaps
1660 with the uncertainty range from other approaches. Last, the ESMs estimate for the net atmosphere-to-
1661 land flux during 2014-2023 is a $2.3 [-0.1, 3.6]$ GtC yr⁻¹ sink, larger than all other estimates (Table 5).

1662 As discussed in Section 3.5.3, the atmospheric growth rate of CO₂ derived from the NOAA surface
1663 stations was very high in 2024, 7.9 GtC (3.73 ppm) the largest on the 65 years long observational
1664 record. Both DGVMs and inversions assign this large CO₂ growth rate to a continued reduction of the
1665 net atmosphere to land flux since 2023, in particular in the tropics (Figures 11 and 14), especially
1666 pronounced in the inversions. DGVMs simulate a 2024 global net atmosphere-to-land flux of 1.1 GtC
1667 yr⁻¹, a 50% decline relative to the 2.2 GtC yr⁻¹ sink in 2022, primarily driven by the severe reduction in
1668 S_{land} (-37%, see Section 3.7.3). The tropics (30°N-30°S) are recording a dramatic decrease in the net
1669 atmosphere-to-land flux from a 1.3 GtC yr⁻¹ sink in 2022 to a 0.2 GtC yr⁻¹ source in 2024. The
1670 atmospheric inversions show a continued reduction with the global net atmosphere-to-land flux
1671 declining from 2.9 GtC yr⁻¹ in 2022 to 0.8 GtC yr⁻¹ in 2023 to 0.2 GtC yr⁻¹ in 2024 (-94% from 2022 to
1672 2024), with the tropics turning from a 1.3 GtC yr⁻¹ sink in 2022 to a 1.2 GtC yr⁻¹ source in 2024. This

1673 discrepancy between the DGVMs and inversions estimates of the tropical and hence global atmosphere-
1674 land flux largely explains the negative B_{IM} in 2024, (see also Section 3.8.2.2 below).

1675 **3.8.1.2 Net atmosphere-to-ocean flux**

1676 For the 2015-2024 period, the GOBMs (2.7 ± 0.4 GtC yr⁻¹) produce a lower estimate of the ocean sink
1677 than the fCO_2 -products with 3.3 [2.9, 3.8] GtC yr⁻¹, which shows up in Figure 13 as separate peaks in
1678 the distribution from the GOBMs (dark blue symbols) and from the fCO_2 -products (light blue symbols).
1679 Atmospheric inversions (3.0 ± 0.3 GtC yr⁻¹) suggest an ocean uptake more in line with the average of
1680 the GOBMs and fCO_2 -products for the recent decade (Table 6). The inversions are not fully
1681 independent as 7 out of 14 inversions covering the last decade use fCO_2 -products as ocean priors and
1682 one uses a GOBM (Table S4). The independent constraint based on atmospheric O_2 (3.5 ± 0.5 GtC yr
1683 ⁻¹) is at the high end of the distribution of the other methods. However, as mentioned in section 2.8, the
1684 O_2 method requires a correction for global air-sea O_2 flux, which induces a non-negligible uncertainty
1685 on the decadal estimates (about 0.5 GtC yr⁻¹). The large growth in the ocean carbon sink from O_2 is
1686 compatible with the GOBMs and fCO_2 -products estimates when accounting for their uncertainty ranges.
1687 Lastly, the ESMs estimate, 2.5 [2.2, 2.8] GtC yr⁻¹, suggest a lower average ocean carbon sink than the
1688 other estimates. We caution that the riverine transport of carbon taken up on land and outgassing from
1689 the ocean, accounted for here, is a substantial (0.65 ± 0.3 GtC yr⁻¹) and uncertain term (Crisp et al.,
1690 2022; Gruber et al., 2023; DeVries et al., 2023) that separates the GOBMs, ESMs and oxygen-based
1691 estimates on the one hand from the fCO_2 -products and atmospheric inversions on the other hand.

1692 **3.8.2 Regional partitioning**

1693 Figure 14 shows the latitudinal partitioning of the global atmosphere-to-ocean (S_{OCEAN}), atmosphere-to-
1694 land ($S_{LAND} - E_{LUC}$), and their sum ($S_{OCEAN} + S_{LAND} - E_{LUC}$) according to the estimates from GOBMs
1695 and ocean fCO_2 -products (S_{OCEAN}), DGVMs ($S_{LAND} - E_{LUC}$), and from atmospheric inversions (S_{OCEAN}
1696 and $S_{LAND} - E_{LUC}$). S_{OCEAN} estimates were not corrected for the regional analysis.

1697 **3.8.2.1 North**

1698 Despite being one of the most densely observed and studied regions of our globe, annual mean carbon
1699 sink estimates in the northern extra-tropics (north of 30°N) continue to differ. The atmospheric
1700 inversions suggest an atmosphere-to-surface sink ($S_{OCEAN} + S_{LAND} - E_{LUC}$) for 2015-2024 of 2.7 ± 0.4
1701 GtC yr⁻¹, which is higher than the process models' estimate of 2.0 ± 0.4 GtC yr⁻¹ (Figure 14). The
1702 GOBMs (1.1 ± 0.2 GtC yr⁻¹), fCO_2 -products (1.4 [1.2-1.6] GtC yr⁻¹), and inversion systems (1.2 ± 0.1
1703 GtC yr⁻¹) produce largely consistent estimates of the ocean sink. However, the larger flux in the fCO_2 -
1704 products may be related to data sparsity (Mayot et al., 2024). Thus, the difference mainly arises from

1705 the net land flux ($S_{\text{LAND}} - E_{\text{LUC}}$) estimate, which is $0.9 \pm 0.3 \text{ GtC yr}^{-1}$ in the DGVMs compared to $1.5 \pm$
1706 0.4 GtC yr^{-1} in the atmospheric inversions (Figure 14, second row).

1707 Discrepancies in the northern land fluxes conform with persistent issues surrounding the quantification
1708 of the drivers of the global net land CO_2 flux (Arneeth et al., 2017; Huntzinger et al., 2017; O’Sullivan et
1709 al., 2022) and the distribution of atmosphere-to-land fluxes between the tropics and high northern
1710 latitudes (Baccini et al., 2017; Schimel et al., 2015; Stephens et al., 2007; Ciais et al., 2019; Gaubert et
1711 al., 2019; O’Sullivan et al. 2024).

1712 In the northern extra-tropics, the process models, inversions, and $f\text{CO}_2$ -products consistently suggest
1713 that most of the interannual variability stems from the land (Figure 14). Inversions generally agree on
1714 the magnitude of interannual variations (IAV) over land, more so than DGVMs ($0.27\text{-}0.38$ vs $0.07\text{-}0.55$
1715 GtC yr^{-1} , averaged over 1990-2024).

1716 **3.8.2.2 Tropics**

1717 In the tropics ($30^\circ\text{S}\text{-}30^\circ\text{N}$), both the atmospheric inversions and process models estimate a net carbon
1718 balance ($S_{\text{OCEAN}} + S_{\text{LAND}} - E_{\text{LUC}}$) that is relatively close to neutral over the past decade (inversions: 0.05
1719 $\pm 0.5 \text{ GtC yr}^{-1}$, process models: $0.4 \pm 0.6 \text{ GtC yr}^{-1}$). The GOBMs ($-0.003 \pm 0.3 \text{ GtC yr}^{-1}$), $f\text{CO}_2$ -products
1720 ($0.3 [0.1, 0.6] \text{ GtC yr}^{-1}$), and inversion systems ($0.3 \pm 0.1 \text{ GtC yr}^{-1}$) indicate a neutral to positive tropical
1721 ocean flux (see Figure S5 for spatial patterns). DGVMs indicate a net land sink ($S_{\text{LAND}} - E_{\text{LUC}}$) of 0.4
1722 $\pm 0.5 \text{ GtC yr}^{-1}$, whereas the inversion systems indicate a small source in the net land flux although with
1723 larger model spread ($-0.2 \pm 0.6 \text{ GtC yr}^{-1}$, Figure 14, third row).

1724 A continuing conundrum is the partitioning of the global atmosphere-land flux between the Northern
1725 Hemisphere land and the tropical land (Stephens et al., 2017; Pan et al., 2011; Gaubert et al., 2019). It is
1726 of importance because each region has its own history of land-use change, climate drivers, and impact
1727 of increasing atmospheric CO_2 and nitrogen deposition. Quantifying the magnitude of each sink is a
1728 prerequisite to understanding how each individual driver impacts the tropical and mid/high-latitude
1729 carbon balance. We define the North-South (N-S) difference as net atmosphere-land flux north of 30°N
1730 minus the net atmosphere-land flux south of 30°N . For the inversions, the N-S difference is 1.7 ± 1.0
1731 GtC yr^{-1} across this year’s inversion ensemble. In the ensemble of DGVMs the N-S difference is $0.6 \pm$
1732 0.5 GtC yr^{-1} , a much narrower range than the one from atmospheric inversions. The smaller spread
1733 across DGVMs than across inversions is to be expected as there is no correlation between Northern and
1734 Tropical land sinks in the DGVMs as opposed to the inversions where the sum of the two regions being
1735 well-constrained by atmospheric observations leads to an anti-correlation between these two regions.

1736 The tropical lands are the origin of most of the atmospheric CO_2 interannual variability (Ahlström et al.,
1737 2015), consistently among the process models and inversions (Figure 14). The interannual variability in

1738 the tropics is similar among the ocean $f\text{CO}_2$ -products (0.06-0.18 GtC yr⁻¹) and the GOBMs (0.07-0.16
1739 GtC yr⁻¹). The DGVMs and inversions indicate that atmosphere-to-land CO₂ fluxes are more variable
1740 than atmosphere-to-ocean CO₂ fluxes in the tropics, with interannual variability of 0.3 to 1.13 and 0.96
1741 GtC yr⁻¹ for DGVMs and inversions, respectively for 1990-2024. The year 2024 saw the largest growth
1742 rate in the atmosphere so far, largely caused by reductions in the tropical land sink, similar to earlier
1743 extreme years, such as during the 2015-2016 El Niño period. The inversions seem to capture the
1744 response of the tropical land sink to a larger degree than the DGVMs, with a 2024 tropical land source
1745 of 1.2 ± 0.9 GtC yr⁻¹ for the inversions versus a 0.2 ± 0.7 sink for the DGVMs.

1746 3.8.2.3 South

1747 In the southern extra-tropics (south of 30°S), the atmospheric inversions suggest a net atmosphere-to-
1748 surface sink ($S_{\text{OCEAN}}+S_{\text{LAND}}-E_{\text{LUC}}$) for 2015-2024 of 1.6 ± 0.2 GtC yr⁻¹, similar to the process models'
1749 estimate of 1.5 ± 0.4 GtC yr⁻¹ (Figure 14). An approximately neutral net land flux ($S_{\text{LAND}}-E_{\text{LUC}}$) for the
1750 southern extra-tropics is estimated by both the DGVMs (0.05 ± 0.1 GtC yr⁻¹) and the inversion systems
1751 (0.01 ± 0.1 GtC yr⁻¹). This means nearly all carbon uptake is due to oceanic sinks south of 30°S. The
1752 Southern Ocean flux in the $f\text{CO}_2$ -products (1.6 [1.5, 1.9 GtC] yr⁻¹) and inversion estimates (1.6 ± 0.2
1753 GtC yr⁻¹) is marginally higher than in the GOBMs (1.5 ± 0.4 GtC yr⁻¹) (Figure 14, bottom row). This
1754 agreement is subject to the choice of the river flux adjustment (Lacroix et al., 2020, Hauck et al.,
1755 2023b). Nevertheless, the time-series of atmospheric inversions and $f\text{CO}_2$ -products diverge from the
1756 GOBMs. A substantial overestimation of the trends in the $f\text{CO}_2$ -products could be explained by sparse
1757 and unevenly distributed observations, especially in wintertime (Figure S5; Hauck et al., 2023a; Gloege
1758 et al., 2021). Model biases likely contribute as well, with biases in mode water formation, stratification,
1759 and the chemical buffer capacity known to play a role in Earth System Models (Terhaar et al., 2021,
1760 Bourgeois et al., 2022, Terhaar et al., 2022).

1761 The interannual variability in the southern extra-tropics is low because of the dominance of ocean areas
1762 with low variability compared to land areas. The split between land ($S_{\text{LAND}}-E_{\text{LUC}}$) and ocean (S_{OCEAN})
1763 shows a substantial contribution to variability in the south coming from the land, with no consistency
1764 between the DGVMs and the inversions or among inversions. This is expected due to the difficulty of
1765 separating exactly the land and oceanic fluxes when viewed from atmospheric observations alone. The
1766 S_{OCEAN} interannual variability was found to be higher in the $f\text{CO}_2$ -products (0.04-0.18 GtC yr⁻¹)
1767 compared to GOBMs (0.03 to 0.06 GtC yr⁻¹) in 1990-2024. Inversions give an interannual variability
1768 of 0.13 to 0.15 GtC yr⁻¹. Model subsampling experiments recently illustrated that $f\text{CO}_2$ -products may
1769 overestimate decadal variability in the Southern Ocean carbon sink by 30% and the trend since 2000 by
1770 50-130% due to data sparsity, based on one and two $f\text{CO}_2$ -products with strong variability (Gloege et
1771 al., 2021, Hauck et al., 2023a). The trend benchmark test using the method of Hauck et al., (2023a) and
1772 a subset of 6 $f\text{CO}_2$ -products confirms the sensitivity of the decadal trends in $f\text{CO}_2$ -products to

1773 reconstruction biases, particularly in the Southern Ocean, indicating an overestimation of the ensemble
1774 mean trend (See Supplement S.3.4). However, we also find compensating positive biases in the
1775 ensemble so that the ensemble mean bias is smaller than the bias from some individual $f\text{CO}_2$ -products.

1776 **3.8.2.4 RECCAP2 regions**

1777 Aligning with the RECCAP-2 initiative (Ciais et al., 2022; Poulter et al., 2022; DeVries et al., 2023),
1778 we provide a breakdown of this GCB paper estimate of the E_{LUC} , S_{LAND} , Net land ($S_{\text{LAND}} - E_{\text{LUC}}$), and
1779 S_{OCEAN} fluxes over the 10 land, and 5 ocean RECCAP-2 regions, averaged over the period 2015-2024
1780 (Figure 15). The DGVMs and inversions suggest a positive net land sink in all regions, except for South
1781 America, Africa, and Southeast Asia, where the inversions indicate a small net source of respectively -
1782 $0.1 \pm 0.5 \text{ GtC yr}^{-1}$, $-0.3 \pm 0.3 \text{ GtC yr}^{-1}$, and $-0.1 \pm 0.3 \text{ GtC yr}^{-1}$ compared to a small sink of $0.1 \pm 0.3 \text{ GtC}$
1783 yr^{-1} , $0.1 \pm 0.3 \text{ GtC yr}^{-1}$, and $0.03 \pm 0.1 \text{ GtC yr}^{-1}$ for the DGVMs. The uncertainty in the sign of net
1784 tropical carbon fluxes is driven by opposing gross fluxes and relatively large uncertainty in the gross
1785 fluxes themselves. For South America, DGVMs estimate S_{LAND} of $0.4 \pm 0.4 \text{ GtC yr}^{-1}$ and E_{LUC} of
1786 $0.3 \pm 0.2 \text{ GtC yr}^{-1}$. Bookkeeping models suggest a larger E_{LUC} source of around 0.5 GtC yr^{-1} . Similarly,
1787 in Southeast Asia, the DGVMs estimate an E_{LUC} of $0.2 \pm 0.1 \text{ GtC yr}^{-1}$, compared with the bookkeeping
1788 model estimate of $0.4 \pm 0.02 \text{ GtC yr}^{-1}$. Therefore, DGVMs may underestimate E_{LUC} in these regions,
1789 which could explain the net sink discrepancy with inversions. In Africa, E_{LUC} is similar for DGVMs and
1790 bookkeeping models ($\sim 0.4 \text{ GtC yr}^{-1}$), and DGVMs estimate an S_{LAND} of $0.5 \pm 0.2 \text{ GtC yr}^{-1}$.

1791 The inversions suggest the largest net land sinks are located in North America ($0.4 \pm 0.3 \text{ GtC yr}^{-1}$),
1792 Russia ($0.6 \pm 0.2 \text{ GtC yr}^{-1}$), Europe ($0.3 \pm 0.2 \text{ GtC yr}^{-1}$), and East Asia ($0.2 \pm 0.3 \text{ GtC yr}^{-1}$). This agrees
1793 well with the DGVMs in North America ($0.4 \pm 0.1 \text{ GtC yr}^{-1}$), which indicate a large natural land sink
1794 (S_{LAND}) of $0.4 \pm 0.2 \text{ GtC yr}^{-1}$, and near-zero net land-use related carbon losses ($0.02 \pm 0.1 \text{ GtC yr}^{-1}$). The
1795 DGVMs suggest a smaller net land sink in Russia compared to inversions ($0.3 \pm 0.1 \text{ GtC yr}^{-1}$), and a
1796 similar net sink in East Asia ($0.2 \pm 0.1 \text{ GtC yr}^{-1}$).

1797 There is generally a higher level of agreement in the estimates of regional S_{OCEAN} between the different
1798 data streams (GOBMs, $f\text{CO}_2$ -products and atmospheric inversions) on decadal scale, compared to the
1799 agreement between the different land flux estimates. All data streams agree that the largest contribution
1800 to S_{OCEAN} stems from the Southern Ocean due to a combination of high flux density and large surface
1801 area, but with important contributions also from the Atlantic (high flux density) and Pacific (large area)
1802 basins. In the Southern Ocean, GOBMs suggest a sink of $1.1 \pm 0.4 \text{ GtC yr}^{-1}$, in line with the $f\text{CO}_2$ -
1803 products ($1.1 [1.0, 1.2] \text{ GtC yr}^{-1}$) and atmospheric inversions ($1.1 \pm 0.2 \text{ GtC yr}^{-1}$). There is similar
1804 agreement in the Pacific Ocean, with GOBMs, $f\text{CO}_2$ -products, and atmospheric inversions indicating a
1805 sink of $0.6 \pm 0.1 \text{ GtC yr}^{-1}$, $0.7 [0.6, 0.9] \text{ GtC yr}^{-1}$, and $0.6 \pm 0.2 \text{ GtC yr}^{-1}$, respectively. However, in the

1806 Atlantic Ocean, GOBMs simulate a sink of $0.5 \pm 0.1 \text{ GtC yr}^{-1}$, noticeably lower than both the $f\text{CO}_2$ -
1807 products ($0.8 [0.7, 0.9] \text{ GtC yr}^{-1}$) and atmospheric inversions ($0.8 \pm 0.1 \text{ GtC yr}^{-1}$). It is important to note
1808 the $f\text{CO}_2$ -products and atmospheric inversions have a substantial and uncertain river flux adjustment in
1809 the Atlantic Ocean (0.3 GtC yr^{-1}) that also leads to a mean offset between GOBMs and $f\text{CO}_2$ -
1810 products/inversions in the latitude band of the tropics (Figure 14). The Indian Ocean due its smaller size
1811 and the Arctic Ocean due to its size and sea-ice cover that prevents air-sea gas-exchange are responsible
1812 for smaller but non negligible S_{OCEAN} fluxes (Indian Ocean: $(0.3 \pm 0.1 \text{ GtC yr}^{-1}, 0.3 [0.3, 0.4] \text{ GtC yr}^{-1},$
1813 and $0.3 \pm 0.1 \text{ GtC yr}^{-1}$ for GOBMs, $f\text{CO}_2$ -products, and atmospheric inversions, respectively, and Arctic
1814 Ocean: $(0.1 \pm 0.03 \text{ GtC yr}^{-1}, 0.2 [0.1, 0.3] \text{ GtC yr}^{-1},$ and $0.1 \pm 0.04 \text{ GtC yr}^{-1}$ for GOBMs, $f\text{CO}_2$ -products,
1815 and atmospheric inversions, respectively). Note that the S_{OCEAN} numbers presented here deviate from
1816 numbers reported in RECCAP-2 where the net air-sea CO_2 flux is reported (i.e. without river flux
1817 adjustment for $f\text{CO}_2$ -products and inversions, and with river flux adjustment subtracted from GOBMs
1818 in most chapters, or comparing unadjusted datasets with discussion of uncertain regional riverine fluxes
1819 as major uncertainty, e.g. Sarma et al., 2023, DeVries et al., 2023).

1820 **3.8.3 Fire emissions in 2025**

1821 Fire emissions so far in 2025 have been below the average of recent decades, chiefly due to the lowest
1822 emissions on record since 2003 across the tropics. Figure S14 shows global and regional emissions
1823 estimates for the period 1st Jan-30th September in each year 2003-2025. Estimates derive from two
1824 global fire emissions products: the global fire emissions database (GFED, version 4.1s; van der Werf et
1825 al., 2017), and the global fire assimilation system (GFAS, operated by the Copernicus Atmosphere
1826 Service; Kaiser et al., 2012). The two products estimate that global emissions from fires were 1.2-1.4
1827 GtC (the range reflecting the difference between the two fire emission datasets, actual uncertainties are
1828 larger and estimates are likely conservative, see Chen et al. (2023)) during January-September 2025.
1829 These estimates are 19-20% below the 2015-2024 average for the same months (1.5-1.7 GtC). Both the
1830 GFED4.1s and GFAS products show the second-lowest January-September fire emissions since 2003
1831 (2022 is the lowest year in both products).

1832 Notably, the year 2025 follows two years with above-average global fire emissions (Figure S14), with
1833 global emissions through September totalling 1.7-2.1 GtC in 2023 and 1.6-2.2 GtC in 2024. These high
1834 emissions totals were caused by high emissions in North America in 2023 principally in Canada; Jones
1835 et al., 2024b), and in both North America and South America in 2024 (principally in Canada and Brazil;
1836 Kelley et al., 2025). For example, in January-September 2024, GFED4.1s suggests that global
1837 emissions totalled 2.2 GtC, the highest total on record for these months and 32% above the average for
1838 the decade prior (2014-2023; GFAS also suggests that emissions were 11% above the average for
1839 January-September).

1840 Despite low global fire emissions so far in 2025, a pattern of extremely high fire emissions from
1841 Canada has now persisted for three consecutive years commencing with the record-breaking year in
1842 2023 (Jones et al., 2024b, Byrne et al., 2024; Kelley et al., 2025). In January-September 2025, fire
1843 emissions from Canada (0.3-0.4 GtC) were slightly greater than in the same months of 2024 (0.2-0.3
1844 GtC yr⁻¹) and around half as large as those in the same months of 2023 (0.5-0.8 GtC). The emissions
1845 totals for Canada in January-September 2025 were 2.2 times the average of January-September periods
1846 during the prior decade 2015-2024 and 4-6 times greater than the average of those months in 2003-2022
1847 [excluding the record-breaking year in 2023]; Figure S14). According to GFED4.1s, January-
1848 September fire emissions from Canada in just the past three years (1.5 GtC) exceeded the country's
1849 total January-September fire emissions throughout the 20 years prior (1.2 GtC during 2003-2022). The
1850 continued anomaly in Canada propagated to the Northern Hemisphere, where January-September 2025
1851 emissions of 0.4-0.5 GtC were 13-21% above the average of 2015-2024.

1852 Fire emissions anomalies in Africa strongly influence global fire emissions totals because the continent
1853 typically contributed near 50% of global fire emissions during 2015-2024 (average of January-
1854 September periods). For 2025, fire emissions in Africa through September were 0.4-0.6 GtC, 19-25%
1855 below the average of 2015-2024 (0.6-0.8 GtC). Synchronously, emissions through September from
1856 South America were around 0.1 GtC in both GFED4.1s and GFAS systems, less than half of the
1857 average for 2015-2024 (0.2-0.3 GtC), and emissions from Southeast Asia were around 0.05 GtC, also
1858 less than half of the average for 2015-2024 (0.1 GtC in both GFED4.1s and GFAS). Low emissions
1859 from the tropical parts of Africa, South America, and Southeast Asia contribute to low emissions across
1860 the global tropics so far in 2025 (0.7-0.9 GtC), which were only around two-thirds of the average for
1861 2015-2024 (1.1-1.3 GtC) in both GFED4.1s and GFAS.

1862 We caution that the fire emissions fluxes presented here should not be compared directly with other
1863 fluxes of the budget (e.g. S_{LAND} or E_{LUC}) due to incompatibilities between the observable fire emission
1864 fluxes and what is quantified in the S_{LAND} and E_{LUC} components of the budget. The fire emission
1865 estimates from global fire products relate to all fire types that can be observed in Earth Observations
1866 (Giglio et al., 2018; Randerson et al., 2012; Kaiser et al., 2012), including (i) fires occurring as part of
1867 natural disturbance-recovery cycles that would also have occurred in the pre-industrial period (Yue et
1868 al., 2016; Keeley and Pausas, 2019; Zou et al., 2019), (ii) fires occurring above and beyond natural
1869 disturbance-recovery cycle due to changes in climate, CO₂ and N fertilisation and to an increased
1870 frequency of extreme drought and heatwave events (Abatzoglou et al., 2019; Jones et al., 2022; Zheng
1871 et al., 2021; Burton et al., 2024), and (iii) fires occurring in relation to land use and land use change,
1872 such as deforestation fires and agricultural fires (van der Werf et al., 2010; Magi et al., 2012). In the
1873 context of the global carbon budget, fire emissions associated with (ii) should be included in the S_{LAND}
1874 component, fire emissions associated with (iii) should already be accounted for in the E_{LUC} component,
1875 while fire emissions associated with (i) should not be included in the global carbon budget as part of the

1876 natural carbon cycle. However, it is not currently possible to derive specific estimates for fluxes (i), (ii),
1877 and (iii) using global fire emission products such as GFED or GFAS. In addition, the fire emissions
1878 estimates from global fire emissions products represent a gross flux of carbon to the atmosphere,
1879 whereas the S_{LAND} component of the budget is a net flux that should also include post-fire recovery
1880 fluxes. Even if emissions from fires of type (ii) could be separated from those of type (i), these fluxes
1881 may be partially or wholly offset in subsequent years by post-fire fluxes as vegetation recovers,
1882 sequestering carbon from the atmosphere to the terrestrial biosphere (Yue et al., 2016; Jones et al.,
1883 2024c). Increases in forest fire emissions and severity (emissions per unit area) globally during the past
1884 two decades have highlighted the increasing potential for fire emissions fluxes to outweigh post-fire
1885 recovery fluxes, though long-term monitoring of vegetation recovery is required to quantify the net
1886 effect on terrestrial C storage (Jones et al., 2024c).

1887 **3.9 Closing the global carbon cycle**

1888 **3.9.1 Partitioning of cumulative emissions and sink fluxes**

1889 Emissions during the period 1850-2024 amounted to 745 ± 65 GtC and were partitioned among the
1890 atmosphere (290 ± 5 GtC; 39%), ocean (200 ± 40 GtC; 27%), and land (175 ± 50 GtC; 24%). The
1891 cumulative land sink is lower than the cumulative land-use emissions (250 ± 65 GtC), making the
1892 global land a source of 75 ± 80 GtC over the whole 1850-2024 period (Table 8).

1893 The use of nearly independent estimates for the individual terms of the global carbon budget shows a
1894 cumulative budget imbalance of 80 GtC (11% of total emissions) during 1850-2024 (Table 8), which
1895 suggests that emissions could be slightly too high by the same proportion or that the combined land and
1896 ocean sinks are underestimated (by up to 20%). A large part of the B_{IM} occurs over the first half of the
1897 20th century (Figure 3, red dashed line) and could originate from the estimation of significant increase
1898 in E_{FOS} and E_{LUC} between the mid 1920s and the mid 1960s which is unmatched by a similar growth in
1899 atmospheric CO_2 concentration as recorded in ice cores (Figure 3). Also, we now correct the S_{LAND}
1900 estimate for historical reduction in forest cover (RSS, see Section 2.6). This reduces the S_{LAND} estimate
1901 by about 40 GtC over the 1850-2024 period, contributing to the increase of the historical budget
1902 imbalance in comparison to GCB2024 (Friedlingstein et al., 2025a).

1903 For the more recent 1959-2024 period where direct atmospheric CO_2 measurements are available, total
1904 emissions ($E_{\text{FOS}} + E_{\text{LUC}}$) amounted to 530 ± 50 GtC, of which 420 ± 20 GtC (79%) were caused by
1905 fossil CO_2 emissions, and 110 ± 45 GtC (21%) by land-use change (Table 8). The total emissions were
1906 partitioned among the atmosphere (230 ± 5 GtC; 44%), ocean (145 ± 30 GtC; 27%), and the land (120
1907 ± 30 GtC; 23%), with a budget imbalance of 35 GtC (7% of total emissions). All components except
1908 land-use change emissions have significantly grown since the 1960s, with important interannual
1909 variability in the growth rate in atmospheric CO_2 concentration primarily mirrored in the land CO_2 sink

1910 (Figure 4), and some decadal variability in all terms (Table 7). Differences with previous budget
1911 releases are documented in Figure S15.

1912 The global carbon budget averaged over the last decade (2015-2024) is shown in Figure 2 and Table 7.
1913 For this period, 88% of the total emissions ($E_{\text{FOS}} + E_{\text{LUC}}$) were from fossil CO₂ emissions (E_{FOS}), and
1914 12% from land-use change (E_{LUC}). The total emissions were partitioned among the atmosphere (50%),
1915 ocean (29%) and land (21%), with a near zero budget imbalance (0.1%, $<0.1 \text{ GtC yr}^{-1}$). We note that,
1916 compared to GCB2024, the corrections on S_{OCEAN} and S_{LAND} largely reduced the B_{IM} over the 2015-
1917 2024 period, by about 0.4 GtC, but at the cost of increasing the cumulated B_{IM} over the longer 1959-
1918 2024 period, from 17 GtC (uncorrected estimate) to 37 GtC (corrected estimate).

1919 For single years, the budget imbalance can be larger (Figure 4f). For 2024, the combination of our
1920 estimated anthropogenic sources ($11.6 \pm 0.9 \text{ GtC yr}^{-1}$) and partitioning in atmosphere, land and ocean
1921 ($13.3 \pm 0.9 \text{ GtC yr}^{-1}$) leads to a large negative B_{IM} of -1.7 GtC (Table 7), indicating that, despite the
1922 lower than average S_{LAND} in 2024, the land sink is still too large to explain the record-high atmospheric
1923 CO₂ growth rate of 2024. We note that using the 2024 GRESO atmospheric growth rate of $6.8 \pm 0.2 \text{ GtC}$
1924 yr^{-1} (Section 3.5.3) would reduce the 2024 B_{IM} to about -0.6 GtC.

1925 **3.9.2 Trend and variability in the carbon budget imbalance**

1926 The carbon budget imbalance (B_{IM} ; Eq. 1, Figure 4f) quantifies the mismatch between the estimated
1927 total emissions and the estimated changes in the atmosphere, land, and ocean reservoirs. The budget
1928 imbalance from 1959 to 2024 is small (35 GtC cumulated over the period, i.e. 0.5 GtC yr^{-1} on average)
1929 and shows no significant trend over the 1959-2024 period (Figure 4). The process models (GOBMs and
1930 DGVMs) and $f\text{CO}_2$ -products have been selected to match observational constraints in the 1990s, but no
1931 further constraints have been applied to their representation of trend and variability. Therefore, the
1932 small mean and trend in the budget imbalance can be seen as evidence of a coherent community
1933 understanding of the emissions and their partitioning on those time scales (Figure 4). However, the
1934 budget imbalance shows substantial variability of the order of $\pm 1 \text{ GtC yr}^{-1}$, particularly over semi-
1935 decadal time scales, although most of the variability is within the uncertainty of the estimates.

1936 We cannot attribute the cause of the budget imbalance with our analysis, we only note that the budget
1937 imbalance is unlikely to be explained by errors in the emissions alone because of its large semi-decadal
1938 variability component, a variability that is atypical of emissions, and also because the budget imbalance
1939 has not increased in the past 60 years despite a near tripling in anthropogenic emissions (Figure 4).

1940 Errors in S_{LAND} and S_{OCEAN} are more likely to be the main cause for the budget imbalance, especially on
1941 interannual to semi-decadal timescales. For example, underestimation of the S_{LAND} by DGVMs has
1942 been reported following the eruption of Mount Pinatubo in 1991 possibly due to missing responses to
1943 changes in diffuse radiation (Mercado et al., 2009). Although we account for aerosol effects on solar

1944 radiation quantity and quality (diffuse vs direct), most DGVMs only used the former as input (i.e., total
1945 solar radiation) (Table S1). Thus, the ensemble mean may not capture the full effects of volcanic
1946 eruptions, i.e. associated with high light scattering sulphate aerosols, on the land carbon sink
1947 (O'Sullivan et al., 2021), potentially explaining the large positive B_{IM} in 1991-1992. DGVMs are
1948 suspected to underestimate the land sink reduction in response to El Niño events (see Section 3.7.3),
1949 which could explain the large negative B_{IM} in 1986-1987, 1997-1998 or 2023-2024). Quasi-decadal
1950 variability in the ocean sink has also been reported, with all methods agreeing on smaller than expected
1951 ocean CO₂ sink in the 1990s and a larger than expected sink in the 2000s (Figure 10b; Landschützer et
1952 al., 2016, DeVries et al., 2019, Hauck et al., 2020, McKinley et al., 2020, Gruber et al., 2023) and the
1953 climate-driven variability could be substantial but is not well constrained (DeVries et al., 2023, Müller
1954 et al., 2023). Errors in sink estimates could also be partly driven by errors in the climatic forcing data,
1955 particularly precipitation for S_{LAND} and wind for S_{OCEAN} .

1956 Although the budget imbalance is near zero for the most recent decade, it could be due to a
1957 compensation of errors. We cannot exclude an overestimation of CO₂ emissions, particularly from land-
1958 use change, given their large uncertainty, as has been suggested elsewhere (Piao et al., 2018), and/or an
1959 underestimate of the land or ocean sinks. A larger estimate of the atmosphere-land CO₂ flux (S_{LAND-}
1960 E_{LUC}) over the extra-tropics would reconcile bottom-up model results with inversion estimates (Figure
1961 14). Likewise, a larger S_{OCEAN} is also possible given the higher estimates from the fCO_2 -products and
1962 the oxygen based estimates (see Table 6 and Figure 10b), the underestimation of interior ocean
1963 anthropogenic carbon accumulation in the GOBMs (Section 3.6.5, Müller et al., 2023), or known biases
1964 of ocean models (e.g., Terhaar et al., 2022; 2024). More integrated use of observations in the global
1965 carbon budget, either on their own or for further constraining model results, should help resolve some
1966 of the budget imbalance.

1967 **4 Tracking progress towards mitigation targets**

1968 The average growth in global fossil CO₂ emissions peaked at nearly +3% per year during the 2000s,
1969 driven by the rapid growth in emissions in China. In the last decade, however, the global growth rate
1970 has slowly declined, reaching a low +0.8% per year over 2015-2024. While this slowdown in global
1971 fossil CO₂ emissions growth is welcome, global fossil CO₂ emissions continue to grow, far from the
1972 rapid emission decreases needed to be consistent with the temperature goals of the Paris Agreement.

1973 Since the 1990s, the average growth rate of fossil CO₂ emissions has continuously declined across the
1974 group of developed countries of the Organisation for Economic Co-operation and Development
1975 (OECD), with emissions peaking in around 2005 and declining at 1.5% yr⁻¹ in the decade 2015-2024,
1976 compared to a decline of 0.9% yr⁻¹ during the 2005-2014 period (Table 9). In the non-OECD countries,
1977 emissions rose 4.6% yr⁻¹ from 2005-2014, but growth has lowered to 2.1% yr⁻¹ from 2015-2024. In the
1978 decade 2015-2024, territorial fossil CO₂ emissions decreased significantly (at the 95% confidence level)

1979 in 35 economies whose gross domestic product (GDP) grew significantly (also at the 95% confidence
1980 level): Andorra, Australia, Austria, Belgium, Bulgaria, Czechia, Denmark, Estonia, Finland, France,
1981 Germany, Greece, Hungary, Ireland, Israel, Jordan, Latvia, Luxembourg, Netherlands, New Zealand,
1982 Norway, Poland, Portugal, South Korea, Romania, Serbia, Slovakia, Slovenia, Spain, Sweden,
1983 Switzerland, Taiwan, Thailand, United Kingdom, and USA (updated from Le Quéré et al., 2019).
1984 Altogether, these 35 economies emitted 2.7 GtC yr⁻¹ (9.7 GtCO₂ yr⁻¹) on average over the last decade,
1985 about 27% of world CO₂ fossil emissions. For comparison, over the previous decade (2005-2014), 18
1986 economies showed a significant decrease in territorial fossil CO₂ emissions while significantly growing
1987 their GDP (Austria, Belgium, Bulgaria, Czechia, France, Germany, Luxembourg, North Macedonia,
1988 Netherlands, New Zealand, Romania, Serbia, Slovakia, Sweden, Switzerland, United Kingdom, USA,
1989 Uzbekistan). These 18 economies emitted an average 2.0 GtC yr⁻¹ over 2005–2014, or 20% of the
1990 global total.

1991 Decomposing emission changes into the components of growth, a Kaya decomposition, helps give an
1992 initial understanding of the drivers of emission changes (Peters et al., 2017b). The reduction in growth
1993 in global fossil CO₂ emissions in the last decade (2015-2024, 0.8% yr⁻¹) relative to the previous decade
1994 (2005-2014, 2.2% yr⁻¹) is due to slightly weaker economic growth (3.5% yr⁻¹ to 2.4% yr⁻¹), increasing
1995 declines in CO₂ emissions per unit energy (0% yr⁻¹ to 0.7% yr⁻¹), and weakening declines in energy per
1996 unit GDP (1.6% yr⁻¹ to 1.3% yr⁻¹) (Figure S17). Fossil CO₂ emission declines in the USA and the EU27
1997 are primarily driven by sustained or increasing declines in energy per GDP and CO₂ emissions per unit
1998 energy. China has seen emissions growth decline from 6.7% yr⁻¹ in the 2005-2014 decade to 2.5% yr⁻¹
1999 from 2015-2024, driven by weaker economic growth (five percentage points), offset by a considerable
2000 weakening in the rate of reduction in the energy per GDP (four percentage points), with sustained
2001 improvements in CO₂ emissions per unit energy (Figure S17). India has had strong economic growth
2002 that is not offset by declines in energy per GDP or declines in CO₂ emissions per unit energy, driving
2003 up fossil CO₂ emissions. In the rest of the world, economic growth has slowed considerably in the last
2004 decade, and carbon intensity has increased, with declines in energy per GDP unable to counteract these
2005 increases leading to growing emissions. Despite the high deployment of renewables in some countries
2006 (e.g., China, India), fossil energy sources continue to grow to meet growing energy demand (Le Quéré
2007 et al., 2019). In summary, the carbon intensity of energy has consistently decreased over the past
2008 decade globally (-0.7% yr⁻¹), indicating decarbonisation of the global energy system, with declines in
2009 China (-1.4% yr⁻¹), the European Union (-1.5% yr⁻¹), the USA (-1.3% yr⁻¹), but no change in India and
2010 increases (carbonisation) in the Rest of the World. The global decarbonation trends are not sufficient to
2011 offset the growth in global energy demand, with energy demand growing faster than expected due to
2012 weakening declines in energy per GDP in China, US, and globally.

2013 The slower growth of global fossil CO₂ emissions in the last decade is due in part to the emergence of
2014 climate policy (Eskander and Fankhauser 2020; Le Quere et al 2019; Hoppe et al., 2023) and

2015 technological change, which is leading to a shift from coal to gas and growth in renewable energies, and
2016 reduced expansion of coal capacity. At the aggregated global level, decarbonisation shows a strong and
2017 growing signal in the last decade, with smaller contributions from lower economic growth and declines
2018 in energy per GDP. Altogether, global fossil CO₂ emissions are still growing, far from the reductions
2019 needed to meet the ambitious climate goals of the UNFCCC Paris agreement.

2020 Last, we update the remaining carbon budget (RCB) based on two studies, the IPCC AR6 (Canadell et
2021 al., 2021) and the revision of the IPCC AR6 estimates (Forster et al., 2025, Lamboll et al., 2023). We
2022 update the RCB assessed by the IPCC AR6 (Canadell et al., 2021), accounting for the 2020 to 2025
2023 GCB estimated anthropogenic emissions from fossil combustion (E_{FOS}) and land use change (ELUC).
2024 From January 2026, the IPCC AR6 RCB (50% likelihood) for limiting global warming to 1.5°C, 1.7°C
2025 and 2°C is estimated to amount to 70, 165, and 300 GtC (250, 600, 1100 GtCO₂). The Forster et al.
2026 (2025) study proposed a significantly lower RCB than IPCC AR6, with the largest reduction being due
2027 to an update of the climate emulator (MAGICC) used to estimate the warming contribution of non-CO₂
2028 agents, and to the warming (i.e. emissions) that occurred over the 2020-2024 period. We update the
2029 Forster et al., budget accounting for the 2025 GCB estimated anthropogenic emissions. From January
2030 2026, the Forster et al., (2025) RCB (50% likelihood) for limiting global warming to 1.5°C, 1.7°C and
2031 2°C is estimated to amount to 25, 120, and 275 GtC (90, 450, 1010 GtCO₂), significantly smaller than
2032 the updated IPCC AR6 estimate. Both the original IPCC AR6 and Forster et al. (2025) estimates
2033 include the Earth System uncertainty on the climate response to cumulative CO₂ emissions, which is
2034 reflected through the percent likelihood of exceeding the given temperature threshold, an additional
2035 uncertainty of ±220GtCO₂ due to alternative non-CO₂ emission scenarios, and other sources of
2036 uncertainties (see Canadell et al., 2021). The two sets of estimates overlap when considering all
2037 uncertainties.

2038 Here, we take the average of our update of both IPCC AR6 and Forster et al. (2025) estimates, giving a
2039 remaining carbon (50% likelihood) for limiting global warming to 1.5°C, 1.7°C and 2°C of respectively
2040 45, 145, and 290 GtC (170, 525, 1055 GtCO₂) starting from January 2026. We emphasise the large
2041 uncertainties, particularly when close to the global warming limit of 1.5°C. These 1.5°C, 1.7°C and 2°C
2042 remaining carbon budgets correspond respectively to about 4, 12 and 25 years from the beginning of
2043 2026, at the 2025 level of total anthropogenic CO₂ emissions. Reaching net-zero CO₂ emissions by
2044 2050 entails cutting total anthropogenic CO₂ emissions by about 0.5 GtC (1.7 GtCO₂), 4% of 2025
2045 emissions, each year on average, comparable to the decrease in E_{FOS} observed in 2020 during the
2046 COVID-19 pandemic. However, this would lead to cumulative emissions over 2025-2050 of 140 GtC
2047 (520 GtCO₂), well above the remaining carbon budget of 50 GtC to limit global warming to 1.5°C, but
2048 still within the remaining budget of 145 GtC to limit warming to 1.7°C (in phase with the “well below
2049 2°C” ambition of the Paris Agreement).

2050 **5 Discussion**

2051 Each year when the global carbon budget is published, each flux component is updated for all previous
2052 years to consider corrections that are the result of further scrutiny and verification of the underlying
2053 data in the primary input datasets. Annual estimates may be updated with improvements in data quality
2054 and timeliness (e.g., to eliminate the need for extrapolation of forcing data such as land use). Of all
2055 terms in the global budget, only the fossil CO₂ emissions and the growth rate in atmospheric CO₂
2056 concentration are based primarily on empirical inputs supporting annual estimates in this carbon
2057 budget. The carbon budget imbalance, yet an imperfect measure, provides a strong indication of the
2058 limitations in observations, in understanding and representing processes in models, and/or in the
2059 integration of the carbon budget components.

2060 The persistent unexplained variability in the carbon budget imbalance limits our ability to verify
2061 reported emissions (Peters et al., 2017a) and suggests we do not yet have a complete understanding of
2062 the underlying carbon cycle dynamics on annual to decadal timescales. Resolving most of this
2063 unexplained variability should be possible through different and complementary approaches. First, as
2064 intended with our annual updates, the imbalance as an error term should be reduced by improvements
2065 of individual components of the global carbon budget that follow from improving the underlying data
2066 and statistics and by improving the models through the resolution of some of the key uncertainties
2067 detailed in Table 10. Second, additional clues to the origin and processes responsible for the variability
2068 in the budget imbalance could be obtained through a closer scrutiny of carbon variability in light of
2069 other Earth system data (e.g., heat balance, water balance), and the use of a wider range of
2070 biogeochemical observations to better understand the land-ocean partitioning of the carbon imbalance
2071 such as the constraint from atmospheric oxygen. Finally, additional information could also be obtained
2072 through better inclusion of process knowledge at the regional level. The limit for reducing the carbon
2073 budget imbalance is yet unclear, but most certainly not yet reached given the possibilities for
2074 improvements that lie ahead.

2075 Estimates of global fossil CO₂ emissions from different datasets are in relatively good agreement when
2076 the different system boundaries of these datasets are considered (Andrew, 2020a). While estimates of
2077 E_{FOS} are derived from reported activity data requiring much fewer complex transformations than some
2078 other components of the budget, uncertainties remain, and one reason for the apparently low variation
2079 between datasets is precisely the reliance on the same underlying reported energy data. The budget
2080 excludes some sources of fossil CO₂ emissions, which available evidence suggests are relatively small
2081 (<1%) (see Supplement S.8.2). We have added emissions from lime production in China and the US,
2082 but these are still absent in reporting from most other non-Annex I countries, and before 1990 in other
2083 Annex I countries.

2084 Estimates of E_{LUC} suffer from a range of intertwined issues (Obermeier et al., 2025), including the poor
2085 knowledge of historical land-cover and land-use change (particularly before the 1960s when FAO
2086 reporting started), the rudimentary representation of management processes in most models, and the
2087 diversity in methodologies and boundary conditions used across methods (e.g., Armeth et al., 2017;
2088 Pongratz et al., 2014; Bastos et al., 2021). Uncertainties in current and historical carbon stocks in soils
2089 and vegetation also contribute to uncertainty in E_{LUC} estimates. Major efforts are thus necessary to
2090 resolve the different issues concerning E_{LUC} (Obermeier et al., 2025). The large uncertainty and limited
2091 reliability of E_{LUC} estimates are particularly concerning given the growing importance of E_{LUC} for
2092 climate mitigation strategies, and the large issues in the quantification of the cumulative emissions over
2093 the historical period that arise from large uncertainties in E_{LUC} .

2094 By adding the natural land sink in managed forests estimated by DGVMs (part of S_{LAND} in this budget)
2095 to the budget E_{LUC} estimate, we reconcile most of the large gap between our E_{LUC} estimate and the land-
2096 use flux estimates from NGHGs (Figure 8). This reconciliation (translation) can be used as potential
2097 adjustment in the policy context, for instance to help assess the collective countries' progress towards
2098 the goal of the Paris Agreement avoiding double-accounting for the natural sink in managed forests. In
2099 the absence of this translation, collective progress would appear better than it is (Grassi et al., 2021). A
2100 clear understanding of these implications is thus essential for policymakers for developing effective
2101 climate targets (Grassi et al., 2025). The application of this translation is also recommended in the
2102 UNFCCC Synthesis report for the first Global Stocktake (UNFCCC, 2022) whenever a comparison
2103 between LULUCF fluxes reported by countries and the global emission estimates of the IPCC is
2104 conducted. However, this translation should be seen as a short-term and pragmatic fix based on existing
2105 data, rather than a definitive solution to bridge the differences between global models and national
2106 inventories. Platforms for dataset comparisons (e.g., Melo et al., 2025) help strengthening the dialogue
2107 across communities and identify the additional steps needed to understand and reconcile the remaining
2108 differences, some of which are relevant at the country level (Grassi, et al., 2023, Schwingshackl, et al.,
2109 2022).

2110 The comparison of GOBMs, fCO_2 -products, and inversions highlights discrepancies in the temporal
2111 evolution of S_{OCEAN} in the Southern Ocean and northern high-latitudes (Figure 14, Hauck et al., 2023a)
2112 and in the mean S_{OCEAN} in the tropics. A large part of the uncertainty in the mean fluxes stems from the
2113 regional distribution of the river flux adjustment term. The current distribution simulates the largest
2114 share of the outgassing to occur in the tropics (Lacroix et al., 2020). The long-standing sparse data
2115 coverage of fCO_2 observations in the Southern compared to the Northern Hemisphere (e.g., Takahashi
2116 et al., 2009) continues to exist (Bakker et al., 2016, 2025a, Figure S5) and to lead to substantially higher
2117 uncertainty in the S_{OCEAN} estimate for the Southern Hemisphere (Watson et al., 2020, Gloege et al.,
2118 2021, Hauck et al., 2023a). This discrepancy, which also hampers model improvement, points to the
2119 need for increased high-quality fCO_2 observations especially in the Southern Ocean. At the same time,

2120 model uncertainty is illustrated by the large spread of individual GOBM estimates (indicated by
2121 shading in Figure 14) and highlights the need for model improvement, now also supported by the
2122 IOMB benchmarking. The issue of diverging trends in S_{OCEAN} from different methods remains a matter
2123 of concern. Recent and on-going work suggests that the $f\text{CO}_2$ -products may overestimate the trend
2124 although biases in the $f\text{CO}_2$ -product ensemble may partly cancel out (Supplement section S3.4). A data-
2125 constrained model approach suggests that the GOBMs underestimate the amplitude of decadal
2126 variability, but that the $f\text{CO}_2$ -products overestimate the trend (Mayot et al., 2024). The various methods,
2127 now also including ocean interior observation-based estimates, agree within uncertainties on the mean
2128 ocean sink in the last decade, although the independent estimate from atmospheric oxygen
2129 measurements still shows the largest sink estimate for the past decade and has a steeper trend (Table 6).
2130 However, the estimate is consistent within uncertainties with S_{OCEAN} , with the relatively larger ocean
2131 sink in the $f\text{CO}_2$ -products and some of the GOBMs. The assessment of the net land-atmosphere
2132 exchange from DGVMs and atmospheric inversions also shows substantial discrepancy, particularly for
2133 the estimate of the net land flux over the northern extra-tropic. This discrepancy highlights the
2134 difficulty to quantify complex processes (CO_2 fertilisation, nitrogen deposition and fertilisers, climate
2135 change and variability, land management, etc.) that collectively determine the net land CO_2 flux.
2136 Resolving the differences in the Northern Hemisphere land sink will require the consideration and
2137 inclusion of larger volumes of observations.

2138 The adjustments introduced in this budget for S_{LAND} and S_{OCEAN} to account for known biases (RSS for
2139 DGVMs, cold skin/warm layer for $f\text{CO}_2$ products, ocean sink underestimation for GOBMs) lead to a
2140 smaller net land sink ($S_{\text{LAND-ELUC}}$) and a larger ocean sink (S_{OCEAN}), more in line with the atmospheric
2141 inversions and independent oxygen based estimates (Table 7), and also consistent with a recent study
2142 based on satellite derived changes in aboveground biomass over the 2000-2019 period (Randerson et
2143 al., 2025).

2144 We provide metrics for the evaluation of the ocean and land models and the atmospheric inversions
2145 (Figure S6-S8 and S13, Table S12). These metrics expand the use of observations in the global carbon
2146 budget, helping 1) to support improvements in the ocean and land carbon models that produce the sink
2147 estimates, and 2) to constrain the representation of key underlying processes in the models and to
2148 allocate the regional partitioning of the CO_2 fluxes. The use of process-based metrics in an objective
2149 evaluation framework (IOMB) targeted to evaluate the simulation of S_{OCEAN} in the ocean
2150 biogeochemistry models is an important advance. This is another step in the endeavour to use a broader
2151 range of observations and more stringent model evaluation that we hope will support continued
2152 improvements in the models and in the annual estimates of the global carbon budget.

2153 We assessed before that a sustained decrease of -1% in global emissions could be detected at the 66%
2154 likelihood level after a decade only (Peters et al., 2017a). Similarly, a change in behaviour of the land
2155 and/or ocean carbon sink would take as long to detect, and much longer if it emerges more slowly. To

2156 continue reducing the carbon imbalance on annual to decadal time scales, regionalising the carbon
2157 budget, and integrating multiple variables are powerful ways to shorten the detection limit and ensure
2158 the research community can rapidly identify issues of concern in the evolution of the global carbon
2159 cycle under the current rapid and unprecedented changing environmental conditions.

2160 **6 Conclusions**

2161 The estimation of global CO₂ emissions and sinks is a major effort by the carbon cycle research
2162 community that requires a careful compilation and synthesis of measurements, statistical estimates, and
2163 model results. The delivery of an annual carbon budget serves two purposes. First, there is a large
2164 demand for up-to-date information on the state of the anthropogenic perturbation of the climate system
2165 and its underpinning causes. A broad stakeholder community relies on the datasets associated with the
2166 annual carbon budget including scientists, policy makers, businesses, journalists, and non-governmental
2167 organisations engaged in adapting to and mitigating human-driven climate change. Second, over the last
2168 decades we have seen unprecedented changes in the human and biophysical environments (e.g.,
2169 changes in the growth of fossil fuel emissions, impact of COVID-19 pandemic, Earth's warming,
2170 extreme events, and strength of the carbon sinks), which call for frequent assessments of the state of the
2171 planet, a better quantification of the causes of changes in the contemporary global carbon cycle, and an
2172 improved capacity to anticipate its evolution in the future. Building this scientific understanding to meet
2173 the extraordinary climate mitigation challenge requires frequent, robust, transparent, and traceable
2174 datasets and methods that can be scrutinised and replicated. This paper via 'living data' helps to keep
2175 track of new budget updates.

2176 **7 Data availability**

2177 The data presented here are made available in the belief that their wide dissemination will lead to
2178 greater understanding and new scientific insights of how the carbon cycle works, how humans are
2179 altering it, and how we can mitigate the resulting human-driven climate change. Full contact details and
2180 information on how to cite the data shown here are given at the top of each page in the accompanying
2181 database and summarised in Table 2.

2182 The accompanying database includes three Excel files organised in the following spreadsheets:

2183 File `Global_Carbon_Budget_2025v1.0.xlsx` includes the following:

- 2184 1. Summary
- 2185 2. The global carbon budget (1959-2024);
- 2186 3. The historical global carbon budget (1750-2024);

- 2187 4. Global CO₂ emissions from fossil fuels and cement production by fuel type, and the per-capita
2188 emissions (1850-2024);
- 2189 5. CO₂ emissions from land-use change from the individual bookkeeping models (1959-2024);
- 2190 6. Ocean CO₂ sink from the individual global ocean biogeochemistry models and f CO₂-products
2191 (1959-2024);
- 2192 7. Terrestrial CO₂ sink from the individual DGVMs (1959-2024);
- 2193 8. Cement carbonation CO₂ sink (1959-2024).

2194 File National_Fossil_Carbon_Emissions_2025v1.0.xlsx includes the following:

- 2195 1. Summary
- 2196 2. Territorial country CO₂ emissions from fossil fuels and cement production (1850-2024);
- 2197 3. Consumption country CO₂ emissions from fossil fuels and cement production and emissions
2198 transfer from the international trade of goods and services (1990-2020) using CDIAC/UNFCCC
2199 data as reference;
- 2200 4. Emissions transfers (Consumption minus territorial emissions; 1990-2020);
- 2201 5. Country definitions.

2202 File National_LandUseChange_Carbon_Emissions_2024v1.0.xlsx includes the following:

- 2203 1. Summary
- 2204 2. Territorial country CO₂ emissions from Land Use Change (1850-2024) from three bookkeeping
2205 models;

2206 All three spreadsheets are published by the Integrated Carbon Observation System (ICOS) Carbon
2207 Portal and are available at <https://doi.org/10.18160/GCP-2025> (Friedlingstein et al., 2025c). National
2208 emissions data are also available at <https://doi.org/10.5281/zenodo.5569234> (Andrew and Peters, 2025),
2209 from the Global Carbon Atlas (<http://www.globalcarbonatlas.org/>, last access: 23 October 2025) and
2210 from Our World in Data (<https://ourworldindata.org/co2-emissions>, last access: 23 October 2025).

2211 **Author contributions**

2212 PF, MOS, MWJ, DCEB, RMA, JH, PL, CLQ, HL, ITL, GPP, WP, JP, CSc, and SS designed the study,
2213 conducted the analysis, and wrote the paper with input from JGC and PC. RMA, GPP, JIK and TK

2214 produced the fossil CO₂ emissions and their uncertainties and analysed the emissions data. ME and GM
2215 provided fossil fuel emission data. ZL provided the Carbon Monitor fossil emission projection. JP, CSc,
2216 TG and ZQ provided the bookkeeping land-use change emissions with synthesis by JP and CSc. KH
2217 and JDM provided the estimates of non-vegetation CDR fluxes. LB, MAC, ÖG, NG, TI, TJ, LR, JS,
2218 RS, and HTs provided an update of the global ocean biogeochemical models; LD, DJF, MG, LG, YI,
2219 AJ, GMK, CR, JZ, and PC provided an update of the ocean fCO₂-data products, with synthesis on both
2220 streams by JH, PL and AR. SRA, LBa, NRB, AB, CFB, MC, MPE, KE, WE, RAF, TGk, CL, NM,
2221 DRM, SN, AO, AMO, DP, GR, IS, AJS, CSw, ST, BT, SJvdV, EVO, and RW provided ocean fCO₂
2222 measurements for the year 2024, with synthesis by DCEB and SDJ. KA, PA, THC, JHE, AFo, BG, JG,
2223 AI, AKJ, EK, JK, EM, JM, LM, TN, QS, TLS, HT, APW, WY, XYa, XYu and CK provided an update
2224 of the Dynamic Global Vegetation Models, with synthesis by SS and MOS. RB, FF, HL, VS, DS, and
2225 HiT provided estimates of land and ocean sinks from Earth System Models, as well as a projection of
2226 the atmospheric growth rate for 2025, with synthesis by HL. FC, NC, LF, ARJ, FJ, ITL, JL, LRN, YN,
2227 CR, XT, YK, and ZL provided an updated atmospheric inversion, WP, FC, and ITL developed the
2228 protocol and produced the synthesis and evaluation of the atmospheric inversions. EJM and RFK
2229 provided the atmospheric oxygen estimate of surface net carbon sinks. RMA provided projections of
2230 the 2025 fossil emissions and atmospheric CO₂ growth rate. PL provided the predictions of the 2025
2231 ocean sink. IBMB, LPC, KKG, GCH, TMR and GRvdW provided forcing data for land-use change. FT
2232 and GG provided data for the land-use change NGHGI harmonisation. XL provided the atmospheric
2233 CO₂ data. SP provided the satellite OCO-2 atmospheric CO₂ growth rate. MWJ provided the historical
2234 atmospheric CO₂ concentration and growth rate. IH provided the climate forcing data for the DGVMs.
2235 NP provided the nitrogen fertilizer forcing data for the DGVMs. MOS and NB produced the aerosol
2236 diffuse radiative forcing for the DGVMs. PCM provided the iLAMB evaluation of the DGVMs. NOC
2237 and MGS provided the iOMB evaluation of the GOBMs. PR provided the historical land carbon export
2238 estimate, MWJ provided the emissions prior for use in the inversion systems. XD provided seasonal
2239 emissions data, based on GRACED (Global gridded daily CO₂ emissions dataset), for most recent years
2240 for the emission prior. PF, MO and MWJ coordinated the effort, revised all figures, tables, text and

2241 numbers to ensure the update was clear from the 2024 edition and in line with the
2242 globalcarbonatlas.org.

2243

2244 **Competing interests.**

2245 At least one of the authors is a member of the editorial board of Earth System Science Data

2246

2247 **Acknowledgements**

2248 First, we wish to thank Richard ‘Skee’ Houghton for his tremendous contribution to the Global Carbon
2249 Budget since its inception, pioneering the estimate of land use change emissions with bookkeeping
2250 models. We thank all people and institutions who provided the data used in this global carbon budget
2251 2025 and the Global Carbon Project members for their input throughout the development of this
2252 publication. We thank Christian Ethé, Xavier Perrot, Damian Loher, Fatemeh Chegini, Fabrice Lacroix,
2253 Yangyang Zhao, Paridhi Rustogi, Sarah Berthet, Aurore Voldoire, Laurent Oziel, T. Toyoda, Y.
2254 Kitamura, K. Toyama, H. Nakano, L. S. Urakawa, Philip Townsend, Nathaniel O. Collier, Min Xu, James
2255 D. Shutler, Andrew J. Watson, T. Holding, I.G.C. Ashton, D. K. Woolf, Lonneke Goddijn-Murphy,
2256 Richard Sims, Stefanie Falk, Pengyue Du, Peter Lawrence, Sean Swenson, Daniel Kennedy, Sam Levis,
2257 Erik Kluzek, Lachlan Whyborn, Drew Holzworth, Ian Harman, Naiqing Pan, Shufen Pan for their
2258 involvement in the development, use, and analysis of the models and data products used here. We thank
2259 Kim Currie, Hannelore Theetaert, and Coraline Leseurre who contributed to the provision of surface
2260 ocean CO₂ observations for the year 2024 (see Table S8). We also thank Kevin O'Brien and Eugene
2261 Burger of NOAA's Pacific Marine Environmental Laboratory and Alex Kozyr of NOAA's National
2262 Centers for Environmental Information, for their contribution to surface ocean CO₂ data and metadata
2263 management. We thank the scientists, institutions, and funding agencies responsible for the collection
2264 and quality control of the data in SOCAT as well as the International Ocean Carbon Coordination Project
2265 (IOCCP) and the Surface Ocean Lower Atmosphere Study (SOLAS) program for their support. ITL and
2266 WP thank the CarbonTracker Europe team at Wageningen University, including Remco de Kok, Joram
2267 Hooghiem and Auke van der Woude. The inverse modelling team thanks all data providers of
2268 atmospheric CO₂ data provided through multiple ObsPack products. HL thanks Tatiana Ilyina for
2269 supporting the coordination of ESMs' contributions to GCBs, and Sebastian Brune and Kristina Frölich
2270 for helping with the MPI-ESM1-2-LR assimilation. Zhangcai Qin thanks Ziwang Fu and Dr. Yakun Zhu
2271 for contributing to LUCE modeling. We thank Ram Alkama and Simone Rossi for helping in filtering
2272 S_{LAND} data from DGVMs with managed forest area and Joana Melo for extracting and processing data

2273 from NGHGs. FT acknowledges support of member countries to the FAO regular budget and
2274 FAOSTAT. The conclusions in this paper are the authors' only and do not represent FAO views and
2275 position on the subject matter. This is PMEL contribution 5802. MC thanks Tobias Steinhoff (MACID),
2276 Lukasz Pawlikowski, Ian Murphy and Gordon Furey (P&O Maritime Services), and Aodhan Fitzgerald
2277 (Marine Institute) for their support. TG and the VLIZ team are thankful to the management group and
2278 crew of the research vessels Simon Stevin, Skagerak and Neil Armstrong for all the support and help they
2279 provided. pCO₂ measurements on the Marion Dufresne were collected in the frame of the French
2280 COOL/OISO long-term monitoring program with support from the National Institute of Sciences of the
2281 Universe (INSU), the French Polar Institute (IPEV) and the French Oceanographic Fleet (FOF). AMO
2282 thanks the captain and crew on the Sea-Cargo Express for their help. DP would like to thank Kevin
2283 Sullivan for processing and quality controlling AOML data and facilitating submission to SOCATv2025.
2284 GR thanks the "Finnmaid science and tech-teams" at IOW and SYKE for their support, and is indebted
2285 to the crew of the ship and the people involved at Finnlines. IS thanks the captain and crew on the G. O.
2286 Sars for their help. BT and EvO thank Australia's Integrated Marine Observing System (IMOS) for
2287 sourcing CO₂ data. IMOS is enabled by the National Collaborative Research Infrastructure Strategy
2288 (NCRIS). SJV thanks Andrew Marriner for maintaining the pCO₂ underway system on the RV Tangaroa.
2289 PCM thanks Tristan Quaife, Eddy Robertson, Emily Black and Anthony Walker for support. FC thanks
2290 Adrien Martinez who maintained the atmospheric transport model for the CAMS inversion. We
2291 acknowledge the contributions of Jeongmin Yun, Anthony Bloom, and Kevin Bowman to the CMS-Flux
2292 inversion submission. YN thanks Suman Maity who performed the NISMON-GOSAT inversion. LF
2293 thanks Paul I. Palmer and acknowledges ongoing support from the National Centre for Earth Observation.
2294 Xiangjun Tian thanks Zhe Jin, Yilong Wang, Hongqin Zhang, Min Zhao, Tao Wang, Jinzhi Ding, and
2295 Shilong Piao for their contributions to the GONGGA inversion system. We thank Ning Zeng, Yun Liu,
2296 Eugenia Kalnay, and Gassem Asrar for their contributions to the COLA system. CarbonTracker CT2025
2297 results provided by NOAA GML, Boulder, Colorado, USA from the website at
2298 <http://carbontracker.noaa.gov>. FJ thanks Weimin Ju for running the BEPS model. LN thanks Shamil
2299 Maksyutov, Rajesh Janardanan and Tsuneo Matsunaga for contributing to NTFVAR inverse model study.
2300 YK acknowledges Bo Zheng from Tsinghua University for his contribution to the THU inversion system.
2301 RSA thanks William Merryfield, Woosung Lee, Jason Cole for their help to set up and produce the model
2302 runs. The IPSL contribution was achieved thanks to the valuable contributions of Patricia Cadule, Juliette
2303 Mignot and Olivier Torres. GAM acknowledges contributions from Amanda Fay to updating the LDEO-
2304 HPD fCO₂ product. JRM thanks Gesa Meyer for assistance setting up the DGVM simulations. LMD
2305 thanks Pedro. M. S. Monteiro (SCS-SU) and Sandy Thomalla (SOCCO-CSIR) for their continued support
2306 to make the CSIR-ML6 fCO₂-product up-to-date. CFB is grateful to the technicians and crew of the
2307 research vessel Víctor Angelescu for all the support and assistance they provided. This is INIDEP
2308 contribution 2460.

2309

2310

Financial and computing support

2311 This research was supported by the following sources of funding: Instituto Nacional de Investigación y
2312 Desarrollo Pesquero (INIDEP) (Argentina); Joint Technical Commission of the Maritime Front
2313 (CTMFM, Argentina-Uruguay) (Argentina); Integrated Marine Observing System (IMOS) (Australia);
2314 National Environmental Science Program (NESP) (Australia); Research Foundation Flanders (grant no.
2315 I001821N) (Belgium); ICOS (Integrated Carbon Observing System) Belgium (Belgium); Tula
2316 Foundation (Canada); National Key Research and Development Program of China (grant no.
2317 2023YFF0805400) (China); Copernicus Atmosphere Monitoring Service, implemented by ECMWF on
2318 behalf of the European Commission (Grant no. CAMS2 55 bis) (EC); European Research Council (ERC-
2319 2022-STG OceanPeak, grant 101077209) (EC); Horizon Europe (NextGenCarbon: grant no. 101184989)
2320 (EC); Horizon Europe (RESCUE: grant no. 101056939) (EC); Horizon 2020 (ESM2025: grant no.
2321 101003536) (EC); Horizon Europe (TRICUSO: grant no. 101199028) (EC); Horizon Europe
2322 (GreenFeedBack: grant no. 101056921) (EC); H2020 (JERICO-S3: grant no. 871153) (EC); Horizon
2323 Europe (GEORGE: grant no. 101094716) (EC); Horizon Europe (AI4PEX: grant no.101137682) (EC); ;
2324 MOB TAC project of the European Copernicus Marine Environment Monitoring Service (EC); Horizon
2325 Europe (TipESM: grant no. 101137673) (EC); European Union under grant agreement no. 101083922
2326 (OceanICU) and UK Research and Innovation (UKRI) under the UK government's Horizon Europe
2327 funding guarantee [grant number 10054454, 10063673, 10064020, 10059241, 10079684, 10059012,
2328 10048179]. Views and opinions expressed are however those of the author(s) only and do not necessarily
2329 reflect those of the European Union or European Research Executive Agency. Neither the European
2330 Union nor the granting authority can be held responsible for them; Climate Space RECCAP-2 (grant no.
2331 4000144908/24/1-LR) (European Space Agency); EO-LINCS (European Space Agency); Ocean Carbon
2332 for Climate (grant no. 3-18399/24/I-NB) (European Space Agency); Satellite-based observations of
2333 Carbon in the Ocean: Pools, Fluxes and Exchanges (grant no. 4000142532/23/I-DT) (European Space
2334 Agency); THRAC3E (grant no. 4000149569/25/I-AG) (European Space Agency); ; ICOS Germany
2335 (Germany); Federal Ministry of Education and Research (BMBF) (STEPSEC: grant no. 01LS2102A)
2336 (Germany); Marine Institute (Ireland); Japan Meteorological Agency (Japan); Global Environmental
2337 Research Coordination System, Ministry of the Environment (grant nos. E2152 and E2252) (Japan);
2338 NIES GOSAT Project (Japan); the Environment Research and Technology Development Fund
2339 (JPMEERF24S12200) of the Environmental Restoration and Conservation Agency provided by Ministry
2340 of the Environment of Japan (Japan); Environment Research and Technology Development Fund (grant
2341 no. JPMEERF24S12205, Co-PI: P. K. Patra) of the Environmental Restoration and Conservation Agency
2342 of Japan, and the Arctic Challenge for Sustainability phase III project (ArCS-3; grant no.
2343 JPMXD1720251001; Co-PI: P. K. Patra) (Japan); Environment Research and Technology Development
2344 Fund (grant no. JPMEERF24S12206) of the Environmental Restoration and Conservation Agency of
2345 Japan (Japan); Ministry of Business, Innovation and Employment (Strategic Science Investment Fund
2346 via the NIWA Ocean-Climate Interaction programme) (New Zealand); Research Council of Norway

2347 (ICOS-3, grant no. 350341) (Norway); Research Council of Norway (grant no. 352474) (Norway);
2348 Research Council of Norway (grant no. 352204) (Norway); South African Department of Science,
2349 Technology and Innovation (grant no. DSI/CON C3184/2023) (South Africa); UK Research and
2350 Innovation (Horizon Europe GreenFeedBack: grant no. 10040851) (UK); NCAS at the University of
2351 Reading (UK); NERC NE/V011103/1 “Frontiers of instability in marine ecosystems and carbon
2352 export”UK Natural Environment Research Council (NE/V01417X/1) (UK); Department of Energy,
2353 Office of Science, Office of Biological and Environmental Research (USA); NOAA (Global Ocean
2354 Monitoring and Observing Program: Open Funder Registry no. 100018302) (USA); NOAA (Ocean
2355 Acidification Program: Open Funder Registry no. 100018228) (USA); NOAA (Cooperative Agreement
2356 NA20OAR4320472) (USA); NOAA (Cooperative Agreement NA-03-AR4320179) (USA); Alaska
2357 Ocean Observing System (USA); NASA Carbon Monitoring System (grant no. 80NSSC25K7221)
2358 (USA); NASA Early Career Investigator Program in Earth Science (grant no. 80NSSC24K1632) (USA);
2359 NASA Land Cover and Land Use Change Program (Grants: 80NSSC24K0920 and 80NSSC25K7497)
2360 (USA); NSF (Cooperative Agreement No. 1852977) (USA); NASA Orbiting Carbon Observatory
2361 Science Team Program (grant no. NNH23ZDA001N-OCOST) (USA); NASA Carbon Monitoring
2362 System (grant no.NNH22ZDA001N-CMS) (USA); Work of J.L. and S.P. was conducted at the Jet
2363 Propulsion Laboratory, California Institute of Technology, under a contract with the National Aeronautics
2364 and Space Administration (80NM0018D0004) (USA); NOAA (Cooperative Institute for Marine, Earth
2365 and Atmospheric Systems, Award No. NA25NMF432C0003-T1-01) (USA); NSF (OPP-2329254)
2366 (USA); ORNL is managed by UT-Battelle, LLC, for the DOE (grant no. DE-AC05-1008 00OR22725)
2367 (USA); Schmidt Sciences (VESRI CALIPSO) (USA); Schmidt Sciences (OBVI InMOS) (USA); NSF
2368 (OPP-1922922) (USA); NOAA grant NA24NESX432C0001 (Cooperative Institute for Satellite Earth
2369 System Studies - CISESS) (USA); NOAA cooperative agreement NA22OAR4320151 (CIRES: Andrew
2370 Jacobson and Xin Lan) (USA); Schmidt Sciences (CLARiTy project, part of the Virtual Institute for the
2371 Carbon Cycle) (USA); Schmidt Sciences (COCO2 project, part of the Virtual Institute for the Carbon
2372 Cycle) (USA); NSF (LEAP STC Award no 2019625) (USA); NASA (grant no. 80NSSC22K0150)
2373 (USA); NOAA (GOMO, grant no. NA24OARX431G0151-T1-01) (USA).

2374 The US National Science Foundation (grant nos. OPP-1922922, OPP-2329254), a NOAA cooperative
2375 agreement, the Cooperative Institute for Marine, Earth and Atmospheric Systems (CIMEAS, grant nos.
2376 NA20OAR4320278-T1-01 and NA25NMF432C0003-T3-01S022); although NSF grants 1922922 and
2377 2329254 and NOAA grants NA20OAR4320278-T1-01 and NA25NMF432C0003-T3-01S022 have
2378 been identified for conflict of interest management based on the overall scope of the project and its
2379 potential benefit to the Keeling Curve Foundation, the research findings included in this particular
2380 publication may not necessarily relate to the interests of Keeling Curve Foundation. The terms of this
2381 arrangement have been reviewed and approved by the University of California, San Diego in accordance
2382 with its conflict of interest policies.

2383 We also acknowledge support from the following computing facilities: Australian Community Climate
2384 and Earth System Simulator – National Research Infrastructure (ACCESS-NRI) (Australia); National
2385 Computational Infrastructure (NCI) (Australia); High-Performance Computing Center (HPCC) of
2386 Nanjing University for doing the inversions on its blade cluster system (China); HPC computing and
2387 storage resources by GENCI at IDRIS and TGCC thanks to the grant 2024-2201 on the supercomputers
2388 Jean Zay's V100 and Joliot Curie's SKL and V100 partitions. (France); The ORCHIDEE simulations
2389 were performed using HPC resources from GENCI-TGCC on grant 2024-00006328 (France); IPSL
2390 Climate Modelling Centre (<https://mesocentre.ipsl.fr>) (France); HPC resources from GENCI - TGCC
2391 (Grant A005-017403) (France); Deutsches Klimarechenzentrum (DKRZ) (Projects: bm0891, bm1124
2392 and bg1446) (Germany); NIES Supercomputer system, GOSAT Supercomputing Facility (GOFC)
2393 (Japan); NEC SX-Aurora TSUBASA at NIES (Japan);Fugaku provided by the RIKEN Center for
2394 Computational Science (Project ID: hp250024) (Japan); JAMSTEC's ES4 Super Computer system
2395 (Japan); Sigma2 - the National Infrastructure for High-Performance Computing and Data Storage in
2396 Norway (Norway); NICIS Centre for High-Performance Computing (South Africa); UK CEDA JASMIN
2397 supercomputer (UK); Compute and Data Environment for Science (CADES) at the Oak Ridge National
2398 Laboratory (USA); LEAP Pangeo cloud platform (USA);NASA Ames Supercomputers (USA).

- 2400 Andela, N., Morton, D. C., Giglio, L., Chen, Y., van der Werf, G. R., Kasibhatla, P. S., DeFries, R. S., Collatz, G.
2401 J., Hantson, S., Kloster, S., Bachelet, D., Forrest, M., Lasslop, G., Li, F., Mangeon, S., Melton, J. R., Yue, C., and
2402 Randerson, J. T.: A human-driven decline in global burned area, *Science*, 356, 1356–1362,
2403 <https://doi.org/10.1126/science.aal4108>, 2017.
- 2404 Andrew, R. M.: A comparison of estimates of global carbon dioxide emissions from fossil carbon sources, *Earth*
2405 *Syst. Sci. Data*, 12, 1437–1465, <https://doi.org/10.5194/essd-12-1437-2020>, 2020a.
- 2406 Andrew, R. M.: Timely estimates of India's annual and monthly fossil CO₂ emissions, *Earth Syst. Sci. Data*, 12,
2407 2411–2421, <https://doi.org/10.5194/essd-12-2411-2020>, 2020b.
- 2408 Andrew, R. M.: Towards near real-time, monthly fossil CO₂ emissions estimates for the European Union with
2409 current-year projections, *Atmospheric Pollution Research*, 12, 101229, <https://doi.org/10.1016/j.apr.2021.101229>,
2410 2021.
- 2411 Andrew, R. M., & Peters, G. P.: The Global Carbon Project's fossil CO₂ emissions dataset (Version 251022) [Data
2412 set]. Zenodo. <https://doi.org/10.5281/zenodo.5569234>, 2025.
- 2413 Aragão, L. E. O. C., Anderson, L. O., Fonseca, M. G., Rosan, T. M., Vedovato, L. B., Wagner, F. H., Silva, C. V.
2414 J., Silva Junior, C. H. L., Arai, E., Aguiar, A. P., Barlow, J., Berenguer, E., Deeter, M. N., Domingues, L. G., Gatti,
2415 L., Gloor, M., Malhi, Y., Marengo, J. A., Miller, J. B., Phillips, O. L., and Saatchi, S.: 21st Century drought-related
2416 fires counteract the decline of Amazon deforestation carbon emissions, *Nat Commun*, 9, 536,
2417 <https://doi.org/10.1038/s41467-017-02771-y>, 2018.
- 2418 Archer, D., Eby, M., Brovkin, V., Ridgwell, A., Cao, L., Mikolajewicz, U., Caldeira, K., Matsumoto, K.,
2419 Munhoven, G., Montenegro, A., and Tokos, K.: Atmospheric Lifetime of Fossil Fuel Carbon Dioxide, *Annu. Rev.*
2420 *Earth Planet. Sci.*, 37, 117–134, <https://doi.org/10.1146/annurev.earth.031208.100206>, 2009.
- 2421 Arneth, A., Sitch, S., Pongratz, J., Stocker, B. D., Ciais, P., Poulter, B., Bayer, A. D., Bondeau, A., Calle, L., Chini,
2422 L. P., Gasser, T., Fader, M., Friedlingstein, P., Kato, E., Li, W., Lindeskog, M., Nabel, J. E. M. S., Pugh, T. A. M.,
2423 Robertson, E., Viovy, N., Yue, C., and Zaehle, S.: Historical carbon dioxide emissions caused by land-use changes
2424 are possibly larger than assumed, *Nature Geosci*, 10, 79–84, <https://doi.org/10.1038/ngeo2882>, 2017.
- 2425 Asaadi, A., Arora, V. K., Melton, J. R., and Bartlett, P.: An improved parameterization of leaf area index (LAI)
2426 seasonality in the Canadian Land Surface Scheme (CLASS) and Canadian Terrestrial Ecosystem Model (CTEM)
2427 modelling framework, 15, 6885–6907, <https://doi.org/10.5194/bg-15-6885-2018>, 2018.
- 2428 Aumont, O., Orr, J. C., Monfray, P., Ludwig, W., Amiotte-Suchet, P., and Probst, J.-L.: Riverine-driven
2429 interhemispheric transport of carbon, *Global Biogeochem. Cycles*, 15, 393–405,
2430 <https://doi.org/10.1029/1999GB001238>, 2001.
- 2431 Aumont, O., Ethé, C., Tagliabue, A., Bopp, L., and Gehlen, M.: PISCES-v2: an ocean biogeochemical model for
2432 carbon and ecosystem studies, 8, 2465–2513, <https://doi.org/10.5194/gmd-8-2465-2015>, 2015.
- 2433 Babiker, M., G. Berndes, K. Blok, B. Cohen, A. Cowie, O. Geden, V. Ginzburg, A. Leip, P. Smith, M. Sugiyama,
2434 F. Yamba, Al Khourdajie, A., Arneth, A., Lima de Azevedo, I. M., Bataille, C., Beerling, D., Bezner Kerr, R.,
2435 Bradley, J., Buck, H. J., Cabeza, L. F., Calvin, K., Campbell, D., Carnicer Cols, J., Daioglou, V., Harmsen, M.,
2436 Höglund-Isaksson, L., House, J. I., Keller, D., de Kleijne, K., Kugelberg, S., Makarov, I., Meza, F., Minx, J. C.,
2437 Morecroft, M., Nabuurs, G. J., Neufeldt, H., Novikova, A., Nugroho, S. B., Oshlies, A., Parmesan, C., Peters, G.
2438 P., Poore, J., Portugal-Pereira, J., Postigo, J. C., Pradhan, P., Renforth, P., Rivera-Ferre, M. G., Roe, S., Singh, P.
2439 K., Slade, R., Smith, S. M., Tirado von der Pahlen, M. C., and Toribio Ramirez, D.: Cross sectoral perspectives. In:
2440 *Climate Change 2022: Mitigation of Climate Change. Contribution of Working Group III to the Sixth Assessment*
2441 *Report of the Intergovernmental Panel on Climate Change* [P.R. Shukla, J. Skea, R. Slade, A. Al Khourdajie, R.
2442 van Diemen, D. McCollum, M. Pathak, S. Some, P. Vyas, R. Fradera, M. Belkacemi, A. Hasija, G. Lisboa, S. Luz,
2443 J. Malley, (eds.)]. Cambridge University Press, Cambridge, UK and New York, NY, USA. doi:
2444 10.1017/9781009157926.014, 2022.

- 2445 Baccini, A., Walker, W., Carvalho, L., Farina, M., Sulla-Menashe, D., and Houghton, R. A.: Tropical forests are a
 2446 net carbon source based on aboveground measurements of gain and loss, *Science*, 358, 230–234,
 2447 <https://doi.org/10.1126/science.aam5962>, 2017.
- 2448 Bakker, D. C. E., Pfeil, B., Landa, C. S., Metz, N., O'Brien, K. M., Olsen, A., Smith, K., Cosca, C., Harasawa, S.,
 2449 Jones, S. D., Nakaoka, S., Nojiri, Y., Schuster, U., Steinhoff, T., Sweeney, C., Takahashi, T., Tilbrook, B., Wada,
 2450 C., Wanninkhof, R., Alin, S. R., Balestrini, C. F., Barbero, L., Bates, N. R., Bianchi, A. A., Bonou, F., Boutin, J.,
 2451 Bozec, Y., Burger, E. F., Cai, W.-J., Castle, R. D., Chen, L., Chierici, M., Currie, K., Evans, W., Featherstone, C.,
 2452 Feely, R. A., Fransson, A., Goyet, C., Greenwood, N., Gregor, L., Hankin, S., Hardman-Mountford, N. J., Harlay,
 2453 J., Hauck, J., Hoppema, M., Humphreys, M. P., Hunt, C. W., Huss, B., Ibáñez, J. S. P., Johannessen, T., Keeling,
 2454 R., Kitidis, V., Körtzinger, A., Kozyr, A., Krasakopoulou, E., Kuwata, A., Landschützer, P., Lauvset, S. K.,
 2455 Lefèvre, N., Lo Monaco, C., Manke, A., Mathis, J. T., Merlivat, L., Monteiro, F. J., Monteiro, P. M. S., Munro, D.
 2456 R., Murata, A., Newberger, T., Omar, A. M., Ono, T., Paterson, K., Pearce, D., Pierrot, D., Robbins, L. L., Saito,
 2457 S., Salisbury, J., Schlitzer, R., Schneider, B., Schweitzer, R., Sieger, R., Skjelvan, I., Sullivan, K. F., Sutherland, S.
 2458 C., Sutton, A. J., Tadokoro, K., Telszewski, M., Tuma, M., van Heuven, S. M. A. C., Vandemark, D., Ward, B.,
 2459 Watson, A. J., and Xu, S.: A multi-decade record of high-quality CO₂ data in version 3 of the Surface Ocean CO₂
 2460 Atlas (SOCAT), *Earth Syst. Sci. Data*, 8, 383–413, <https://doi.org/10.5194/essd-8-383-2016>, 2016.
- 2461 Bakker, D. C. E., Alin, S. R., Aramaki, T., Barbero, L., Bates, N. R., Gkritzalis, T., Jones, S. D., Kozyr, A.,
 2462 Lauvset, S. K., Macovei, V., Metz, N., Munro, D. R., Nakaoka, S.-i., O'Brien, K. M., Olsen, A., Pierrot, D.,
 2463 Steinhoff, T., Sullivan, K. F., Sutton, A. J., Sweeney, C., Wada, C., Wanninkhof, R., Akl, J., Arbilla, L. A., Azetsu-
 2464 Scott, K., Battisti, R., Beatty, C. M., Becker, M., Benoit-Cattin, A., Berghoff, C. F., Bittig, H. C., Bonin, J. A.,
 2465 Bott, R., Bozzano, R., Burger, E. F., Brunetti, F., Cantoni, C., Castelli, G., Chambers, D. P., Chierici, M., Corbo,
 2466 A., Cronin, M., Cross, J. N., Currie, K. I., Dentico, C., Emerson, S. R., Enochs, I., Enright, M. P., Enyo, K.,
 2467 Ericson, Y., Evans, W., Fay, A. R., Feely, R. A., Fragiaco, E., Fransson, A., Gehrung, M., Giani, M., Glockzin,
 2468 M., Hamna, S., Holodkov, N., Hoppema, M., Ibáñez, J. S. P., Kadono, K., Kamb, L., Kralj, M., Kristensin, T. O.,
 2469 Laudicella, V. A., Lefèvre, N., Leseurre, C., Lo Monaco, C., Maenner Jones, S. M., Maenza, R. A., McAuliffe, A.
 2470 M., Mdokwana, B. W., Monacci, N. M., Musielewicz, S., Neill, C., Newberger, T., Nojiri, Y., Ohman, M. D.,
 2471 Ólafsdóttir, S. R., Olivier, L., Omar, A., Osborne, J., Pensieri, S., Petersen, W., Plueddemann, A. J., Rehder, G.,
 2472 Roden, N. P., Rutgersson, A., Sallée, J.-B., Sanders, R., Sarpe, D., Schirnik, C., Schlitzer, R., Send, U., Skjelvan,
 2473 I., Sutherland, S., C., T'Jampens, M., Tamsitt, V., Telszewski, M., Theetaert, H., Tilbrook, B., Trull, T., Tsanwani,
 2474 M., Van de Velde, S., Van Heuven, S. M. A. C., Vecchia, M. H., Voynova, Y. G., Weller, R. A., Williams, N. L.:
 2475 Surface Ocean CO₂ Atlas Database Version 2025 (SOCATv2025) (NCEI Accession 0304549), NOAA National
 2476 Centers for Environmental Information, Dataset, <https://doi.org/10.25921/648f-fv35>, 2025a.
- 2477 Bakker, D. C. E., Alin, S. R., Aramaki, T., Barbero, L., Bates, N. R., Gkritzalis, T., Jones, S. D., Kozyr, A.,
 2478 Lauvset, S. K., Macovei, V. A., Metz, N., Munro, D. R., Nakaoka, S. i., O'Brien, K. M., Olsen, A., Pierrot, D.,
 2479 Steinhoff, T., Sullivan, K. F., Sutton, A. J., Sweeney, C., Wada, C., Wanninkhof, R.: SOCAT version 2025: Open
 2480 ocean CO₂ data submissions stabilise, <https://socat.info/index.php/posters/>, Poster published on 05/06/2025. Last
 2481 access 23 October 2025, 2025b.
- 2482 Ballantyne, A. P., Alden, C. B., Miller, J. B., Tans, P. P., and White, J. W. C.: Increase in observed net carbon
 2483 dioxide uptake by land and oceans during the past 50 years, *Nature*, 488, 70–72,
 2484 <https://doi.org/10.1038/nature11299>, 2012.
- 2485 Ballantyne, A. P., Andres, R., Houghton, R., Stocker, B. D., Wanninkhof, R., Anderegg, W., Cooper, L. A.,
 2486 DeGrandpre, M., Tans, P. P., Miller, J. B., Alden, C., and White, J. W. C.: Audit of the global carbon budget:
 2487 estimate errors and their impact on uptake uncertainty, *Biogeosciences*, 12, 2565–2584, <https://doi.org/10.5194/bg-12-2565-2015>, 2015.
- 2489 Bar-On, Y. M., Li, X., O'Sullivan, M., Wigneron, J.-P., Sitch, S., Ciais, P., Frankenberg, C., Fischer, W. W.: Recent
 2490 gains in global terrestrial carbon stocks are mostly stored in nonliving pools, *Science* 387, 1291–1295, 2025.
- 2491 Bastos, A., Hartung, K., Nützel, T. B., Nabel, J. E. M. S., Houghton, R. A., and Pongratz, J.: Comparison of
 2492 uncertainties in land-use change fluxes from bookkeeping model parameterisation, 12, 745–762,
 2493 <https://doi.org/10.5194/esd-12-745-2021>, 2021.
- 2494 Battle, M. O., Raynor, R., Kesler, S., and Keeling, R.: Technical Note: The impact of industrial activity on the
 2495 amount of atmospheric O₂, *Atmospheric Chem. Phys. Discuss.*, 1–17, <https://doi.org/10.5194/acp-2022-765>, 2023.

- 2496 Bellenger, H., Bopp, L., Ethé, C., Ho, D., Duvel, J. P., Flavoni, S., Guez, L., Kataoka, T., Perrot, X., Parc, L., and
2497 Watanabe, M.: Sensitivity of the Global Ocean Carbon Sink to the Ocean Skin in a Climate Model, *J. Geophys.*
2498 *Res. Oceans*, 128, e2022JC019479, <https://doi.org/10.1029/2022JC019479>, 2023.
- 2499 Bennington, V., Gloege, L., and McKinley, G. A.: Variability in the Global Ocean Carbon Sink From 1959 to 2020
2500 by Correcting Models with Observations, *Geophys. Res. Lett.*, 49, e2022GL098632,
2501 <https://doi.org/10.1029/2022GL098632>, 2022.
- 2502 Bernardello, R., Sicardi, V., Lapin, V., Ortega, P., Ruprich-Robert, Y., Tourigny, E. and Ferrer, E.: Ocean
2503 biogeochemical reconstructions to estimate historical ocean CO₂ uptake. *Earth System Dynamics*, 15(5), pp.1255-
2504 1275, <https://doi.org/10.5194/esd-15-1255-2024>, 2024.
- 2505 Berthet, S., Séférian, R., Bricaud, C., Chevallier, M., Voltaire, A., and Ethé, C.: Evaluation of an Online Grid-
2506 Coarsening Algorithm in a Global Eddy-Admitting Ocean Biogeochemical Model, *J. Adv. Model Earth Sy.*, 11,
2507 1759–1783, <https://doi.org/10.1029/2019MS001644>, 2019.
- 2508 Bethke, I., Wang, Y., Counillon, F., Keenlyside, N., Kimmritz, M., Fransner, F., Samuelsen, A., Langehaug, H.,
2509 Svendsen, L., Chiu, P.-G., Passos, L., Bentsen, M., Guo, C., Gupta, A., Tjiputra, J., Kirkevåg, A., Olivé, D.,
2510 Seland, Ø., Solsvik Vågane, J., Fan, Y., and Eldevik, T.: NorCPM1 and its contribution to CMIP6 DCPP, *Geosci.*
2511 *Model Dev.*, 14, 7073–7116, <https://doi.org/10.5194/gmd-14-7073-2021>, 2021.
- 2512 Betts, R. A., Jones, C. D., Knight, J. R., Keeling, R. F., and Kennedy, J. J.: El Niño and a record CO₂ rise, *Nat.*
2513 *Clim. Change*, 6, 806–810, <https://doi.org/10.1038/nclimate3063>, 2016.
- 2514 Bilbao, R., Wild, S., Ortega, P., Acosta-Navarro, J., Arsouze, T., Bretonnière, P.A., Caron, L.P., Castrillo, M.,
2515 Cruz-García, R., Cvijanovic, I. and Doblas-Reyes, F.J.: Assessment of a full-field initialised decadal climate
2516 prediction system with the CMIP6 version of EC-Earth. *Earth System Dynamics Discussions*, 2020, pp.1-30,
2517 <https://doi.org/10.5194/esd-12-173-2021>, 2020.
- 2518 Bloom, A. A. and Williams, M.: Constraining ecosystem carbon dynamics in a data-limited world: integrating
2519 ecological “common sense” in a model–data fusion framework, *Biogeosciences*, 12, 1299–1315,
2520 <https://doi.org/10.5194/bg-12-1299-2015>, 2015.
- 2521 Bloom, A. A., Exbrayat, J.-F., van der Velde, I. R., Feng, L., and Williams, M.: The decadal state of the terrestrial
2522 carbon cycle: Global retrievals of terrestrial carbon allocation, pools, and residence times, *Proc. Natl. Acad. Sci.*,
2523 113, 1285–1290, <https://doi.org/10.1073/pnas.1515160113>, 2016.
- 2524 Boer, G. J., Smith, D. M., Cassou, C., Doblas-Reyes, F., Danabasoglu, G., Kirtman, B., Kushnir, Y., Kimoto, M.,
2525 Meehl, G. A., Msadek, R., Mueller, W. A., Taylor, K. E., Zwiers, F., Rixen, M., Ruprich-Robert, Y., and Eade, R.:
2526 The Decadal Climate Prediction Project (DCPP) contribution to CMIP6, *Geosci. Model Dev.*, 9, 3751–3777,
2527 <https://doi.org/10.5194/gmd-9-3751-2016>, 2016.
- 2528 Boucher, O., Servonnat, J., Albright, A. L., Aumont, O., Balkanski, Y., Bastrikov, V., Bekki, S., Bonnet, R., Bony,
2529 S., Bopp, L., Braconnot, P., Brockmann, P., Cadule, P., Caubel, A., Cheruy, F., Codron, F., Cozic, A., Cugnet, D.,
2530 D’Andrea, F., Davini, P., de Lavergne, C., Denvil, S., Deshayes, J., Devilliers, M., Ducharne, A., Dufresne, J.-L.,
2531 Dupont, E., Ethé, C., Fairhead, L., Falletti, L., Flavoni, S., Foujols, M.-A., Gardoll, S., Gastineau, G., Ghattas, J.,
2532 Grandpeix, J.-Y., Guenet, B., Guez, E., Lionel, Guilyardi, E., Guimberteau, M., Hauglustaine, D., Hourdin, F.,
2533 Idelkadi, A., Joussaume, S., Kageyama, M., Khodri, M., Krinner, G., Lebas, N., Levvasseur, G., Lévy, C., Li, L.,
2534 Lott, F., Lurton, T., Luyssaert, S., Madec, G., Madeleine, J.-B., Maignan, F., Marchand, M., Marti, O., Mellul, L.,
2535 Meurdesoif, Y., Mignot, J., Musat, I., Ottlé, C., Peylin, P., Planton, Y., Polcher, J., Rio, C., Rochetin, N., Rousset,
2536 C., Sepulchre, P., Sima, A., Swingedouw, D., Thiéblemont, R., Traore, A. K., Vancoppenolle, M., Vial, J., Vialard,
2537 J., Viovy, N., and Vuichard, N.: Presentation and Evaluation of the IPSL-CM6A-LR Climate Model, *J. Adv.*
2538 *Model. Earth Syst.*, 12, e2019MS002010, <https://doi.org/10.1029/2019MS002010>, 2020.
- 2539 Bourgeois, T., Goris, N., Schwinger, J., and Tjiputra, J. F.: Stratification constrains future heat and carbon uptake
2540 in the Southern Ocean between 30°S and 55°S, *Nat. Commun.*, 13, 340, <https://doi.org/10.1038/s41467-022-27979-5>, 2022.
- 2542 Bourgoïn, C., Beuchle, R., Branco, A., Carreiras, J., Ceccherini, G., Oom, D., San-Miguel-Ayanz, J., and Sedano,
2543 F.: Extensive fire-driven degradation in 2024 marks worst Amazon forest disturbance in over 2 decades,
2544 *Biogeosciences*, 22, 5247–5256, <https://doi.org/10.5194/bg-22-5247-2025>, 2025.

- 2545 Bray, E.: 2017 Minerals Yearbook: Aluminum [Advance Release], Tech. rep., U.S. Geological Survey, <https://d9-wret.s3-us-west-2.amazonaws.com/assets/palladium/production/atoms/files/myb1-2017-alumi.pdf>, 2020.
- 2547 Brienens, R. J. W., Caldwell, L., Duchesne, L., Voelker, S., Barichivich, J., Baliva, M., Ceccantini, G., Di Filippo,
2548 A., Helama, S., Locosselli, G. M., Lopez, L., Piovesan, G., Schöngart, J., Villalba, R., and Gloor, E.: Forest carbon
2549 sink neutralized by pervasive growth-lifespan trade-offs, *Nat. Commun.*, 11, 4241, <https://doi.org/10.1038/s41467-020-17966-z>, 2020.
- 2551 Brienens, R. J. W., Phillips, O. L., Feldpausch, T. R., Gloor, E., Baker, T. R., Lloyd, J., Lopez-Gonzalez, G.,
2552 Monteagudo-Mendoza, A., Malhi, Y., Lewis, S. L., Vásquez Martínez, R., Alexiades, M., Álvarez Dávila, E.,
2553 Alvarez-Loayza, P., Andrade, A., Aragão, L. E. O. C., Araujo-Murakami, A., Arets, E. J. M. M., Arroyo, L.,
2554 Aymard C., G. A., Bánki, O. S., Baraloto, C., Barroso, J., Bonal, D., Boot, R. G. A., Camargo, J. L. C., Castilho, C.
2555 V., Chama, V., Chao, K. J., Chave, J., Comiskey, J. A., Cornejo Valverde, F., da Costa, L., de Oliveira, E. A., Di
2556 Fiore, A., Erwin, T. L., Fauset, S., Forsthofer, M., Galbraith, D. R., Grahame, E. S., Groot, N., Hérault, B.,
2557 Higuchi, N., Honorio Coronado, E. N., Keeling, H., Killeen, T. J., Laurance, W. F., Laurance, S., Licona, J.,
2558 Magnussen, W. E., Marimon, B. S., Marimon-Junior, B. H., Mendoza, C., Neill, D. A., Nogueira, E. M., Núñez, P.,
2559 Pallqui Camacho, N. C., Parada, A., Pardo-Molina, G., Peacock, J., Peña-Claros, M., Pickavance, G. C., Pitman, N.
2560 C. A., Poorter, L., Prieto, A., Quesada, C. A., Ramírez, F., Ramírez-Angulo, H., Restrepo, Z., Roopsind, A., Rudas,
2561 A., Salomão, R. P., Schwarz, M., Silva, N., Silva-Espejo, J. E., Silveira, M., Stropp, J., Talbot, J., ter Steege, H.,
2562 Teran-Aguilar, J., Terborgh, J., Thomas-Caesar, R., Toledo, M., Torello-Raventos, M., Umetsu, R. K., van der
2563 Heijden, G. M. F., van der Hout, P., Guimarães Vieira, I. C., Vieira, S. A., Vilanova, E., Vos, V. A., and Zagt, R.
2564 J.: Long-term decline of the Amazon carbon sink, 519, 344–348, <https://doi.org/10.1038/nature14283>, 2015.
- 2565 Bronselaer, B., Winton, M., Russell, J., Sabine, C. L., and Khatiwala, S.: Agreement of CMIP5 Simulated and
2566 Observed Ocean Anthropogenic CO₂ Uptake, *Geophys. Res. Lett.*, 44, 12,298–12,305,
2567 <https://doi.org/10.1002/2017GL074435>, 2017.
- 2568 Bruno, M. and Joos, F.: Terrestrial carbon storage during the past 200 years: A Monte Carlo Analysis of CO₂ data
2569 from ice core and atmospheric measurements, *Global Biogeochem. Cycles*, 11, 111–124,
2570 <https://doi.org/10.1029/96GB03611>, 1997.
- 2571 Burrows, S. M., Maltrud, M., Yang, X., Zhu, Q., Jeffery, N., Shi, X., Ricciuto, D., Wang, S., Bisht, G., Tang, J.,
2572 Wolfe, J., Harrop, B. E., Singh, B., Brent, L., Baldwin, S., Zhou, T., Cameron-Smith, P., Keen, N., Collier, N., Xu,
2573 M., Hunke, E. C., Elliott, S. M., Turner, A. K., Li, H., Wang, H., Golaz, J.-C., Bond-Lamberty, B., Hoffman, F. M.,
2574 Riley, W. J., Thornton, P. E., Calvin, K., and Leung, L. R.: The DOE E3SM v1.1 Biogeochemistry Configuration:
2575 Description and Simulated Ecosystem-Climate Responses to Historical Changes in Forcing, *J. Adv. Model. Earth
2576 Syst.*, 12, e2019MS001766, <https://doi.org/10.1029/2019MS001766>, 2020.
- 2577 Bunsen, F., Nissen, C., and Hauck, J.: The Impact of Recent Climate Change on the Global Ocean Carbon Sink.
2578 *Geophysical Research Letters*, 51(4), e2023GL107030, <https://doi.org/10.1029/2023GL107030>, 2024.
- 2579 Burton, C., Betts, R., Cardoso, M., Feldpausch, T. R., Harper, A., Jones, C. D., Kelley, D. I., Robertson, E., and
2580 Wiltshire, A.: Representation of fire, land-use change and vegetation dynamics in the Joint UK Land Environment
2581 Simulator vn4.9 (JULES), *Geosci. Model Dev.*, 12, 179–193, <https://doi.org/10.5194/gmd-12-179-2019>, 2019.
- 2582 Burton, C., Lampe, S., Kelley, D. I., Thiery, W., Hantson, S., Christidis, N., Gudmundsson, L., Forrest, M., Burke,
2583 E., Chang, J., Huang, H., Ito, A., Kou-Giesbrecht, S., Lasslop, G., Li, W., Nieradzik, L., Li, F., Chen, Y.,
2584 Randerson, J., Reyer, C. P. O., and Mengel, M.: Global burned area increasingly explained by climate change,
2585 *Nature Climate Change*, <https://doi.org/10.1038/s41558-024-02140-w>, 2024.
- 2586 Bushinsky, S. M., Landschützer, P., Rödenbeck, C., Gray, A. R., Baker, D., Mazloff, M. R., Resplandy, L.,
2587 Johnson, K. S., and Sarmiento, J. L.: Reassessing Southern Ocean Air-Sea CO₂ Flux Estimates With the Addition
2588 of Biogeochemical Float Observations, *Global Biogeochem. Cycles*, 33, 1370–1388,
2589 <https://doi.org/10.1029/2019GB006176>, 2019.
- 2590 Byrne, B., Liu, J., Bowman, K. W., Pascolini-Campbell, M., Chatterjee, A., Pandey, S., Miyazaki, K., van der Werf,
2591 G. R., Wunch, D., Wennberg, P. O., Roehl, C. M., and Sinha, S.: Carbon emissions from the 2023 Canadian
2592 wildfires. *Nature*, 633, 835–839, <https://doi.org/10.1038/s41586-024-07878-z>, 2024.
- 2593 Canadell, J. G., Le Quere, C., Raupach, M. R., Field, C. B., Buitenhuis, E. T., Ciais, P., Conway, T. J., Gillett, N.
2594 P., Houghton, R. A., and Marland, G.: Contributions to accelerating atmospheric CO₂ growth from economic

- 2595 activity, carbon intensity, and efficiency of natural sinks, *Proceedings of the National Academy of Sciences*, 104,
2596 18866–18870, <https://doi.org/10.1073/pnas.0702737104>, 2007.
- 2597 Canadell, J. G., Monteiro, P. M. S., Costa, M. H., Cotrim da Cunha, L., Cox, P. M., Eliseev, A. V., Henson, S.,
2598 Ishii, M., Jaccard, S., Koven, C., Lohila, A., Patra, P. K., Piao, S., Rogelj, J., Syampungani, S., Zaehle, S., and
2599 Zickfeld, K.: Global Carbon and other Biogeochemical Cycles and Feedbacks. In: *Climate Change 2021: The
2600 Physical Science Basis. Contribution of Working Group I to the Sixth Assessment Report of the Intergovernmental
2601 Panel on Climate Change* [Masson-Delmotte, V., P. Zhai, A. Pirani, S. L. Connors, C. Péan, S. Berger, N. Caud, Y.
2602 Chen, L. Goldfarb, M. I. Gomis, M. Huang, K. Leitzell, E. Lonnoy, J.B.R. Matthews, T. K. Maycock, T.
2603 Waterfield, O. Yelekçi, R. Yu and B. Zhou (eds.)]. Cambridge University Press, Cambridge, United Kingdom and
2604 New York, NY, USA, pp. 673–816, <https://doi.org/10.1017/9781009157896.007>, 2021.
- 2605 Cao, Z., Myers, R. J., Lupton, R. C., Duan, H., Sacchi, R., Zhou, N., Reed Miller, T., Cullen, J. M., Ge, Q., and
2606 Liu, G.: The sponge effect and carbon emission mitigation potentials of the global cement cycle, *Nat Commun*, 11,
2607 3777, <https://doi.org/10.1038/s41467-020-17583-w>, 2020.
- 2608 Carbon Monitor: Year in Review: Global carbon emissions and decarbonization in 2024, available at:
2609 <https://carbonmonitor.org/>, last access: 23 October 2025, 2025.
- 2610 Centro Nacional de Monitoramento e Alertas de Desastres Naturais (CEMADEN): Monitoramento de secas e
2611 impactos no Brasil - Agosto 2024, available at: [https://www.gov.br/cemaden/pt-
2612 br/assuntos/monitoramento/monitoramento-de-seca-para-o-brasil/monitoramento-de-secas-e-impactos-no-brasil-
2613 agosto-2024](https://www.gov.br/cemaden/pt-br/assuntos/monitoramento/monitoramento-de-seca-para-o-brasil/monitoramento-de-secas-e-impactos-no-brasil-agosto-2024), last access: 23 October 2025.
- 2614 Céspedes, J., Sylvester, J. M., Pérez-Marulanda, L., Paz-García, P., Reymondin, L., Khodadadi, M., Tello, J. J., and
2615 Castro-Nunez, A.: Has global deforestation accelerated due to the COVID-19 pandemic?, *J. For. Res.*, 34, 1153–
2616 1165, <https://doi.org/10.1007/s11676-022-01561-7>, 2023.
- 2617 Chandra, N., Patra, P. K., Niwa, Y., Ito, A., Iida, Y., Goto, D., Morimoto, S., Kondo, M., Takigawa, M., Hajima,
2618 T., and Watanabe, M.: Estimated regional CO₂ flux and uncertainty based on an ensemble of atmospheric CO₂
2619 inversions, *Atmospheric Chem. Phys.*, 22, 9215–9243, <https://doi.org/10.5194/acp-22-9215-2022>, 2022.
- 2620 Chatfield, C.: The Holt-Winters Forecasting Procedure, *J. Roy. Stat. Soc. C.*, 27, 264–279,
2621 <https://doi.org/10.2307/2347162>, 1978.
- 2622 Chau, T. T. T., Gehlen, M., and Chevallier, F.: A seamless ensemble-based reconstruction of surface ocean pCO₂
2623 and air–sea CO₂ fluxes over the global coastal and open oceans, *Biogeosciences*, 19, 1087–1109,
2624 <https://doi.org/10.5194/bg-19-1087-2022>, 2022.
- 2625 Chen, Y., Hall, J., Van Wees, D., Andela, N., Hantson, S., Giglio, L., Van Der Werf, G. R., Morton, D. C., and
2626 Randerson, J. T.: Multi-decadal trends and variability in burned area from the fifth version of the Global Fire
2627 Emissions Database (GFED5), *Earth Syst. Sci. Data*, 15, 5227–5259, <https://doi.org/10.5194/essd-15-5227-2023>,
2628 2023.
- 2629 Chevallier, F., Fisher, M., Peylin, P., Serrar, S., Bousquet, P., Bréon, F.-M., Chédin, A., and Ciais, P.: Inferring CO
2630 2 sources and sinks from satellite observations: Method and application to TOVS data, *J. Geophys. Res.*, 110,
2631 D24309, <https://doi.org/10.1029/2005JD006390>, 2005.
- 2632 Chevallier, F., Martinez, A., Lloret, Z., Takache, S., and Cozic, A.: Offline Atmospheric Transport on a Global
2633 Mesh of Hexagons, *JGR Atmospheres*, 130, e2025JD043579, <https://doi.org/10.1029/2025JD043579>, 2025.
- 2634 Ciais, P., Sabine, C., Bala, G., Bopp, L., Brovkin, V., Canadell, J. G., Chhabra, A., DeFries, R., Galloway, J.,
2635 Heimann, M., Jones, C., Le Quéré, C., Myneni, R., Piao, S., Thornton, P., Willem, J., Friedlingstein, P., and
2636 Munhoven, G.: Carbon and Other Biogeochemical Cycles, in *Climate Change 2013: The Physical Science Basis,
2637 Contribution of Working Group I to the Fifth Assessment Report of the Intergovernmental Panel on Climate
2638 Change*, edited by: Intergovernmental Panel on Climate Change, Cambridge University Press, Cambridge, United
2639 Kingdom and New York, NY, USA, <https://doi.org/10.1017/CBO9781107415324.015>, 2013.
- 2640 Ciais, P., Tan, J., Wang, X., Roedenbeck, C., Chevallier, F., Piao, S.-L., Moriarty, R., Broquet, G., Le Quéré, C.,
2641 Canadell, J. G., Peng, S., Poulter, B., Liu, Z., and Tans, P.: Five decades of northern land carbon uptake revealed
2642 by the interhemispheric CO₂ gradient, *Nature*, 568, 221–225, <https://doi.org/10.1038/s41586-019-1078-6>, 2019.

- 2643 Ciais, P., Bastos, A., Chevallier, F., Lauerwald, R., Poulter, B., Canadell, P., Hugelius, G., Jackson, R. B., Jain, A.,
 2644 Jones, M., Kondo, M., Lujikx, I. T., Patra, P. K., Peters, W., Pongratz, J., Petrescu, A. M. R., Piao, S., Qiu, C., Von
 2645 Randow, C., Regnier, P., Saunois, M., Scholes, R., Shvidenko, A., Tian, H., Yang, H., Wang, X., and Zheng, B.:
 2646 Definitions and methods to estimate regional land carbon fluxes for the second phase of the REgional Carbon
 2647 Cycle Assessment and Processes Project (RECCAP-2), *Geosci. Model Dev.*, 15, 1289–1316,
 2648 <https://doi.org/10.5194/gmd-15-1289-2022>, 2022.
- 2649 Ciais, P., Ke, P., Yao, Y., Sitch, S., Li, W., Xu, Y., Du, X., Gui, X., Bastos, A., Zaehle, S., Poulter, B., Colligan, T.,
 2650 van der Woude, A. M., Peters, W., Liu, Z., Jin, Z., Tian, X., Wang, Y., Liu, J., Pandey, S., O'Dell, C., Bian, J.,
 2651 Zhou, C., Miller, J., Lan, X., Goncalves De Souza, J., O'Sullivan, M., Friedlingstein, P., van der Werf, G. R.,
 2652 Peters, G. P., and Chevallier, F.: Low latency global carbon budget indicates reduced land carbon sink in the year
 2653 2024, *National Science Review*, submitted.
- 2654 Collier, N., Hoffman, F. M., Lawrence, D. M., Keppel-Aleks, G., Koven, C. D., Riley, W. J., Mu, M., and
 2655 Randerson, J. T.: The International Land Model Benchmarking (ILAMB) System: Design, Theory, and
 2656 Implementation, *J. Adv. Model. Earth Syst.*, 10, 2731–2754, <https://doi.org/10.1029/2018MS001354>, 2018.
- 2657 Conchedda, G. and Tubiello, F. N.: Drainage of organic soils and GHG emissions: Validation with country data,
 2658 *Biosphere – Biogeosciences*, <https://doi.org/10.5194/essd-2020-202>, 2020.
- 2659 Cox, P. M., Pearson, D., Booth, B. B., Friedlingstein, P., Huntingford, C., Jones, C. D., and Luke, C. M.:
 2660 Sensitivity of tropical carbon to climate change constrained by carbon dioxide variability, *Nature*, 494, 341–344,
 2661 <https://doi.org/10.1038/nature11882>, 2013.
- 2662 De Kauwe, M. G., Medlyn, B. E., Zaehle, S., Walker, A. P., Dietze, M. C., Wang, Y.-P., Luo, Y., Jain, A. K., El-
 2663 Masri, B., Hickler, T., Wårlind, D., Weng, E., Parton, W. J., Thornton, P. E., Wang, S., Prentice, I. C., Asao, S.,
 2664 Smith, B., McCarthy, H. R., Iversen, C. M., Hanson, P. J., Warren, J. M., Oren, R., and Norby, R. J.: Where does
 2665 the carbon go? A model–data intercomparison of vegetation carbon allocation and turnover processes at two
 2666 temperate forest free-air CO₂ enrichment sites, *New Phytol.*, 203, 883–899, <https://doi.org/10.1111/nph.12847>,
 2667 2014.
- 2668 Delire, C., Séférian, R., Decharme, B., Alkama, R., Calvet, J.-C., Carrer, D., Gibelin, A.-L., Joetzjer, E., Morel, X.,
 2669 Rocher, M., and Tzanos, D.: The Global Land Carbon Cycle Simulated With ISBA-CTRIP: Improvements Over
 2670 the Last Decade, *J. Adv. Model. Earth Syst.*, 12, e2019MS001886, <https://doi.org/10.1029/2019MS001886>, 2020.
- 2671 Denman, K. L., Brasseur, G., Chidthaisong, A., Ciais, P., Cox, P. M., Dickinson, R. E., Hauglustaine, D., Heinze,
 2672 C., Holland, E., Jacob, D., Lohmann, U., Ramachandran, S., Leite da Silva Dias, P., Wofsy, S. C., and Zhang, X.:
 2673 Couplings Between Changes in the Climate System and Biogeochemistry, in: *Climate Change 2007: The Physical
 2674 Science Basis. Contribution of Working Group I to the Fourth Assessment Report of the Intergovernmental Panel
 2675 on Climate Change*, edited by: Solomon, S., Qin, D., Manning, M., Marquis, M., Averyt, K., Tignor, M. M. B.,
 2676 Miller, H. L., and Chen, Z. L., Cambridge University Press, Cambridge, UK and New York, USA, 499–587, ISBN:
 2677 9780521705967, 2007.
- 2678 Denvil-Sommer, A., Gehlen, M., and Vrac, M.: Observation system simulation experiments in the Atlantic Ocean
 2679 for enhanced surface ocean pCO₂ reconstructions, *Ocean Sci.*, 17, 1011–1030, [https://doi.org/10.5194/os-17-1011-](https://doi.org/10.5194/os-17-1011-2021)
 2680 2021, 2021.
- 2681 DeVries, T., Holzer, M., and Primeau, F.: Recent increase in oceanic carbon uptake driven by weaker upper-ocean
 2682 overturning, *Nature*, 542, 215–218, <https://doi.org/10.1038/nature21068>, 2017.
- 2683 DeVries, T.: The oceanic anthropogenic CO₂ sink: Storage, air-sea fluxes, and transports over the industrial era,
 2684 *Global Biogeochem. Cycles*, 28, 631–647, <https://doi.org/10.1002/2013GB004739>, 2014.
- 2685 DeVries, T., Quéré, C. L., Andrews, O., Berthet, S., Hauck, J., Ilyina, T., Landschützer, P., Lenton, A., Lima, I. D.,
 2686 Nowicki, M., Schwinger, J., and Séférian, R.: Decadal trends in the ocean carbon sink, *PNAS*, 116, 11646–11651,
 2687 <https://doi.org/10.1073/pnas.1900371116>, 2019.
- 2688 DeVries, T.: Atmospheric CO₂ and Sea Surface Temperature Variability Cannot Explain Recent Decadal
 2689 Variability of the Ocean CO₂ Sink, *Geophysical Research Letters*, 49, e2021GL096018,
 2690 <https://doi.org/10.1029/2021GL096018>, 2022.

- 2691 DeVries, T., Yamamoto, K., Wanninkhof, R., Gruber, N., Hauck, J., Müller, J. D., Bopp, L., Carroll, D., Carter, B.,
2692 Chau, T.-T., Doney, S. C., Gehlen, M., Gloege, L., Gregor, L., Henson, S., Kim, J. H., Iida, Y., Ilyina, T.,
2693 Landschützer, P., Le Quéré, C., Munro, D., Nissen, C., Patara, L., Pérez, F. F., Resplandy, L., Rodgers, K. B.,
2694 Schwinger, J., Séférian, R., Sicardi, V., Terhaar, J., Triñanes, J., Tsujino, H., Watson, A., Yasunaka, S., and Zeng,
2695 J.: Magnitude, trends, and variability of the global ocean carbon sink from 1985-2018, *Glob. Biogeochem. Cycles*,
2696 n/a, e2023GB007780, <https://doi.org/10.1029/2023GB007780>, 2023.
- 2697 Döscher, R., Acosta, M., Alessandri, A., Anthoni, P., Arneth, A., Arsouze, T., Bergmann, T., Bernadello, R.,
2698 Boussetta, S., Caron, L.P. and Carver, G.: The EC-earth3 Earth system model for the climate model intercomparison
2699 project 6. *Geoscientific Model Development Discussions*, 2021, pp.1-90, [https://doi.org/10.5194/gmd-15-2973-](https://doi.org/10.5194/gmd-15-2973-2022)
2700 2022, 2021.
- 2701 Doney, S. C., Lima, I., Feely, R. A., Glover, D. M., Lindsay, K., Mahowald, N., Moore, J. K., and Wanninkhof, R.:
2702 Mechanisms governing interannual variability in upper-ocean inorganic carbon system and air–sea CO₂ fluxes:
2703 Physical climate and atmospheric dust, *Deep Sea Research Part II: Topical Studies in Oceanography*, 56, 640–655,
2704 <https://doi.org/10.1016/j.dsr2.2008.12.006>, 2009.
- 2705 Dong, Y., Bakker, D. C. E., Bell, T. G., Huang, B., Landschützer, P., Liss, P. S., and Yang, M.: Update on the
2706 Temperature Corrections of Global Air–Sea CO₂ Flux Estimates, *Glob. Biogeochem. Cycles*, 36, e2022GB007360,
2707 <https://doi.org/10.1029/2022GB007360>, 2022.
- 2708 Dong, Y., Bakker, D. C. E., Bell, T. G., Yang, M., Landschützer, P., Hauck, J., Rödenbeck, C., Kitidis, V.,
2709 Bushinsky, S. M., and Liss, P. S. (2024). Direct observational evidence of strong CO₂ uptake in the Southern
2710 Ocean. *Science Advances*, 10(30), eadn5781, <https://doi.org/10.1126/sciadv.adn5781>, 2024a.
- 2711 Dong, Y., Bakker, D. C. E., and Landschützer, P.: Accuracy of ocean CO₂ uptake estimates at a risk by a reduction
2712 in the data collection. *Geophysical Research Letters*, 51, e2024GL108502, <https://doi.org/10.1029/2024GL108502>,
2713 2024b.
- 2714 Dorgeist, L., Schwingshackl, C., Bultan, S., and Pongratz, J.: A consistent budgeting of terrestrial carbon fluxes.
2715 *Nature Communications*, 15(1), 7426, <https://doi.org/10.1038/s41467-024-51126-x>, 2024.
- 2716 Dou, X., Wang, Y., Ciais, P., Chevallier, F., Davis, S. J., Crippa, M., Janssens-Maenhout, G., Guizzardi, D.,
2717 Solazzo, E., Yan, F., Huo, D., Zheng, B., Zhu, B., Cui, D., Ke, P., Sun, T., Wang, H., Zhang, Q., Gentile, P., Deng,
2718 Z., and Liu, Z.: Near-real-time global gridded daily CO₂ emissions, *The Innovation*, 3, 100182,
2719 <https://doi.org/10.1016/j.xinn.2021.100182>, 2022.
- 2720 Eckes-Shephard, A. H., Argles, A. P. K., Brzeziecki, B., Cox, P. M., De Kauwe, M. G., Esquivel-Muelbert, A.,
2721 Fisher, R. A., Hurtt, G. C., Knauer, J., Koven, C. D., Lehtonen, A., Luyssaert, S., Marqués, L., Ma, L., Marie, G.,
2722 Moore, J. R., Needham, J. F., Olin, S., Peltoniemi, M., Piltz, K., Sato, H., Sitch, S., Stocker, B. D., Weng, E.,
2723 Zuleta, D., and Pugh, T. A. M. Pugh: Demography, dynamics and data: building confidence for simulating changes
2724 in the world’s forests, *New Phytologist*, doi: 10.1111/nph.70643, 2025.
- 2725 Edson, J. B., Jampana, V., Weller, R. A., Bigorre, S. P., Plueddemann, A. J., Fairall, C. W., Miller, S. D., Mahrt,
2726 L., Vickers, D., and Hersbach, H.: On the Exchange of Momentum over the Open Ocean, *J. Phys. Oceanogr.*, 43,
2727 1589–1610, <https://doi.org/10.1175/JPO-D-12-0173.1>, 2013.
- 2728 EIA: Short-Term Energy Outlook: March 2026. U.S. Energy Information Administration [Data set]. Available at:
2729 <http://www.eia.gov/forecasts/steo/outlook.cfm>, last access: 23 March 2026, 2023.
- 2730 Embury, O., Merchant, C.J., Good, S.A., Rayner, N.A., Hoyer, J.L., Atkinson, C., Block, T., Alerskans, E.,
2731 Pearson, K.J., Worsfold, M. and McCarroll, N. and Donlon, C.: Satellite-based time-series of sea-surface
2732 temperature since 1980 for climate applications. *Scientific Data*, 11(1), 326, [https://doi.org/10.1038/s41597-024-](https://doi.org/10.1038/s41597-024-03147-w)
2733 03147-w, 2024.
- 2734 Erb, K.-H., Kastner, T., Luyssaert, S., Houghton, R. A., Kuemmerle, T., Olofsson, P., and Haberl, H.: Bias in the
2735 attribution of forest carbon sinks, *Nature Clim Change*, 3, 854–856, <https://doi.org/10.1038/nclimate2004>, 2013.
- 2736 Erb, K.-H., Kastner, T., Plutzer, C., Bais, A. L. S., Carvalhais, N., Fetzel, T., Gingrich, S., Haberl, H., Lauk, C.,
2737 Niedertscheider, M., Pongratz, J., Thurner, M., and Luyssaert, S.: Unexpectedly large impact of forest management
2738 and grazing on global vegetation biomass, *Nature*, 553, 73–76, <https://doi.org/10.1038/nature25138>, 2018.

- 2739 Erb, M. and Marland G.: Global, Regional, and National Fossil-Fuel CO₂ Emissions: 1751–2022 CDIAC-FF,
2740 Research Institute for Environment, Energy, and Economics, Appalachian State University.
2741 <https://ricee.appstate.edu/projects-programs/cdiac/>, last access: 23 October 2025, 2025.
- 2742 Eskander, S. M. S. U. and Fankhauser, S.: Reduction in greenhouse gas emissions from national climate legislation,
2743 *Nat. Clim. Chang.*, 10, 750–756, <https://doi.org/10.1038/s41558-020-0831-z>, 2020.
- 2744 Etheridge, D. M., Steele, L. P., Langenfelds, R. L., Francey, R. J., Barnola, J.-M., and Morgan, V. I.: Natural and
2745 anthropogenic changes in atmospheric CO₂ over the last 1000 years from air in Antarctic ice and firn, *J. Geophys.*
2746 *Res.*, 101, 4115–4128, <https://doi.org/10.1029/95JD03410>, 1996.
- 2747 FAO, Food and Agriculture Organization of the United Nations (FAO): Impact of the Ukraine-Russia conflict on
2748 global food security and related matters under the mandate of the Food and Agriculture Organization of the United
2749 Nations (FAO), Hundred and Seventieth Session of the Council, <https://www.fao.org/3/nj164en/nj164en.pdf>, last
2750 access: 23 October 2025, 2023.
- 2751 FAO: FAOSTAT Emissions from drained organic soils. Available at <http://www.fao.org/faostat/en/#data/GV>, last
2752 access: 23 October 2025, 2025a.
- 2753 FAO: Forest emissions and removals – Global, regional and country trends 1990–2025. FAOSTAT Analytical
2754 Briefs, No. 114. Rome., available at: <https://doi.org/10.4060/cd7163en>, last access: 23 October 2025, 2025b.
- 2755 FAO: Land statistics 2001–2023 – Global, regional and country trends. FAOSTAT Analytical Briefs, No.107.
2756 Rome, available at: <https://doi.org/10.4060/cd5765en>, last access: 23 October 2025, 2025c.
- 2757 FAO: FAOSTAT Emissions totals database, available at: <https://faostat.fao.org/internal/en/#data/GT>, FAO, Rome,
2758 , last access: 23 October 2025, 2025d.
- 2759 Fay, A. R., Gregor, L., Landschützer, P., McKinley, G. A., Gruber, N., Gehlen, M., Iida, Y., Laruelle, G. G.,
2760 Rödenbeck, C., Roobaert, A., and Zeng, J.: SeaFlux: harmonization of air–sea CO₂ fluxes from surface pCO₂ data
2761 products using a standardized approach, *Earth System Science Data*, 13, 4693–4710, [https://doi.org/10.5194/essd-](https://doi.org/10.5194/essd-13-4693-2021)
2762 [13-4693-2021](https://doi.org/10.5194/essd-13-4693-2021), 2021.
- 2763 Fay, A. R., McKinley, G. A., Lovenduski, N. S., Eddebbar, Y., Levy, M. N., Long, M. C., Olivarez, H. C., and
2764 Rustagi, R. R.: Immediate and Long-Lasting Impacts of the Mt. Pinatubo Eruption on Ocean Oxygen and Carbon
2765 Inventories. *Global Biogeochemical Cycles*, 37(2). <https://doi.org/10.1029/2022gb007513>, 2023.
- 2766 Fay, A. R., Carroll, D., McKinley, G. A., Menemenlis, D., and Zhang, H.: Scale-Dependent Drivers of Air-Sea
2767 CO₂ Flux Variability, *Geophysical Research Letters*, 51, e2024GL111911, <https://doi.org/10.1029/2024GL111911>,
2768 2024.
- 2769 Fay, A. R., Heimdal, T. H., Acquaviva, V., Shaum, A. P., and McKinley, G. A.: Sensitivity of Ocean Carbon Sink
2770 Estimates to Rare Observations, *Geophysical Research Letters*, 52, e2025GL117961,
2771 <https://doi.org/10.1029/2025GL117961>, 2025.
- 2772 Felzer, B. S.: Carbon, nitrogen, and water response to climate and land use changes in Pennsylvania during the
2773 20th and 21st centuries, *Ecological Modelling*, 240, 49–63, <https://doi.org/10.1016/j.ecolmodel.2012.05.003>, 2012.
- 2774 Felzer, B. S. and Jiang, M.: Effect of Land Use and Land Cover Change in Context of Growth Enhancements in the
2775 United States Since 1700: Net Source or Sink?, *JGR Biogeosciences*, 123, 3439–3457,
2776 <https://doi.org/10.1029/2017JG004378>, 2018.
- 2777 Felzer, B. S., Cronin, T. W., Melillo, J. M., Kicklighter, D. W., and Schlosser, C. A.: Importance of carbon-
2778 nitrogen interactions and ozone on ecosystem hydrology during the 21st century, *J. Geophys. Res.*, 114,
2779 2008JG000826, <https://doi.org/10.1029/2008JG000826>, 2009.
- 2780 Felzer, B. S., Cronin, T. W., Melillo, J. M., Kicklighter, D. W., Schlosser, C. A., and Dangal, S. R. S.: Nitrogen
2781 effect on carbon-water coupling in forests, grasslands, and shrublands in the arid western United States, *J.*
2782 *Geophys. Res.*, 116, G03023, <https://doi.org/10.1029/2010JG001621>, 2011.
- 2783 Feng, L., Palmer, P. I., Bösch, H., and Dance, S.: Estimating surface CO₂ fluxes from space-borne CO₂ dry air
2784 mole fraction observations using an ensemble Kalman Filter, *Atmospheric Chem. Phys.*, 9, 2619–2633,
2785 <https://doi.org/10.5194/acp-9-2619-2009>, 2009.

- 2786 Feng, L., Palmer, P. I., Parker, R. J., Deutscher, N. M., Feist, D. G., Kivi, R., Morino, I., and Sussmann, R.:
 2787 Estimates of European uptake of CO₂ inferred from GOSAT XCO₂ retrievals: sensitivity to measurement bias
 2788 inside and outside Europe, *Atmos. Chem. Phys.*, 16, 1289–1302, <https://doi.org/10.5194/acp-16-1289-2016>, 2016.
- 2789 Fisher, R. A., Muszala, S., Versteinstein, M., Lawrence, P., Xu, C., McDowell, N. G., Knox, R. G., Koven, C.,
 2790 Holm, J., Rogers, B. M., Spessa, A., Lawrence, D., and Bonan, G.: Taking off the training wheels: the properties of
 2791 a dynamic vegetation model without climate envelopes, *CLM4.5(ED)*, *Geosci. Model Dev.*, 8, 3593–3619,
 2792 <https://doi.org/10.5194/gmd-8-3593-2015>, 2015.
- 2793 Flanagan, D.: 2017 Minerals Yearbook: Copper [Advance Release], Tech. rep., U.S. Geological Survey,
 2794 <https://pubs.usgs.gov/myb/vol1/2017/myb1-2017-copper.pdf>, 2021.
- 2795 Ford, D. J., Blannin, J., Watts, J., Watson, A. J., Landschützer, P., Jersild, A., and Shutler, J. D.: A Comprehensive
 2796 Analysis of Air-Sea CO₂ Flux Uncertainties Constructed From Surface Ocean Data Products, *Global*
 2797 *Biogeochemical Cycles*, 38, e2024GB008188, <https://doi.org/10.1029/2024GB008188>, 2024.
- 2798 Ford, D.J., Shutler, J.D., Blanco-Sacristán, J. et al. Enhanced ocean CO₂ uptake due to near-surface temperature
 2799 gradients. *Nat. Geosci.* 17, 1135–1140 . <https://doi.org/10.1038/s41561-024-01570-7>, 2024a
- 2800 Ford, D. J., Shutler, J. D., Ashton, I., Sims, R. P., and Holding, T.: Recalculated (depth and temperature consistent)
 2801 surface ocean CO₂ atlas (SOCAT) version 2025 (v0-1), <https://doi.org/10.5281/ZENODO.15656803>, 2025.
- 2802 Forster, P. M., Smith, C., Walsh, T., Lamb, W. F., Lamboll, R., Cassou, C., Hauser, M., Hausfather, Z., Lee, J.-Y.,
 2803 Palmer, M. D., Von Schuckmann, K., Slangen, A. B. A., Szopa, S., Trewin, B., Yun, J., Gillett, N. P., Jenkins, S.,
 2804 Matthews, H. D., Raghavan, K., Ribes, A., Rogelj, J., Rosen, D., Zhang, X., Allen, M., Aleluia Reis, L., Andrew,
 2805 R. M., Betts, R. A., Borger, A., Broersma, J. A., Burgess, S. N., Cheng, L., Friedlingstein, P., Domingues, C. M.,
 2806 Gambarini, M., Gasser, T., Gütschow, J., Ishii, M., Kadow, C., Kennedy, J., Killick, R. E., Krummel, P. B., Liné,
 2807 A., Monselesan, D. P., Morice, C., Mühle, J., Naik, V., Peters, G. P., Pirani, A., Pongratz, J., Minx, J. C., Rigby,
 2808 M., Rohde, R., Savita, A., Seneviratne, S. I., Thorne, P., Wells, C., Western, L. M., Van Der Werf, G. R., Wijffels,
 2809 S. E., Masson-Delmotte, V., and Zhai, P.: Indicators of Global Climate Change 2024: annual update of key
 2810 indicators of the state of the climate system and human influence, *Earth Syst. Sci. Data*, 17, 2641–2680,
 2811 <https://doi.org/10.5194/essd-17-2641-2025>, 2025.
- 2812 Friedlingstein, P., Houghton, R. A., Marland, G., Hackler, J., Boden, T. A., Conway, T. J., Canadell, J. G.,
 2813 Raupach, M. R., Ciais, P., and Le Quéré, C.: Update on CO₂ emissions, *Nature Geosci.* 3, 811–812,
 2814 <https://doi.org/10.1038/ngeo1022>, 2010.
- 2815 Friedlingstein, P., Andrew, R. M., Rogelj, J., Peters, G. P., Canadell, J. G., Knutti, R., Luderer, G., Raupach, M. R.,
 2816 Schaeffer, M., van Vuuren, D. P., and Le Quéré, C.: Persistent growth of CO₂ emissions and implications for
 2817 reaching climate targets, *Nature Geosci.* 7, 709–715, <https://doi.org/10.1038/ngeo2248>, 2014.
- 2818 Friedlingstein, P., Jones, M. W., O’Sullivan, M., Andrew, R. M., Hauck, J., Peters, G. P., Peters, W., Pongratz, J.,
 2819 Sitch, S., Le Quéré, C., Bakker, D. C. E., Canadell, J. G., Ciais, P., Jackson, R. B., Athoni, P., Barbero, L., Bastos,
 2820 A., Bastrikov, V., Becker, M., Bopp, L., Buitenhuis, E., Chandra, N., Chevallier, F., Chini, L. P., Currie, K. I.,
 2821 Feely, R. A., Gehlen, M., Gilfillan, D., Gkritzalis, T., Goll, D. S., Gruber, N., Gutekunst, S., Harris, I., Haverd, V.,
 2822 Houghton, R. A., Hurtt, G., Ilyina, T., Jain, A. K., Joetzier, E., Kaplan, J. O., Kato, E., Klein Goldewijk, K.,
 2823 Korsbakken, J. I., Landschützer, P., Lauvset, S. K., Lefèvre, N., Lenton, A., Lienert, S., Lombardozi, D., Marland,
 2824 G., McGuire, P. C., Melton, J. R., Metzl, N., Munro, D. R., Nabel, J. E. M. S., Nakaoka, S.-I., Neill, C., Omar, A.
 2825 M., Ono, T., Peregon, A., Pierrot, D., Poulter, B., Rehder, G., Resplandy, L., Robertson, E., Rödenbeck, C.,
 2826 Séférian, R., Schwinger, J., Smith, N., Tans, P. P., Tian, H., Tilbrook, B., Tubiello, F. N., van der Werf, G. R.,
 2827 Wiltshire, A. J., and Zaehle, S.: Global Carbon Budget 2019, *Earth Syst. Sci. Data*, 11, 1783–1838,
 2828 <https://doi.org/10.5194/essd-11-1783-2019>, 2019.
- 2829 Friedlingstein, P., O’Sullivan, M., Jones, M. W., Andrew, R. M., Hauck, J., Olsen, A., Peters, G. P., Peters, W.,
 2830 Pongratz, J., Sitch, S., Le Quéré, C., Canadell, J. G., Ciais, P., Jackson, R. B., Alin, S., Aragão, L. E. O. C., Arneth,
 2831 A., Arora, V., Bates, N. R., Becker, M., Benoit-Cattin, A., Bittig, H. C., Bopp, L., Bultan, S., Chandra, N.,
 2832 Chevallier, F., Chini, L. P., Evans, W., Florentie, L., Forster, P. M., Gasser, T., Gehlen, M., Gilfillan, D.,
 2833 Gkritzalis, T., Gregor, L., Gruber, N., Harris, I., Hartung, K., Haverd, V., Houghton, R. A., Ilyina, T., Jain, A. K.,
 2834 Joetzier, E., Kadono, K., Kato, E., Kitidis, V., Korsbakken, J. I., Landschützer, P., Lefèvre, N., Lenton, A., Lienert,
 2835 S., Liu, Z., Lombardozi, D., Marland, G., Metzl, N., Munro, D. R., Nabel, J. E. M. S., Nakaoka, S.-I., Niwa, Y.,
 2836 O’Brien, K., Ono, T., Palmer, P. I., Pierrot, D., Poulter, B., Resplandy, L., Robertson, E., Rödenbeck, C.,
 2837 Schwinger, J., Séférian, R., Skjelvan, I., Smith, A. J. P., Sutton, A. J., Tanhua, T., Tans, P. P., Tian, H., Tilbrook,

- 2838 B., van der Werf, G., Vuichard, N., Walker, A. P., Wanninkhof, R., Watson, A. J., Willis, D., Wiltshire, A. J.,
 2839 Yuan, W., Yue, X., and Zaehle, S.: Global Carbon Budget 2020, *Earth Syst. Sci. Data*, 12, 3269–3340,
 2840 <https://doi.org/10.5194/essd-12-3269-2020>, 2020.
- 2841 Friedlingstein, P., Jones, M. W., O’Sullivan, M., Andrew, R. M., Bakker, D. C. E., Hauck, J., Le Quéré, C., Peters,
 2842 G. P., Peters, W., Pongratz, J., Sitch, S., Canadell, J. G., Ciais, P., Jackson, R. B., Alin, S. R., Anthoni, P., Bates, N.
 2843 R., Becker, M., Bellouin, N., Bopp, L., Chau, T. T. T., Chevallier, F., Chini, L. P., Cronin, M., Currie, K. I.,
 2844 Decharme, B., Djeutchouang, L. M., Dou, X., Evans, W., Feely, R. A., Feng, L., Gasser, T., Gilfillan, D.,
 2845 Gkritzalis, T., Grassi, G., Gregor, L., Gruber, N., Gürses, Ö., Harris, I., Houghton, R. A., Hurtt, G. C., Iida, Y.,
 2846 Ilyina, T., Luijckx, I. T., Jain, A., Jones, S. D., Kato, E., Kennedy, D., Klein Goldewijk, K., Knauer, J., Korsbakken,
 2847 J. I., Körtzinger, A., Landschützer, P., Lauvset, S. K., Lefèvre, N., Lienert, S., Liu, J., Marland, G., McGuire, P. C.,
 2848 Melton, J. R., Munro, D. R., Nabel, J. E. M. S., Nakaoka, S.-I., Niwa, Y., Ono, T., Pierrot, D., Poulter, B., Rehder,
 2849 G., Resplandy, L., Robertson, E., Rödenbeck, C., Rosan, T. M., Schwinger, J., Schwingshackl, C., Séférian, R.,
 2850 Sutton, A. J., Sweeney, C., Tanhua, T., Tans, P. P., Tian, H., Tilbrook, B., Tubiello, F., van der Werf, G. R.,
 2851 Vuichard, N., Wada, C., Wanninkhof, R., Watson, A. J., Willis, D., Wiltshire, A. J., Yuan, W., Yue, C., Yue, X.,
 2852 Zaehle, S., and Zeng, J.: Global Carbon Budget 2021, *Earth Syst. Sci. Data*, 14, 1917–2005,
 2853 <https://doi.org/10.5194/essd-14-1917-2022>, 2022a.
- 2854 Friedlingstein, P., O’Sullivan, M., Jones, M. W., Andrew, R. M., Gregor, L., Hauck, J., Le Quéré, C., Luijckx, I. T.,
 2855 Olsen, A., Peters, G. P., Peters, W., Pongratz, J., Schwingshackl, C., Sitch, S., Canadell, J. G., Ciais, P., Jackson, R.
 2856 B., Alin, S. R., Alkama, R., Arneeth, A., Arora, V. K., Bates, N. R., Becker, M., Bellouin, N., Bittig, H. C., Bopp,
 2857 L., Chevallier, F., Chini, L. P., Cronin, M., Evans, W., Falk, S., Feely, R. A., Gasser, T., Gehlen, M., Gkritzalis, T.,
 2858 Gloege, L., Grassi, G., Gruber, N., Gürses, Ö., Harris, I., Hefner, M., Houghton, R. A., Hurtt, G. C., Iida, Y., Ilyina,
 2859 T., Jain, A. K., Jersild, A., Kadono, K., Kato, E., Kennedy, D., Klein Goldewijk, K., Knauer, J., Korsbakken, J. I.,
 2860 Landschützer, P., Lefèvre, N., Lindsay, K., Liu, J., Liu, Z., Marland, G., Mayot, N., McGrath, M. J., Metzl, N.,
 2861 Monacci, N. M., Munro, D. R., Nakaoka, S., Niwa, Y., O’Brien, K., Ono, T., Palmer, P. I., Pan, N., Pierrot, D.,
 2862 Pockock, K., Poulter, B., Resplandy, L., Robertson, E., Rödenbeck, C., Rodriguez, C., Rosan, T. M., Schwinger, J.,
 2863 Séférian, R., Shutler, J. D., Skjelvan, I., Steinhoff, T., Sun, Q., Sutton, A. J., Sweeney, C., Takao, S., Tanhua, T.,
 2864 Tans, P. P., Tian, X., Tian, H., Tilbrook, B., Tsujino, H., Tubiello, F., van der Werf, G. R., Walker, A. P.,
 2865 Wanninkhof, R., Whitehead, C., Willstrand Wranne, A., Wright, R., Yuan, W., Yue, C., Yue, X., Zaehle, S., Zeng,
 2866 J., and Zheng, B.: Global Carbon Budget 2022, *Earth Syst. Sci. Data*, 14, 4811–4900, <https://doi.org/10.5194/essd-14-4811-2022>, 2022b.
- 2868 Friedlingstein, P., O’Sullivan, M., Jones, M. W., Andrew, R. M., Bakker, D. C. E., Hauck, J., Landschützer, P., Le
 2869 Quéré, C., Luijckx, I. T., Peters, G. P., Peters, W., Pongratz, J., Schwingshackl, C., Sitch, S., Canadell, J. G., Ciais,
 2870 P., Jackson, R. B., Alin, S. R., Anthoni, P., Barbero, L., Bates, N. R., Becker, M., Bellouin, N., Decharme, B.,
 2871 Bopp, L., Brasika, I. B. M., Cadule, P., Chamberlain, M. A., Chandra, N., Chau, T.-T.-T., Chevallier, F., Chini, L.
 2872 P., Cronin, M., Dou, X., Enyo, K., Evans, W., Falk, S., Feely, R. A., Feng, L., Ford, D. J., Gasser, T., Ghattas, J.,
 2873 Gkritzalis, T., Grassi, G., Gregor, L., Gruber, N., Gürses, Ö., Harris, I., Hefner, M., Heinke, J., Houghton, R. A.,
 2874 Hurtt, G. C., Iida, Y., Ilyina, T., Jacobson, A. R., Jain, A. K., Jarníková, T., Jersild, A., Jiang, F., Jin, Z., Joos, F.,
 2875 Kato, E., Keeling, R. F., Kennedy, D., Klein Goldewijk, K., Knauer, J., Korsbakken, J. I., Körtzinger, A., Lan, X.,
 2876 Lefèvre, N., Li, H., Liu, J., Liu, Z., Ma, L., Marland, G., Mayot, N., McGuire, P. C., McKinley, G. A., Meyer, G.,
 2877 Morgan, E. J., Munro, D. R., Nakaoka, S., Niwa, Y., O’Brien, K. M., Olsen, A., Omar, A. M., Ono, T., Paulsen, M.,
 2878 Pierrot, D., Pockock, K., Poulter, B., Powis, C. M., Rehder, G., Resplandy, L., Robertson, E., Rödenbeck, C., Rosan,
 2879 T. M., Schwinger, J., Séférian, R., Smallman, T. L., Smith, S. M., Sospedra-Alfonso, R., Sun, Q., Sutton, A. J.,
 2880 Sweeney, C., Takao, S., Tans, P. P., Tian, H., Tilbrook, B., Tsujino, H., Tubiello, F., van der Werf, G. R., van
 2881 Ooijen, E., Wanninkhof, R., Watanabe, M., Wimart-Rousseau, C., Yang, D., Yang, X., Yuan, W., Yue, X., Zaehle,
 2882 S., Zeng, J., and Zheng, B.: Global Carbon Budget 2023, *Earth Syst. Sci. Data*, 15, 5301–5369,
 2883 <https://doi.org/10.5194/essd-15-5301-2023>, 2023.
- 2884 Friedlingstein, P., O’Sullivan, M., Jones, M. W., Andrew, R. M., Hauck, J., Landschützer, P., Le Quéré, C., Li, H.,
 2885 Luijckx, I. T., Olsen, A., Peters, G. P., Peters, W., Pongratz, J., Schwingshackl, C., Sitch, S., Canadell, J. G., Ciais,
 2886 P., Jackson, R. B., Alin, S. R., Arneeth, A., Arora, V., Bates, N. R., Becker, M., Bellouin, N., Berghoff, C. F., Bittig,
 2887 H. C., Bopp, L., Cadule, P., Campbell, K., Chamberlain, M. A., Chandra, N., Chevallier, F., Chini, L. P., Colligan,
 2888 T., Decayeux, J., Djeutchouang, L. M., Dou, X., Duran Rojas, C., Enyo, K., Evans, W., Fay, A. R., Feely, R. A.,
 2889 Ford, D. J., Foster, A., Gasser, T., Gehlen, M., Gkritzalis, T., Grassi, G., Gregor, L., Gruber, N., Gürses, Ö., Harris,
 2890 I., Hefner, M., Heinke, J., Hurtt, G. C., Iida, Y., Ilyina, T., Jacobson, A. R., Jain, A. K., Jarníková, T., Jersild, A.,
 2891 Jiang, F., Jin, Z., Kato, E., Keeling, R. F., Klein Goldewijk, K., Knauer, J., Korsbakken, J. I., Lan, X., Lauvset, S.
 2892 K., Lefèvre, N., Liu, Z., Liu, J., Ma, L., Maksyutov, S., Marland, G., Mayot, N., McGuire, P. C., Metzl, N.,
 2893 Monacci, N. M., Morgan, E. J., Nakaoka, S.-I., Neill, C., Niwa, Y., Nützel, T., Olivier, L., Ono, T., Palmer, P. I.,
 2894 Pierrot, D., Qin, Z., Resplandy, L., Roobaert, A., Rosan, T. M., Rödenbeck, C., Schwinger, J., Smallman, T. L.,
 2895 Smith, S. M., Sospedra-Alfonso, R., Steinhoff, T., Sun, Q., Sutton, A. J., Séférian, R., Takao, S., Tatebe, H., Tian,

- 2896 H., Tilbrook, B., Torres, O., Tourigny, E., Tsujino, H., Tubiello, F., van der Werf, G., Wanninkhof, R., Wang, X.,
2897 Yang, D., Yang, X., Yu, Z., Yuan, W., Yue, X., Zaehle, S., Zeng, N., and Zeng, J.: Global Carbon Budget 2024,
2898 Earth Syst. Sci. Data, 17, 965–1039, <https://doi.org/10.5194/essd-17-965-2025>, 2025a.
- 2899 Friedlingstein, P., Le Quéré, C., O’Sullivan, M., Hauck, J., Landschützer, P., Luijckx, I.T., Li, H., van der Woude,
2900 A., Schwingshackl, C., Pongratz, P., Regnier, P., Andrew, R.M., Bakker, D.C.E., Canadell, J.G., Ciais, P., Gasser,
2901 T., Jones, M.W., Lan, X., Morgan, E., Olsen, A., Peters, G.P., Peters, W., Sitch, S., and Tian, H.: Emerging climate
2902 impact on carbon sinks in a consolidated carbon budget, *Nature*, <https://doi.org/10.1038/s41586-025-09802-5>,
2903 2025b.
- 2904 Friedlingstein, P., O’Sullivan, M., Jones, M. W., Andrew, R. M., Bakker, D. C. E., Hauck, J., Landschützer, P., Le
2905 Quéré, C., Li, H., Luijckx, I. T., Peters, G. P., Peters, W., Pongratz, J., Schwingshackl, C., Sitch, S., Canadell, J. G.,
2906 Ciais, P., Aas, K., Alin, S. R., Anthoni, P., Barbero, L., Bates, N. R., Bellouin, N., Benoit-Cattin, A., Berghoff, C.
2907 F., Bernardello, R., Bopp, L., Brasika, I. B. M., Chamberlain, M. A., Chandra, N., Chevallier, F., Chini, L. P.,
2908 Collier, N. O., Colligan, T. H., Cronin, M., Djeutchouang, L. M., Dou, X., Enright, M. P., Enyo, K., Erb, M.,
2909 Evans, W., Feely, R. A., Feng, L., Ford, D. J., Foster, A., Fransner, F., Gasser, T., Gehlen, M., Gkritzalis, T.,
2910 Goncalves De Souza, J., Grassi, G., Gregor, L., Gruber, N., Guenet, B., Gürses, Ö., Harrington, K., Harris, I.,
2911 Heinke, J., Hurtt, G. C., Iida, Y., Ilyina, T., Ito, A., Jacobson, A. R., Jain, A. K., Jarníková, T., Jersild, A., Jiang, F.,
2912 Jones, S. D., Kato, E., Keeling, R. F., Klein Goldewijk, K., Knauer, J., Kong, Y., Korsbakken, J. I., Koven, C.,
2913 Kunimitsu, T., Lan, X., Liu, J., Liu, Z., Liu, Z., Lo Monaco, C., Ma, L., Marland, G., McGuire, P. C., McKinley,
2914 G. A., Melton, J. R., Monacci, N., Monier, E., Morgan, E. J., Munro, D. R., Müller, J. D., Nakaoka, S., Nayagam,
2915 L. R., Niwa, Y., Nutzelt, T., Olsen, A., Omar, A. M., Pan, N., Pandey, S., Pierrot, D., Qin, Z., Regnier, P., Rehder,
2916 G., Resplandy, L., Roobaert, A., Rosan, T. M., Rödenbeck, C., Schwinger, J., Skjelvan, I., Smallman, T. L., Spada,
2917 V., Sreeush, M. G., Sun, Q., Sutton, A. J., Sweeney, C., Swingedouw, D., Séférian, R., Takao, S., Tatebe, H., Tian,
2918 H., Tian, X., Tilbrook, B., Tsujino, H., Tubiello, F., van Ooijen, E., van der Werf, G. R., van de Velde, S. J.,
2919 Walker, A. P., Wanninkhof, R., Yang, X., Yuan, W., Yue, X., and Zeng, J.: Supplemental data of the Global
2920 Carbon Budget 2025, ICOS-ERIC Carbon Portal, <https://doi.org/10.18160/GCP-2025>, 2025c.
- 2921 Fu, W., Moore, J. K., Primeau, F., Collier, N., Ogunro, O. O., Hoffman, F. M., and Randerson, J. T.: Evaluation of
2922 Ocean Biogeochemistry and Carbon Cycling in CMIP Earth System Models With the International Ocean Model
2923 Benchmarking (IOMB) Software System, *JGR Oceans*, 127, e2022JC018965,
2924 <https://doi.org/10.1029/2022JC018965>, 2022.
- 2925 Ganzenmüller, R., Bultan, S., Winkler, K., Fuchs, R., Zabel, F., and Pongratz, J.: Land-use change emissions based
2926 on high-resolution activity data substantially lower than previously estimated, *Environ. Res. Lett.*, 17, 064050,
2927 <https://doi.org/10.1088/1748-9326/ac70d8>, 2022.
- 2928 Gasser, T., Crepin, L., Quilcaille, Y., Houghton, R. A., Ciais, P., and Obersteiner, M.: Historical CO₂ emissions
2929 from land use and land cover change and their uncertainty, *Biogeosciences*, 17, 4075–4101,
2930 <https://doi.org/10.5194/bg-17-4075-2020>, 2020.
- 2931 Gaubert, B., Stephens, B. B., Basu, S., Chevallier, F., Deng, F., Kort, E. A., Patra, P. K., Peters, W., Rödenbeck,
2932 C., Saeki, T., Schimel, D., Van der Laan-Luijckx, I., Wofsy, S., and Yin, Y.: Global atmospheric CO₂ inverse
2933 models converging on neutral tropical land exchange, but disagreeing on fossil fuel and atmospheric growth rate,
2934 *Biogeosciences*, 16, 117–134, <https://doi.org/10.5194/bg-16-117-2019>, 2019.
- 2935 Gauthier, C. B., Melton, J. R., Meyer, G., Raj Deepak, S. N., and Sonnentag, O.: Parameter Optimization for
2936 Global Soil Carbon Simulations: Not a Simple Problem, *J Adv Model Earth Syst*, 17, e2024MS004577,
2937 <https://doi.org/10.1029/2024MS004577>, 2025.
- 2938 GCP: The Global Carbon Budget 2007, available at: [http://www.
2939 globalcarbonproject.org/carbonbudget/archive.htm](http://www.globalcarbonproject.org/carbonbudget/archive.htm), last access: 23 October 2025, 2007.
- 2940 Giglio, L., Schroeder, W., and Justice, C. O.: The collection 6 MODIS active fire detection algorithm and fire
2941 products, *Remote Sensing of Environment*, 178, 31–41, <https://doi.org/10.1016/j.rse.2016.02.054>, 2016.
- 2942 Gitz V, Ciais P. Amplifying effects of land-use change on future atmospheric CO₂ levels. *Global Biogeochemical
2943 Cycles*. <https://doi.org/10.1029/2002GB001963>, 2003.
- 2944 Gloege, L., McKinley, G. A., Landschützer, P., Fay, A. R., Frölicher, T. L., Fyfe, J. C., Ilyina, T., Jones, S.,
2945 Lovenduski, N. S., Rodgers, K. B., Schlunegger, S., and Takano, Y.: Quantifying Errors in Observationally Based

- 2946 Estimates of Ocean Carbon Sink Variability, *Global Biogeochem. Cy.*, 35, e2020GB006788,
2947 <https://doi.org/10.1029/2020GB006788>, 2021.
- 2948 Gloege, L., Yan, M., Zheng, T., and McKinley, G. A.: Improved Quantification of Ocean Carbon Uptake by Using
2949 Machine Learning to Merge Global Models and pCO₂ Data, *J. Adv. Model. Earth Syst.*, 14, e2021MS002620,
2950 <https://doi.org/10.1029/2021MS002620>, 2022.
- 2951 Golar, G., Malik, A., Muis, H., Herman, A., Nurudin, N., and Lukman, L.: The social-economic impact of COVID-
2952 19 pandemic: implications for potential forest degradation, *Heliyon*, 6, e05354,
2953 <https://doi.org/10.1016/j.heliyon.2020.e05354>, 2020.
- 2954 Goris, N., Tjiputra, J. F., Olsen, A., Schwinger, J., Lauvset, S. K., and Jeansson, E.: Constraining Projection-Based
2955 Estimates of the Future North Atlantic Carbon Uptake, *J. Clim.*, 31, 3959–3978, <https://doi.org/10.1175/JCLI-D-17-0564.1>, 2018.
- 2957 Grassi, G., House, J., Kurz, W. A., Cescatti, A., Houghton, R. A., Peters, G. P., Sanz, M. J., Viñas, R. A., Alkama,
2958 R., Arneth, A., Bondeau, A., Dentener, F., Fader, M., Federici, S., Friedlingstein, P., Jain, A. K., Kato, E., Koven,
2959 C. D., Lee, D., Nabel, J. E. M. S., Nassikas, A. A., Perugini, L., Rossi, S., Sitch, S., Viovy, N., Wiltshire, A., and
2960 Zaehle, S.: Reconciling global-model estimates and country reporting of anthropogenic forest CO₂ sinks, *Nature
2961 Clim Change*, 8, 914–920, <https://doi.org/10.1038/s41558-018-0283-x>, 2018.
- 2962 Grassi, G., Stehfest, E., Rogelj, J., van Vuuren, D., Cescatti, A., House, J., Nabuurs, G.-J., Rossi, S., Alkama, R.,
2963 Viñas, R. A., Calvin, K., Ceccherini, G., Federici, S., Fujimori, S., Gusti, M., Hasegawa, T., Havlik, P.,
2964 Humpenöder, F., Korosuo, A., Perugini, L., Tubiello, F. N., and Popp, A.: Critical adjustment of land mitigation
2965 pathways for assessing countries' climate progress, *Nat. Clim. Chang.*, 11, 425–434,
2966 <https://doi.org/10.1038/s41558-021-01033-6>, 2021.
- 2967 Grassi, G., Schwingshackl, C., Gasser, T., Houghton, R. A., Sitch, S., Canadell, J. G., Cescatti, A., Ciais, P.,
2968 Federici, S., Friedlingstein, P., Kurz, W. A., Sanz Sanchez, M. J., Abad Viñas, R., Alkama, R., Bultan, S.,
2969 Ceccherini, G., Falk, S., Kato, E., Kennedy, D., Knauer, J., Korosuo, A., Melo, J., McGrath, M. J., Nabel, J. E. M.
2970 S., Poulter, B., Romanovskaya, A. A., Rossi, S., Tian, H., Walker, A. P., Yuan, W., Yue, X., and Pongratz, J.:
2971 Harmonising the land-use flux estimates of global models and national inventories for 2000–2020, *Earth Syst. Sci.
2972 Data*, 15, 1093–1114, <https://doi.org/10.5194/essd-15-1093-2023>, 2023.
- 2973 Grassi, G., Peters, G. P., Canadell, J. G., Cescatti, A., Federici, S., Gidden, M. J., Harris, N., Herold, M., Krug, T.,
2974 O'Sullivan, M., Pongratz, J., Sanz, M. J., Schwingshackl, C., and Van Vuuren, D.: Improving land-use emission
2975 estimates under the Paris Agreement, *Nat Sustain*, 8, 579–581, <https://doi.org/10.1038/s41893-025-01565-1>, 2025.
- 2976 Gregor, L., Lebehot, A. D., Kok, S., and Scheel Monteiro, P. M.: A comparative assessment of the uncertainties of
2977 global surface ocean CO₂ estimates using a machine-learning ensemble (CSIR-ML6 version 2019a)—have we hit
2978 the wall?. *Geoscientific Model Development*, 12(12), 5113–5136, <https://doi.org/10.5194/gmd-12-5113-2019>,
2979 2019.
- 2980 Gregor, L., Shutler, J., and Gruber, N.: High-resolution variability of the ocean carbon sink. *Global
2981 Biogeochemical Cycles*, 38(8), e2024GB008127, <https://doi.org/10.1029/2024GB008127>, 2024.
- 2982 Gruber, N., Bakker, D. C. E., DeVries, T., Gregor, L., Hauck, J., Landschützer, P., McKinley, G. A., and Müller, J.
2983 D.: Trends and variability in the ocean carbon sink, *Nat. Rev. Earth Environ.*, 4, 119–134,
2984 <https://doi.org/10.1038/s43017-022-00381-x>, 2023.
- 2985 Gruber, N., Clement, D., Carter, B. R., Feely, R. A., van Heuven, S., Hoppema, M., Ishii, M., Key, R. M., Kozyr,
2986 A., Lauvset, S. K., Lo Monaco, C., Mathis, J. T., Murata, A., Olsen, A., Perez, F. F., Sabine, C. L., Tanhua, T., and
2987 Wanninkhof, R.: The oceanic sink for anthropogenic CO₂ from 1994 to 2007, 363, 1193–1199,
2988 <https://doi.org/10.1126/science.aau5153>, 2019.
- 2989 Guan, D., Liu, Z., Geng, Y., Lindner, S., and Hubacek, K.: The gigatonne gap in China's carbon dioxide
2990 inventories, *Nature Clim Change*, 2, 672–675, <https://doi.org/10.1038/nclimate1560>, 2012.
- 2991 Gulev, S. K., Thorne, P. W., Ahn, J., Dentener, F. J., Domingues, C. M., Gerland, S., Gong, D. S., Kaufman, S.,
2992 Nnamchi, H. C., Quaas, J., Rivera, J. A., Sathyendranath, S., Smith, S. L., Trewin, B., von Shuckmann, K., and
2993 Vose, R. S.: Changing State of the Climate System. In: *Climate Change 2021: The Physical Science Basis.
2994 Contribution of Working Group I to the Sixth Assessment Report of the Intergovernmental Panel on Climate*

- 2995 Change [Masson-Delmotte, V., Zhai, P., Pirani, A., Connors, S. L., Péan, C., Berger, S., Caud, N., Chen, Y.,
2996 Goldfarb, L., Gomis, M. I., Huang, M., Leitzell, K., Lonnoy, E., Matthews, J.B.R., Maycock, T.K., Waterfield, T.,
2997 Yelekçi, O., Yu, R. and Zhou, B. (eds.)]. Cambridge University Press, Cambridge, United Kingdom and New
2998 York, NY, USA, pp. 287–422, <https://doi.org/10.1017/9781009157896.004>, 2021.
- 2999 Guo, R., Wang, J., Bing, L., Tong, D., Ciais, P., Davis, S. J., Andrew, R. M., Xi, F., and Liu, Z.: Global CO₂
3000 uptake by cement from 1930 to 2019, 13, 1791–1805, <https://doi.org/10.5194/essd-13-1791-2021>, 2021.
- 3001 Gürses, Ö., Oziel, L., Karakuş, O., Sidorenko, D., Völker, C., Ye, Y., Zeising, M., Butzin, M., and Hauck, J.:
3002 Ocean biogeochemistry in the coupled ocean–sea ice–biogeochemistry model FESOM2.1–REcoM3, *Geosci.*
3003 *Model Dev.*, 16, 4883–4936, <https://doi.org/10.5194/gmd-16-4883-2023>, 2023.
- 3004 Gütschow, J., Jeffery, M. L., Gieseke, R., Gebel, R., Stevens, D., Krapp, M., and Rocha, M.: The PRIMAP-hist
3005 national historical emissions time series, 8, 571–603, <https://doi.org/10.5194/essd-8-571-2016>, 2016.
- 3006 Gütschow, J., Busch, D. and Pflüger, M.: The PRIMAP-hist national historical emissions time series (1750–2023)
3007 v2.6, Zenodo [Data set], <https://doi.org/10.5281/zenodo.13752654>, 2023.
- 3008 Hall, B. D., Crotwell, A. M., Kitzis, D. R., Mefford, T., Miller, B. R., Schibig, M. F., and Tans, P. P.: Revision of
3009 the World Meteorological Organization Global Atmosphere Watch (WMO/GAW) CO₂ calibration scale, 14,
3010 3015–3032, <https://doi.org/10.5194/amt-14-3015-2021>, 2021.
- 3011 Hansis, E., Davis, S. J., and Pongratz, J.: Relevance of methodological choices for accounting of land use change
3012 carbon fluxes, *Global Biogeochem. Cycles*, 29, 1230–1246, <https://doi.org/10.1002/2014GB004997>, 2015.
- 3013 Hauck, J., Nissen, C., Landschützer, P., Rödenbeck, C., Bushinsky, S., and Olsen, A.: Sparse observations induce
3014 large biases in estimates of the global ocean CO₂ sink: an ocean model subsampling experiment, *Philos. Trans. R.*
3015 *Soc. Math. Phys. Eng. Sci.*, 381, 20220063, <https://doi.org/10.1098/rsta.2022.0063>, 2023a.
- 3016 Hauck, J., Gregor, L., Nissen, C., Patara, L., Hague, M., Mongwe, P., Bushinsky, S., Doney, S. C., Gruber, N., Le
3017 Quéré, C., Manizza, M., Mazloff, M., Monteiro, P. M. S., and Terhaar, J.: The Southern Ocean Carbon Cycle
3018 1985–2018: Mean, Seasonal Cycle, Trends, and Storage. *Global Biogeochemical Cycles*, 37(11), e2023GB007848,
3019 <https://doi.org/10.1029/2023GB007848>, 2023b.
- 3020 Hauck, J., Zeising, M., Le Quéré, C., Gruber, N., Bakker, D. C. E., Bopp, L., Chau, T. T. T., Gürses, Ö., Ilyina, T.,
3021 Landschützer, P., Lenton, A., Resplandy, L., Rödenbeck, C., Schwinger, J., and Séférian, R.: Consistency and
3022 Challenges in the Ocean Carbon Sink Estimate for the Global Carbon Budget, *Front. Mar. Sci.*, 7, 571720,
3023 <https://doi.org/10.3389/fmars.2020.571720>, 2020.
- 3024 Haverd, V., Smith, B., Nieradzik, L., Briggs, P. R., Woodgate, W., Trudinger, C. M., Canadell, J. G., and Cuntz,
3025 M.: A new version of the CABLE land surface model (Subversion revision r4601) incorporating land use and land
3026 cover change, woody vegetation demography, and a novel optimisation-based approach to plant coordination of
3027 photosynthesis, *Geosci. Model Dev.*, 11, 2995–3026, <https://doi.org/10.5194/gmd-11-2995-2018>, 2018.
- 3028 Heinke, J., Rolinski, S., and Müller, C.: Modelling the role of livestock grazing in C and N cycling in grasslands
3029 with LPJmL5.0-grazing, *Geosci. Model Dev.*, 16, 2455–2475, <https://doi.org/10.5194/gmd-16-2455-2023>, 2023.
- 3030 Hickler, T., Smith, B., Prentice, I. C., Mjöfors, K., Miller, P., Arneth, A., and Sykes, M. T.: CO₂ fertilization in
3031 temperate FACE experiments not representative of boreal and tropical forests, *Glob. Change Biol.*, 14, 1531–1542,
3032 <https://doi.org/10.1111/j.1365-2486.2008.01598.x>, 2008.
- 3033 Hoesly, R. M., Smith, S. J., Feng, L., Klimont, Z., Janssens-Maenhout, G., Pitkanen, T., Seibert, J. J., Vu, L.,
3034 Andres, R. J., Bolt, R. M., Bond, T. C., Dawidowski, L., Kholod, N., Kurokawa, J., Li, M., Liu, L., Lu, Z., Moura,
3035 M. C. P., O'Rourke, P. R., and Zhang, Q.: Historical (1750–2014) anthropogenic emissions of reactive gases and
3036 aerosols from the Community Emissions Data System (CEDS), *Geosci. Model Dev.*, 11, 369–408,
3037 <https://doi.org/10.5194/gmd-11-369-2018>, 2018.
- 3038 Hoesly, R., Smith, S. J., Prime, N., Ahsan, H., Suchyta, H., O'Rourke, P., Crippa, M., Klimont, Z., Guizzardi, D.,
3039 Behrendt, J., Feng, L., Harkins, C., McDonald, B., Mott, A., McDuffie, A., Nicholson, M. and Wang, S.: CEDS
3040 v_2024_07_08 Release Emission Data, Zenodo [Data set], <https://doi.org/10.5281/zenodo.12803196>, 2024.

- 3041 Hong, C., Burney, J. A., Pongratz, J., Nabel, J. E. M. S., Mueller, N. D., Jackson, R. B., and Davis, S. J.: Global
3042 and regional drivers of land-use emissions in 1961–2017, *Nature*, 589, 554–561, [https://doi.org/10.1038/s41586-](https://doi.org/10.1038/s41586-020-03138-y)
3043 020-03138-y, 2021.
- 3044 Holding, T., Ashton, I. G., Shutler, J. D., Land, P. E., Nightingale, P. D., Rees, A. P., Brown, I., Piolle, J.-F., Kock,
3045 A., Bange, H. W., Woolf, D. K., Goddijn-Murphy, L., Pereira, R., Paul, F., Girard-Ardhuin, F., Chapron, B.,
3046 Rehder, G., Ardhuin, F., and Donlon, C. J.: The FluxEngine air–sea gas flux toolbox: simplified interface and
3047 extensions for in situ analyses and multiple sparingly soluble gases, *Ocean Sci.*, 15, 1707–1728,
3048 <https://doi.org/10.5194/os-15-1707-2019>, 2019.
- 3049 Hoppe, J., Hinder, B., Rafaty, R., Patt, A., and Grubb, M.: Three Decades of Climate Mitigation Policy: What Has
3050 It Delivered?, *Annu. Rev. Environ. Resour.*, 48, 615–650, [https://doi.org/10.1146/annurev-environ-112321-](https://doi.org/10.1146/annurev-environ-112321-103821)
3051 103821, 2023.
- 3052 Houghton, R. A. and Castanho, A.: Annual emissions of carbon from land use, land-use change, and forestry from
3053 1850 to 2020, *Earth Syst. Sci. Data*, 15, 2025–2054, <https://doi.org/10.5194/essd-15-2025-2023>, 2023.
- 3054 Houghton, R. A., House, J. I., Pongratz, J., van der Werf, G. R., DeFries, R. S., Hansen, M. C., Le Quéré, C., and
3055 Ramankutty, N.: Carbon emissions from land use and land-cover change, *Biogeosciences*, 9, 5125–5142,
3056 <https://doi.org/10.5194/bg-9-5125-2012>, 2012.
- 3057 Houghton, R. A. and Nassikas, A. A.: Global and regional fluxes of carbon from land use and land cover change
3058 1850–2015: Carbon Emissions From Land Use, *Global Biogeochem. Cycles*, 31, 456–472,
3059 <https://doi.org/10.1002/2016GB005546>, 2017.
- 3060 Huang, B., Thorne, P. W., Banzon, V. F., Boyer, T., Chepurin, G., Lawrimore, J. H., Menne, M. J., Smith, T. M.,
3061 Vose, R. S., and Zhang, H.-M.: NOAA Extended Reconstructed Sea Surface Temperature (ERSST), Version 5,
3062 <https://doi.org/10.7289/V5T72FNM>, 2017.
- 3063 Hubau, W., Lewis, S.L., Phillips, O.L., Affum-Baffoe, K., Beeckman, H., Cuní-Sanchez, A., Daniels, A.K.,
3064 Ewango, C.E.N., Fauset, S., Mukinzi, J.M., Sheil, D., Sonké, B., Sullivan, M.J.P., Sunderland, T.C.H., Taedoumg,
3065 H., Thomas, S.C., White, L.J.T., Abernethy, K.A., Adu-Bredu, S., Amani, C.A., Baker, T.R., Banin, L.F., Baya, F.,
3066 Begne, S.K., Bennett, A.C., Benedet, F., Bitariho, R., Bocko, Y.E., Boeckx, P., Boundja, P., Brienen, R.J.W.,
3067 Brncic, T., Chezeaux, E., Chuyong, G.B., Clark, C.J., Collins, M., Comiskey, J.A., Coomes, D.A., Dargie, G.C., de
3068 Haulleville, T., Kamdem, M.N.D., Doucet, J.-L., Esquivel-Muelbert, A., Feldpausch, T.R., Fofanah, A., Foli, E.G.,
3069 Gilpin, M., Gloor, E., Gonmadje, C., Gourlet-Fleury, S., Hall, J.S., Hamilton, A.C., Harris, D.J., Hart, T.B.,
3070 Hockemba, M.B.N., Hladik, A., Ifo, S.A., Jeffery, K.J., Jucker, T., Yakusu, E.K., Kearsley, E., Kenfack, D., Koch,
3071 A., Leal, M.E., Levesley, A., Lindsell, J.A., Lisingo, J., Lopez-Gonzalez, G., Lovett, J.C., Makana, J.-R., Malhi,
3072 Y., Marshall, A.R., Martin, J., Martin, E.H., Mbayu, F.M., Medjibe, V.P., Mihindou, V., Mitchard, E.T.A., Moore,
3073 S., Munishi, P.K.T., Bengone, N.N., Ojo, L., Ondo, F.E., Peh, K.S.-H., Pickavance, G.C., Poulsen, A.D., Poulsen,
3074 J.R., Qie, L., Reitsma, J., Rovero, F., Swaine, M.D., Talbot, J., Taplin, J., Taylor, D.M., Thomas, D.W., Toirambe,
3075 B., Mukendi, J.T., Tuagben, D., Umunay, P.M., van der Heijden, G.M.F., Verbeeck, H., Vleminckx, J., Willcock,
3076 S., Wöll, H., Woods, J.T., Zemagho, L.: Asynchronous carbon sink saturation in African and Amazonian tropical
3077 forests, *Nature*, 579, 80–87, <https://doi.org/10.1038/s41586-020-2035-0>, 2020.
- 3078 Humphrey, V., Zscheischler, J., Ciais, P., Gudmundsson, L., Sitch, S., and Seneviratne, S. I.: Sensitivity of
3079 atmospheric CO₂ growth rate to observed changes in terrestrial water storage, *Nature*, 560, 628–631,
3080 <https://doi.org/10.1038/s41586-018-0424-4>, 2018.
- 3081 Humphrey, V., Berg, A., Ciais, P., Gentile, P., Jung, M., Reichstein, M., Seneviratne, S. I., and Frankenberg, C.:
3082 Soil moisture–atmosphere feedback dominates land carbon uptake variability, *Nature*, 592, 65–69,
3083 <https://doi.org/10.1038/s41586-021-03325-5>, 2021.
- 3084 Huntzinger, D. N., Michalak, A. M., Schwalm, C., Ciais, P., King, A. W., Fang, Y., Schaefer, K., Wei, Y., Cook,
3085 R. B., Fisher, J. B., Hayes, D., Huang, M., Ito, A., Jain, A. K., Lei, H., Lu, C., Maignan, F., Mao, J., Parazoo, N.,
3086 Peng, S., Poulter, B., Ricciuto, D., Shi, X., Tian, H., Wang, W., Zeng, N., and Zhao, F.: Uncertainty in the response
3087 of terrestrial carbon sink to environmental drivers undermines carbon-climate feedback predictions, *Sci Rep*, 7,
3088 4765, <https://doi.org/10.1038/s41598-017-03818-2>, 2017.
- 3089 Iida, Y., Takatani, Y., Kojima, A., and Ishii, M.: Global trends of ocean CO₂ sink and ocean acidification: an
3090 observation-based reconstruction of surface ocean inorganic carbon variables, *J Oceanogr*, 77, 323–358,
3091 <https://doi.org/10.1007/s10872-020-00571-5>, 2021.

- 3092 Ilyina, T., Li, H., Spring, A., Müller, W. A., Bopp, L., Chikamoto, M. O., Danabasoglu, G., Dobrynin, M., Dunne,
3093 J., Fransner, F., Friedlingstein, P., Lee, W., Lovenduski, N. S., Merryfield, W. J., Mignot, J., Park, J. Y., Séférian,
3094 R., Sospedra-Alfonso, R., Watanabe, M., and Yeager, S.: Predictable Variations of the Carbon Sinks and
3095 Atmospheric CO₂ Growth in a Multi-Model Framework, *Geophys. Res. Lett.*, 48, e2020GL090695,
3096 <https://doi.org/10.1029/2020GL090695>, 2021.
- 3097 IMF: International Monetary Fund: World Economic Outlook, available at: <http://www.imf.org>, last access: 23
3098 October 2025, 2025.
- 3099 Instituto Nacional de Pesquisas Espaciais (INPE): Portal TerraBrasilis, available at:
3100 <http://terrabrasilis.dpi.inpe.br/en/home-page/>, last access: 23 October 2025.
- 3101 Ito, A.: Disequilibrium of terrestrial ecosystem CO₂ budget caused by disturbance-induced emissions and non-CO₂
3102 carbon export flows: a global model assessment, *Earth Syst. Dynam.*, 10, 685–709, [https://doi.org/10.5194/esd-10-](https://doi.org/10.5194/esd-10-685-2019)
3103 685-2019, 2019.
- 3104 Ito, A. and Inatomi, M.: Use of a process-based model for assessing the methane budgets of global terrestrial
3105 ecosystems and evaluation of uncertainty, 9, 759–773, <https://doi.org/10.5194/bg-9-759-2012>, 2012.
- 3106 Jackson, R. B., Canadell, J. G., Le Quéré, C., Andrew, R. M., Korsbakken, J. I., Peters, G. P., and Nakicenovic, N.:
3107 Reaching peak emissions, *Nature Clim Change*, 6, 7–10, <https://doi.org/10.1038/nclimate2892>, 2016.
- 3108 Jackson, R. B., Le Quéré, C., Andrew, R. M., Canadell, J. G., Korsbakken, J. I., Liu, Z., Peters, G. P., and Zheng,
3109 B.: Global energy growth is outpacing decarbonization, *Environ. Res. Lett.*, 13, 120401,
3110 <https://doi.org/10.1088/1748-9326/aaf303>, 2018.
- 3111 Jackson, R. B., Friedlingstein, P., Andrew, R. M., Canadell, J. G., Le Quéré, C., and Peters, G. P.: Persistent fossil
3112 fuel growth threatens the Paris Agreement and planetary health, *Environ. Res. Lett.*, 14, 121001,
3113 <https://doi.org/10.1088/1748-9326/ab57b3>, 2019.
- 3114 Jackson, R. B., Friedlingstein, P., Quéré, C. L., Abernethy, S., Andrew, R. M., Canadell, J. G., Ciais, P., Davis, S.
3115 J., Deng, Z., Liu, Z., Korsbakken, J. I., and Peters, G. P.: Global fossil carbon emissions rebound near pre-COVID-
3116 19 levels, *Environ. Res. Lett.*, 17, 031001, <https://doi.org/10.1088/1748-9326/ac55b6>, 2022.
- 3117 Jacobson, A. R., Schuldt, K. N., Tans, P., Andrews, A., Miller, J. B., Oda, T., Basu, S., Mund, J., Weir, B., Ott, L.,
3118 Aalto, T., Abshire, J. B., Aikin, K., Aoki, S., Apadula, F., Arnold, S., Baier, B., Bartyzel, J., Beyersdorf, A.,
3119 Biermann, T., Biraud, S. C., Boenisch, H., Brailsford, G., Brand, W. A., Chen, G., Chen, H., Chmura, L., Clark, S.,
3120 Colomb, A., Commane, R., Conil, S., Couret, C., Cox, A., Cristofanelli, P., Cuevas, E., Curcoll, R., Daube, B.,
3121 Davis, K. J., De Wekker, S., Della Coletta, J., Delmotte, M., DiGangi, E., DiGangi, J. P., di Sarra, A. G.,
3122 Dlugokencky, E., Elkins, J. W., Emmenegger, L., Fang, S., Fischer, M. L., Forster, G., Frumau, A., Galkowski, M.,
3123 Gatti, L. V., Gehrlein, T., Gerbig, C., Gheusi, F., Gloor, E., Gomez-Trueba, V., Goto, D., Griffis, T., Hammer, S.,
3124 Hanson, C., Haszpra, L., Hatakka, J., Heimann, M., Heliasz, M., Hensen, A., Hermansen, O., Hints, E., Holst, J.,
3125 Ivakhov, V., Jaffe, D. A., Jordan, A., Joubert, W., Karion, A., Kawa, S. R., Kazan, V., Keeling, R. F., Keronen, P.,
3126 Kneuer, T., Kolari, P., Kominková, K., Kort, E., Kozlova, E., Krummel, P., Kubistin, D., Labuschagne, C., Lam,
3127 D. H. Y., Lan, X., Langenfelds, R. L., Laurent, O., Laurila, T., Lauvaux, T., Lavric, J., Law, B. E., Lee, J., Lee, O.
3128 S. M., Lehner, I., Lehtinen, K., Leppert, R., Leskinen, A., Leuenberger, M., Levin, I., Levula, J., Lin, J., Lindauer,
3129 M., Loh, Z., Lopez, M., Luijkx, I. T., Lunder, C. R., Machida, T., Mammarella, I., Manca, G., Manning, A.,
3130 Manning, A., Marek, M. V., Martin, M. Y., Matsueda, H., McKain, K., Meijer, H., Meinhardt, F., Merchant, L.,
3131 Mihalopoulos, N., Miles, N. L., Miller, C. E., Mitchell, L., Mölder, M., Montzka, S., Moore, F., Moossen, H.,
3132 Morgan, E., Morgui, J.-A., Morimoto, S., Müller-Williams, J., Munger, J. W., Munro, D., Myhre, C. L., Nakaoka,
3133 S.-I., Necki, J., Newman, S., Nichol, S., Niwa, Y., Obersteiner, F., O'Doherty, S., Paplawsky, B., Peischl, J.,
3134 Peltola, O., Piacentino, S., Pichon, J.-M., Pickers, P., Piper, S., Pitt, J., Plass-Dülmer, C., Platt, S. M., Prinzivalli,
3135 S., Ramonet, M., Ramos, R., Reyes-Sanchez, E., Richardson, S. J., Riris, H., Rivas, P. P., Ryerson, T., Saito, K.,
3136 Sargent, M., Sasakawa, M., Scheeren, B., Schuck, T., Schumacher, M., Seifert, T., Sha, M. K., Shepson, P., Shook,
3137 M., Sloop, C. D., Smith, P., Stanley, K., Steinbacher, M., Stephens, B., Sweeney, C., Thoning, K., Timas, H., Torn,
3138 M., Tørseth, K., Trisolino, P., Turnbull, J., van den Bulk, P., van Dinter, D., Vermeulen, A., Viner, B., Vitkova,
3139 G., Walker, S., Watson, A., Wofsy, S. C., Worsley, J., Worthy, D., Young, D., Zaehle, S., Zahn, A., and Zimnoch,
3140 M.: CarbonTracker CT2022, NOAA GML [Data set], <https://doi.org/10.25925/Z1GJ-3254>, 2023a.
- 3141 Jacobson, A. R., Schuldt, K. N., Tans, P., Andrews, A., Miller, J. B., Oda, T., Basu, S., Mund, J., Weir, B., Ott, L.,
3142 Aalto, T., Abshire, J. B., Aikin, K., Aoki, S., Apadula, F., Arnold, S., Baier, B., Bartyzel, J., Beyersdorf, A.,
3143 Biermann, T., Biraud, S. C., Boenisch, H., Brailsford, G., Brand, W. A., Chen, G., Chen, H., Chmura, L., Clark, S.,

- 3144 Colomb, A., Commane, R., Conil, S., Couret, C., Cox, A., Cristofanelli, P., Cuevas, E., Curcoll, R., Daube, B.,
3145 Davis, K. J., De Wekker, S., Della Coletta, J., Delmotte, M., DiGangi, E., DiGangi, J. P., di Sarra, A. G.,
3146 Dlugokencky, E., Elkins, J. W., Emmenegger, L., Fang, S., Fischer, M. L., Forster, G., Frumau, A., Galkowski, M.,
3147 Gatti, L. V., Gehrlein, T., Gerbig, C., Gheusi, F., Gloor, E., Gomez-Trueba, V., Goto, D., Griffiths, T., Hammer, S.,
3148 Hanson, C., Haszpra, L., Hatakka, J., Heimann, M., Heliasz, M., Hensen, A., Hermansen, O., Hintsä, E., Holst, J.,
3149 Ivakhov, V., Jaffe, D. A., Jordan, A., Joubert, W., Karion, A., Kawa, S. R., Kazan, V., Keeling, R. F., Keronen, P.,
3150 Kneuer, T., Kolari, P., Komínková, K., Kort, E., Kozlova, E., Krummel, P., Kubistin, D., Labuschagne, C., Lam,
3151 D. H. Y., Lan, X., Langenfelds, R. L., Laurent, O., Laurila, T., Lauvaux, T., Lavric, J., Law, B. E., Lee, J., Lee, O.
3152 S. M., Lehner, I., Lehtinen, K., Leppert, R., Leskinen, A., Leuenberger, M., Levin, I., Levula, J., Lin, J., Lindauer,
3153 M., Loh, Z., Lopez, M., Luijkx, I. T., Lunder, C. R., Machida, T., Mammarella, I., Manca, G., Manning, A.,
3154 Manning, A., Marek, M. V., Martin, M. Y., Matsueda, H., McKain, K., Meijer, H., Meinhardt, F., Merchant, L.,
3155 Mihalopoulos, N., Miles, N. L., Miller, C. E., Mitchell, L., Mölder, M., Montzka, S., Moore, F., Moossen, H.,
3156 Morgan, E., Morgui, J.-A., Morimoto, S., Müller-Williams, J., Munger, J. W., Munro, D., Myhre, C. L., Nakaoka,
3157 S.-I., Necki, J., Newman, S., Nichol, S., Niwa, Y., Obersteiner, F., O'Doherty, S., Paplawsky, B., Peischl, J.,
3158 Peltola, O., Piacentino, S., Pichon, J.-M., Pickers, P., Piper, S., Pitt, J., Plass-Dülmer, C., Platt, S. M., Prinzivalli,
3159 S., Ramonet, M., Ramos, R., Reyes-Sanchez, E., Richardson, S. J., Riris, H., Rivas, P. P., Ryerson, T., Saito, K.,
3160 Sargent, M., Sasakawa, M., Scheeren, B., Schuck, T., Schumacher, M., Seifert, T., Sha, M. K., Shepson, P., Shook,
3161 M., Sloop, C. D., Smith, P., Stanley, K., Steinbacher, M., Stephens, B., Sweeney, C., Thoning, K., Timas, H., Torn,
3162 M., Tørseth, K., Trisolino, P., Turnbull, J., van den Bulk, P., van Dinter, D., Vermeulen, A., Viner, B., Vitkova,
3163 G., Walker, S., Watson, A., Wofsy, S. C., Worsey, J., Worthy, D., Young, D., Zaehle, S., Zahn, A., and Zimnoch,
3164 M.: CarbonTracker CT-NRT.v2023-3, NOAA GML [Data set], <https://doi.org/10.25925/7TAF-J322>, 2023b.
- 3165 Jain, A. K., Meiyappan, P., Song, Y., and House, J. I.: CO₂ emissions from land-use change affected more by
3166 nitrogen cycle, than by the choice of land-cover data, *Global Change Biology*, 19, 2893–2906,
3167 <https://doi.org/10.1111/gcb.12207>, 2013.
- 3168 Jain, P., Barber, Q. E., Taylor, S. W., Whitman, E., Castellanos Acuna, D., Boulanger, Y., Chavardès, R. D., Chen,
3169 J., Englefield, P., Flannigan, M., Girardin, M. P., Hanes, C. C., Little, J., Morrison, K., Skakun, R. S., Thompson,
3170 D. K., Wang, X., Parisien, M.-A.: Drivers and Impacts of the Record-Breaking 2023 Wildfire Season in Canada.
3171 *Nature Communications*, 15(1), p.6764, <https://doi.org/10.1038/s41467-024-51154-7>, 2024.
- 3172 Janssens-Maenhout, G., Crippa, M., Guizzardi, D., Muntean, M., Schaaf, E., Dentener, F., Bergamaschi, P.,
3173 Pagliari, V., Olivier, J. G. J., Peters, J. A. H. W., van Aardenne, J. A., Monni, S., Doering, U., Petrescu, A. M. R.,
3174 Solazzo, E., and Oreggioni, G. D.: EDGAR v4.3.2 Global Atlas of the three major greenhouse gas emissions for
3175 the period 1970–2012, *Earth Syst. Sci. Data*, 11, 959–1002, <https://doi.org/10.5194/essd-11-959-2019>, 2019.
- 3176 Jean-Michel, L., Eric, G., Romain, B.-B., Gilles, G., Angélique, M., Marie, D., Clément, B., Mathieu, H., Olivier,
3177 L. G., Charly, R., Tony, C., Charles-Emmanuel, T., Florent, G., Giovanni, R., Mounir, B., Yann, D., and Pierre-
3178 Yves, L. T.: The Copernicus Global 1/12° Oceanic and Sea Ice GLORYS12 Reanalysis, *Front. Earth Sci.*, 9, 2021.
- 3179 Jiang, F., Ju, W., He, W., Wu, M., Wang, H., Wang, J., Jia, M., Feng, S., Zhang, L., and Chen, J. M.: A 10-year
3180 global monthly averaged terrestrial net ecosystem exchange dataset inferred from the ACOS GOSAT v9 XCO₂
3181 retrievals (GCAS2021), *Earth Syst. Sci. Data*, 14, 3013–3037, <https://doi.org/10.5194/essd-14-3013-2022>, 2022.
- 3182 Jiang, F., Wang, H., Chen, J. M., Ju, W., Tian, X., Feng, S., Li, G., Chen, Z., Zhang, S., Lu, X., Liu, J., Wang, H.,
3183 Wang, J., He, W., and Wu, M.: Regional CO₂ fluxes from 2010 to 2015 inferred from GOSAT XCO₂ retrievals
3184 using a new version of the Global Carbon Assimilation System, *Atmospheric Chem. Phys.*, 21, 1963–1985,
3185 <https://doi.org/10.5194/acp-21-1963-2021>, 2021.
- 3186 Jin, Y., Keeling, R. F., Stephens, B. B., Long, M. C., Patra, P. K., Rödenbeck, C., Morgan, E. J., Kort, E. A., and
3187 Sweeney, C.: Improved atmospheric constraints on Southern Ocean CO₂ exchange. *Proceedings of the National
3188 Academy of Sciences*, 121(6), e2309333121, <https://doi.org/10.1073/pnas.2309333121>, 2024.
- 3189 Jin, Z., Wang, T., Zhang, H., Wang, Y., Ding, J., and Tian, X.: Constraint of satellite CO₂ retrieval on the global
3190 carbon cycle from a Chinese atmospheric inversion system, *Sci. China Earth Sci.*, 66, 609–618,
3191 <https://doi.org/10.1007/s11430-022-1036-7>, 2023.
- 3192 Joos, F. and Spahni, R.: Rates of change in natural and anthropogenic radiative forcing over the past 20,000 years,
3193 *Proceedings of the National Academy of Sciences*, 105, 1425–1430, <https://doi.org/10.1073/pnas.0707386105>,
3194 2008.

- 3195 Jones, C. D., Hickman, J. E., Rumbold, S. T., Walton, J., Lamboll, R. D., Skeie, R. B., Fiedler, S., Forster, P. M.,
3196 Rogelj, J., Abe, M., Botzet, M., Calvin, K., Cassou, C., Cole, J. N. S., Davini, P., Deushi, M., Dix, M., Fyfe, J. C.,
3197 Gillett, N. P., Ilyina, T., Kawamiya, M., Kelley, M., Kharin, S., Koshiro, T., Li, H., Mackallah, C., Müller, W. A.,
3198 Nabat, P., van Noije, T., Nolan, P., Ohgaito, R., Oliví, D., Oshima, N., Parodi, J., Reerink, T. J., Ren, L.,
3199 Romanou, A., Séférian, R., Tang, Y., Timmreck, C., Tjiputra, J., Tourigny, E., Tsigaridis, K., Wang, H., Wu, M.,
3200 Wyser, K., Yang, S., Yang, Y., and Ziehn, T.: The Climate Response to Emissions Reductions Due to COVID-19:
3201 Initial Results From CovidMIP, *Geophys. Res. Lett.*, 48, e2020GL091883, <https://doi.org/10.1029/2020GL091883>,
3202 2021a.
- 3203 Jones, M. W., Abatzoglou, J. T., Veraverbeke, S., Andela, N., Lasslop, G., Forkel, M., Smith, A. J. P., Burton, C.,
3204 Betts, R. A., van der Werf, G. R., Sitch, S., Canadell, J. G., Santín, C., Kolden, C., Doerr, S. H., and Le Quéré, C.:
3205 Global and Regional Trends and Drivers of Fire Under Climate Change, *Rev. Geophys.*, 60, e2020RG000726,
3206 <https://doi.org/10.1029/2020RG000726>, 2022.
- 3207 Jones, M. W., Andrew, R. M., Peters, G. P., Janssens-Maenhout, G., De-Gol, A. J., Ciais, P., Patra, P. K.,
3208 Chevallier, F., and Le Quéré, C.: Gridded fossil CO₂ emissions and related O₂ combustion consistent with national
3209 inventories 1959–2018, *Sci Data*, 8, 2, <https://doi.org/10.1038/s41597-020-00779-6>, 2021b.
- 3210 Jones, M. W., Andrew, R. M., Peters, G. P., Janssens-Maenhout, G., De-Gol, A. J., Dou, X., Liu, Z., Pickers, P.,
3211 Ciais, P., Patra, P. K., Chevallier, F., and Le Quéré, C.: Gridded fossil CO₂ emissions and related O₂ combustion
3212 consistent with national inventories, Zenodo [Data set], <https://doi.org/10.5281/zenodo.17467681>, 2025.
- 3213 Jones, M. W., Kelley, D. I., Burton, C. A., Di Giuseppe, F., Barbosa, M. L. F., Brambleby, E., Hartley, A. J.,
3214 Lombardi, A., Mataveli, G., McNorton, J. R., Spuler, F. R., Wessel, J. B., Abatzoglou, J. T., Anderson, L. O.,
3215 Andela, N., Archibald, S., Armenteras, D., Burke, E., Carmenta, R., Chuvieco, E., Clarke, H., Doerr, S. H.,
3216 Fernandes, P. M., Giglio, L., Hamilton, D. S., Hantson, S., Harris, S., Jain, P., Kolden, C. A., Kurvits, T., Lampe,
3217 S., Meier, S., New, S., Parrington, M., Perron, M. M. G., Qu, Y., Ribeiro, N. S., Saharjo, B. H., San-Miguel-Ayanz,
3218 J., Shuman, J. K., Tanpipat, V., van der Werf, G. R., Veraverbeke, S., and Xanthopoulos, G.: State of Wildfires
3219 2023–2024, *Earth System Science Data*, 16, 3601–3685, <https://doi.org/10.5194/essd-16-3601-2024>, 2024b.
- 3220 Jones, M. W., Veraverbeke, S., Andela, N., Doerr, S. H., Kolden, C., Mataveli, G., Pettinari, M. L., Le Quéré, C.,
3221 Rosan, T. M., van der Werf, G. R. and van Wees, D.: Global rise in forest fire emissions linked to climate change in
3222 the extratropics. *Science*, 386(6719), p.ead15889, 2024c.
- 3223 Jung, M., Reichstein, M., Schwalm, C. R., Huntingford, C., Sitch, S., Ahlström, A., Arneth, A., Camps-Valls, G.,
3224 Ciais, P., Friedlingstein, P., Gans, F., Ichii, K., Jain, A. K., Kato, E., Papale, D., Poulter, B., Raduly, B.,
3225 Rödenbeck, C., Tramontana, G., Viovy, N., Wang, Y.-P., Weber, U., Zaehle, S., and Zeng, N.: Compensatory
3226 water effects link yearly global land CO₂ sink changes to temperature, *Nature*, 541, 516–520,
3227 <https://doi.org/10.1038/nature20780>, 2017.
- 3228 Kaiser, J. W., Heil, A., Andreae, M. O., Benedetti, A., Chubarova, N., Jones, L., Morcrette, J.-J., Razinger, M.,
3229 Schultz, M. G., Suttie, M., and van der Werf, G. R.: Biomass burning emissions estimated with a global fire
3230 assimilation system based on observed fire radiative power, *Biogeosciences*, 9, 527–554,
3231 <https://doi.org/10.5194/bg-9-527-2012>, 2012.
- 3232 Kato, E., Kinoshita, T., Ito, A., Kawamiya, M., and Yamagata, Y.: Evaluation of spatially explicit emission
3233 scenario of land-use change and biomass burning using a process-based biogeochemical model, *J. Land Use Sci.*, 8,
3234 104–122, <https://doi.org/10.1080/1747423X.2011.628705>, 2013.
- 3235 Kawasaki, T., Hasumi, H., and Tanaka, Y.: Role of tide-induced vertical mixing in the deep Pacific Ocean
3236 circulation, *J. Oceanogr.*, 77, 173–184, <https://doi.org/10.1007/s10872-020-00584-0>, 2021.
- 3237 Ke, P., Ciais, P., Sitch, S., Li, W., Bastos, A., Liu, Z., Xu, Y., Gui, X., Bian, J., Goll, D. S., Xi, Y., Li, W.,
3238 O'Sullivan, M., Goncalves de Souza, J., Friedlingstein, P., Chevallier, F.: Low latency carbon budget analysis
3239 reveals a large decline of the land carbon sink in 2023. *National Science Review*, p.nwae367,
3240 <https://doi.org/10.1093/nsr/nwae367>, 2024.
- 3241 Keeley, J. E. and Pausas, J. G.: Distinguishing disturbance from perturbations in fire-prone ecosystems, *Int. J.*
3242 *Wildland Fire*, 28, 282–287, <https://doi.org/10.1071/WF18203>, 2019.

- 3243 Keeling, C. D., Bacastow, R. B., Bainbridge, A. E., Ekdahl, C. A., Guenther, P. R., Waterman, L. S., and Chin, J.
 3244 F. S.: Atmospheric carbon dioxide variations at Mauna Loa Observatory, Hawaii, *Tellus A.*, 28, 538–551,
 3245 <https://doi.org/10.1111/j.2153-3490.1976.tb00701.x>, 1976.
- 3246 Keeling R.F.: Development of an Interferometric Oxygen Analyzer for Precise Measurement of the Atmospheric
 3247 O₂ Mole Fraction, PhD thesis, Harvard University, Cambridge, Massachusetts, available at:
 3248 https://bluemoon.ucsd.edu/publications/ralph/34_PhDthesis.pdf, last access: 23 October 2025, 1988.
- 3249 Keeling, R. F., Manning, A. C., Paplawsky, W. J., and Cox, A. C.: On the long-term stability of reference gases for
 3250 atmospheric O₂/N₂ and CO₂ measurements, *Tellus B Chem. Phys. Meteorol.*, 59, 3–14,
 3251 <https://doi.org/10.1111/j.1600-0889.2006.00196.x>, 2007.
- 3252 Keeling, R. F. and Manning, A. C.: 5.15 - Studies of Recent Changes in Atmospheric O₂ Content, in: *Treatise on*
 3253 *Geochemistry (Second Edition)*, edited by: Holland, H. D. and Turekian, K. K., Elsevier, Oxford, 385–404,
 3254 <https://doi.org/10.1016/B978-0-08-095975-7.00420-4>, 2014.
- 3255 Kelley, D. I., Burton, C., Di Giuseppe, F., Jones, M. W., Barbosa, M. L. F., Brambleby, E., McNorton, J. R., Liu,
 3256 Z., Bradley, A. S. I., Blackford, K., Burke, E., Ciavarella, A., Di Tomaso, E., Eden, J., Ferreira, I. J. M., Fiedler, L.,
 3257 Hartley, A. J., Keeping, T. R., Lampe, S., Lombardi, A., Mataveli, G., Qu, Y., Silva, P. S., Spuler, F. R.,
 3258 Steinmann, C. B., Torres-Vázquez, M. Á., Veiga, R., Van Wees, D., Wessel, J. B., Wright, E., Bilbao, B.,
 3259 Bourbonnais, M., Gao, C., Di Bella, C. M., Dintwe, K., Donovan, V. M., Harris, S., Kukavskaya, E. A., N’Dri, A.
 3260 B., Santín, C., Selaya, G., Sjöström, J., Abatzoglou, J. T., Andela, N., Carmenta, R., Chuvieco, E., Giglio, L.,
 3261 Hamilton, D. S., Hantson, S., Meier, S., Parrington, M., Sadegh, M., San-Miguel-Ayanz, J., Sedano, F., Turco, M.,
 3262 Van Der Werf, G. R., Veraverbeke, S., Anderson, L. O., Clarke, H., Fernandes, P. M., and Kolden, C. A.: State of
 3263 Wildfires 2024–2025, *Earth Syst. Sci. Data*, 17, 5377–5488, <https://doi.org/10.5194/essd-17-5377-2025>, 2025.
- 3264 Keppler, L. and Landschützer, P.: Regional Wind Variability Modulates the Southern Ocean Carbon Sink, *Sci Rep*,
 3265 9, 7384, <https://doi.org/10.1038/s41598-019-43826-y>, 2019.
- 3266 Kharin, V. V., Boer, G. J., Merryfield, W. J., Scinocca, J. F., and Lee, W. -S.: Statistical adjustment of decadal
 3267 predictions in a changing climate, *Geophysical Research Letters*, 39, 2012GL052647,
 3268 <https://doi.org/10.1029/2012GL052647>, 2012.
- 3269 Khatiwala, S., Primeau, F., and Hall, T.: Reconstruction of the history of anthropogenic CO₂ concentrations in the
 3270 ocean, *Nature*, 462, 346–349, <https://doi.org/10.1038/nature08526>, 2009.
- 3271 Khatiwala, S., Tanhua, T., Mikaloff Fletcher, S., Gerber, M., Doney, S. C., Graven, H. D., Gruber, N., McKinley,
 3272 G. A., Murata, A., Ríos, A. F., and Sabine, C. L.: Global ocean storage of anthropogenic carbon, *Biogeosciences*,
 3273 10, 2169–2191, <https://doi.org/10.5194/bg-10-2169-2013>, 2013.
- 3274 Kong, Y., Zheng, B., Zhang, Q., and He, K.: Global and regional carbon budget for 2015–2020 inferred from
 3275 OCO-2 based on an ensemble Kalman filter coupled with GEOS-Chem, *Atmospheric Chem. Phys.*, 22, 10769–
 3276 10788, <https://doi.org/10.5194/acp-22-10769-2022>, 2022.
- 3277 Kou-Giesbrecht, S. and Arora, V. K.: Representing the Dynamic Response of Vegetation to Nitrogen Limitation
 3278 via Biological Nitrogen Fixation in the CLASSIC Land Model, *Global Biogeochemical Cycles*, 36,
 3279 e2022GB007341, <https://doi.org/10.1029/2022GB007341>, 2022.
- 3280 Korsbakken, J. I., Peters, G. P., and Andrew, R. M.: Uncertainties around reductions in China’s coal use and CO₂
 3281 emissions, *Nature Clim Change*, 6, 687–690, <https://doi.org/10.1038/nclimate2963>, 2016.
- 3282 Koven, C. D., Knox, R. G., Fisher, R. A., Chambers, J. Q., Christoffersen, B. O., Davies, S. J., Detto, M., Dietze,
 3283 M. C., Faybishenko, B., Holm, J., Huang, M., Kovenock, M., Kueppers, L. M., Lemieux, G., Massoud, E.,
 3284 McDowell, N. G., Muller-Landau, H. C., Needham, J. F., Norby, R. J., Powell, T., Rogers, A., Serbin, S. P.,
 3285 Shuman, J. K., Swann, A. L. S., Varadharajan, C., Walker, A. P., Wright, S. J., and Xu, C.: Benchmarking and
 3286 parameter sensitivity of physiological and vegetation dynamics using the Functionally Assembled Terrestrial
 3287 Ecosystem Simulator (FATES) at Barro Colorado Island, Panama, *Biogeosciences*, 17, 3017–3044,
 3288 <https://doi.org/10.5194/bg-17-3017-2020>, 2020.
- 3289 Krinner, G., Viovy, N., de Noblet-Ducoudré, N., Ogée, J., Polcher, J., Friedlingstein, P., Ciais, P., Sitch, S., and
 3290 Prentice, I. C.: A dynamic global vegetation model for studies of the coupled atmosphere-biosphere system:

- 3291 DVGM for coupled climate studies, *Global Biogeochem. Cycles*, 19, GB1015,
3292 <https://doi.org/10.1029/2003GB002199>, 2005.
- 3293 Lacroix, F., Ilyina, T., and Hartmann, J.: Oceanic CO₂ outgassing and biological production hotspots induced by
3294 pre-industrial river loads of nutrients and carbon in a global modeling approach, *Biogeosciences*, 17, 55–88,
3295 <https://doi.org/10.5194/bg-17-55-2020>, 2020.
- 3296 Lacroix, F., Ilyina, T., Mathis, M., Laruelle, G. G., and Regnier, P.: Historical increases in land-derived nutrient
3297 inputs may alleviate effects of a changing physical climate on the oceanic carbon cycle, *Glob Change Biol*, 27,
3298 5491–5513, <https://doi.org/10.1111/gcb.15822>, 2021.
- 3299 Lamboll, R. D., Nicholls, Z. R. J., Smith, C. J., Kikstra, J. S., Byers, E., and Rogelj, J.: Assessing the size and
3300 uncertainty of remaining carbon budgets, *Nat. Clim. Change*, <https://doi.org/10.1038/s41558-023-01848-5>, 2023.
- 3301 Lamboll, R. D., Jones, C. D., Skeie, R. B., Fiedler, S., Samset, B. H., Gillett, N. P., Rogelj, J., Forster, P. M., 2021:
3302 Modifying emissions scenario projections to account for the effects of COVID-19: protocol for CovidMIP, *Geosci.
3303 Model Dev.*, 14, 3683–3695, <https://doi.org/10.5194/gmd-14-3683-2021>, 2021.
- 3304 Lan, X., Tans, P. and Thoning, K.: NOAA Greenhouse Gas Marine Boundary Layer Reference - CO₂ [Data set].
3305 NOAA Global Monitoring Laboratory, <https://doi.org/10.15138/DVNP-F961>, 2024.
- 3306 Lan, X., Tans, P. and Thoning, K. W.: Trends in globally-averaged CO₂ determined from NOAA Global
3307 Monitoring Laboratory measurements, <https://doi.org/10.15138/9N0H-ZH07>, 2025.
- 3308 Landschützer, P., Gruber, N., Haumann, F. A., Rödenbeck, C., Bakker, D. C. E., van Heuven, S., Hoppema, M.,
3309 Metzl, N., Sweeney, C., Takahashi, T., Tilbrook, B., and Wanninkhof, R.: The reinvigoration of the Southern
3310 Ocean carbon sink, *Science*, 349, 1221–1224, <https://doi.org/10.1126/science.aab2620>, 2015.
- 3311 Landschützer, P., Gruber, N., and Bakker, D. C. E.: Decadal variations and trends of the global ocean carbon sink:
3312 decadal air-sea CO₂ flux variability, *Global Biogeochem. Cycles*, 30, 1396–1417,
3313 <https://doi.org/10.1002/2015GB005359>, 2016.
- 3314 Lapola, D. M., Pinho, P., Barlow, J., Aragão, L. E. O. C., Berenguer, E., Carmenta, R., Liddy, H. M., Seixas, H.,
3315 Silva, C. V. J., Silva-Junior, C. H. L., Alencar, A. A. C., Anderson, L. O., Armenteras, D., Brovkin, V., Calders,
3316 K., Chambers, J., Chini, L., Costa, M. H., Faria, B. L., Fearnside, P. M., Ferreira, J., Gatti, L., Gutierrez-Velez, V.
3317 H., Han, Z., Hibbard, K., Koven, C., Lawrence, P., Pongratz, J., Portela, B. T. T., Rounsevell, M., Ruane, A. C.,
3318 Schaldach, R., da Silva, S. S., von Randow, C., Walker, W. S.: The drivers and impacts of Amazon forest
3319 degradation. *Science*, 379(6630), p.cabp8622, <https://doi.org/10.1126/science.abp8622>, 2023.
- 3320 Law, R. M., Ziehn, T., Matear, R. J., Lenton, A., Chamberlain, M. A., Stevens, L. E., Wang, Y.-P., Sribnovsky, J.,
3321 Bi, D., Yan, H., and Vohralik, P. F.: The carbon cycle in the Australian Community Climate and Earth System
3322 Simulator (ACCESS-ESM1) – Part 1: Model description and pre-industrial simulation, *Geosci. Model Dev.*, 10,
3323 2567–2590, <https://doi.org/10.5194/gmd-10-2567-2017>, 2017.
- 3324 Laughner, J. L., Roche, S., Kiel, M., Toon, G. C., Wunch, D., Baier, B. C., Biraud, S., Chen, H., Kivi, R.,
3325 Laemmle, T., McKain, K., Quéhé, P.-Y., Rousogonous, C., Stephens, B. B., Walker, K., and Wennberg, P. O.: A
3326 new algorithm to generate a priori trace gas profiles for the GGG2020 retrieval algorithm, *Atmos. Meas. Tech.*, 16,
3327 1121–1146, <https://doi.org/10.5194/amt-16-1121-2023>, 2023.
- 3328 Lauvset, S. K., Lange, N., Tanhua, T., Bittig, H. C., Olsen, A., Kozyr, A., Álvarez, M., Azetsu-Scott, K., Brown, P.
3329 J., Carter, B. R., Cotrim Da Cunha, L., Hoppema, M., Humphreys, M. P., Ishii, M., Jeansson, E., Murata, A.,
3330 Müller, J. D., Pérez, F. F., Schirnack, C., Steinfeldt, R., Suzuki, T., Ulfso, A., Velo, A., Woosley, R. J., and Key,
3331 R. M.: The annual update GLODAPv2.2023: the global interior ocean biogeochemical data product, *Earth Syst.
3332 Sci. Data*, 16, 2047–2072, <https://doi.org/10.5194/essd-16-2047-2024>, 2024.
- 3333 Lawrence, D. M., Fisher, R. A., Koven, C. D., Oleson, K. W., Swenson, S. C., Bonan, G., Collier, N., Ghimire, B.,
3334 van Kampenhout, L., Kennedy, D., Kluzek, E., Lawrence, P. J., Li, F., Li, H., Lombardozzi, D., Riley, W. J.,
3335 Sacks, W. J., Shi, M., Vertenstein, M., Wieder, W. R., Xu, C., Ali, A. A., Badger, A. M., Bisht, G., van den
3336 Broeke, M., Brunke, M. A., Burns, S. P., Buzan, J., Clark, M., Craig, A., Dahlin, K., Drewniak, B., Fisher, J. B.,
3337 Flanner, M., Fox, A. M., Gentile, P., Hoffman, F., Keppel-Aleks, G., Knox, R., Kumar, S., Lenaerts, J., Leung, L.
3338 R., Lipscomb, W. H., Lu, Y., Pandey, A., Pelletier, J. D., Perket, J., Randerson, J. T., Ricciuto, D. M., Sanderson,
3339 B. M., Slater, A., Subin, Z. M., Tang, J., Thomas, R. Q., Val Martin, M., and Zeng, X.: The Community Land

- 3340 Model Version 5: Description of New Features, Benchmarking, and Impact of Forcing Uncertainty, *J. Adv. Model*
 3341 *Earth, Sy.*, 11, 4245–4287, <https://doi.org/10.1029/2018MS001583>, 2019.
- 3342 Le Quéré, C., Rödenbeck, C., Buitenhuis, E. T., Conway, T. J., Langenfelds, R., Gomez, A., Labuschagne, C.,
 3343 Ramonet, M., Nakazawa, T., Metzl, N., Gillett, N., and Heimann, M.: Saturation of the Southern Ocean CO₂ Sink
 3344 Due to Recent Climate Change, *Science*, 316, 1735–1738, <https://doi.org/10.1126/science.1136188>, 2007.
- 3345 Le Quéré, C., Raupach, M. R., Canadell, J. G., Marland, G., Bopp, L., Ciais, P., Conway, T. J., Doney, S. C., Feely,
 3346 R. A., Foster, P., Friedlingstein, P., Gurney, K., Houghton, R. A., House, J. I., Huntingford, C., Levy, P. E., Lomas,
 3347 M. R., Majkut, J., Metzl, N., Ometto, J. P., Peters, G. P., Prentice, I. C., Randerson, J. T., Running, S. W.,
 3348 Sarmiento, J. L., Schuster, U., Sitch, S., Takahashi, T., Viovy, N., van der Werf, G. R., and Woodward, F. I.:
 3349 Trends in the sources and sinks of carbon dioxide, *Nature Geosci*, 2, 831–836, <https://doi.org/10.1038/ngeo689>,
 3350 2009.
- 3351 Le Quéré, C., Andres, R. J., Boden, T., Conway, T., Houghton, R. A., House, J. I., Marland, G., Peters, G. P., van
 3352 der Werf, G. R., Ahlström, A., Andrew, R. M., Bopp, L., Canadell, J. G., Ciais, P., Doney, S. C., Enright, C.,
 3353 Friedlingstein, P., Huntingford, C., Jain, A. K., Jourdain, C., Kato, E., Keeling, R. F., Klein Goldewijk, K., Levis,
 3354 S., Levy, P., Lomas, M., Poulter, B., Raupach, M. R., Schwinger, J., Sitch, S., Stocker, B. D., Viovy, N., Zaehle,
 3355 S., and Zeng, N.: The global carbon budget 1959–2011, *Earth Syst. Sci. Data*, 5, 165–185,
 3356 <https://doi.org/10.5194/essd-5-165-2013>, 2013.
- 3357 Le Quéré, C., Peters, G. P., Andres, R. J., Andrew, R. M., Boden, T. A., Ciais, P., Friedlingstein, P., Houghton, R.
 3358 A., Marland, G., Moriarty, R., Sitch, S., Tans, P., Arneeth, A., Arvanitis, A., Bakker, D. C. E., Bopp, L., Canadell, J.
 3359 G., Chini, L. P., Doney, S. C., Harper, A., Harris, I., House, J. I., Jain, A. K., Jones, S. D., Kato, E., Keeling, R. F.,
 3360 Klein Goldewijk, K., Körtzinger, A., Koven, C., Lefèvre, N., Maignan, F., Omar, A., Ono, T., Park, G.-H., Pfeil,
 3361 B., Poulter, B., Raupach, M. R., Regnier, P., Rödenbeck, C., Saito, S., Schwinger, J., Segsneider, J., Stocker, B.
 3362 D., Takahashi, T., Tilbrook, B., van Heuven, S., Viovy, N., Wanninkhof, R., Wiltshire, A., and Zaehle, S.: Global
 3363 carbon budget 2013, *Earth Syst. Sci. Data*, 6, 235–263, <https://doi.org/10.5194/essd-6-235-2014>, 2014.
- 3364 Le Quéré, C., Moriarty, R., Andrew, R. M., Peters, G. P., Ciais, P., Friedlingstein, P., Jones, S. D., Sitch, S., Tans,
 3365 P., Arneeth, A., Boden, T. A., Bopp, L., Bozec, Y., Canadell, J. G., Chini, L. P., Chevallier, F., Cosca, C. E., Harris,
 3366 I., Hoppema, M., Houghton, R. A., House, J. I., Jain, A. K., Johannessen, T., Kato, E., Keeling, R. F., Kitidis, V.,
 3367 Klein Goldewijk, K., Koven, C., Landa, C. S., Landschützer, P., Lenton, A., Lima, I. D., Marland, G., Mathis, J. T.,
 3368 Metzl, N., Nojiri, Y., Olsen, A., Ono, T., Peng, S., Peters, W., Pfeil, B., Poulter, B., Raupach, M. R., Regnier, P.,
 3369 Rödenbeck, C., Saito, S., Salisbury, J. E., Schuster, U., Schwinger, J., Séférian, R., Segsneider, J., Steinhoff, T.,
 3370 Stocker, B. D., Sutton, A. J., Takahashi, T., Tilbrook, B., van der Werf, G. R., Viovy, N., Wang, Y.-P.,
 3371 Wanninkhof, R., Wiltshire, A., and Zeng, N.: Global carbon budget 2014, *Earth Syst. Sci. Data*, 7, 47–85,
 3372 <https://doi.org/10.5194/essd-7-47-2015>, 2015a.
- 3373 Le Quéré, C., Moriarty, R., Andrew, R. M., Canadell, J. G., Sitch, S., Korsbakken, J. I., Friedlingstein, P., Peters,
 3374 G. P., Andres, R. J., Boden, T. A., Houghton, R. A., House, J. I., Keeling, R. F., Tans, P., Arneeth, A., Bakker, D. C.
 3375 E., Barbero, L., Bopp, L., Chang, J., Chevallier, F., Chini, L. P., Ciais, P., Fader, M., Feely, R. A., Gkritzalis, T.,
 3376 Harris, I., Hauck, J., Ilyina, T., Jain, A. K., Kato, E., Kitidis, V., Klein Goldewijk, K., Koven, C., Landschützer, P.,
 3377 Lausvet, S. K., Lefèvre, N., Lenton, A., Lima, I. D., Metzl, N., Millero, F., Munro, D. R., Murata, A., Nabel, J. E.
 3378 M. S., Nakaoka, S., Nojiri, Y., O'Brien, K., Olsen, A., Ono, T., Pérez, F. F., Pfeil, B., Pierrot, D., Poulter, B.,
 3379 Rehder, G., Rödenbeck, C., Saito, S., Schuster, U., Schwinger, J., Séférian, R., Steinhoff, T., Stocker, B. D.,
 3380 Sutton, A. J., Takahashi, T., Tilbrook, B., van der Laan-Luijkx, I. T., van der Werf, G. R., van Heuven, S.,
 3381 Vandemark, D., Viovy, N., Wiltshire, A., Zaehle, S., and Zeng, N.: Global Carbon Budget 2015, *Earth Syst. Sci.*
 3382 *Data*, 7, 349–396, <https://doi.org/10.5194/essd-7-349-2015>, 2015b.
- 3383 Le Quéré, C., Andrew, R. M., Canadell, J. G., Sitch, S., Korsbakken, J. I., Peters, G. P., Manning, A. C., Boden, T.
 3384 A., Tans, P. P., Houghton, R. A., Keeling, R. F., Alin, S., Andrews, O. D., Anthoni, P., Barbero, L., Bopp, L.,
 3385 Chevallier, F., Chini, L. P., Ciais, P., Currie, K., Delire, C., Doney, S. C., Friedlingstein, P., Gkritzalis, T., Harris,
 3386 I., Hauck, J., Haverd, V., Hoppema, M., Klein Goldewijk, K., Jain, A. K., Kato, E., Körtzinger, A., Landschützer,
 3387 P., Lefèvre, N., Lenton, A., Lienert, S., Lombardozi, D., Melton, J. R., Metzl, N., Millero, F., Monteiro, P. M. S.,
 3388 Munro, D. R., Nabel, J. E. M. S., Nakaoka, S., O'Brien, K., Olsen, A., Omar, A. M., Ono, T., Pierrot, D., Poulter,
 3389 B., Rödenbeck, C., Salisbury, J., Schuster, U., Schwinger, J., Séférian, R., Skjelvan, I., Stocker, B. D., Sutton, A. J.,
 3390 Takahashi, T., Tian, H., Tilbrook, B., van der Laan-Luijkx, I. T., van der Werf, G. R., Viovy, N., Walker, A. P.,
 3391 Wiltshire, A. J., and Zaehle, S.: Global Carbon Budget 2016, *Earth Syst. Sci. Data*, 8, 605–649,
 3392 <https://doi.org/10.5194/essd-8-605-2016>, 2016.

- 3393 Le Quéré, C., Andrew, R. M., Friedlingstein, P., Sitch, S., Pongratz, J., Manning, A. C., Korsbakken, J. I., Peters,
3394 G. P., Canadell, J. G., Jackson, R. B., Boden, T. A., Tans, P. P., Andrews, O. D., Arora, V. K., Bakker, D. C. E.,
3395 Barbero, L., Becker, M., Betts, R. A., Bopp, L., Chevallier, F., Chini, L. P., Ciais, P., Cosca, C. E., Cross, J.,
3396 Currie, K., Gasser, T., Harris, I., Hauck, J., Haverd, V., Houghton, R. A., Hunt, C. W., Hurtt, G., Ilyina, T., Jain, A.
3397 K., Kato, E., Kautz, M., Keeling, R. F., Klein Goldewijk, K., Körtzinger, A., Landschützer, P., Lefèvre, N., Lenton,
3398 A., Lienert, S., Lima, I., Lombardozi, D., Metzl, N., Millero, F., Monteiro, P. M. S., Munro, D. R., Nabel, J. E. M.
3399 S., Nakaoka, S., Nojiri, Y., Padin, X. A., Peregón, A., Pfeil, B., Pierrot, D., Poulter, B., Rehder, G., Reimer, J.,
3400 Rödenbeck, C., Schwinger, J., Séférian, R., Skjelvan, I., Stocker, B. D., Tian, H., Tilbrook, B., Tubiello, F. N., van
3401 der Laan-Luijkx, I. T., van der Werf, G. R., van Heuven, S., Viovy, N., Vuichard, N., Walker, A. P., Watson, A. J.,
3402 Wiltshire, A. J., Zaehle, S., and Zhu, D.: Global Carbon Budget 2017, *Earth Syst. Sci. Data*, 10, 405–448,
3403 <https://doi.org/10.5194/essd-10-405-2018>, 2018a.
- 3404 Le Quéré, C., Andrew, R. M., Friedlingstein, P., Sitch, S., Hauck, J., Pongratz, J., Pickers, P. A., Korsbakken, J. I.,
3405 Peters, G. P., Canadell, J. G., Arneeth, A., Arora, V. K., Barbero, L., Bastos, A., Bopp, L., Chevallier, F., Chini, L.
3406 P., Ciais, P., Doney, S. C., Gkritzalis, T., Goll, D. S., Harris, I., Haverd, V., Hoffman, F. M., Hoppema, M.,
3407 Houghton, R. A., Hurtt, G., Ilyina, T., Jain, A. K., Johannessen, T., Jones, C. D., Kato, E., Keeling, R. F., Klein
3408 Goldewijk, K., Landschützer, P., Lefèvre, N., Lienert, S., Liu, Z., Lombardozi, D., Metzl, N., Munro, D. R.,
3409 Nabel, J. E. M. S., Nakaoka, S., Neill, C., Olsen, A., Ono, T., Patra, P., Peregón, A., Peters, W., Peylin, P., Pfeil,
3410 B., Pierrot, D., Poulter, B., Rehder, G., Resplandy, L., Robertson, E., Rocher, M., Rödenbeck, C., Schuster, U.,
3411 Schwinger, J., Séférian, R., Skjelvan, I., Steinhoff, T., Sutton, A., Tans, P. P., Tian, H., Tilbrook, B., Tubiello, F.
3412 N., van der Laan-Luijkx, I. T., van der Werf, G. R., Viovy, N., Walker, A. P., Wiltshire, A. J., Wright, R., Zaehle,
3413 S., and Zheng, B.: Global Carbon Budget 2018, *Earth Syst. Sci. Data*, 10, 2141–2194, <https://doi.org/10.5194/essd-10-2141-2018>, 2018b.
- 3415 Le Quéré, C., Korsbakken, J. I., Wilson, C., Tosun, J., Andrew, R., Andres, R. J., Canadell, J. G., Jordan, A.,
3416 Peters, G. P., and van Vuuren, D. P.: Drivers of declining CO₂ emissions in 18 developed economies, *Nat. Clim.*
3417 *Chang.*, 9, 213–217, <https://doi.org/10.1038/s41558-019-0419-7>, 2019.
- 3418 Le Quéré, C., Peters, G. P., Friedlingstein, P., Andrew, R. M., Canadell, J. G., Davis, S. J., Jackson, R. B., and
3419 Jones, M. W.: Fossil CO₂ emissions in the post-COVID-19 era, *Nat. Clim. Chang.*, 11, 197–199,
3420 <https://doi.org/10.1038/s41558-021-01001-0>, 2021.
- 3421 Levitus, S., Antonov, J. I., Boyer, T. P., Baranova, O. K., Garcia, H. E., Locarnini, R. A., Mishonov, A. V.,
3422 Reagan, J. R., Seidov, D., Yarosh, E. S., and Zweng, M. M.: World ocean heat content and thermocline sea level
3423 change (0–2000 m), 1955–2010, *Geophys. Res. Lett.*, 39, <https://doi.org/10.1029/2012GL051106>, 2012.
- 3424 Li, H., Ilyina, T., Müller, W. A., and Sienz, F.: Decadal predictions of the North Atlantic CO₂ uptake, *Nat.*
3425 *Commun.*, 7, 11076, <https://doi.org/10.1038/ncomms11076>, 2016.
- 3426 Li, H., Ilyina, T., Müller, W. A., and Landschützer, P.: Predicting the variable ocean carbon sink, *Sci. Adv.*, 5,
3427 eaav6471, <https://doi.org/10.1126/sciadv.aav6471>, 2019.
- 3428 Li, H., Ilyina, T., Loughran, T., Spring, A., and Pongratz, J.: Reconstructions and predictions of the global carbon
3429 budget with an emission-driven Earth system model, *Earth Syst. Dyn.*, 14, 101–119, <https://doi.org/10.5194/esd-14-101-2023>, 2023.
- 3431 Li, W., Ciais, P., Peng, S., Yue, C., Wang, Y., Thurner, M., Saatchi, S. S., Arneeth, A., Avitabile, V., Carvalhais, N.,
3432 Harper, A. B., Kato, E., Koven, C., Liu, Y. Y., Nabel, J. E. M. S., Pan, Y., Pongratz, J., Poulter, B., Pugh, T. A. M.,
3433 Santoro, M., Sitch, S., Stocker, B. D., Viovy, N., Wiltshire, A., Yousefpour, R., and Zaehle, S.: Land-use and land-
3434 cover change carbon emissions between 1901 and 2012 constrained by biomass observations, *Biogeosciences*, 14,
3435 5053–5067, <https://doi.org/10.5194/bg-14-5053-2017>, 2017.
- 3436 Liao, E., Resplandy, L., Liu, J., and Bowman, K. W.: Amplification of the Ocean Carbon Sink During El Niños:
3437 Role of Poleward Ekman Transport and Influence on Atmospheric CO₂, *Global Biogeochem. Cy.*, 34,
3438 e2020GB006574, <https://doi.org/10.1029/2020GB006574>, 2020.
- 3439 Lienert, S. and Joos, F.: A Bayesian ensemble data assimilation to constrain model parameters and land-use carbon
3440 emissions, *Biogeosciences*, 15, 2909–2930, <https://doi.org/10.5194/bg-15-2909-2018>, 2018.
- 3441 Liu, J., Baskaran, L., Bowman, K., Schimel, D., Bloom, A. A., Parazoo, N. C., Oda, T., Carroll, D., Menemenlis,
3442 D., Joiner, J., Commane, R., Daube, B., Gatti, L. V., McKain, K., Miller, J., Stephens, B. B., Sweeney, C., and

- 3443 Wofsy, S.: Carbon Monitoring System Flux Net Biosphere Exchange 2020 (CMS-Flux NBE 2020), 13, 299–330,
3444 <https://doi.org/10.5194/essd-13-299-2021>, 2021.
- 3445 Liu, Z., Guan, D., Wei, W., Davis, S. J., Ciais, P., Bai, J., Peng, S., Zhang, Q., Hubacek, K., Marland, G., Andres,
3446 R. J., Crawford-Brown, D., Lin, J., Zhao, H., Hong, C., Boden, T. A., Feng, K., Peters, G. P., Xi, F., Liu, J., Li, Y.,
3447 Zhao, Y., Zeng, N., and He, K.: Reduced carbon emission estimates from fossil fuel combustion and cement
3448 production in China, *Nature*, 524, 335–338, <https://doi.org/10.1038/nature14677>, 2015.
- 3449 Liu, Z., Zeng, N., Liu, Y., Kalnay, E., Asrar, G., Wu, B., Cai, Q., Liu, D., and Han, P.: Improving the joint
3450 estimation of CO₂ and surface carbon fluxes using a constrained ensemble Kalman filter in COLA (v1.0), *Geosci.*
3451 *Model Dev.*, 15, 5511–5528, <https://doi.org/10.5194/gmd-15-5511-2022>, 2022.
- 3452 Liu, Z., Ciais, P., Deng, Z., Lei, R., Davis, S. J., Feng, S., Zheng, B., Cui, D., Dou, X., Zhu, B., Guo, R., Ke, P.,
3453 Sun, T., Lu, C., He, P., Wang, Y., Yue, X., Wang, Y., Lei, Y., Zhou, H., Cai, Z., Wu, Y., Guo, R., Han, T., Xue, J.,
3454 Boucher, O., Boucher, E., Chevallier, F., Tanaka, K., Wei, Y., Zhong, H., Kang, C., Zhang, N., Chen, B., Xi, F.,
3455 Liu, M., Bréon, F.-M., Lu, Y., Zhang, Q., Guan, D., Gong, P., Kammen, D. M., He, K., and Schellnhuber, H. J.:
3456 Near-real-time monitoring of global CO₂ emissions reveals the effects of the COVID-19 pandemic, *Nat Commun*,
3457 11, 5172, <https://doi.org/10.1038/s41467-020-18922-7>, 2020a.
- 3458 Liu, Z., Ciais, P., Deng, Z., Davis, S. J., Zheng, B., Wang, Y., Cui, D., Zhu, B., Dou, X., Ke, P., Sun, T., Guo, R.,
3459 Zhong, H., Boucher, O., Bréon, F.-M., Lu, C., Guo, R., Xue, J., Boucher, E., Tanaka, K., and Chevallier, F.:
3460 Carbon Monitor, a near-real-time daily dataset of global CO₂ emission from fossil fuel and cement production, *Sci*
3461 *Data*, 7, 392, <https://doi.org/10.1038/s41597-020-00708-7>, 2020b.
- 3462 Long, M. C., Stephens, B. B., McKain, K., Sweeney, C., Keeling, R. F., Kort, E. A., Morgan, E. J., Bent, J. D.,
3463 Chandra, N., Chevallier, F., Commane, R., Daube, B. C., Krummel, P. B., Loh, Z., Luijkx, I. T., Munro, D., Patra,
3464 P., Peters, W., Ramonet, M., Rödenbeck, C., Stavert, A., Tans, P., Wofsy, S. C.: Strong Southern Ocean carbon
3465 uptake evident in airborne observations. *Science*, 374(6572), 1275–1280, <https://doi.org/10.1126/science.abi4355>,
3466 2021.
- 3467 Lovenduski, N. S., Bonan, G. B., Yeager, S. G., Lindsay, K., and Lombardozzi, D. L.: High predictability of
3468 terrestrial carbon fluxes from an initialized decadal prediction system, *Environ. Res. Lett.*, 14, 124074,
3469 <https://doi.org/10.1088/1748-9326/ab5c55>, 2019a.
- 3470 Lovenduski, N. S., Yeager, S. G., Lindsay, K., and Long, M. C.: Predicting near-term variability in ocean carbon
3471 uptake, *Earth Syst. Dyn.*, 10, 45–57, <https://doi.org/10.5194/esd-10-45-2019>, 2019b.
- 3472 Lutz, F., Herzfeld, T., Heinke, J., Rolinski, S., Schaphoff, S., von Bloh, W., Stoorvogel, J. J., and Müller, C.:
3473 Simulating the effect of tillage practices with the global ecosystem model LPJmL (version 5.0-tillage), *Geosci.*
3474 *Model Dev.*, 12, 2419–2440, <https://doi.org/10.5194/gmd-12-2419-2019>, 2019.
- 3475 Ma, L., Hurtt, G., Ott, L., Sahajpal, R., Fisk, J., Lamb, R., Tang, H., Flanagan, S., Chini, L., Chatterjee, A., and
3476 Sullivan, J.: Global evaluation of the Ecosystem Demography model (ED v3.0), *Geosci. Model Dev.*, 15, 1971–
3477 1994, <https://doi.org/10.5194/gmd-15-1971-2022>, 2022.
- 3478 Magi, B. I., Rabin, S., Shevliakova, E., and Pacala, S.: Separating agricultural and non-agricultural fire seasonality
3479 at regional scales, *Biogeosciences*, 9, 3003–3012, <https://doi.org/10.5194/bg-9-3003-2012>, 2012.
- 3480 Maksyutov, S., Oda, T., Saito, M., Janardan, R., Belikov, D., Kaiser, J. W., Zhuravlev, R., Ganshin, A., Valsala,
3481 V. K., Andrews, A., Chmura, L., Dlugokencky, E., Haszpra, L., Langenfelds, R. L., Machida, T., Nakazawa, T.,
3482 Ramonet, M., Sweeney, C., and Worthy, D.: Technical note: A high-resolution inverse modelling technique for
3483 estimating surface CO₂ fluxes based on the NIES-TM-FLEXPART coupled transport model and its adjoint,
3484 *Atmos. Chem. Phys.*, 21, 1245–1266, <https://doi.org/10.5194/acp-21-1245-2021>, 2021.
- 3485 Masarie, K. A. and Tans, P. P.: Extension and integration of atmospheric carbon dioxide data into a globally
3486 consistent measurement record, *J. Geophys. Res.*, 100, 11593, <https://doi.org/10.1029/95JD00859>, 1995.
- 3487 Mataveli, G., Jones, M.W., Carmenta, R., Sanchez, A., Dutra, D.J., Chaves, M., de Oliveira, G., Anderson, L.O.
3488 and Aragão, L.E.: Deforestation falls but rise of wildfires continues degrading Brazilian Amazon forests. *Global*
3489 *Change Biology*, 30(2), p.e17202, <https://doi.org/10.1111/gcb.17202>, 2024.

- 3490 Mather, A. S.: The transition from deforestation to reforestation in Europe, in: *Agricultural technologies and*
3491 *tropical deforestation* (eds. Angelsen, A.; Kaimowitz, D.), CABI in association with centre for international
3492 *Forestry Research*, 35–52, 2001.
- 3493 Mauritsen, T., Bader, J., Becker, T., Behrens, J., Bittner, M., Brokopf, R., Brovkin, V., Claussen, M., Crueger, T.,
3494 Esch, M., Fast, I., Fiedler, S., Fläschner, D., Gayler, V., Giorgetta, M., Goll, D. S., Haak, H., Hagemann, S.,
3495 Hedemann, C., Hohenegger, C., Ilyina, T., Jahns, T., Jimenéz-de-la-Cuesta, D., Jungclaus, J., Kleinen, T., Kloster,
3496 S., Kracher, D., Kinne, S., Kleberg, D., Lasslop, G., Kornblueh, L., Marotzke, J., Matei, D., Meraner, K.,
3497 Mikolajewicz, U., Modali, K., Möbis, B., Müller, W. A., Nabel, J. E. M. S., Nam, C. C. W., Notz, D., Nyawira, S.-
3498 S., Paulsen, H., Peters, K., Pincus, R., Pohlmann, H., Pongratz, J., Popp, M., Raddatz, T. J., Rast, S., Redler, R.,
3499 Reick, C. H., Rohrschneider, T., Schemann, V., Schmidt, H., Schnur, R., Schulzweida, U., Six, K. D., Stein, L.,
3500 Stemmler, I., Stevens, B., von Storch, J.-S., Tian, F., Voigt, A., Vrese, P., Wieners, K.-H., Wilkenskjeld, S.,
3501 Winkler, A., and Roeckner, E.: Developments in the MPI-M Earth System Model version 1.2 (MPI-ESM1.2) and
3502 Its Response to Increasing CO₂, *J. Adv. Model Earth Sy.*, 11, 998–1038, <https://doi.org/10.1029/2018MS001400>,
3503 2019.
- 3504 Mayot, N., Buitenhuis, E. T., Wright, R. M., Hauck, J., Bakker, D. C. E., and Le Quéré, C.: Constraining the trend
3505 in the ocean CO₂ sink during 2000–2022. *Nat Commun* 15, 8429, <https://doi.org/10.1038/s41467-024-52641-7>,
3506 2024.
- 3507 McGrath, M. J., Luyssaert, S., Meyfroidt, P., Kaplan, J. O., Bürgi, M., Chen, Y., Erb, K., Gimmi, U., McNerney,
3508 D., Naudts, K., Otto, J., Pasztor, F., Ryder, J., Schelhaas, M.-J., and Valade, A.: Reconstructing European forest
3509 management from 1600 to 2010, *12*, 4291–4316, <https://doi.org/10.5194/bg-12-4291-2015>, 2015.
- 3510 McKinley, G. A., Fay, A. R., Eddebbar, Y. A., Gloege, L., and Lovenduski, N. S.: External Forcing Explains
3511 Recent Decadal Variability of the Ocean Carbon Sink, *AGU Advances*, 1, e2019AV000149,
3512 <https://doi.org/10.1029/2019AV000149>, 2020.
- 3513 McKinley, G. A., Fay, A. R., Lovenduski, N. S., and Pilcher, D. J.: Natural Variability and Anthropogenic Trends
3514 in the Ocean Carbon Sink, *Annu. Rev. Mar. Sci.*, 9, 125–150, <https://doi.org/10.1146/annurev-marine-010816-060529>, 2017.
- 3516 Meiyappan, P., Jain, A. K., and House, J. I.: Increased influence of nitrogen limitation on CO₂ emissions from
3517 future land use and land use change, *Global Biogeochem. Cycles*, 29, 1524–1548,
3518 <https://doi.org/10.1002/2015GB005086>, 2015.
- 3519 Melo, J., Rossi, S., Achard, F., Alkama, R., Canadell, J. G., Federici, S., Friedlingstein, P., Gibbs, D., Harris, N.,
3520 Heinrich, V., O’Sullivan, M., Peters, G., Pongratz, J., Rose, M., Roman-Cuesta, R., Sanz Sanchez, M. J.,
3521 Schwingshackl, C., Sitch, S., and Grassi, G.: The LULUCF Data Hub: translating global land use emissions
3522 estimates into the national GHG inventory framework (Version 3.0, 2025 NGHGI release) (3.0),
3523 <https://doi.org/10.5281/ZENODO.17140775>, 2025.
- 3524 Melton, J. R., Arora, V. K., Wisernig-Cojoc, E., Seiler, C., Fortier, M., Chan, E., and Teckentrup, L.: CLASSIC
3525 v1.0: the open-source community successor to the Canadian Land Surface Scheme (CLASS) and the Canadian
3526 Terrestrial Ecosystem Model (CTEM) – Part 1: Model framework and site-level performance, *Geosci. Model Dev.*,
3527 13, 2825–2850, <https://doi.org/10.5194/gmd-13-2825-2020>, 2020.
- 3528 Mercado, L. M., Bellouin, N., Sitch, S., Boucher, O., Huntingford, C., Wild, M., and Cox, P. M.: Impact of
3529 changes in diffuse radiation on the global land carbon sink, *Nature*, 458, 1014–1017,
3530 <https://doi.org/10.1038/nature07949>, 2009.
- 3531 Merchant, C. J., Embury, O., Bulgin, C. E., Block, T., Corlett, G. K., Fiedler, E., Good, S. A., Mittaz, J., Rayner,
3532 N. A., Berry, D., Eastwood, S., Taylor, M., Tsushima, Y., Waterfall, A., Wilson, R., and Donlon, C.: Satellite-
3533 based time-series of sea-surface temperature since 1981 for climate applications, *Sci. Data*, 6, 223,
3534 <https://doi.org/10.1038/s41597-019-0236-x>, 2019.
- 3535 Moorcroft, P. R., Hurtt, G. C., and Pacala, S. W.: A Method for Scaling Vegetation Dynamics: The Ecosystem
3536 Demography Model (ed), *Ecol. Monogr.*, 71, 557–586, [https://doi.org/10.1890/0012-9615\(2001\)071\[0557:AMFSVD\]2.0.CO;2](https://doi.org/10.1890/0012-9615(2001)071[0557:AMFSVD]2.0.CO;2), 2001.

- 3538 Müller, J. D., Gruber, N., Carter, B., Feely, R., Ishii, M., Lange, N., Lauvset, S. K., Murata, A., Olsen, A., Pérez, F.
3539 F., Sabine, C., Tanhua, T., Wanninkhof, R., and Zhu, D.: Decadal Trends in the Oceanic Storage of Anthropogenic
3540 Carbon From 1994 to 2014, *AGU Adv.*, 4, e2023AV000875, <https://doi.org/10.1029/2023AV000875>, 2023.
- 3541 Müller, J. D., Gruber, N., Schneuwly, A., Bakker, D. C. E., Gehlen, M., Gregor, L., Hauck, J., Landschützer, P.,
3542 and McKinley, G. A.: Unexpected decline in the ocean carbon sink under record-high sea surface temperatures in
3543 2023, *Nat. Clim. Chang.*, 15, 978–985, <https://doi.org/10.1038/s41558-025-02380-4>, 2025.
- 3544 Müller, J. and Joos, F.: Committed and projected future changes in global peatlands – continued transient model
3545 simulations since the Last Glacial Maximum, *Biogeosciences*, 18, 3657–3687, [https://doi.org/10.5194/bg-18-3657-](https://doi.org/10.5194/bg-18-3657-2021)
3546 2021, 2021.
- 3547 Nayagam, L., Maksyutov, S., Oda, T., Janardanan, R., Trisolino, P., Zeng J., Kaiser, J.W. and Matsunaga, T.: A
3548 top-down estimation of subnational CO₂ budget using a global high-resolution inverse model with data from
3549 regional surface networks, *Environ. Res. Lett.*, 19, 0140312024, <https://doi.org/10.1088/1748-9326/ad0f74>, 2024.
- 3550 NCEP: National Centers for Environmental Prediction. ONI Index. Cold & Warm Episodes by Season [Data set],
3551 available at: https://www.cpc.ncep.noaa.gov/products/analysis_monitoring/ensostuff/ONI_v5.php, last access: 23
3552 October 2025, 2025.
- 3553 Nayagam, L., Maksyutov, S., Janardanan, R., Oda, T., Tiwari, Y. K., Sreenivas, G., Datye, A., Jain, C. D., Ratnam,
3554 M. V., Sinha, V., Hakkim, H., Terao, Y., Naja, M., Ahmed, Md. K., Mukai, H., Zeng, J., Kaiser, J. W., Someya,
3555 Y., Yoshida, Y., and Matsunaga, T.: Indian Land Carbon Sink Estimated from Surface and GOSAT Observations,
3556 *Remote Sensing*, 17, 450, <https://doi.org/10.3390/rs17030450>, 2025.
- 3557 Nevison, C.D., Mahowald, N.M., Doney, S.C., Lima, I.D. and Cassar, N.: Impact of variable air-sea O₂ and CO₂
3558 fluxes on atmospheric potential oxygen (APO) and land-ocean carbon sink partitioning, *Biogeosciences*, 5(3),
3559 pp.875-889, <https://doi.org/10.5194/bg-5-875-2008>, 2008.
- 3560 Niu, G.-Y., Yang, Z.-L., Mitchell, K. E., Chen, F., Ek, M. B., Barlage, M., Kumar, A., Manning, K., Niyogi, D.,
3561 Rosero, E., Tewari, M., and Xia, Y.: The community Noah land surface model with multiparameterization options
3562 (Noah-MP): 1. Model description and evaluation with local-scale measurements, *J. Geophys. Res. Atmospheres*,
3563 116, <https://doi.org/10.1029/2010JD015139>, 2011.
- 3564 Niwa, Y., Ishijima, K., Ito, A., and Iida, Y.: Toward a long-term atmospheric CO₂ inversion for elucidating natural
3565 carbon fluxes: technical notes of NISMOM-CO₂ v2021.1, *Prog. Earth Planet Sci.*, 9, 42,
3566 <https://doi.org/10.1186/s40645-022-00502-6>, 2022.
- 3567 Niwa, Y., Fujii, Y., Sawa, Y., Iida, Y., Ito, A., Satoh, M., Imasu, R., Tsuboi, K., Matsueda, H., and Saigusa, N.: A
3568 4D-Var inversion system based on the icosahedral grid model (NICAM-TM 4D-Var v1.0) – Part 2: Optimization
3569 scheme and identical twin experiment of atmospheric CO₂ inversion, *Geosci. Model Dev.*,
3570 10, 2201–2219, <https://doi.org/10.5194/gmd-10-2201-2017>, 2017.
- 3571 Niwa, Y., Langenfelds, R., Krummel, P., Loh, Zoe, Worthy, Doug, Hatakka, Juha, Aalto, Tuula, Ramonet, Michel,
3572 Delmotte, Marc, Schmidt, Martina, Gheusi, Francois, Mihalopoulos, N., Morgui, J.A., Andrews, Arlyn,
3573 Dlugokencky, Ed, Lee, John, Sweeney, Colm, Thoning, Kirk, Tans, Pieter, De Wekker, Stephan, Fischer, Marc L.,
3574 Jaffe, Dan, McKain, Kathryn, Viner, Brian, Miller, John B., Karion, Anna, Miller, Charles, Sloop, Christopher D.,
3575 Saito, Kazuyuki, Aoki, Shuji, Morimoto, Shinji, Goto, Daisuke, Steinbacher, Martin, Myhre, Cathrine Lund,
3576 Hermanssen, Ove, Stephens, Britton, Keeling, Ralph, Afshar, Sara, Paplawsky, Bill, Cox, Adam, Walker, Stephen,
3577 Schuldt, Kenneth, Mukai, Hitoshi, Machida, Toshinobu, Sasakawa, Motoki, Nomura, Shohei, Ito, Akihiko, Iida,
3578 Yosuke, and Jones, Matthew W.: Long-term global CO₂ fluxes estimated by NICAM-based Inverse Simulation for
3579 Monitoring CO₂ (NISMOM-CO₂) (ver.2022.1), National Institute for Environmental Studies Japan [Data set],
3580 <https://doi.org/10.17595/20201127.001>, 2020.
- 3581 Norby, R.J.: Forest productivity response to elevated CO₂ in free-air CO₂ enrichment experiments: the 23 percent
3582 solution, revisited, *New Phytologist*, <https://doi.org/10.1111/nph.70162>, 2025.
- 3583 Obermeier, W. A., Nabel, J. E. M. S., Loughran, T., Hartung, K., Bastos, A., Havermann, F., Anthoni, P., Arneth,
3584 A., Goll, D. S., Lienert, S., Lombardozi, D., Luyssaert, S., McGuire, P. C., Melton, J. R., Poulter, B., Sitch, S.,
3585 Sullivan, M. O., Tian, H., Walker, A. P., Wiltshire, A. J., Zaehle, S., and Pongratz, J.: Modelled land use and land
3586 cover change emissions – a spatio-temporal comparison of different approaches, 12, 635–670,
3587 <https://doi.org/10.5194/esd-12-635-2021>, 2021.

- 3588 Obermeier, W. A., Schwingshackl, C., Ganzenmüller, R., Grassi, G., Heinrich, V., Luijkx, I. T., Bastos, A., Ciais,
3589 P., Sitch, S., and Pongratz, J.: Differences and uncertainties in land-use CO₂ flux estimates, *Nat Rev Earth*
3590 *Environ*, <https://doi.org/10.1038/s43017-025-00730-6>, 2025.
- 3591 O'Dell, C. W., Eldering, A., Wennberg, P. O., Crisp, D., Gunson, M. R., Fisher, B., Frankenberg, C., Kiel, M.,
3592 Lindqvist, H., Mandrake, L., Merrelli, A., Natraj, V., Nelson, R. R., Osterman, G. B., Payne, V. H., Taylor, T. E.,
3593 Wunch, D., Drouin, B. J., Oyafuso, F., Chang, A., McDuffie, J., Smyth, M., Baker, D. F., Basu, S., Chevallier, F.,
3594 Crowell, S. M. R., Feng, L., Palmer, P. I., Dubey, M., García, O. E., Griffith, D. W. T., Hase, F., Iraci, L. T., Kivi,
3595 R., Morino, I., Notholt, J., Ohyama, H., Petri, C., Roehl, C. M., Sha, M. K., Strong, K., Sussmann, R., Te, Y.,
3596 Uchino, O., and Velazco, V. A.: Improved retrievals of carbon dioxide from Orbiting Carbon Observatory-2 with
3597 the version 8 ACOS algorithm, *Atmos. Meas. Tech.*, 11, 6539–6576, <https://doi.org/10.5194/amt-11-6539-2018>,
3598 2018.
- 3599 O'Rourke, P. R., Smith, S. J., Mott, A., Ahsan, H., McDuffie, E. E., Crippa, M., Klimont, Z., McDonald, B., Wang,
3600 S., Nicholson, M. B., Feng, L., and Hoesly, R. M.: CEDS v_2021_04_21 Release Emission Data, Zenodo [Data
3601 set], <https://doi.org/10.5281/zenodo.4741285>, 2021.
- 3602 O'Sullivan, M., Zhang, Y., Bellouin, N., Harris, I., Mercado, L. M., Sitch, S., Ciais, P., and Friedlingstein, P.:
3603 Aerosol–light interactions reduce the carbon budget imbalance, *Environ. Res. Lett.*, 16, 124072,
3604 <https://doi.org/10.1088/1748-9326/ac3b77>, 2021.
- 3605 O'Sullivan, M., Friedlingstein, P., Sitch, S., Anthoni, P., Arneeth, A., Arora, V. K., Bastrikov, V., Delire, C., Goll,
3606 D. S., Jain, A., Kato, E., Kennedy, D., Knauer, J., Lienert, S., Lombardozzi, D., McGuire, P. C., Melton, J. R.,
3607 Nabel, J. E. M. S., Pongratz, J., Poulter, B., Séférian, R., Tian, H., Vuichard, N., Walker, A. P., Yuan, W., Yue, X.,
3608 and Zaehle, S.: Process-oriented analysis of dominant sources of uncertainty in the land carbon sink, *Nat.*
3609 *Commun.*, 13, 4781, <https://doi.org/10.1038/s41467-022-32416-8>, 2022.
- 3610 O'Sullivan, M., Spracklen, D. V., Batterman, S. A., Arnold, S. R., Gloor, M., and Buermann, W.: Have Synergies
3611 Between Nitrogen Deposition and Atmospheric CO₂ Driven the Recent Enhancement of the Terrestrial Carbon
3612 Sink?, *Glob. Biogeochem. Cycles*, 33, 163–180, <https://doi.org/10.1029/2018GB005922>, 2019.
- 3613 O'Sullivan, M., Sitch, S., Friedlingstein, P., Luijkx, I. T., Peters, W., Rosan, T. M., Arneeth, A., Arora, V. K.,
3614 Chandra, N., Chevallier, F., Ciais, P., Falk, S., Feng, L., Gasser, T., Houghton, R. A., Jain, A. K., Kato, E.,
3615 Kennedy, D., Knauer, J., McGrath, M. J., Niwa, Y., Palmer, P. I., Patra, P. K., Pongratz, J., Poulter, B., Rödenbeck,
3616 C., Schwingshackl, C., Sun, Q., Tian, H., Walker, A. P., Yang, D., Yuan, W., Yue, X., and Zaehle, S.: The key role
3617 of forest disturbance in reconciling estimates of the northern carbon sink. *Commun Earth Environ* 5, 705,
3618 <https://doi.org/10.1038/s43247-024-01827-4>, 2024.
- 3619 O'Sullivan, M., Friedlingstein, P., Sitch, S., Pongratz, J., Schwingshackl, C., Gasser, T., Ciais, P., Arora, V., Kato,
3620 E., Knauer, J., Nützel, T., Sun, Q., Yuan, W., and Zaehle, S.: An improved approach to estimate the natural land
3621 carbon sink, 27 July 2025, PREPRINT (Version 1) available at Research Square [<https://doi.org/10.21203/rs.3.rs-7207206/v1>], 2025.
- 3623 Palmer, P. I., Feng, L., Baker, D., Chevallier, F., Bösch, H., and Somkuti, P.: Net carbon emissions from African
3624 biosphere dominate pan-tropical atmospheric CO₂ signal, *Nat Commun*, 10, 3344, <https://doi.org/10.1038/s41467-019-11097-w>, 2019.
- 3626 Pan, Y., Birdsey, R. A., Fang, J., Houghton, R., Kauppi, P. E., Kurz, W. A., Phillips, O. L., Shvidenko, A., Lewis,
3627 S. L., Canadell, J. G., Ciais, P., Jackson, R. B., Pacala, S. W., McGuire, A. D., Piao, S., Rautiainen, A., Sitch, S.,
3628 and Hayes, D.: A Large and Persistent Carbon Sink in the World's Forests, *Science*, 333, 988–993,
3629 <https://doi.org/10.1126/science.1201609>, 2011.
- 3630 Pandey, S., Miller, J. B., Basu, S., Liu, J., Weir, B., Byrne, B., Chevallier, F., Bowman, K. W., Liu, Z., Deng, F.,
3631 O'Dell, C. W., and Chatterjee, A.: Toward Low-Latency Estimation of Atmospheric CO₂ Growth Rates Using
3632 Satellite Observations: Evaluating Sampling Errors of Satellite and In Situ Observing Approaches, *AGU Advances*,
3633 5, e2023AV001145, <https://doi.org/10.1029/2023AV001145>, 2024.
- 3634 Pandey, S., Chevallier, F., Rödenbeck, C., Byrne, B., Chatterjee, A., Liu, J., and Frankenberg, C.: Reduction in
3635 Earth's carbon budget imbalance, *Nat Commun*, 16, 6818, <https://doi.org/10.1038/s41467-025-61588-2>, 2025.

- 3636 Patra, P. K., Takigawa, M., Watanabe, S., Chandra, N., Ishijima, K., and Yamashita, Y.: Improved Chemical
3637 Tracer Simulation by MIROC4.0-based Atmospheric Chemistry-Transport Model (MIROC4-ACTM), SOLA, 14,
3638 91–96, <https://doi.org/10.2151/sola.2018-016>, 2018.
- 3639 Pendrill, F., Persson, U. M., Godar, J., Kastner, T., Moran, D., Schmidt, S., and Wood, R.: Agricultural and
3640 forestry trade drives large share of tropical deforestation emissions, *Global Environmental Change*, 56, 1–10,
3641 <https://doi.org/10.1016/j.gloenvcha.2019.03.002>, 2019.
- 3642 Pérez, F. F., Becker, M., Goris, N., Gehlen, M., López-Mozos, M., Tjiputra, J., Olsen, A., Müller, J. D., Huertas, I.
3643 E., Chau, T. T. T., Cainzos, V., Velo, A., Benard, G., Hauck, J., Gruber, N., and Wanninkhof, R.: An Assessment
3644 of CO₂ Storage and Sea-Air Fluxes for the Atlantic Ocean and Mediterranean Sea Between 1985 and 2018. *Global*
3645 *Biogeochemical Cycles*, 38(4), e2023GB007862, <https://doi.org/10.1029/2023GB007862>, 2024.
- 3646 Peters, G. P., Minx, J. C., Weber, C. L., and Edenhofer, O.: Growth in emission transfers via international trade
3647 from 1990 to 2008, *Proceedings of the National Academy of Sciences*, 108, 8903–8908,
3648 <https://doi.org/10.1073/pnas.1006388108>, 2011a.
- 3649 Peters, G. P., Marland, G., Le Quéré, C., Boden, T., Canadell, J. G., and Raupach, M. R.: Rapid growth in CO₂
3650 emissions after the 2008–2009 global financial crisis, *Nature Clim Change*, 2, 2–4,
3651 <https://doi.org/10.1038/nclimate1332>, 2012a.
- 3652 Peters, G. P., Andrew, R. M., Boden, T., Canadell, J. G., Ciais, P., Le Quéré, C., Marland, G., Raupach, M. R., and
3653 Wilson, C.: The challenge to keep global warming below 2 °C, *Nature Clim Change*, 3, 4–6,
3654 <https://doi.org/10.1038/nclimate1783>, 2013.
- 3655 Peters, G. P., Le Quéré, C., Andrew, R. M., Canadell, J. G., Friedlingstein, P., Ilyina, T., Jackson, R. B., Joos, F.,
3656 Korsbakken, J. I., McKinley, G. A., Sitch, S., and Tans, P.: Towards real-time verification of CO₂ emissions,
3657 *Nature Clim Change*, 7, 848–850, <https://doi.org/10.1038/s41558-017-0013-9>, 2017a.
- 3658 Peters, G. P., Andrew, R. M., Canadell, J. G., Fuss, S., Jackson, R. B., Korsbakken, J. I., Le Quéré, C. and
3659 Nakicenovic, N.: Key indicators to track current progress and future ambition of the Paris Agreement, 7, 118–122,
3660 <https://doi.org/10.1038/nclimate3202>, 2017b.
- 3661 Peters, G. P., Andrew, R. M., Canadell, J. G., Friedlingstein, P., Jackson, R. B., Korsbakken, J. I., Le Quéré, C.,
3662 and Peregón, A.: Carbon dioxide emissions continue to grow amidst slowly emerging climate policies, *Nat. Clim.*
3663 *Chang.*, 10, 3–6, <https://doi.org/10.1038/s41558-019-0659-6>, 2020.
- 3664 Peters, W., Miller, J. B., Whitaker, J., Denning, A. S., Hirsch, A., Krol, M. C., Zupanski, D., Bruhwiler, L., and
3665 Tans, P. P.: An ensemble data assimilation system to estimate CO₂ surface fluxes from atmospheric trace gas
3666 observations, *J. Geophys. Res. Atmospheres*, 110, <https://doi.org/10.1029/2005JD006157>, 2005.
- 3667 Petrescu, A. M. R., Peters, G. P., Janssens-Maenhout, G., Ciais, P., Tubiello, F. N., Grassi, G., Nabuurs, G.-J.,
3668 Leip, A., Carmona-García, G., Winiwarter, W., Höglund-Isaksson, L., Günther, D., Solazzo, E., Kiesow, A.,
3669 Bastos, A., Pongratz, J., Nabel, J. E. M. S., Conchedda, G., Pilli, R., Andrew, R. M., Schelhaas, M.-J., and Dolman,
3670 A. J.: European anthropogenic AFOLU greenhouse gas emissions: a review and benchmark data, *Earth Syst. Sci.*
3671 *Data*, 12, 961–1001, <https://doi.org/10.5194/essd-12-961-2020>, 2020.
- 3672 Pfeil, B., Olsen, A., Bakker, D. C. E., Hankin, S., Koyuk, H., Kozyr, A., Malczyk, J., Manke, A., Metz, N., Sabine,
3673 C. L., Akl, J., Alin, S. R., Bates, N., Bellerby, R. G. J., Borges, A., Boutin, J., Brown, P. J., Cai, W.-J., Chavez, F.
3674 P., Chen, A., Cosca, C., Fassbender, A. J., Feely, R. A., González-Dávila, M., Goyet, C., Hales, B., Hardman-
3675 Mountford, N., Heinze, C., Hood, M., Hoppema, M., Hunt, C. W., Hydes, D., Ishii, M., Johannessen, T., Jones, S.
3676 D., Key, R. M., Körtzinger, A., Landschützer, P., Lauvset, S. K., Lefèvre, N., Lenton, A., Lourantou, A., Merlivat,
3677 L., Midorikawa, T., Mintrop, L., Miyazaki, C., Murata, A., Nakadate, A., Nakano, Y., Nakaoka, S., Nojiri, Y.,
3678 Omar, A. M., Padin, X. A., Park, G.-H., Paterson, K., Perez, F. F., Pierrot, D., Poisson, A., Ríos, A. F., Santana-
3679 Casiano, J. M., Salisbury, J., Sarma, V. V. S. S., Schlitzer, R., Schneider, B., Schuster, U., Sieger, R., Skjelvan, I.,
3680 Steinhoff, T., Suzuki, T., Takahashi, T., Tedesco, K., Telszewski, M., Thomas, H., Tilbrook, B., Tjiputra, J.,
3681 Vandemark, D., Veness, T., Wanninkhof, R., Watson, A. J., Weiss, R., Wong, C. S., and Yoshikawa-Inoue, H.: A
3682 uniform, quality controlled Surface Ocean CO₂ Atlas (SOCAT), *Earth Syst. Sci. Data*, 5, 125–143,
3683 <https://doi.org/10.5194/essd-5-125-2013>, 2013.

- 3684 Piao, S., Ciais, P., Friedlingstein, P., de Noblet-Ducoudré, N., Cadule, P., Viovy, N., and Wang, T.: Spatiotemporal
3685 patterns of terrestrial carbon cycle during the 20th century, *Global Biogeochem. Cy.*, 23, GB4026,
3686 <https://doi.org/10.1029/2008GB003339>, 2009.
- 3687 Piao, S., Huang, M., Liu, Z., Wang, X., Ciais, P., Canadell, J. G., Wang, K., Bastos, A., Friedlingstein, P.,
3688 Houghton, R. A., Le Quéré, C., Liu, Y., Myneni, R. B., Peng, S., Pongratz, J., Sitch, S., Yan, T., Wang, Y., Zhu, Z.,
3689 Wu, D., and Wang, T.: Lower land-use emissions responsible for increased net land carbon sink during the slow
3690 warming period, *Nature Geosci*, 11, 739–743, <https://doi.org/10.1038/s41561-018-0204-7>, 2018.
- 3691 Pongratz, J., Reick, C.H., Raddatz, T. and Claussen, M.: Effects of anthropogenic land cover change on the carbon
3692 cycle of the last millennium. *Global Biogeochemical Cycles*, 23(4), doi:10.1029/2009GB003488, 2009.
- 3693 Pongratz, J., Reick, C. H., Houghton, R. A., and House, J. I.: Terminology as a key uncertainty in net land use and
3694 land cover change carbon flux estimates, *Earth Syst. Dynam.*, 5, 177–195, <https://doi.org/10.5194/esd-5-177-2014>,
3695 2014.
- 3696 Pongratz, J., Smith, S. M., Schwingshackl, C., Dayathilake, L., Gasser, T., Grassi, G. and Pilli, R.: Chapter 7:
3697 Current levels of CDR. in *The State of Carbon Dioxide Removal 2024 – 2nd Edition*,
3698 <https://doi.org/10.17605/OSF.IOZXSKB>, 2024.
- 3699 Poulter, B., Bastos, A., Canadell, J., Ciais, P., Gruber, N., Hauck, J., Jackson, R., Ishii, M., Müller, J., Patra, P., and
3700 Tian, H.: Inventorying Earth’s Land and Ocean Greenhouse Gases, *Eos*, 103,
3701 <https://doi.org/10.1029/2022EO179084>, 2022.
- 3702 Poulter, B., Frank, D. C., Hodson, E. L., and Zimmermann, N. E.: Impacts of land cover and climate data selection
3703 on understanding terrestrial carbon dynamics and the CO₂ airborne fraction, *Biogeosciences*, 8, 2027–2036,
3704 <https://doi.org/10.5194/bg-8-2027-2011>, 2011.
- 3705 Poulter, B., Freeborn, P. H., Jolly, W. M., and Varner, J. M.: COVID-19 lockdowns drive decline in active fires in
3706 southeastern United States, *PNAS*, 118, e2105666118, <https://doi.org/10.1073/pnas.2105666118>, 2021.
- 3707 Powis, C. M., Smith, S. M., Minx, J. C., and Gasser, T.: Quantifying global carbon dioxide removal deployment,
3708 *Environ. Res. Lett.*, 18, 024022, <https://doi.org/10.1088/1748-9326/acb450>, 2023.
- 3709 Prentice, I. C., Farquhar, G. D., Fasham, M. J. R., Goulden, M. L., Heimann, M., Jaramillo, V. J., Khashgi, H. S.,
3710 Le Quéré, C., Scholes, R. J., and Wallace, D. W. R.: The Carbon Cycle and Atmospheric Carbon Dioxide, in
3711 *Climate Change 2001: The Scientific Basis. Contribution of Working Group I to the Third Assessment Report of*
3712 *the Intergovernmental Panel on Climate Change*, edited by: Houghton, J. T., Ding, Y., Griggs, D. J., Noguer, M.,
3713 van der Linden, P. J., Dai, X., Maskell, K., and Johnson, C. A., Cambridge University Press, Cambridge, United
3714 Kingdom and New York, NY, USA, 183–237, ISBN: 978-0521014953, 2001.
- 3715 Price, J. T. and Warren, R.: Literature Review of the Potential of “Blue Carbon” Activities to Reduce Emissions,
3716 available at: [https://avoid-net-uk.cc.ic.ac.uk/wp-content/uploads/delightful-downloads/2016/03/Literature-review-](https://avoid-net-uk.cc.ic.ac.uk/wp-content/uploads/delightful-downloads/2016/03/Literature-review-of-the-potential-of-blue-carbon-activities-to-reduce-emissions-AVOID2-WPE2.pdf)
3717 [of-the-potential-of-blue-carbon-activities-to-reduce-emissions-AVOID2-WPE2.pdf](https://avoid-net-uk.cc.ic.ac.uk/wp-content/uploads/delightful-downloads/2016/03/Literature-review-of-the-potential-of-blue-carbon-activities-to-reduce-emissions-AVOID2-WPE2.pdf), last access: 23 October 2025,
3718 2016.
- 3719 Qin, Y., Xiao, X., Wigneron, J.-P., Ciais, P., Brandt, M., Fan, L., Li, X., Crowell, S., Wu, X., Doughty, R., Zhang,
3720 Y., Liu, F., Sitch, S., and Moore, B.: Carbon loss from forest degradation exceeds that from deforestation in the
3721 Brazilian Amazon, *Nat. Clim. Chang.*, 11, 442–448, <https://doi.org/10.1038/s41558-021-01026-5>, 2021.
- 3722 Qin, Z., Zhu, Y., Canadell, J.G., Chen, M., Li, T., Mishra, U. and Yuan, W.: Global spatially explicit carbon
3723 emissions from land-use change over the past six decades (1961–2020). *One Earth*, 7(5), pp.835-847,
3724 <https://doi.org/10.1016/j.oneear.2024.04.002>, 2024.
- 3725 Qiu, C., Ciais, P., Zhu, D., Guenet, B., Peng, S., Petrescu, A. M. R., Lauerwald, R., Makowski, D., Gallego-Sala,
3726 A. V., Charman, D. J., and Brewer, S. C.: Large historical carbon emissions from cultivated northern peatlands,
3727 *Sci. Adv.*, 7, eabf1332, <https://doi.org/10.1126/sciadv.abf1332>, 2021.
- 3728 Randerson, J. T., Chen, Y., van der Werf, G. R., Rogers, B. M., and Morton, D. C.: Global burned area and
3729 biomass burning emissions from small fires: BURNED AREA FROM SMALL FIRES, *J. Geophys. Res.*
3730 *Biogeosciences*, 117, n/a-n/a, <https://doi.org/10.1029/2012JG002128>, 2012.

- 3731 Randerson, J. T., Li, Y., Fu, W., Primeau, F., Kim, J. E., Mu, M., Hoffman, F. M., Trugman, A. T., Yang, L., Wu,
3732 C., Wang, J. A., Anderegg, W. R. L., Baccini, A., Friedl, M. A., Saatchi, S. S., Denning, A. S., and Goulden, M. L.:
3733 The weak land carbon sink hypothesis, *Sci. Adv.*, 11, eadr5489, <https://doi.org/10.1126/sciadv.adr5489>, 2025.
- 3734 Raupach, M. R., Marland, G., Ciais, P., Le Quere, C., Canadell, J. G., Klepper, G., and Field, C. B.: Global and
3735 regional drivers of accelerating CO₂ emissions, *Proceedings of the National Academy of Sciences*, 104, 10288–
3736 10293, <https://doi.org/10.1073/pnas.0700609104>, 2007.
- 3737 Regnier, P., Resplandy, L., Najjar, R. G., and Ciais, P.: The land-to-ocean loops of the global carbon cycle, *Nature*,
3738 603, 401–410, <https://doi.org/10.1038/s41586-021-04339-9>, 2022.
- 3739 Reick, C. H., Gayler, V., Goll, D., Hagemann, S., Heidkamp, M., Nabel, J. E. M. S., Raddatz, T., Roeckner, E.,
3740 Schnur, R., 110 and Wilkenskjeld, S.: JSBACH 3 – The land component of the MPI Earth System Model:
3741 documentation of version 3.2, available at: <https://doi.org/10.17617/2.3279802>, 2021.
- 3742 Remaud, M., Chevallier, F., Cozic, A., Lin, X., and Bousquet, P.: On the impact of recent developments of the
3743 LMDz atmospheric general circulation model on the simulation of CO₂ transport, 11, 4489,
3744 <https://doi.org/10.5194/gmd-11-4489-2018>, 2018.
- 3745 Resplandy, L., Keeling, R. F., Rödenbeck, C., Stephens, B. B., Khatiwala, S., Rodgers, K. B., Long, M. C., Bopp,
3746 L., and Tans, P. P.: Revision of global carbon fluxes based on a reassessment of oceanic and riverine carbon
3747 transport, *Nature Geosci*, 11, 504–509, <https://doi.org/10.1038/s41561-018-0151-3>, 2018.
- 3748 Resplandy, L., Keeling, R. F., Eddebbar, Y., Brooks, M., Wang, R., Bopp, L., Long, M. C., Dunne, J. P., Koeve,
3749 W., and Oeschies, A.: Quantification of ocean heat uptake from changes in atmospheric O₂ and CO₂ composition,
3750 *Scientific Reports*, 9, 20244, <https://doi.org/10.1038/s41598-019-56490-z>, 2019.
- 3751 Rödenbeck, C., Houweling, S., Gloor, M., and Heimann, M.: CO₂ flux history 1982–2001 inferred from
3752 atmospheric data using a global inversion of atmospheric transport, *Atmos Chem Phys*, 3, 1919–1964, 2003.
- 3753 Rödenbeck, C., Bakker, D. C. E., Metzl, N., Olsen, A., Sabine, C., Cassar, N., Reum, F., Keeling, R. F., and
3754 Heimann, M.: Interannual sea–air CO₂ flux variability from an observation-driven ocean mixed-layer scheme, 11,
3755 4599–4613, <https://doi.org/10.5194/bg-11-4599-2014>, 2014.
- 3756 Rödenbeck, C., Zaehle, S., Keeling, R., and Heimann, M.: History of El Niño impacts on the global carbon cycle
3757 1957–2017: a quantification from atmospheric CO₂ data, 373, 20170303, <https://doi.org/10.1098/rstb.2017.0303>,
3758 2018.
- 3759 Rödenbeck, C., DeVries, T., Hauck, J., Le Quéré, C., and Keeling, R. F.: Data-based estimates of interannual sea–
3760 air CO₂ flux variations 1957–2020 and their relation to environmental drivers, *Biogeosciences*, 19, 2627–2652,
3761 <https://doi.org/10.5194/bg-19-2627-2022>, 2022.
- 3762 Rosan, T. M., Klein Goldewijk, K., Ganzenmüller, R., O’Sullivan, M., Pongratz, J., Mercado, L. M., Aragao, L. E.
3763 O. C., Heinrich, V., Randow, C. V., Wiltshire, A., Tubiello, F. N., Bastos, A., Friedlingstein, P., and Sitch, S.: A
3764 multi-data assessment of land use and land cover emissions from Brazil during 2000–2019, *Environ. Res. Lett.*, 16,
3765 074004, <https://doi.org/10.1088/1748-9326/ac08c3>, 2021.
- 3766 Rosan, T. M., Sitch, S., O’Sullivan, M., Basso, L. S., Wilson, C., Silva, C., Gloor, E., Fawcett, D., Heinrich, V.,
3767 Souza, J. G. and Bezerra, F.G.S.: Synthesis of the land carbon fluxes of the Amazon region between 2010 and
3768 2020. *Communications Earth & Environment*, 5(1), p.46. <https://doi.org/10.1038/s43247-024-01205-0>, 2024.
- 3769 Sakamoto, K., H. Nakano, S. Urakawa, T. Toyoda, Y. Kawakami, H. Tsujino, G. Yamanaka, 2023: Reference
3770 manual for the Meteorological Research Institute Community Ocean Model version 5 (MRI.COMv5), Technical
3771 Reports of the Meteorological Research Institute, No.87, <https://doi.org/10.11483/mritechrepo.87>.
- 3772 Sarma, V. V. S. S., Sridevi, B., Metzl, N., Patra, P. K., Lachkar, Z., Chakraborty, K., Goyet, C., Levy, M., Mehari,
3773 M., and Chandra, N.: Air-Sea Fluxes of CO₂ in the Indian Ocean Between 1985 and 2018: A Synthesis Based on
3774 Observation-Based Surface CO₂, Hindcast and Atmospheric Inversion Models, *Glob. Biogeochem. Cycles*, 37,
3775 e2023GB007694, <https://doi.org/10.1029/2023GB007694>, 2023.
- 3776 Schaphoff, S., von Bloh, W., Rammig, A., Thonicke, K., Biemans, H., Forkel, M., Gerten, D., Heinke, J.,
3777 Jägermeyr, J., Knauer, J., Langerwisch, F., Lucht, W., Müller, C., Rolinski, S., and Waha, K.: LPJmL4 – a dynamic

- 3778 global vegetation model with managed land – Part 1: Model description, *Geosci. Model Dev.*, 11, 1343–1375,
3779 <https://doi.org/10.5194/gmd-11-1343-2018>, 2018.
- 3780 Schimel, D., Alves, D., Enting, I. G., Heimann, M., Joos, F., Raynaud, D., Wigley, T., Prater, M., Derwent, R.,
3781 Ehhalt, D., Fraser, P., Sanhueza, E., Zhou, X., Jonas, P., Charlson, R., Rodhe, H., Sadasivan, S., Shine, K. P.,
3782 Fouquart, Y., Ramaswamy, V., Solomon, S., Srinivasan, J., Albritton, D., Derwent, R., Isaksen, I., Lal, M., and
3783 Wuebbles, D.: Radiative Forcing of Climate Change, in: *Climate Change 1995: The Science of Climate Change*,
3784 Contribution of Working Group I to the Second Assessment Report of the Intergovernmental Panel on Climate
3785 Change [Houghton, J. T., Meira Rillo, L. G., Callander, B. A., Harris, N., Kattenberg, A., and Maskell, K. (eds.)],
3786 Cambridge University Press, Cambridge, United Kingdom and New York, NY, USA, ISBN: 978-0521559621,
3787 1995.
- 3788 Schimel, D., Stephens, B. B., and Fisher, J. B.: Effect of increasing CO₂ on the terrestrial carbon cycle, *Proc Natl*
3789 *Acad Sci USA*, 112, 436–441, <https://doi.org/10.1073/pnas.1407302112>, 2015.
- 3790 Schuh, A. E., Jacobson, A. R., Basu, S., Weir, B., Baker, D., Bowman, K., Chevallier, F., Crowell, S., Davis, K. J.,
3791 Deng, F., Denning, S., Feng, L., Jones, D., Liu, J., and Palmer, P. I.: Quantifying the Impact of Atmospheric
3792 Transport Uncertainty on CO₂ Surface Flux Estimates, *Global Biogeochem. Cycles*, 33, 484–500,
3793 <https://doi.org/10.1029/2018GB006086>, 2019.
- 3794 Schuld, K. N., Mund, J., Aalto, T., Abshire, J. B., Aikin, K., Allen, G., Andrade, M., Andrews, A., Apadula, F.,
3795 Arnold, S., Baier, B., Bakwin, P., Bartyzel, J., Bentz, G., Bergamaschi, P., Beyersdorf, A., Biermann, T., Biraud, S.
3796 C., Blanc, P.-E., Boenisch, H., Bowling, D., Brailsford, G., Brand, W. A., Brunner, D., Bui, T. P., Burban, B.,
3797 Bani, L., Calzolari, F., Chang, C. S., Chen, H., Chen, G., Chmura, L., Clark, S., Climadat, S., Colomb, A.,
3798 Commane, R., Condori, L., Conen, F., Conil, S., Couret, C., Cristofanelli, P., Cuevas, E., Curcoll, R., Daube, B.,
3799 Davis, K. J., De Mazière, M., De Wekker, S., Dean-Day, J. M., Della Coletta, J., Delmotte, M., Di Iorio, T.,
3800 DiGangi, E., DiGangi, J. P., Dickerson, R., Elsassner, M., Emmenegger, L., Fang, S., Forster, G., France, J.,
3801 Frumau, A., Fuente-Lastra, M., Galkowski, M., Gatti, L. V., Gehrlein, T., Gerbig, C., Gheusi, F., Gloor, E., Goto,
3802 D., Griffiths, T., Hammer, S., Hanisco, T. F., Hanson, C., Haszpra, L., Hatakka, J., Heimann, M., Heliasz, M., Heltai,
3803 D., Henne, S., Hensen, A., Hermans, C., Hermansen, O., Hints, E., Hoheisel, A., Holst, J., Iraci, L. T., Ivakhov,
3804 V., Jaffe, D. A., Jordan, A., Joubert, W., Kang, H.-Y., Karion, A., Kawa, S. R., Kazan, V., Keeling, R. F., Keronen,
3805 P., Kim, J., Klausen, J., Kneuer, T., Ko, M.-Y., Kolari, P., Kominkova, K., Kort, E., Kozlova, E., Krummel, P. B.,
3806 Kubistin, D., Kulawik, S. S., Kumps, N., Labuschagne, C., Lam, D. H., Lan, X., Langenfelds, R. L., Lanza, A.,
3807 Laurent, O., Laurila, T., Lauvaux, T., Lavric, J., Law, B. E., Lee, C.-H., Lee, J., Lehner, I., Lehtinen, K., Leppert,
3808 R., Leskinen, A., Leuenberger, M., Leung, W. H., Levin, I., Levula, J., Lin, J., Lindauer, M., Lindroth, A., Loh, Z.
3809 M., Lopez, M., Lunder, C. R., Löfvenius, M. O., Machida, T., Mammarella, I., Manca, G., Manning, A., Manning,
3810 A., Marek, M. V., Marklund, P., Marrero, J. E., Martin, M. Y., Martin, D., Martins, G. A., Matsueda, H., McKain,
3811 K., Meijer, H., Meinhardt, F., Merchant, L., Metzger, J.-M., Mihalopoulos, N., Miles, N. L., Miller, C. E., Miller, J.
3812 B., Mitchell, L., Monteiro, V., Montzka, S., Moossen, H., Moreno, C., Morgan, E., Morgui, J.-A., Morimoto, S.,
3813 Munger, J. W., Munro, D., Mutuku, M., Myhre, C. L., Mölder, M., Müller-Williams, J., Nakaoka, S.-I., Necki, J.,
3814 Newman, S., Nichol, S., Nisbet, E., Niwa, Y., Njiru, D. M., Noe, S. M., Nojiri, Y., O'Doherty, S., Obersteiner, F.,
3815 Paplawsky, B., Parworth, C. L., Peischl, J., Peltola, O., Peters, W., Philippon, C., Piacentino, S., Pichon, J. M.,
3816 Pickers, P., Piper, S., Pitt, J., Plass-Dülmer, C., Platt, S. M., Prinzivalli, S., Ramonet, M., Ramos, R., Ren, X.,
3817 Reyes-Sanchez, E., Richardson, S. J., Rigoulet, L.-J., Riris, H., Rivas, P. P., Rothe, M., Roulet, Y.-A., Ryerson,
3818 T., Ryoo, J.-M., Sargent, M., Sasakawa, M., Schaefer, H., Scheeren, B., Schmidt, M., Schuck, T., Schumacher, M.,
3819 Seibel, J., Seifert, T., Sha, M. K., Shepson, P., Shin, D., Shook, M., Sloop, C. D., Smale, D., Smith, P. D., Spain,
3820 G., St. Clair, J. M., Steger, D., Steinbacher, M., Stephens, B., Sweeney, C., Sørensen, L. L., Taipale, R., Takatsuji,
3821 S., Tans, P., Thoning, K., Timas, H., Torn, M., Trisolino, P., Turnbull, J., Vermeulen, A., Viner, B., Vitkova, G.,
3822 Walker, S., Watson, A., Weiss, R., Weyrauch, D., Wofsy, S. C., Worsley, J., Worthy, D., Xueref-Remy, I., Yates,
3823 E. L., Young, D., Yver-Kwok, C., Zaehe, S., Zahn, A., Zellweger, C., Zimnoch, M., de Souza, R. A., di Sarra, A.
3824 G., van Dinter, D., van den Bulk, P.: Multi-laboratory compilation of atmospheric carbon dioxide data for the
3825 period 1957-2023; *obspack_co2_1_GLOBALVIEWplus_v10.1_2024-11-13*, <https://doi.org/10.25925/20241101>,
3826 2024.
- 3827 Schuld, K. N., Jacobson, A. R., Aalto, T., Aaltonen, H., Andrews, A., Apadula, F., Arnold, S., Bakwin, P.,
3828 Bartyzel, J., Bergamaschi, P., Biermann, T., Biraud, S. C., Blanc, P.-E., Brunner, D., Bani, L., Calzolari, F., Chen,
3829 H., Chmura, L., Colomb, A., Condori, L., Conen, F., Conil, S., Couret, C., Cristofanelli, P., Cuevas, E., De
3830 Mazière, M., De Wekker, S., Della Coletta, J., Delmotte, M., Di Iorio, T., Elsassner, M., Emmenegger, L., Forster,
3831 G., Frumau, A., Fuente-Lastra, M., Galkowski, M., Gheusi, F., Hammer, S., Haszpra, L., Hatakka, J., Heliasz, M.,
3832 Heltai, D., Henne, S., Hensen, A., Hermans, C., Hermansen, O., Hoheisel, A., Holst, J., Jaffe, D. A., Karion, A.,
3833 Kazan, V., Keronen, P., Kneuer, T., Kolari, P., Kominkova, K., Krummel, P. B., Kubistin, D., Kumps, N., Lan, X.,
3834 Langenfelds, R. L., Lanza, A., Laurent, O., Lee, J., Lehner, I., Lehtinen, K., Leskinen, A., Leuenberger, M., Levin,

- 3835 I., Levula, J., Lindauer, M., Lindroth, A., Loh, Z. M., Lopez, M., Lunder, C. R., Löfvenius, M. O., Mammarella, I.,
3836 Manca, G., Manning, A., Manning, A., Marek, M. V., Marklund, P., McKain, K., Meijer, H., Meinhardt, F.,
3837 Metzger, J.-M., Miller, J. B., Miller, C. E., Myhre, C. L., Mölder, M., Müller-Williams, J., Necki, J., Noe, S. M.,
3838 O'Doherty, S., Peltola, O., Philippon, C., Piacentino, S., Pichon, J. M., Pickers, P., Pitt, J., Plass-Dülmer, C., Platt,
3839 S. M., Ramonet, M., Ramos, R., Reyes-Sanchez, E., Rigouleau, L.-J., Rivas, P. P., Roulet, Y.-A., Scheeren, B.,
3840 Schmidt, M., Schumacher, M., Sha, M. K., Sloop, C. D., Smith, P. D., Steger, D., Steinbacher, M., Sweeney, C.,
3841 Sørensen, L. L., Taipale, R., Tans, P., Thoning, K., Trisolino, P., Vermeulen, A., Viner, B., Vitkova, G., Weyrauch,
3842 D., Worthy, D., Xueref-Remy, I., Young, D., Yver-Kwok, C., Zimnoch, M., di Sarra, A. G., van den Bulk, P.:
3843 Multi-laboratory compilation of atmospheric carbon dioxide data for the year 2024;
3844 obspack_co2_1_NRT_v10.1_2025-02-07, <https://doi.org/10.25925/20250101>, 2025.
- 3845 Schwinger, J., Goris, N., Tjiputra, J. F., Kriest, I., Bentsen, M., Bethke, I., Ilicak, M., Assmann, K. M., and Heinze,
3846 C.: Evaluation of NorESM-OC (versions 1 and 1.2), the ocean carbon-cycle stand-alone configuration of the
3847 Norwegian Earth System Model (NorESM1), *Geosci. Model Dev.*, 9, 2589–2622, [https://doi.org/10.5194/gmd-9-](https://doi.org/10.5194/gmd-9-2589-2016)
3848 2589-2016, 2016.
- 3849 Schwingshackl, C., Obermeier, W. A., Bultan, S., Grassi, G., Canadell, J. G., Friedlingstein, P., Gasser, T.,
3850 Houghton, R. A., Kurz, W. A., Sitch, S., and Pongratz, J.: Differences in land-based mitigation estimates
3851 reconciled by separating natural and land-use CO2 fluxes at the country level, *One Earth*, 5, 1367–1376,
3852 <https://doi.org/10.1016/j.oneear.2022.11.009>, 2022.
- 3853 Séférian, R., Nabat, P., Michou, M., Saint-Martin, D., Voldoire, A., Colin, J., Decharme, B., Delire, C., Berthet, S.,
3854 Chevallier, M., Sénési, S., Franchisteguy, L., Vial, J., Mallet, M., Joetzjer, E., Geoffroy, O., Guérémy, J.-F., Moine,
3855 M.-P., Msadek, R., Ribes, A., Rocher, M., Roehrig, R., Salas-y-Méla, D., Sanchez, E., Terray, L., Valcke, S.,
3856 Waldman, R., Aumont, O., Bopp, L., Deshayes, J., Éthé, C., and Madec, G.: Evaluation of CNRM Earth System
3857 Model, CNRM-ESM2-1: Role of Earth System Processes in Present-Day and Future Climate, *Journal of Advances*
3858 *in Modeling Earth Systems*, 11, 4182–4227, <https://doi.org/10.1029/2019MS001791>, 2019.
- 3859 Seiler, C., Melton, J. R., Arora, V. K., Sitch, S., Friedlingstein, P., Anthoni, P., Goll, D., Jain, A. K., Joetzjer, E.,
3860 Lienert, S., Lombardozzi, D., Luyssaert, S., Nabel, J. E. M. S., Tian, H., Vuichard, N., Walker, A. P., Yuan, W.,
3861 and Zaehle, S.: Are Terrestrial Biosphere Models Fit for Simulating the Global Land Carbon Sink?, *J. Adv. Model.*
3862 *Earth Syst.*, 14, e2021MS002946, <https://doi.org/10.1029/2021MS002946>, 2022.
- 3863 Sellar, A. A., Jones, C. G., Mulcahy, J. P., Tang, Y., Yool, A., Wiltshire, A., O'Connor, F. M., Stringer, M., Hill,
3864 R., Palmieri, J., Woodward, S., Mora, L., Kuhlbrodt, T., Rumbold, S. T., Kelley, D. I., Ellis, R., Johnson, C. E.,
3865 Walton, J., Abraham, N. L., Andrews, M. B., Andrews, T., Archibald, A. T., Berthou, S., Burke, E., Blockley, E.,
3866 Carslaw, K., Dalvi, M., Edwards, J., Folberth, G. A., Gedney, N., Griffiths, P. T., Harper, A. B., Hendry, M. A.,
3867 Hewitt, A. J., Johnson, B., Jones, A., Jones, C. D., Keeble, J., Liddicoat, S., Morgenstern, O., Parker, R. J.,
3868 Predoi, V., Robertson, E., Siahhaan, A., Smith, R. S., Swaminathan, R., Woodhouse, M. T., Zeng, G.,
3869 and Zerroukat, M.: UKESM1: Description and Evaluation of the U.K. Earth System Model, *J. Adv.*
3870 *Model. Earth Syst.*, 11, 4513–4558, <https://doi.org/10.1029/2019MS001739>, 2019.
- 3871 Ship and Bunker, 2026. Bunker demand change, Q3 2025, at key global bunkering locations. Available
3872 at: <https://shipandbunker.com/bi/bunker-volumes>, last access: 23 March 2026.
- 3873 Shu, S., Jain, A. K., Koven, C. D., and Mishra, U.: Estimation of Permafrost SOC Stock and Turnover Time
3874 Using a Land Surface Model With Vertical Heterogeneity of Permafrost Soils, *Global Biogeochem. Cy.*, 34,
3875 e2020GB006585, <https://doi.org/10.1029/2020GB006585>, 2020.
- 3876 Shutler, J. D., Land, P. E., Piolle, J.-F., Woolf, D. K., Goddijn-Murphy, L., Paul, F., Girard-Arduin, F., Chapron,
3877 B., and Donlon, C. J.: FluxEngine: A Flexible Processing System for Calculating Atmosphere–Ocean Carbon
3878 Dioxide Gas Fluxes and Climatologies, *J. Atmospheric Ocean. Technol.*, 33, 741–756,
3879 <https://doi.org/10.1175/JTECH-D-14-00204.1>, 2016.
- 3880 Silva Junior, C.H., Anderson, L.O., Silva, A.L., Almeida, C.T., Dalagnol, R., Pletsch, M.A., Penha, T.V., Paloschi,
3881 R.A. and Aragão, L.E.: Fire responses to the 2010 and 2015/2016 Amazonian droughts. *Frontiers in Earth Science*,
3882 7, p.97, <https://doi.org/10.3389/feart.2019.00097>, 2019.
- 3883 Sitch, S., V. Brovkin, W. von Bloh, D. Van Vuuren, B. Eickhout, and Ganopolski, A.: Impacts of future land cover
3884 on atmospheric CO2 and climate. *Global Biogeochemical Cycles*, 19, GB2013. doi:10.1029/2004GB002311, 2005.

- 3885 Sitch, S., Huntingford, C., Gedney, N., Levy, P. E., Lomas, M., Piao, S. L., Betts, R., Ciais, P., Cox, P.,
3886 Friedlingstein, P., Jones, C. D., Prentice, I. C., and Woodward, F. I.: Evaluation of the terrestrial carbon cycle,
3887 future plant geography and climate-carbon cycle feedbacks using five Dynamic Global Vegetation Models
3888 (DGVMs): Uncertainty In Land Carbon Cycle Feedbacks, *Glob. Change Biol.*, 14, 2015–2039,
3889 <https://doi.org/10.1111/j.1365-2486.2008.01626.x>, 2008.
- 3890 Sitch, S., O’Sullivan, M., Robertson, E., Friedlingstein, P., Albergel, C., Anthoni, P., Arneth, A., Arora, V. K.,
3891 Bastos, A., Bastrikov, V., Bellouin, N., Canadell, J. G., Chini, L., Ciais, P., Falk, S., Harris, I., Hurtt, G., Ito, A.,
3892 Jain, A. K., Jones, M. W., Joos, F., Kato, E., Kennedy, D., Klein Goldewijk, K., Kluzek, E., Knauer, J., Lawrence,
3893 P. J., Lombardozzi, D., Melton, J. R., Nabel, J. E. M. S., Pan, N., Peylin, P., Pongratz, J., Poulter, B., Rosan, T. M.,
3894 Sun, Q., Tian, H., Walker, A. P., Weber, U., Yuan, W., Yue, X., Zaehle, S.: Trends and Drivers of Terrestrial
3895 Sources and Sinks of Carbon Dioxide: An Overview of the TRENDY Project, *Global Biogeochemical Cycles*,
3896 38(7), e2024GB008102, <https://doi.org/10.1029/2024GB008102>, 2024.
- 3897 Smallman, T. L., Milodowski, D. T., Neto, E. S., Koren, G., Ometto, J., and Williams, M.: Parameter uncertainty
3898 dominates C-cycle forecast errors over most of Brazil for the 21st century, *Earth Syst. Dyn.*, 12, 1191–1237,
3899 <https://doi.org/10.5194/esd-12-1191-2021>, 2021.
- 3900 Smith, B., Wårlind, D., Arneth, A., Hickler, T., Leadley, P., Siltberg, J., and Zaehle, S.: Implications of
3901 incorporating N cycling and N limitations on primary production in an individual-based dynamic vegetation model,
3902 *Biogeosciences*, 11, 2027–2054, <https://doi.org/10.5194/bg-11-2027-2014>, 2014.
- 3903 Smith, S. M., Geden, O., Gidden, M. J., Lamb, W. F., Nemet, G. F., Minx, J. C., Buck, H., Burke, J., Cox, E.,
3904 Edwards, M. R., Fuss, S., Johnstone, I., Müller-Hansen, F., Pongratz, J., Probst, B. S., Roe, S., Schneidt, F.,
3905 Schulte, I., and Vaughan, N. E. *The State of Carbon Dioxide Removal 2024 - 2nd Edition*,
3906 <http://dx.doi.org/10.17605/OSF.IO/F85QJ>, 2024.
- 3907 Sospedra-Alfonso, R., Merryfield, W. J., Boer, G. J., Kharin, V. V., Lee, W.-S., Seiler, C., and Christian, J. R.:
3908 Decadal climate predictions with the Canadian Earth System Model version 5 (CanESM5), *Geosci. Model Dev.*,
3909 14, 6863–6891, <https://doi.org/10.5194/gmd-14-6863-2021>, 2021.
- 3910 Steele, L. P., Dlugokencky, E. J., Lang, P. M., Tans, P. P., Martin, R. C., and Masarie, K. A.: Slowing down of the
3911 global accumulation of atmospheric methane during the 1980s, *Nature* 358, 313–316,
3912 <https://doi.org/10.1038/358313a0>, 1992.
- 3913 Stephens, B. B., Gurney, K. R., Tans, P. P., Sweeney, C., Peters, W., Bruhwiler, L., Ciais, P., Ramonet, M.,
3914 Bousquet, P., Nakazawa, T., Aoki, S., Machida, T., Inoue, G., Vinnichenko, N., Lloyd, J., Jordan, A., Heimann,
3915 M., Shibistova, O., Langenfelds, R. L., Steele, L. P., Francey, R. J., and Denning, A. S.: Weak Northern and Strong
3916 Tropical Land Carbon Uptake from Vertical Profiles of Atmospheric CO₂, *Science*, 316, 1732–1735,
3917 <https://doi.org/10.1126/science.1137004>, 2007.
- 3918 Stephens, B. B., Keeling, R. F., Heimann, M., Six, K. D., Murnane, R., and Caldeira, K.: Testing global ocean
3919 carbon cycle models using measurements of atmospheric O₂ and CO₂ concentration, *Glob. Biogeochem. Cycles*,
3920 12, 213–230, <https://doi.org/10.1029/97GB03500>, 1998.
- 3921 Stock, C. A., Dunne, J. P., Luo, J. Y., Ross, A. C., Van Oostende, N., Zadeh, N., Cordero, T. J., Liu, X., and Teng,
3922 Y.: Photoacclimation and Photoadaptation Sensitivity in a Global Ocean Ecosystem Model, *J Adv Model Earth*
3923 *Syst.*, 17, e2024MS004701, <https://doi.org/10.1029/2024MS004701>, 2025.
- 3924 Stocker, T., Qin, D., and Plattner, G.-K.: *Climate Change 2013: The Physical Science Basis. Contribution of*
3925 *Working Group I to the Fifth Assessment Report of the Intergovernmental Panel on Climate Change*
3926 *[Intergovernmental Panel on Climate Change (eds.)]*, Cambridge University Press, Cambridge, ISBN:
3927 9789291691388, 2013.
- 3928 Swart, N. C., Cole, J. N. S., Kharin, V. V., Lazare, M., Scinocca, J. F., Gillett, N. P., Anstey, J., Arora, V.,
3929 Christian, J. R., Hanna, S., Jiao, Y., Lee, W. G., Majaess, F., Saenko, O. A., Seiler, C., Seinen, C., Shao, A.,
3930 Sigmund, M., Solheim, L., von Salzen, K., Yang, D., and Winter, B.: *The Canadian Earth System Model version 5*
3931 *(CanESM5.0.3)*, *Geosci. Model Dev.*, 12, 4823–4873, <https://doi.org/10.5194/gmd-12-4823-2019>, 2019.
- 3932 SX Coal: Monthly coal consumption estimates, <http://www.sxcoal.com/>, last access: 23 October 2025, 2022.

- 3933 Takahashi, T., Sutherland, S. C., Wanninkhof, R., Sweeney, C., Feely, R. A., Chipman, D. W., Hales, B.,
 3934 Friederich, G., Chavez, F., Sabine, C., Watson, A., Bakker, D. C. E., Schuster, U., Metzl, N., Yoshikawa-Inoue, H.,
 3935 Ishii, M., Midorikawa, T., Nojiri, Y., Körtzinger, A., Steinhoff, T., Hoppema, M., Olafsson, J., Arnarson, T. S.,
 3936 Tilbrook, B., Johannessen, T., Olsen, A., Bellerby, R., Wong, C. S., Delille, B., Bates, N. R., and de Baar, H. J. W.:
 3937 Climatological mean and decadal change in surface ocean pCO₂, and net sea–air CO₂ flux over the global oceans,
 3938 Deep Sea Research Part II: Topical Studies in Oceanography, 56, 554–577,
 3939 <https://doi.org/10.1016/j.dsr2.2008.12.009>, 2009.
- 3940 Terhaar, J., Frölicher, T. L., and Joos, F.: Southern Ocean anthropogenic carbon sink constrained by sea surface
 3941 salinity, *Sci. Adv.*, 7, eabd5964, <https://doi.org/10.1126/sciadv.abd5964>, 2021.
- 3942 Terhaar, J., Frölicher, T. L., and Joos, F.: Observation-constrained estimates of the global ocean carbon sink from
 3943 Earth system models, *Biogeosciences*, 19, 4431–4457, <https://doi.org/10.5194/bg-19-4431-2022>, 2022.
- 3944 Terhaar, J., Goris, N., Müller, J. D., DeVries, T., Gruber, N., Hauck, J., Perez, F. F., and Séférian, R.: Assessment
 3945 of Global Ocean Biogeochemistry Models for Ocean Carbon Sink Estimates in RECCAP2 and Recommendations
 3946 for Future Studies. *Journal of Advances in Modeling Earth Systems*, 16(3), e2023MS003840,
 3947 <https://doi.org/10.1029/2023MS003840>, 2024.
- 3948 Tian, H., Xu, X., Lu, C., Liu, M., Ren, W., Chen, G., Melillo, J., and Liu, J.: Net exchanges of CO₂, CH₄, and
 3949 N₂O between China’s terrestrial ecosystems and the atmosphere and their contributions to global climate warming,
 3950 *J. Geophys. Res. Biogeosciences*, 116, G02011, <https://doi.org/10.1029/2010JG001393>, 2011.
- 3951 Tian, H., Chen, G., Lu, C., Xu, X., Hayes, D. J., Ren, W., Pan, S., Huntzinger, D. N., and Wofsy, S. C.: North
 3952 American terrestrial CO₂ uptake largely offset by CH₄ and N₂O emissions: toward a full accounting of the
 3953 greenhouse gas budget, *Climatic Change*, 129, 413–426, <https://doi.org/10.1007/s10584-014-1072-9>, 2015.
- 3954 Tjiputra, J. F., Schwinger, J., Bentsen, M., Morée, A. L., Gao, S., Bethke, I., Heinze, C., Goris, N., Gupta, A., He,
 3955 Y.-C., Olivíe, D., Seland, Ø., and Schulz, M.: Ocean biogeochemistry in the Norwegian Earth System Model
 3956 version 2 (NorESM2), *Geosci. Model Dev.*, 13, 2393–2431, <https://doi.org/10.5194/gmd-13-2393-2020>, 2020.
- 3957 Tsujino, H., Nakano, H., Sakamoto, K., Urakawa, L.S., Toyama, K., Kosugi, N., Kitamura, Y., Ishii, M.,
 3958 Nishikawa, S., Nishikawa, H., Sugiyama, T., and Ishikawa, Y.: Impact of increased horizontal resolution of an
 3959 ocean model on carbon circulation in the North Pacific Ocean. *Journal of Advances in Modeling Earth Systems*,
 3960 16, e2023MS003720, <https://doi.org/10.1029/2023MS003720>, 2024.
- 3961 Tubiello, F. N., Conchedda, G., Wanner, N., Federici, S., Rossi, S., and Grassi, G.: Carbon emissions and removals
 3962 from forests: new estimates, 1990–2020, *Earth Syst. Sci. Data*, 13, 1681–1691, <https://doi.org/10.5194/essd-13-1681-2021>, 2021.
- 3964 Tubiello, F., Pekkarinen, A., Branthomme, A., Piccoli, M., Obli-Laryea, G., Ramadan, N., and Conchedda, G.:
 3965 New FAOSTAT forest emissions and removals estimates: 1990–2025, *Earth Syst. Sci. Data Discussions*,
 3966 <https://doi.org/10.5194/essd-2025-635>, 2025.
- 3967 Tuck, C.: 2022 Mineral Commodity Summary: Iron Ore, Tech. rep., U.S. Geological Survey,
 3968 <https://pubs.usgs.gov/periodicals/mcs2022/mcs2022-iron-ore.pdf>, 2022.
- 3969 UNFCCC: Synthesis report for the technical assessment component of the first global stocktake, available at:
 3970 <https://unfccc.int/documents/461466>, last access: 23 October 2025, 2022.
- 3971 Vale, M. M., Berenguer, E., Argollo de Menezes, M., Viveiros de Castro, E. B., Pugliese de Siqueira, L., and
 3972 Portela, R. de C. Q.: The COVID-19 pandemic as an opportunity to weaken environmental protection in Brazil,
 3973 *Biological Conservation*, 255, 108994, <https://doi.org/10.1016/j.biocon.2021.108994>, 2021.
- 3974 van der Laan-Luijkx, I. T., van der Velde, I. R., van der Veen, E., Tsuruta, A., Stanislawski, K., Babenhauserheide,
 3975 A., Zhang, H. F., Liu, Y., He, W., Chen, H., Masarie, K. A., Krol, M. C., and Peters, W.: The CarbonTracker Data
 3976 Assimilation Shell (CTDAS) v1.0: implementation and global carbon balance 2001–2015, *Geosci. Model Dev.*, 10,
 3977 2785–2800, <https://doi.org/10.5194/gmd-10-2785-2017>, 2017.
- 3978 van der Velde, I. R., van der Werf, G. R., Houweling, S., Maasackers, J. D., Borsdorff, T., Landgraf, J., Tol, P.,
 3979 van Kempen, T. A., van Hees, R., Hoogeveen, R., Veeffkind, J. P., and Aben, I.: Vast CO₂ release from Australian

- 3980 fires in 2019–2020 constrained by satellite, *Nature*, 597, 366–369, <https://doi.org/10.1038/s41586-021-03712-y>,
3981 2021.
- 3982 van der Werf, G. R., Randerson, J. T., Giglio, L., Collatz, G. J., Mu, M., Kasibhatla, P. S., Morton, D. C., DeFries,
3983 R. S., Jin, Y., and van Leeuwen, T. T.: Global fire emissions and the contribution of deforestation, savanna, forest,
3984 agricultural, and peat fires (1997–2009), *Atmospheric Chem. Phys.*, 10, 11707–11735, [https://doi.org/10.5194/acp-](https://doi.org/10.5194/acp-10-11707-2010)
3985 10-11707-2010, 2010.
- 3986 van der Werf, G. R., Randerson, J. T., Giglio, L., van Leeuwen, T. T., Chen, Y., Rogers, B. M., Mu, M., van Marle,
3987 M. J. E., Morton, D. C., Collatz, G. J., Yokelson, R. J., and Kasibhatla, P. S.: Global fire emissions estimates
3988 during 1997–2016, *Earth Syst. Sci. Data*, 9, 697–720, <https://doi.org/10.5194/essd-9-697-2017>, 2017.
- 3989 van Wees, D., van der Werf, G. R., Randerson, J. T., Andela, N., Chen, Y., and Morton, D. C.: The role of fire in
3990 global forest loss dynamics, *Glob. Change Biol.*, 27, 2377–2391, <https://doi.org/10.1111/gcb.15591>, 2021.
- 3991 von Bloh, W., Schaphoff, S., Müller, C., Rolinski, S., Waha, K., and Zaehle, S.: Implementing the nitrogen cycle
3992 into the dynamic global vegetation, hydrology, and crop growth model LPJmL (version 5.0), *Geosci. Model Dev.*,
3993 11, 2789–2812, <https://doi.org/10.5194/gmd-11-2789-2018>, 2018.
- 3994 Vaithinada Ayar, P., Bopp, L., Christian, J. R., Ilyina, T., Krasting, J. P., Séférian, R., Tsujino, H., Watanabe, M.,
3995 Yool, A., and Tjiputra, J.: Contrasting projections of the ENSO-driven CO₂ flux variability in the equatorial
3996 Pacific under high-warming scenario, *Earth Syst. Dynam.*, 13, 1097–1118, [https://doi.org/10.5194/esd-13-1097-](https://doi.org/10.5194/esd-13-1097-2022)
3997 2022, 2022.
- 3998 Vuichard, N., Messina, P., Luysaert, S., Guenet, B., Zaehle, S., Ghattas, J., Bastrikov, V., and Peylin, P.:
3999 Accounting for carbon and nitrogen interactions in the global terrestrial ecosystem model ORCHIDEE (trunk
4000 version, rev 4999): multi-scale evaluation of gross primary production, *Geosci. Model Dev.*, 12, 4751–4779,
4001 <https://doi.org/10.5194/gmd-12-4751-2019>, 2019.
- 4002 Walker, A. P., Quaife, T., Bodegom, P. M., De Kauwe, M. G., Keenan, T. F., Joiner, J., Lomas, M. R., MacBean,
4003 N., Xu, C., Yang, X., and Woodward, F. I.: The impact of alternative trait-scaling hypotheses for the maximum
4004 photosynthetic carboxylation rate (V_{cmax}) on global gross primary production, *New Phytol.*, 215, 1370–1386,
4005 <https://doi.org/10.1111/nph.14623>, 2017.
- 4006 Walker, A. P., De Kauwe, M. G., Bastos, A., Belmecheri, S., Georgiou, K., Keeling, R. F., McMahon, S. M.,
4007 Medlyn, B. E., Moore, D. J. P., Norby, R. J., Zaehle, S., Anderson-Teixeira, K. J., Battipaglia, G., Brienen, R. J.
4008 W., Cabugao, K. G., Cailleret, M., Campbell, E., Canadell, J. G., Ciais, P., Craig, M. E., Ellsworth, D. S., Farquhar,
4009 G. D., Faticchi, S., Fisher, J. B., Frank, D. C., Graven, H., Gu, L., Haverd, V., Heilman, K., Heimann, M., Hungate,
4010 B. A., Iversen, C. M., Joos, F., Jiang, M., Keenan, T. F., Knauer, J., Körner, C., Leshyk, V. O., Leuzinger, S., Liu,
4011 Y., MacBean, N., Malhi, Y., McVicar, T. R., Penuelas, J., Pongratz, J., Powell, A. S., Riutta, T., Sabot, M. E. B.,
4012 Schleucher, J., Sitch, S., Smith, W. K., Sulman, B., Taylor, B., Terrer, C., Torn, M. S., Treseder, K. K., Trugman,
4013 A. T., Trumbore, S. E., van Mantgem, P. J., Voelker, S. L., Whelan, M. E., and Zuidema, P. A.: Integrating the
4014 evidence for a terrestrial carbon sink caused by increasing atmospheric CO₂, *New Phytol.*, 229, 2413–2445,
4015 <https://doi.org/10.1111/nph.16866>, 2021.
- 4016 Watanabe, M., Tatebe, H., Koyama, H., Hajima, T., Watanabe, M., and Kawamiya, M.: Importance of El Niño
4017 reproducibility for reconstructing historical CO₂ flux variations in the equatorial Pacific, *Ocean Sci.*, 16, 1431–
4018 1442, <https://doi.org/10.5194/os-16-1431-2020>, 2020.
- 4019 Watson, A. J., Schuster, U., Shutler, J. D., Holding, T., Ashton, I. G. C., Landschützer, P., Woolf, D. K., and
4020 Goddijn-Murphy, L.: Revised estimates of ocean-atmosphere CO₂ flux are consistent with ocean carbon inventory,
4021 *Nat Commun*, 11, 4422, <https://doi.org/10.1038/s41467-020-18203-3>, 2020.
- 4022 Watson, R. T., Rohde, H., Oeschger, H., and Siegenthaler, U.: Greenhouse Gases and Aerosols, in: *Climate*
4023 *Change: The IPCC Scientific Assessment*. Intergovernmental Panel on Climate Change (IPCC), edited by:
4024 Houghton, J. T., Jenkins, G. J., and Ephraums, J. J., Cambridge University Press, Cambridge, ISBN: 978-
4025 0521403603, 1990.
- 4026 Wenzel, S., Cox, P. M., Eyring, V., and Friedlingstein, P.: Projected land photosynthesis constrained by changes in
4027 the seasonal cycle of atmospheric CO₂, *Nature*, 538, 499–501, <https://doi.org/10.1038/nature19772>, 2016.

- 4028 Wilkenskjeld, S., Kloster, S., Pongratz, J., Raddatz, T., and Reick, C. H.: Comparing the influence of net and gross
4029 anthropogenic land-use and land-cover changes on the carbon cycle in the MPI-ESM, *Biogeosciences*, 11, 4817–
4030 4828, <https://doi.org/10.5194/bg-11-4817-2014>, 2014.
- 4031 Wiltshire, A. J., Burke, E. J., Chadburn, S. E., Jones, C. D., Cox, P. M., Davies-Barnard, T., Friedlingstein, P.,
4032 Harper, A. B., Liddicoat, S., Sitch, S., and Zaehle, S.: JULES-CN: a coupled terrestrial carbon–nitrogen scheme
4033 (JULES vn5.1), 14, 2161–2186, <https://doi.org/10.5194/gmd-14-2161-2021>, 2021.
- 4034 Winkler, K., Yang, H., Ganzenmüller, R., Fuchs, R., Ceccherini, G., Duveiller, G., Grassi, G., Pongratz, J., Bastos,
4035 A., Shvidenko, A., Araza, A., Herold, M., Wigneron, J.-P., and Ciais, P.: Changes in land use and management led
4036 to a decline in Eastern Europe’s terrestrial carbon sink, *Commun. Earth Environ.*, 4, 1–14,
4037 <https://doi.org/10.1038/s43247-023-00893-4>, 2023.
- 4038 Woodward, F. I. and Lomas, M. R.: Vegetation dynamics – simulating responses to climatic change, *Biol. Rev.*, 79,
4039 643–670, <https://doi.org/10.1017/S1464793103006419>, 2004.
- 4040 Wright, R. M., Le Quéré, C., Buitenhuis, E., Pitois, S., and Gibbons, M. J.: Role of jellyfish in the plankton
4041 ecosystem revealed using a global ocean biogeochemical model, 18, 1291–1320, <https://doi.org/10.5194/bg-18-1291-2021>, 2021.
- 4043 Wunch, D., Wennberg, P. O., Osterman, G., Fisher, B., Naylor, B., Roehl, C. M., O’Dell, C., Mandrake, L., Viatte,
4044 C., Kiel, M., Griffith, D. W. T., Deutscher, N. M., Velasco, V. A., Notholt, J., Warneke, T., Petri, C., De Maziere,
4045 M., Sha, M. K., Sussmann, R., Rettinger, M., Pollard, D., Robinson, J., Morino, I., Uchino, O., Hase, F.,
4046 Blumenstock, T., Feist, D. G., Arnold, S. G., Strong, K., Mendonca, J., Kivi, R., Heikkinen, P., Iraci, L., Podolske,
4047 J., Hillyard, P. W., Kawakami, S., Dubey, M. K., Parker, H. A., Sepulveda, E., García, O. E., Te, Y., Jeseck, P.,
4048 Gunson, M. R., Crisp, D., and Eldering, A.: Comparisons of the Orbiting Carbon Observatory-2 (OCO-2) X CO2
4049 measurements with TCCON, *Atmos. Meas. Tech.*, 10, 2209–2238, <https://doi.org/10.5194/amt-10-2209-2017>,
4050 2017.
- 4051 Wunder, S., Kaimowitz, D., Jensen, S., and Feder, S.: Coronavirus, macroeconomy, and forests: What likely
4052 impacts?, *For. Policy Econ.*, 131, 102536, <https://doi.org/10.1016/j.forpol.2021.102536>, 2021.
- 4053 Xi, F., Davis, S. J., Ciais, P., Crawford-Brown, D., Guan, D., Pade, C., Shi, T., Syddall, M., Lv, J., Ji, L., Bing, L.,
4054 Wang, J., Wei, W., Yang, K.-H., Lagerblad, B., Galan, I., Andrade, C., Zhang, Y., and Liu, Z.: Substantial global
4055 carbon uptake by cement carbonation, *Nature Geosci.*, 9, 880–883, <https://doi.org/10.1038/ngeo2840>, 2016.
- 4056 Xia, J., Chen, Y., Liang, S., Liu, D., and Yuan, W.: Global simulations of carbon allocation coefficients for
4057 deciduous vegetation types, *Tellus B*, 67, 28016, <https://doi.org/10.3402/tellusb.v67.28016>, 2015.
- 4058 Xia, X., Ren, P., Wang, X., Liu, D., Chen, X., Dan, L., He, B., He, H., Ju, W., Liang, M., Lu, X., Peng, J., Qin, Z.,
4059 Xia, J., Zheng, B., Wei, J., Yue, X., Yu, G., Piao, S., and Yuan, W.: The carbon budget of China: 1980–2021,
4060 *Science Bulletin*, 69, 114–124, <https://doi.org/10.1016/j.scib.2023.11.016>, 2024.
- 4061 Yang, D., Liu, Y., Feng, L., Wang, J., Yao, L., Cai, Z., Zhu, S., Lu, N., and Lyu, D.: The First Global Carbon
4062 Dioxide Flux Map Derived from TanSat Measurements, *Adv. Atmospheric Sci.*, 38, 1433–1443,
4063 <https://doi.org/10.1007/s00376-021-1179-7>, 2021.
- 4064 Yang, X., Thornton, P., Ricciuto, D., Wang, Y., and Hoffman, F.: Global evaluation of terrestrial biogeochemistry
4065 in the Energy Exascale Earth System Model (E3SM) and the role of the phosphorus cycle in the historical
4066 terrestrial carbon balance, *Biogeosciences*, 20, 2813–2836, <https://doi.org/10.5194/bg-20-2813-2023>, 2023.
- 4067 Yao, Y., Joetzier, E., Ciais, P., Viovy, N., Cresto Aleina, F., Chave, J., Sack, L., Bartlett, M., Meir, P., Fisher, R.,
4068 and Luyssaert, S.: Forest fluxes and mortality response to drought: model description (ORCHIDEE-CAN-NHA
4069 r7236) and evaluation at the Caxiuanã drought experiment, *Geosci. Model Dev.*, 15, 7809–7833,
4070 <https://doi.org/10.5194/gmd-15-7809-2022>, 2022.
- 4071 Yao, Y., Ciais, P., Viovy, N., Joetzier, E. and Chave, J.: How drought events during the last century have impacted
4072 biomass carbon in Amazonian rainforests. *Global Change Biology*, 29(3), pp.747-762,
4073 <https://doi.org/10.1111/gcb.16504>, 2023.
- 4074 You, Y., Tian, H., Pan, S., Shi, H., Bian, Z., Gurgel, A., Huang, Y., Kicklighter, D., Liang, X.-Z., Lu, C., Melillo,
4075 J., Miao, R., Pan, N., Reilly, J., Ren, W., Xu, R., Yang, J., Yu, Q., and Zhang, J.: Incorporating dynamic crop

- 4076 growth processes and management practices into a terrestrial biosphere model for simulating crop production in the
4077 United States: Toward a unified modeling framework, *Agricultural and Forest Meteorology*, 325, 109144,
4078 <https://doi.org/10.1016/j.agrformet.2022.109144>, 2022.
- 4079 Yu, Z., Ciais, P., Piao, S., Houghton, R. A., Lu, C., Tian, H., Agathokleous, E., Kattel, G. R., Sitch, S., Goll, D.,
4080 Yue, X., Walker, A., Friedlingstein, P., Jain, A. K., Liu, S., and Zhou, G.: Forest expansion dominates China's land
4081 carbon sink since 1980, *Nat. Commun.*, 13, 5374, <https://doi.org/10.1038/s41467-022-32961-2>, 2022.
- 4082 Yue, X. and Unger, N.: The Yale Interactive terrestrial Biosphere model version 1.0: description, evaluation and
4083 implementation into NASA GISS ModelE2, *Geosci. Model Dev.*, 8, 2399–2417, [https://doi.org/10.5194/gmd-8-](https://doi.org/10.5194/gmd-8-2399-2015)
4084 [2399-2015](https://doi.org/10.5194/gmd-8-2399-2015), 2015.
- 4085 Yue, X., Zhou, H., Tian, C., Ma, Y., Hu, Y., Gong, C., Zheng, H., and Liao, H.: Development and evaluation of the
4086 interactive Model for Air Pollution and Land Ecosystems (iMAPLE) version 1.0, *Geosci. Model Dev.*, 17, 4621–
4087 4642, <https://doi.org/10.5194/gmd-17-4621-2024>, 2024.
- 4088 Yuan, W., Liu, D., Dong, W., Liu, S., Zhou, G., Yu, G., Zhao, T., Feng, J., Ma, Z., Chen, J., Chen, Y., Chen, S.,
4089 Han, S., Huang, J., Li, L., Liu, H., Liu, S., Ma, M., Wang, Y., Xia, J., Xu, W., Zhang, Q., Zhao, X., and Zhao, L.:
4090 Multiyear precipitation reduction strongly decreases carbon uptake over northern China, *J. Geophys. Res.-Biogeo.*,
4091 119, 881–896, <https://doi.org/10.1002/2014JG002608>, 2014.
- 4092 Yue, C., Ciais, P., Zhu, D., Wang, T., Peng, S. S., and Piao, S. L.: How have past fire disturbances contributed to
4093 the current carbon balance of boreal ecosystems?, *Biogeosciences*, 13, 675–690, [https://doi.org/10.5194/bg-13-675-](https://doi.org/10.5194/bg-13-675-2016)
4094 [2016](https://doi.org/10.5194/bg-13-675-2016), 2016.
- 4095 Zaehle, S. and Friend, A. D.: Carbon and nitrogen cycle dynamics in the O-CN land surface model: 1. Model
4096 description, site-scale evaluation, and sensitivity to parameter estimates: Site-scale evaluation of a C-N model,
4097 *Global Biogeochem. Cycles*, 24, GB1005, <https://doi.org/10.1029/2009GB003521>, 2010.
- 4098 Zaehle, S., Ciais, P., Friend, A. D., and Prieur, V.: Carbon benefits of anthropogenic reactive nitrogen offset by
4099 nitrous oxide emissions, *Nature Geosci*, 4, 601–605, <https://doi.org/10.1038/ngeo1207>, 2011.
- 4100 Zaehle, S., Medlyn, B. E., De Kauwe, M. G., Walker, A. P., Dietze, M. C., Hickler, T., Luo, Y., Wang, Y.-P., El-
4101 Masri, B., Thornton, P., Jain, A., Wang, S., Warlind, D., Weng, E., Parton, W., Iversen, C. M., Gallet-Budynek, A.,
4102 McCarthy, H., Finzi, A., Hanson, P. J., Prentice, I. C., Oren, R., and Norby, R. J.: Evaluation of 11 terrestrial
4103 carbon–nitrogen cycle models against observations from two temperate Free-Air CO₂ Enrichment studies, *New*
4104 *Phytol.*, 202, 803–822, <https://doi.org/10.1111/nph.12697>, 2014.
- 4105 Zeng, J., Iida, Y., Matsunaga, T., and Shirai, T.: Surface ocean CO₂ concentration and air-sea flux estimate by
4106 machine learning with modelled variable trends, *Front. Mar. Sci.*, 9, <https://doi.org/10.3389/fmars.2022.989233>,
4107 2022.
- 4108 Zheng, B., Ciais, P., Chevallier, F., Chuvieco, E., Chen, Y., and Yang, H.: Increasing forest fire emissions despite
4109 the decline in global burned area, *Sci. Adv.*, 7, eabh2646, <https://doi.org/10.1126/sciadv.abh2646>, 2021.
- 4110 Zhu, Y., Xia, X., Canadell, J. G., Piao, S., Lu, X., Mishra, U., Wang, X., Yuan, W., and Qin, Z.: China's carbon
4111 sinks from land-use change underestimated, *Nat. Clim. Chang.*, 15, 428–435, [https://doi.org/10.1038/s41558-025-](https://doi.org/10.1038/s41558-025-02296-z)
4112 [02296-z](https://doi.org/10.1038/s41558-025-02296-z), 2025.
- 4113 Zou, Y., Wang, Y., Ke, Z., Tian, H., Yang, J., and Liu, Y.: Development of a REgion-Specific Ecosystem
4114 Feedback Fire (RESFire) Model in the Community Earth System Model, *J. Adv. Model. Earth Syst.*, 11, 417–445,
4115 <https://doi.org/10.1029/2018MS001368>, 2019.
- 4116 Zscheischler, J., Mahecha, M. D., Avitabile, V., Calle, L., Carvalhais, N., Ciais, P., Gans, F., Gruber, N.,
4117 Hartmann, J., Herold, M., Ichii, K., Jung, M., Landschützer, P., Laruelle, G. G., Lauerwald, R., Papale, D., Peylin,
4118 P., Poulter, B., Ray, D., Regnier, P., Rödenbeck, C., Roman-Cuesta, R. M., Schwalm, C., Tramontana, G.,
4119 Tyukavina, A., Valentini, R., van der Werf, G., West, T. O., Wolf, J. E., and Reichstein, M.: Reviews and
4120 syntheses: An empirical spatiotemporal description of the global surface–atmosphere carbon fluxes: opportunities
4121 and data limitations, *Biogeosciences*, 14, 3685–3703, <https://doi.org/10.5194/bg-14-3685-2017>, 2017.

4122

Tables

4123

4124 **Table 1.** Factors used to convert carbon in various units (by convention, Unit 1 = Unit 2 × conversion).

Unit 1	Unit 2	Conversion	Source
GtC (gigatonnes of carbon)	ppm (parts per million) (a)	2.124 (b)	Ballantyne et al. (2012)
GtC (gigatonnes of carbon)	PgC (petagrams of carbon)	1	SI unit conversion
GtCO ₂ (gigatonnes of carbon dioxide)	GtC (gigatonnes of carbon)	3.664	44.01/12.011 in mass equivalent
(a) Measurements of atmospheric CO ₂ concentration have units of dry-air mole fraction. 'ppm' is an abbreviation for micromole/mol, dry air.			
(b) The use of a factor of 2.124 assumes that all the atmosphere is well mixed within one year. In reality, only the troposphere is well mixed and the growth rate of CO ₂ concentration in the less well-mixed stratosphere is not measured by sites from the NOAA network. Using a factor of 2.124 makes the approximation that the growth rate of CO ₂ concentration in the stratosphere equals that of the troposphere on a yearly basis.			

4125

4126

Table 2. How to cite the individual components of the global carbon budget presented here.

Component	Primary reference
Global fossil CO ₂ emissions (EFOS), total and by fuel type	Andrew and Peters (2025)
National territorial fossil CO ₂ emissions (EFOS)	Erb and Marland (2025), UNFCCC (2022)
National consumption-based fossil CO ₂ emissions (EFOS) by country (consumption)	Peters et al. (2011a) updated as described in this paper
Net land-use change flux (ELUC)	This paper (see Table 4 for individual model references).
Growth rate in atmospheric CO ₂ concentration (GATM)	Lan et al. (2025)
Ocean and land CO ₂ sinks (SOCEAN and SLAND)	This paper (see Table 4 for individual model and data products references).

4127

4128 **Table 3.** Main methodological changes in the global carbon budget this year (GCB2025). Empty cells mean
 4129 there were no methodological changes introduced that year. Table S10 lists methodological changes from the
 4130 first global carbon budget publication up to 2024.

Fossil fuel emissions		LUC emissions	Reservoirs			Other changes
Global	Country (territorial)		Atmosphere	Ocean	Land	
	Projection available for Japan for the first time	Bookkeeping estimates derived from models that estimate ELUC based on transient carbon densities responding to environmental changes (BLUE, OSCAR, LUCE).	Include an assessment of satellite-derived growth rates	Adjustments applied for known underestimation of GOBMs and cool surface skin effect in fCO ₂ -product. Suspension of 19 ocean data sets from SOCAT.	Include the RSS adjustment.	

4131

4132 **Table 4.** References for the process models, bookkeeping models, ocean data products, and atmospheric
 4133 inversions. All models and products are updated with new data to the end of year 2024.

4134

Model/data name	Reference	Change from Global Carbon Budget 2024 (Friedlingstein et al., 2025a)
<i>Bookkeeping models for land-use change emissions</i>		
BLUE	Hansis et al. (2015)	Transient C densities used to estimate ELUC
OSCAR	Gasser et al. (2020)	No change
LUCE	Qin et al. (2024)	Transient C densities used to estimate ELUC
<i>Dynamic global vegetation models</i>		
CABLE-POP	Haverd et al. (2018)	corrected N deposition input data, minor parameter changes
CLASSIC	Melton et al. (2020), Gauthier et al. (2025), Kou-Giesbrecht and Arora (2022)	
CLM6.0	Lawrence et al. (2019)	New dust scheme, new BGC fire method, updates to MEGAN for BVOCs, parameter updates, new surface datasets, new N fixation method
CLM-FATES	Fisher et al. (2015), Koven et al. (2020)	New model
DLEM	Tian et al. (2015), You et al. (2022)	No change
EDv3	Moorcroft et al. (2001), Ma et al. (2022)	Updated meteorology inputs (i.e. hourly air temperature)
ELM	Yang et al.(2023), Burrows et al.(2020)	No change
ELM-FATES	Fisher et al. (2015), Koven et al. (2020), Needham et al. (2025)	New model
GDSTEM	Felzer et al. (2009), Felzer et al. (2011), Felzer (2012), Felzer and Jiang (2018)	New model
IBIS	Xia et al., (2024)	No change
iMAPLE	Yue et al. (2024)	No change.

ISAM	Jain et al. (2013), Meiyappan et al. (2015), Shu et al. (2020)	Vertically resolved soil biogeochemistry (carbon and nitrogen) module, following Shu et al. (2020)
JSBACH	Mauritsen et al. (2019), Reick et al. (2021)	No change
JULES-ES	Wiltshire et al. (2021), Sellar et al. (2019), Burton et al. (2019)	Minor updates to wildfire parameters
LPJ-GUESS	Smith et al. (2014)	Wood harvest without the LUH2 secondary mature, young, and non-forest harvest fraction info
LPJmL	Schaphoff et al. (2018), von Bloh et al. (2018), Lutz et al., (2019), Heinke et al. (2023)	Switch from version 5.7.5 to 5.10.0 incorporating updates to soil temperature scheme, revised N demand and N uptake processes, revised tree phenology, as well as bugfixes and code improvements
LPJ-EOSIM	Poulter et al. (2011) (d)	Incorporation of new respiration temperature responses and leaf respiration acclimation, updated the soil temperature and water scheme to have 8 layers
LPX-Bern	Lienert and Joos (2018)	No change
ORCHIDEEv3	Krinner et al. (2005), Zaehle and Friend (2010), Vuichard et al. (2019)	No change
SDGVM	Woodward and Lomas (2004), Walker et al. (2017)	Reverted to version used in Friedlingstein et al. (2022), but retaining the recent bug fix to monthly heterotrophic respiration output
VISIT	Ito and Inatomi (2012), Kato et al. (2013)	No change
VISIT-UT	Ito (2019)	New model
<i>Intermediate complexity land carbon cycle model</i>		
CARDAMOM	Bloom et al. (2016), Smallman et al. (2021)	Analysis resolution increased from 1 x1 to 0.5x0.5 degree. Estimates of fAPAR from MODIS collection 6.1. New prior constraint on the leaf carbon per unit area parameter (LCA). MODIS burned area forcing was replaced by GFEDv5 burned area estimate
<i>Global ocean biogeochemistry models</i>		
NEMO-PlankTOM12	Wright et al (2021)	No change
NEMO4.2-PISCES (IPSL)	Aumont et al. (2015)	No change to the model version, but switch to ERA5 forcing - A,B,C,D simulations have been re-run starting from GCB2024 simulation restart fields from 1940 onwards
MICOM-HAMOCC (NorESM1-OCv1.2)	Schwinger et al. (2016)	No change, model has been re-run to provide monthly CFC/SF ₆ outputs
MPIOM-	Lacroix et al. (2021)	No change

HAMOCC6		
NEMO3.6- PISCEsv2-gas (CNRM)	Berthet et al. (2019), Séférian et al. (2019)	Updated simulations using 1750 preindustrial conditions instead of 1850. No change in model configuration, except nudging of surface ocean fields applied to minimize the change of atm forcing. The methodology used is based on Sanchez-Gomez et al. (2024)
FESOM2.1- REcoM3	Gürses et al. (2023)	Switched to ERA5 forcing - A,B,C,D simulations have been re-run starting from GCB2024 simulation restart fields
MOM6- COBALTv3 (Princeton)	Stock et al., (2025)	New model configuration MOM6-COBALTv3 with ~1° horizontal resolution (360x210). 1) updated ocean biogeochemical module COBALTv3 with an additional fixed nitrogen removal process - anaerobic ammonium oxidation (anammox); 2) updated air-sea gas exchange scheme - wind-wave-bubble formulation; 3) updated riverine carbon and nutrient inputs following R2OMIP protocol (Lacroix et al., 2024, https://zenodo.org/records/13799103); 4) updated river water discharge files.
CESM-ETHZ	Doney et al. (2009)	Compared to the 2024 submission, we changed the forcing to ERA5. To this end, a new spinup was performed, extending over 500 years.
MRI-ESM2-4	Tsujino et al. (2024), Sakamoto et al. (2023)	Iron circulation is modified according to Moore and Braucher (2008) and iron limitation on primary production is adjusted according to this change. Updated atmospheric CO2 for simulations A and C. The JRA-3Q reanalysis (Kosaka et al. 2024) is used to physically force the model. The model is spun up for 1925 years with xCO2=278ppm.
ACCESS (CSIRO)	Law et al. (2017)	No change in model since GCB2024, but switched to ERA5 forcing and extended spinup.
<i>fCO2-products</i>		
VLIZ-SOMFFN	Landschützer et al. (2016)	Time period extended to 2024
Jena-MLS	Rödenbeck et al. (2014) updated to Rödenbeck et al (2022)	Time period extended to 2024
CMEMS-LSCE- FFNNv2	Chau et al. (2022)	Time period extended to 2024
UExP-FNN-U	Watson et al. (2020) and Ford et al. (2024)	Updated to recalculated SOCATv2025 dataset (Ford et al. 2025). Updated salinity dataset to use a tiered approach (described in Gregor et al. 2024) including ESA CCI-SSS (v5.51) and CMEMS GLORYS12V1. Updated time period to 1980 to 2024
NIES-ML3	Zeng et al. (2022)	Time period extended to 2024.
JMA-MLR	Iida et al. (2021)	Time period extended to 2024. Updated to recalculated SOCATv2025 dataset (Ford et al. 2025)
OceanSODA- ETHZv2	Gregor et al. (2024)	Time period extended to 2024

LDEO-HPD	Gloege et al. (2022) and Bennington et al. (2022)	Time period extended to 2024
CSIR-ML6	Gregor et al. (2019)	Time period extended to 2024
Atmospheric inversions		
Jena CarboScope	Rödenbeck et al. (2018) & Stephens et al. (2007).	Slight change in station set. Numerical flux resolution 2x2. TM3 run on spatial resolution 6x4 (multiple of 2x2)
CarbonTracker Europe (CTE)	van der Laan-Luijkx et al. (2017)	Update of prior fluxes and assimilated observations.
NISMON-CO2	Niwa et al. (2022), Niwa et al. (2017).	Update of prior fluxes, specifically changed GFED to GBEI. Update of the meteorological input to JRA-3Q. Including more CO2 observations.
CT-NOAA	Jacobson et al. (2025), Byrne et al. (2023), Krol et al. (2005), Peiro et al. (2022)	New air-sea gas exchange and new terrestrial NBE (Jacobson et al., 2025). Unlike previous submissions, CT2025 uses only one set of priors.
CMS-Flux	Liu et al. (2021)	Update of prior fluxes and assimilated observations.
CAMS-Satellite	Chevallier et al. (2005) and Chevallier et al. (2025)	Update of the prior fluxes and assimilated observations.
GONGGA	Jin et al. (2024)	Update of the prior fluxes and assimilated observations.
COLA	Liu et al. (2022)	Update of the prior fluxes and assimilated observations.
GCASv2	Jiang et al. (2021) & Emmons et al. (2010)	Update of the prior fluxes and assimilated observations.
UoE	Feng et al. (2016) & Palmer et al. (2019)	Update of the prior fluxes and assimilated observations.
MIROC-ACTM	Chandra et al. (2022) & Patra et al. (2018)	Update of assimilated observations and prior fluxes, specifically changed to MiCASA and GFED. Update of the meteorological input to JRA-3Q.
NTFVAR	Nayagam et al. (2025) & Maksyutov et al. (2021)	Update of prior fluxes and assimilated observations.
THU	Kong et al. (2022)	New this year, after missing out 1 year. Compared to the previous submission: update of prior fluxes and assimilated observations.
NISMON-CO2_GOSAT	Niwa et al. (2022), Niwa et al. (2017).	New this year.
Earth System Models		
CanESM5	Swart et al. (2019), Sospedra-Alfonso et al. (2021)	No change
EC-Earth3-CC	Döscher et al. (2021), Bilbao et al. (2021), Bernardello et al. (2024)	No change
IPSL-CM6A-CO2-LR	Boucher et al. (2020)	No change
MIROC-ES2L	Watanabe et al. (2020)	No change

MPI-ESM1-2-LR	Mauritsen et al. (2019), Li et al. (2023)	No change
NorCPM-CC	Tjiputra et al. (2020), Bethke et al. (2021)	New this year.

4135

4136 **Table 5.** Comparison of results from the bookkeeping method and budget residuals with results from the
4137 DGVMs, as well as additional estimates from atmospheric oxygen, atmospheric inversions and Earth System
4138 Models (ESMs) for different periods, the last decade, and the last year available. All values are in GtC yr⁻¹. The
4139 best estimate for GCB2025 (E_{LUC}) is calculated with the bookkeeping models (1a) and used in the budget Table
4140 7, see Section 2 and Figure 7 for description of the bookkeeping component fluxes. The best estimate for
4141 GCB2025 (S_{LAND}) is calculated with the DGVMs including the RSS correction (2b), and used in the budget
4142 Table 7. The DGVM uncertainties represent ±1σ of the decadal or annual (for 2024) estimates from the
4143 individual DGVMs. For the inverse systems the mean and range of available results is given when the number
4144 of systems is less than 10, otherwise the ±1σ is provided. All values are rounded to the nearest 0.1 GtC and
4145 therefore columns do not necessarily add to zero.

4146

		<i>Mean (GtC yr⁻¹)</i>							
		1960s	1970s	1980s	1990s	2000s	2010s	2015- 2024	2024
Land-use change emissions (E _{LUC})	Bookkeeping (BK) Net flux (1a)	1.9±0 .7	1.7±0 .7	1.7±0 .7	1.7±0 .7	1.7±0 .7	1.6±0 .7	1.4±0 .7	1.3±0 .7
	BK - deforestation (total)	1.8 [1.6,2 .1]	1.8 [1.6,2 .1]	1.7 [1.5,1 .9]	1.9 [1.6,2 .1]	2 [1.7,2 .2]	2 [1.6,2 .4]	1.9 [1.5,2 .3]	1.9 [1.4,2 .4]
	BK - forest regrowth (total)	-0.9 [-1,- 0.7]	-0.9 [-1,- 0.8]	-0.9 [-1,- 0.8]	-1 [- 1.1,- 0.8]	-1.1 [- 1.2,- 0.9]	-1.3 [- 1.4,- 1]	-1.3 [- 1.5,- 1]	-1.3 [- 1.6,- 1]
	BK - other transitions	0.3 [0.3,0 .3]	0.2 [0.2,0 .3]	0.2 [0.1,0 .3]	0.1 [0.1,0 .2]	0.1 [0,0.1]	0.2 [0.1,0 .2]	0.1 [0.1,0 .1]	0.1 [0.1,0 .1]
	BK - peat drainage & peat fires	0.2 [0.1,0 .2]	0.2 [0.1,0 .2]	0.2 [0.2,0 .2]	0.3 [0.2,0 .3]	0.2 [0.2,0 .3]	0.3 [0.3,0 .3]	0.2 [0.2,0 .3]	0.2 [0.2,0 .2]
	BK - wood harvest & forest management	0.4 [0.1,0 .6]	0.4 [0.1,0 .6]	0.5 [0.1,0 .7]	0.5 [0.1,0 .7]	0.5 [0.1,0 .7]	0.4 [0.1,0 .7]	0.4 [0.1,0 .7]	0.4 [0.1,0 .7]
	DGVMs-net flux (1b)	1.3±0 .5	1.2±0 .5	1.2±0 .5	1.2±0 .5	1.2±0 .6	1.1±0 .6	1±0.6	0.9±0 .5
Terrestrial sink (S _{LAND})	Residual sink from global budget (E _{FOS} +E _{LUC} (1a)-G _{ATM} - S _{OCEAN}) (2a)	1.9±0 .8	2±0.8	1.7±0 .9	2.6±0 .9	2.9±0 .9	3±0.9	2.4±0 .9	0.3±1
	DGVMs (2b)	0.9±0 .3	1.6±0 .5	1.4±0 .6	2±0.5	2.2±0 .6	2.5±0 .7	2.4±0 .8	1.9±0 .9
Net land fluxes (S _{LAND} -E _{LUC})	GCB2025 Budget (2b- 1a)	- 0.9±0 .8	- 0.1±0 .9	- 0.3±0 .9	0.2±0 .9	0.5±0 .9	0.9±1	1±1	0.7±1 .1
	Atmospheric O ₂	---	---	---	1.3±0 .6	0.9±0 .7	1±0.8	0.7±0 .8	-

	1960s	1970s	1980s	1990s	2000s	2010s	2015-2024	2024
DGVMs-net (2b-1b)	- 0.3±0 .4	0.4±0 .6	0.2±0 .5	0.8±0 .4	1±0.4	1.4±0 .6	1.4±0 .7	1.1±0 .8
Inversions*	- [-,-]	- [-,-]	- [-,-]	0.7 [0.6,0 .8] (2)	1.4 [1.3,1 .6] (3)	1.5 [1.3,2 .3] (8)	1.3±0 .3 (14)	0.2±0 .7 (14)
ESMs	0 [- 0.7,0. 5]	1.5 [1.2,2]	1.1 [0.5,1 .4]	1.8 [1.2,2 .4]	1.8 [0.4,2 .7]	2 [0.7,3]	2.3 [- 0.1,3. 6]	0.8 [- 2.9- 3.3]

*Estimates are adjusted for the pre-industrial influence of river fluxes, for the cement carbonation sink, and adjusted to common EFOS (Sect. 2.7). The ranges given include varying numbers (in parentheses) of inversions in each decade (Table S4)

4147

4148 **Table 6:** Comparison of results for the un-adjusted ocean sinks from the $f\text{CO}_2$ -products, from global ocean
4149 biogeochemistry models (GOBMs), the best estimate for GCB2025 (adjusted S_{OCEAN}) calculated from $f\text{CO}_2$ -
4150 products and GOBMs) and used in the budget Table 7, as well as additional estimates from ocean interior
4151 observation-based changes in the dissolved inorganic carbon (DIC) inventory, atmospheric oxygen, atmospheric
4152 inversions and Earth System Models (ESMs) for different periods, the last decade, and the last year available.
4153 All values are in GtC yr^{-1} . Uncertainties represent $\pm 1\sigma$ of the estimates from the GOBMs and inversions ($n > 10$)
4154 and range of ensemble members is given for ensembles with $n < 10$ ($f\text{CO}_2$ -products, inversions, ocean interior,
4155 ESMs). The uncertainty of the GCB2025 budget estimate is based on expert judgement (Section 2 and
4156 Supplement S1 to S4) and for oxygen it is the standard deviation of a Monte Carlo ensemble (Section 2.8). Note
4157 that adjustments were applied to the $f\text{CO}_2$ -products and two of the ocean interior estimates to match the
4158 definition of S_{OCEAN} (see section 2.5.1 and S3.6).

4159

<i>Mean (GtC yr⁻¹)</i>								
Product	1960s	1970s	1980s	1990s	2000s	2010s	2015-2024	2024
GCB2025 Budget	1.3±0.4	1.6±0.4	2.1±0.4	2.3±0.4	2.6±0.4	3.1±0.4	3.2±0.4	3.4±0.4
$f\text{CO}_2$ -products	---	---	---	2.3 [2,3]	2.5 [2.4,2.9]	3.1 [2.9,3.5]	3.3 [2.9,3.9]	3.5 [2.8,4.2]
GOBMs	1.1±0.2	1.3±0.3	1.8±0.3	2.0±0.3	2.2±0.3	2.6±0.3	2.7±0.3	2.9±0.3
Atmospheric O ₂	---	---	---	2.0±0.4	2.8±0.4	3.4±0.5	3.5±0.5	-
Inversions	- [-,-]	- [-,-]	- [-,-]	2.4 [2.2,2.5] (2)	2.3 [2.2,2.4] (3)	2.9 [2.1,3.1] (8)	3±0.3 (14)	3±0.4 (14)
Ocean interior	1.1 [-,-]	1.3 [-,-]	1.8 [-,-]	2.1 [2,2.3]	2.2 [1.7,2.5]	3.3 [2.7,4]	---	-
ESMs	0.7 [0.1,1.1]	1 [0.4,1.4]	1.5 [0.7,2]	1.7 [1.1,2.1]	1.9 [1.5,2.2]	2.4 [2,2.7]	2.5 [2.2,2.8]	2.6 [2.2-3.1]

4160

4161 **Table 7:** Decadal mean in the five components of the anthropogenic CO₂ budget for different periods, and last
 4162 year available. All values are in GtC yr⁻¹, and uncertainties are reported as ±1σ. Fossil CO₂ emissions include
 4163 cement carbonation. The table also shows the budget imbalance (B_{IM}), which provides a measure of the
 4164 discrepancies among the nearly independent estimates. A positive imbalance means the emissions are
 4165 overestimated and/or the sinks are too small. All values are rounded to the nearest 0.1 GtC and therefore
 4166 columns do not necessarily add to zero.

4167

Mean (GtC yr⁻¹)

		1960s	1970s	1980s	1990s	2000s	2010s	2015-2024	2024	2025 (Projection)
Total emissions (E _{FOS} + E _{LUC})	Fossil CO ₂ emissions (E _{FOS})*	3±0.2	4.7±0.2	5.4±0.3	6.4±0.3	7.8±0.4	9.5±0.5	9.8±0.5	10.3±0.5	10.4±0.5
	Land-use change emissions (E _{LUC})	1.9±0.7	1.7±0.7	1.7±0.7	1.7±0.7	1.7±0.7	1.6±0.7	1.4±0.7	1.3±0.7	1.1±0.7
	Total emissions	4.9±0.7	6.4±0.7	7.1±0.8	8.1±0.8	9.5±0.8	11.1±0.8	11.2±0.9	11.6±0.9	11.5±0.9
Partitioning	Growth rate in atmos CO ₂ (G _{ATM})	1.7±0.07	2.8±0.07	3.4±0.02	3.1±0.02	4±0.2	5.1±0.02	5.6±0.02	7.9±0.2	4.9±0.2
	Ocean sink (S _{OCEAN})	1.3±0.4	1.6±0.4	2.1±0.4	2.3±0.4	2.6±0.4	3.1±0.4	3.2±0.4	3.4±0.4	3.2±0.4
	Terrestrial sink (S _{LAND})	0.9±0.3	1.6±0.5	1.4±0.6	2±0.5	2.2±0.6	2.5±0.7	2.4±0.8	1.9±0.9	3.4±1
Budget Imbalance	BIM = E _{FOS} + E _{LUC} - (G _{ATM} + S _{OCEAN})	0.9	0.5	0.3	0.7	0.7	0.4	0	-1.7	

	1960s	1970s	1980s	1990s	2000s	2010s	2015-2024	2024	2025 (Projection)
N+SLAND)									

*Fossil emissions excluding the cement carbonation sink amount to 3 ± 0.2 GtC yr⁻¹, 4.7 ± 0.2 GtC yr⁻¹, 5.5 ± 0.3 GtC yr⁻¹, 6.4 ± 0.3 GtC yr⁻¹, 7.9 ± 0.4 GtC yr⁻¹, and 9.7 ± 0.5 GtC yr⁻¹ for the decades 1960s to 2010s respectively and to 10 ± 0.5 GtC yr⁻¹ for 2024, and 10.5 ± 0.5 GtC yr⁻¹ for 2025.

4168

4169 **Table 8.** Cumulative CO₂ for different time periods in gigatonnes of carbon (GtC). Fossil CO₂ emissions
 4170 include cement carbonation. The budget imbalance (BIM) provides a measure of the discrepancies among the
 4171 nearly independent estimates. All values are rounded to the nearest 5 GtC and therefore columns do not
 4172 necessarily add to zero. Uncertainties are reported as follows: E_{FOS} is 5% of cumulative emissions; E_{LUC} prior to
 4173 1959 is 1σ spread from the DGVMs, E_{LUC} post-1959 is 0.7*number of years (where 0.7 GtC yr⁻¹ is the
 4174 uncertainty on the annual E_{LUC} flux estimate); G_{ATM} uncertainty is held constant at 5 GtC for all time periods;
 4175 S_{OCEAN} uncertainty is 20% of the cumulative sink (20% relates to the annual uncertainty of 0.4 GtC yr⁻¹, which
 4176 is ~20% of the current ocean sink); and S_{LAND} is the 1σ spread from the DGVMs estimates.

4177 *Mean (GtC yr⁻¹)*

4178

		1750-2024	1850-2014	1850-2024	1960-2024	1850-2025
Emissions	Fossil CO ₂ emissions (E _{FOS})	500±25	400±20	495±25	415±20	510±25
	Land-use change emissions (E _{LUC})	280±65	235±55	250±60	110±45	250±60
	Total emissions	780±70	635±60	745±65	525±50	755±65
Partitioning	Growth rate in atmos CO ₂ (G _{ATM})	310±5	235±5	290±5	230±5	295±5
	Ocean sink (S _{OCEAN})	210±40	170±35	200±40	145±30	205±40
	Terrestrial sink (S _{LAND})	190±50	150±40	175±50	120±30	175±50
Budget imbalance	BIM = E _{FOS} + E _{LUC} - (G _{ATM} + S _{OCEAN} + S _{LAND})	65	80	80	35	80

4179
4180

4181 **Table 9.** Average annual growth rate in fossil CO₂ emissions over the most recent decade (2015-2024) and the
 4182 previous decade (2005-2014). The data for the World include the cement carbonation sink. IAS are emissions
 4183 from international aviation and shipping. The rest of the world is defined as World minus China, USA, India,
 4184 EU27, and IAS.
 4185

	World	China	USA	India	EU27	OECD	Non-OECD	IAS	Rest of the World
2005-2014	2.1%	6.7%	-1.4%	6.4%	2.2%	-1.0%	4.6%	1.9%	1.8%
2015-2024	0.8%	2.5%	-1.2%	3.6%	-2.5%	-1.5%	2.1%	-1.4%	0.6%

4186

4187

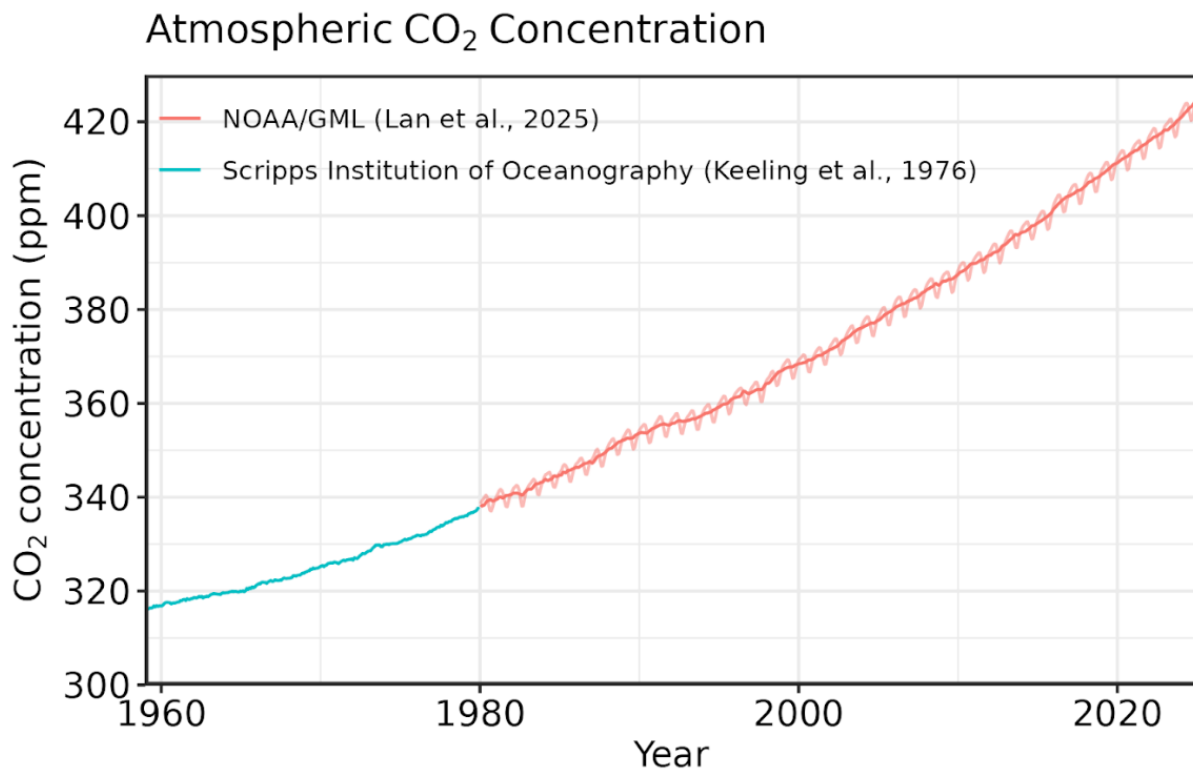
4188 **Table 10.** Major known sources of uncertainties in each component of the Global Carbon Budget, defined as
 4189 input data or processes that have a demonstrated effect of at least $\pm 0.3 \text{ GtC yr}^{-1}$.

Source of uncertainty	Time scale (years)	Location	Evidence
Fossil CO ₂ emissions (EFOS; Section 2.1)			
energy statistics	annual to decadal	global, but mainly China & major developing countries	(Korsbakken et al., 2016, Guan et al., 2012)
carbon content of coal	annual to decadal	global, but mainly China & major developing countries	(Liu et al., 2015)
system boundary	annual to decadal	all countries	(Andrew, 2020a)
Net land-use change flux (ELUC; section 2.2)			
land-cover and land-use change statistics	continuous	global; in particular tropics	(Houghton et al., 2012, Gasser et al., 2020, Ganzenmüller et al., 2022, Yu et al. 2022)
sub-grid-scale transitions	annual to decadal	global	(Wilkenskjeld et al., 2014, Bastos et al., 2021)
vegetation biomass	annual to decadal	global; in particular tropics	(Houghton et al., 2012, Bastos et al., 2021)
forest degradation (fire, selective logging)	annual to decadal	tropics; Amazon	(Aragão et al., 2018, Qin et al., 2021, Lapola et al., 2023)
wood and crop harvest	annual to decadal	global; SE Asia	(Arneth et al., 2017, Erb et al., 2018)
peat burning	multi-decadal trend	global	(van der Werf et al., 2010, 2017)
Atmospheric growth rate (GATM; section 2.4) no demonstrated uncertainties larger than $\pm 0.3 \text{ GtC yr}^{-1}$. The uncertainties in annual GATM have been estimated as $\pm 0.2 \text{ GtC yr}^{-1}$, although the conversion of the growth rate into a global annual flux assuming instantaneous mixing throughout the atmosphere introduces additional errors (see Section 2.4.2).			
Ocean sink (SOCEAN; section 2.5)			
sparsity in surface fCO ₂ observations	mean, decadal variability and trend	global, in particular southern hemisphere	(Gloege et al., 2021, Denvil-Sommer et al., 2021, Hauck et al., 2023a; Dong et al., 2024b)

riverine carbon outgassing and its anthropogenic perturbation	annual to decadal	global, in particular partitioning between Tropics and South	(Aumont et al., 2001, Lacroix et al., 2020, Crisp et al., 2022)
Models underestimate interior ocean anthropogenic carbon storage	annual to decadal	global	(Friedlingstein et al., 2022a, this study, DeVries et al., 2023, Müller et al., 2023)
near-surface temperature and salinity gradients	mean on all time-scales	global	(Watson et al., 2020, Dong et al., 2022, Bellenger et al., 2023, Dong et al., 2024a)
Land sink (SLAND; section 2.6)			
strength of CO2 fertilisation	multi-decadal trend	global	(Wenzel et al., 2016; Walker et al., 2021)
response to variability in temperature and rainfall	annual to decadal	global; in particular tropics	(Cox et al., 2013; Jung et al., 2017; Humphrey et al., 2018; 2021)
nutrient limitation and supply	annual to multi-decadal	global	(Zaehle et al., 2014)
carbon allocation and tissue turnover rates	annual to decadal	global	(De Kauwe et al., 2014; O'Sullivan et al., 2022)
tree mortality	annual	global in particular tropics	(Hubau et al., 2021; Brienen et al., 2020)
response to diffuse radiation	annual	global	(Mercado et al., 2009; O'Sullivan et al., 2021)

4190

4191

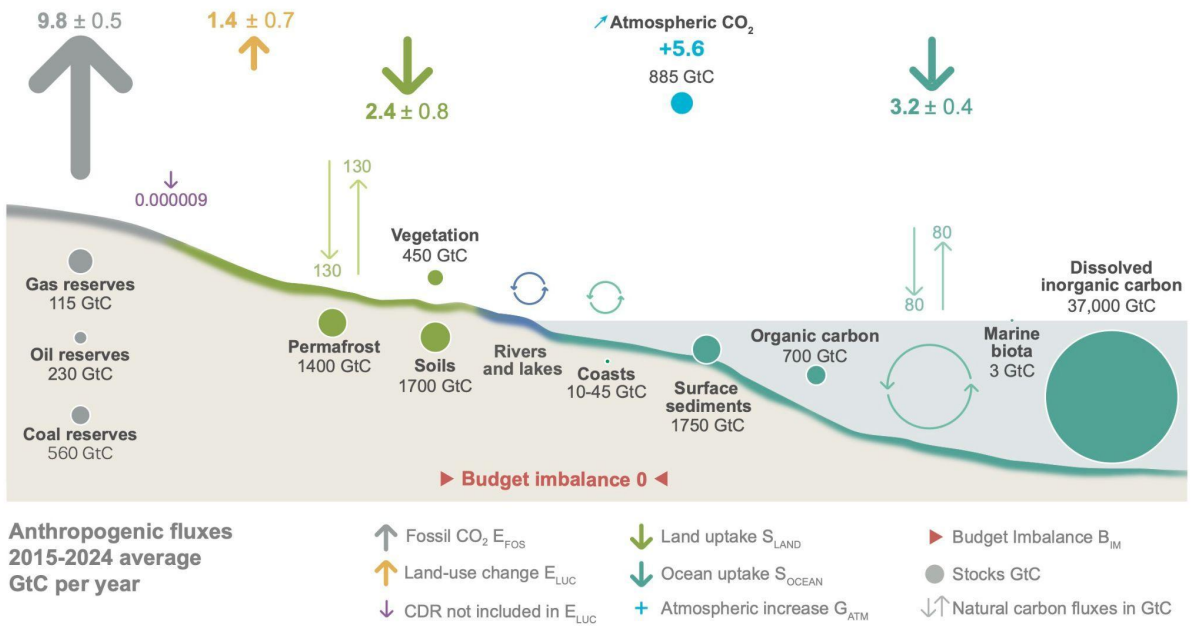


4193

4194 **Figure 1.** Surface average atmospheric CO₂ concentration (ppm). Since 1980, monthly data are from
4195 NOAA/GML (Lan et al., 2025) and are based on an average of direct atmospheric CO₂ measurements from
4196 multiple stations in the marine boundary layer (Masarie and Tans, 1995). The 1958-1979 monthly data are from
4197 the Scripps Institution of Oceanography, based on an average of direct atmospheric CO₂ measurements from the
4198 Mauna Loa and South Pole stations (Keeling et al., 1976). To account for the difference of mean CO₂ and
4199 seasonality between the NOAA/GML and the Scripps station networks used here, the Scripps surface average
4200 (from two stations) was de-seasonalised and adjusted to match the NOAA/GML surface average (from multiple
4201 stations) by adding the mean difference of 0.667 ppm, calculated here from overlapping data during 1980-2012.

4202

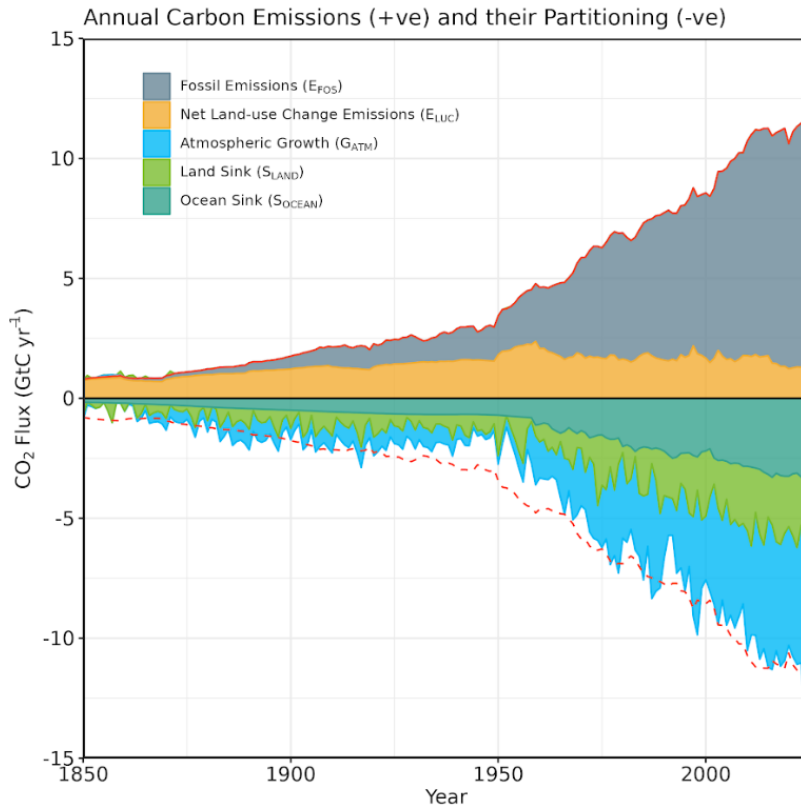
The global carbon cycle



4203

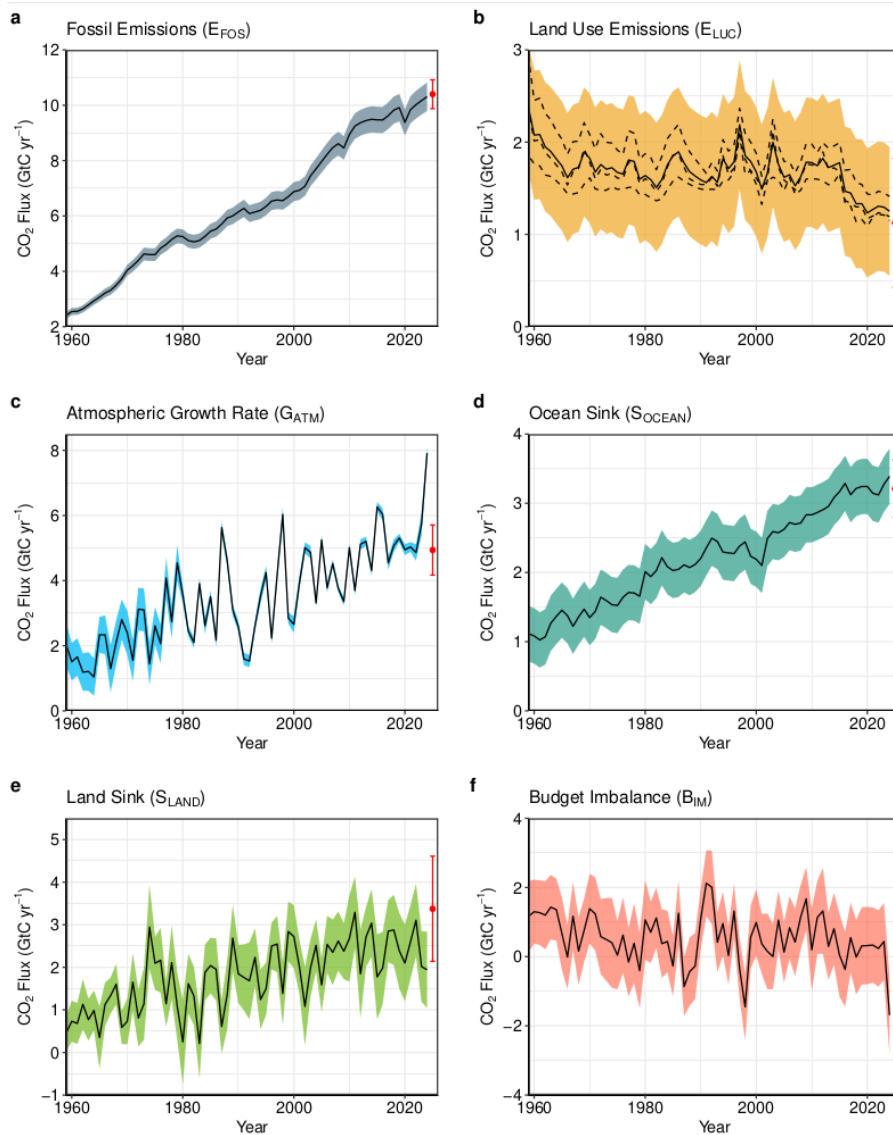
4204 **Figure 2.** Schematic representation of the overall perturbation of the global carbon cycle caused by
 4205 anthropogenic activities, averaged globally for the decade 2015-2024. See legends for the corresponding arrows.
 4206 Fluxes estimates and their 1 standard deviation uncertainty are as reported in Table 7. The CDR estimate is for the
 4207 year 2024. The uncertainty in the atmospheric CO₂ growth rate is very small (± 0.02 GtC yr⁻¹) and is neglected for
 4208 the figure. The anthropogenic perturbation occurs on top of an active carbon cycle, with fluxes and stocks
 4209 represented in the background and taken from Canadell et al. (2021) for all numbers, except for the carbon
 4210 stocks in coasts which is from a literature review of coastal marine sediments (Price and Warren, 2016). Fluxes
 4211 are in GtC yr⁻¹ and reservoirs in GtC. This figure was produced by Nigel Hawtin.

4212



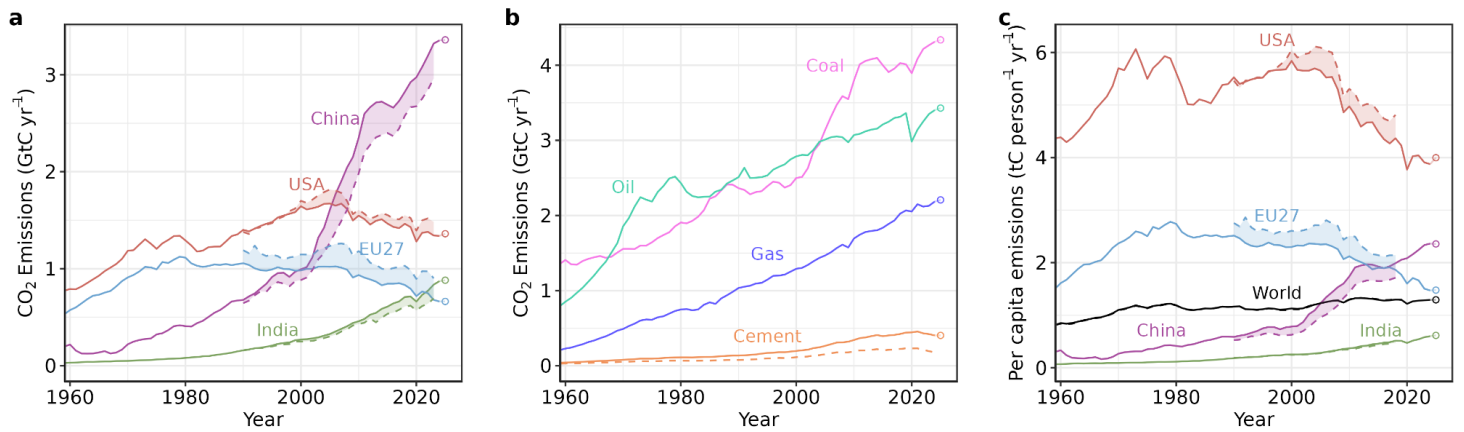
4213

4214 **Figure 3.** Combined components of the global carbon budget as a function of time, for fossil CO₂ emissions
 4215 (E_{FOS}, including a small sink from cement carbonation; grey) and emissions from land-use change (E_{LUC};
 4216 brown), as well as their partitioning among the atmosphere (G_{ATM}; cyan), ocean (S_{OCEAN}; blue), and land (S_{LAND};
 4217 green). The figure shows annual estimates of each flux (in GtC yr⁻¹) since the year 1850. The partitioning is
 4218 based on nearly independent estimates from observations (for G_{ATM}) and from process model ensembles
 4219 constrained by data (for S_{OCEAN} and S_{LAND}) and does not exactly add up to the sum of the emissions, resulting in
 4220 a budget imbalance (B_{IM}) which is represented by the difference between the bottom red line (mirroring total
 4221 emissions) and the sum of carbon fluxes in the ocean, land, and atmosphere reservoirs. The E_{FOS} estimate is
 4222 based on a mosaic of different datasets and has an uncertainty of ±5% (±1σ). The E_{LUC} estimate is from three
 4223 bookkeeping models (Table 4) with uncertainty of ±0.7 GtC yr⁻¹. The G_{ATM} estimates prior to 1959 are from
 4224 Joos and Spahni (2008) with uncertainties equivalent to about ±0.1-0.15 GtC yr⁻¹ and from Lan et al. (2025)
 4225 since 1959 with uncertainties of about ±0.07 GtC yr⁻¹ during 1959-1979 and ±0.02 GtC yr⁻¹ since 1980. The
 4226 S_{OCEAN} estimate prior to 1959 is the average from Khatiwala et al. (2013) and DeVries (2014) with uncertainty
 4227 of about ±30%. After 1959, it is the average of an ensemble of models (GOBMs) and an ensemble of fCO₂-
 4228 products (with adjustments, Table 4) with uncertainties of about ±0.4 GtC yr⁻¹. The S_{LAND} estimate is the
 4229 average of an ensemble of models (DGVMs) (Table 4) with uncertainties of about ±1 GtC yr⁻¹. See the text for
 4230 more details of each component and their uncertainties.



4231
 4232
 4233
 4234
 4235
 4236
 4237
 4238
 4239
 4240

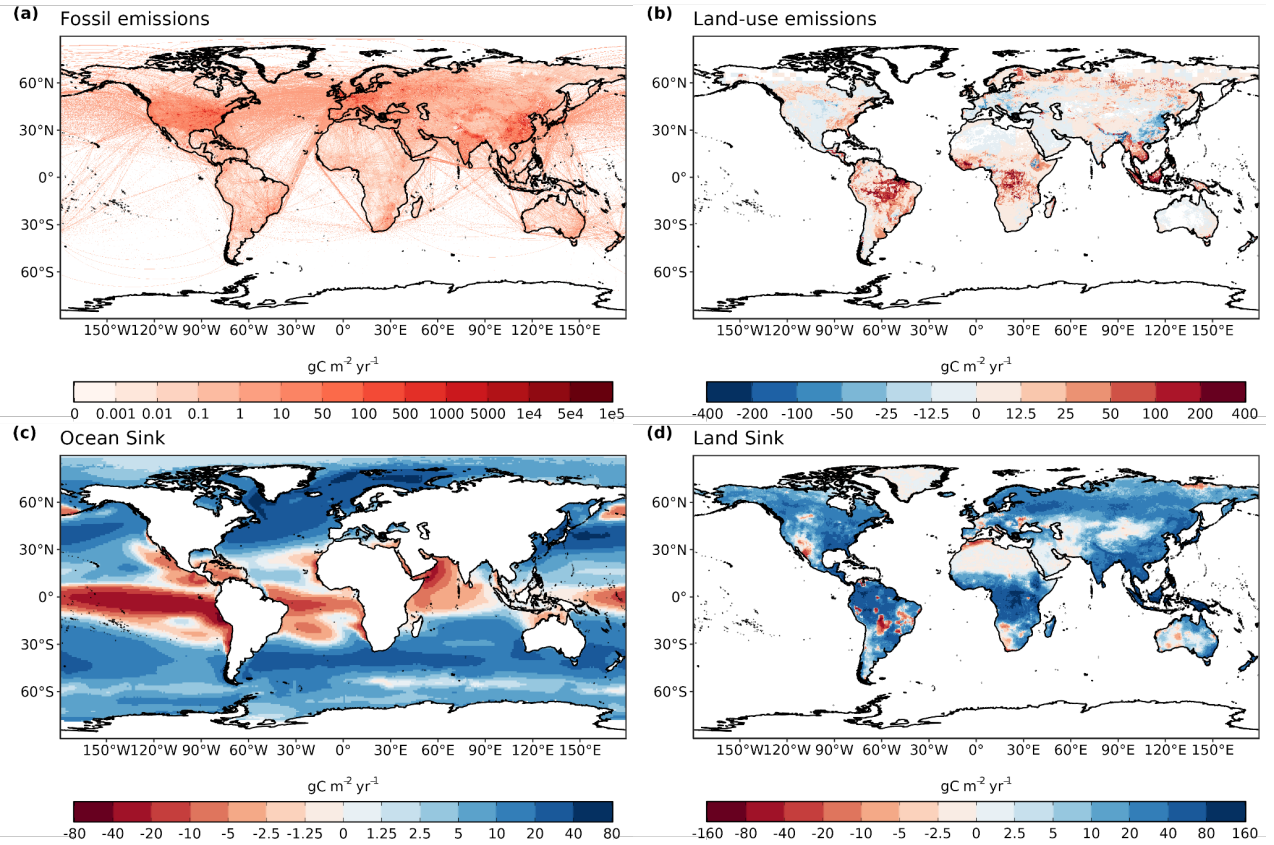
Figure 4. Components of the global carbon budget and their uncertainties as a function of time, presented individually for (a) fossil CO₂, including cement carbonation emissions (E_{FOS}), (b) emissions from land-use change (E_{LUC}), (c) growth rate in atmospheric CO₂ concentration (G_{ATM}), (d) the ocean CO₂ sink (S_{OCEAN}), (e) the land CO₂ sink (S_{LAND}), (f) the budget imbalance (B_{IM}) that is not accounted for by the other terms. Individual estimates from the three bookkeeping models are shown as dashed lines for E_{LUC} in panel (b). Positive values of S_{LAND} and S_{OCEAN} represent a flux from the atmosphere to land or the ocean. All data are in GtC yr⁻¹ with the uncertainty bounds representing ± 1 standard deviation in shaded colour. Data sources are as in Figure 3. The red dots indicate our projections for the year 2025 and the red error bars the uncertainty in the 2025 projections (see methods).



4241

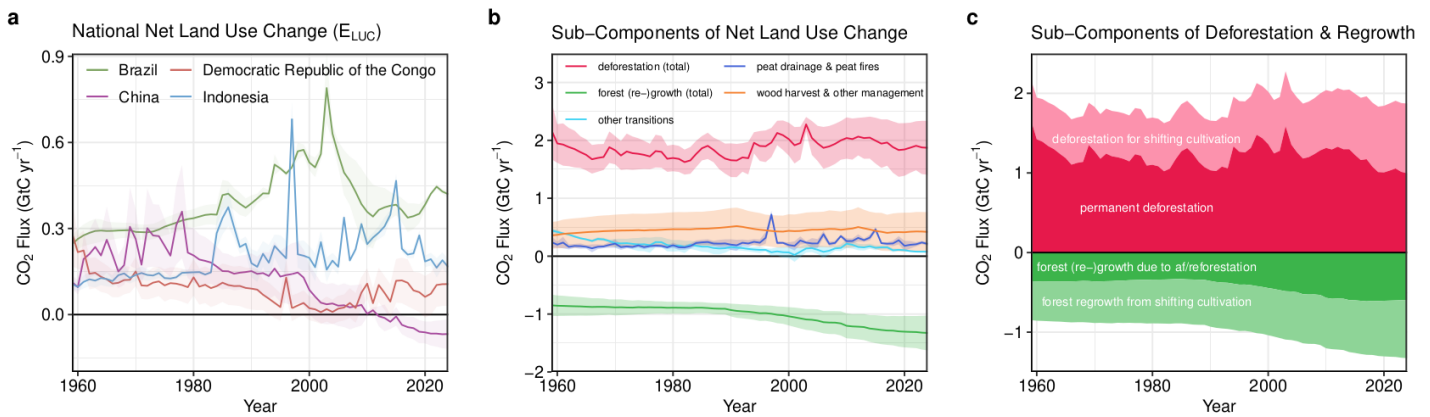
4242 **Figure 5.** Fossil CO₂ emissions for (a) territorial (solid lines) and consumption (dashed lines) emissions for the
 4243 top three country emitters (USA, China, India) and for the European Union (EU27), (b) global emissions by fuel
 4244 type, including coal, oil, gas, and cement, and cement minus cement carbonation (dashed), and (c) per-capita
 4245 emissions the world and for the large emitters as in panel (a). Territorial emissions are from Andrew & Peters
 4246 (2025), while consumption-based emissions are updated from Peters et al. (2011a). See Section 2.1 and
 4247 Supplement S.1 for details of the calculations and data sources.

4248



4249
4250
4251
4252
4253
4254
4255
4256
4257
4258
4259
4260
4261
4262
4263

Figure 6. The 2015-2024 decadal mean components of the global carbon budget, presented for (a) fossil CO₂ emissions (E_{FOS}), (b) land-use change emissions (E_{LUC}), (c) the ocean CO₂ sink (S_{OCEAN}), and (d) the land CO₂ sink (S_{LAND}). Positive values for E_{FOS} and E_{LUC} represent a flux to the atmosphere, whereas positive values of S_{OCEAN} and S_{LAND} represent a flux from the atmosphere to the ocean or the land (carbon sink). In all panels, red colours represent a source (flux from the land/ocean to the atmosphere), blue colours represent a sink (flux from the atmosphere into the land/ocean). All units are in $gC\ m^{-2}\ yr^{-1}$. Note the different scales in each panel. E_{FOS} data shown is from GCP-GridFEDv2025.0 and does not include cement carbonation. The E_{LUC} map shows the average E_{LUC} from the three bookkeeping models plus emissions from peat drainage and peat fires. BLUE and LUCE provide spatially explicit estimates at 0.25° resolution. Gridded E_{LUC} estimates for OSCAR are derived by spatially distributing their national data based on the spatial patterns of BLUE gross fluxes in each country (see Schwingshackl et al., 2022, for more details about the methodology). S_{OCEAN} data shown is the average of un-adjusted GOBMs and fCO_2 -products means, using GOBMs simulation A, no adjustment for bias and drift applied to the gridded fields (see Section 2.5). S_{LAND} data shown is the average of the DGVMs for simulation S2, no adjustment for bias and drift applied to the gridded fields (see Section 2.6).



4265

4266

Figure 7. Net CO₂ exchanges between the atmosphere and the terrestrial biosphere related to land use change.

4267

(a) Net CO₂ emissions from land-use change from the four countries with largest cumulative emissions since 1959. Values shown are the average of the three bookkeeping models, with shaded regions as $\pm 1\sigma$ uncertainty.

4268

4269

(b) Sub-components of E_{LUC} : (i) emissions from deforestation (including permanent deforestation and deforestation in shifting cultivation cycles), (ii) emissions from peat drainage & peat fires, (iii) removals from forest (re-)growth (including forest (re-)growth due to afforestation and reforestation and forest regrowth in shifting cultivation cycles), (iv) fluxes from wood harvest and other forest management (comprising slash and product decay following wood harvest, regrowth after wood harvest, and fire suppression), and (v) emissions and removals related to other land-use transitions. The sum of the five components is E_{LUC} shown in Figure 4b.

4270

4271

4272

4273

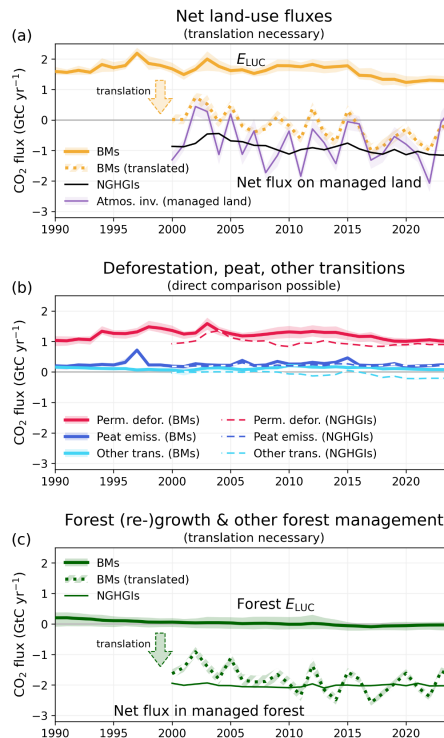
4274

4275

4276

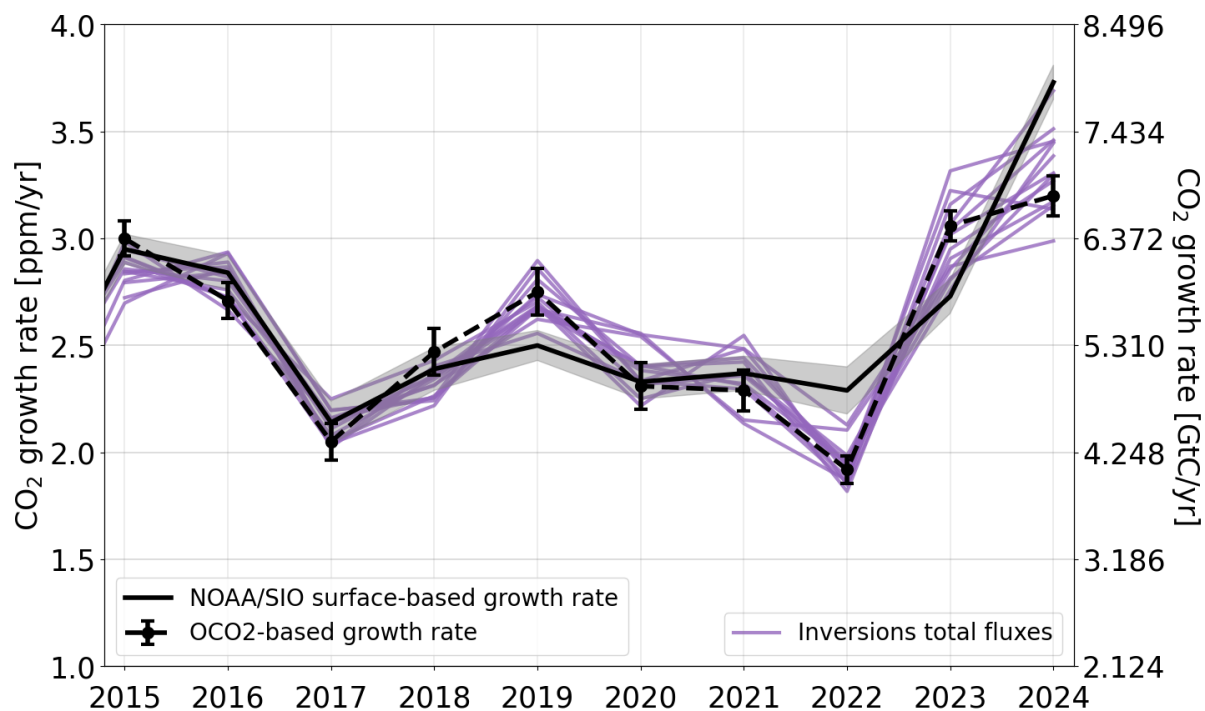
4277

(c) Sub-components of ‘deforestation (total)’ and of ‘forest (re-)growth (total)’: (i) deforestation in shifting cultivation cycles, (ii) permanent deforestation, (iii) forest (re-)growth due to afforestation and/or reforestation, and (iv) forest regrowth in shifting cultivation cycles.



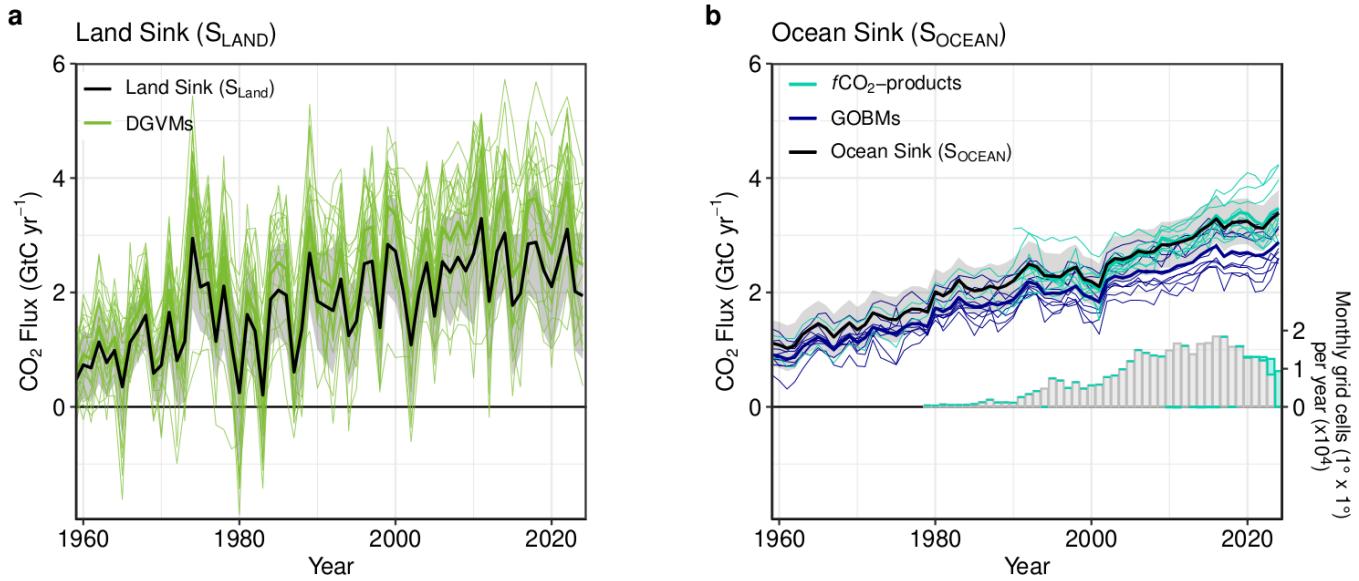
4278

4279 **Figure 8.** Comparison of land-use flux estimates from bookkeeping models (BMs; following the GCB
 4280 definition of E_{LUC}), national GHG inventories (NGHGIs; following IPCC guidelines and thus including all
 4281 carbon fluxes on managed land), and atmospheric inversion systems (considering fluxes on managed land only).
 4282 To compare BM results with NGHGIS, a translation is necessary for some subcomponents. (a) Net land-use
 4283 fluxes, for which a translation of BMs is necessary, (b) subcomponents permanent deforestation, peat drainage
 4284 & peat fires, and other transitions, which can be directly compared and (c) subcomponent forest (re-)growth &
 4285 other forest management, for which a translation is necessary. The lines represent the mean of 3 BMs and 14
 4286 atmospheric inversion estimates, respectively; Shaded areas denote the full range across BM estimates and the
 4287 standard deviation for atmospheric inversions, respectively. The subcomponent forest (re-)growth & other forest
 4288 management includes removals from forest (re-)growth (permanent), emissions and removals from wood
 4289 harvest & other forest management, and emissions and removals in shifting cultivation cycles. The translation of
 4290 BM estimates to NGHGI estimates in (a) and (c) is done by adding the natural land sink in managed forests to
 4291 the BM estimates (see also Table S11). The GCB definition of E_{LUC} and the NGHGI definition of land-use
 4292 fluxes are equally valid, each in its own context. For illustrative purposes we only show the translation of BM
 4293 estimates to the NGHGI definition. NGHGI data are from the LULUCF data hub V3.1 (Melo et al. 2025).

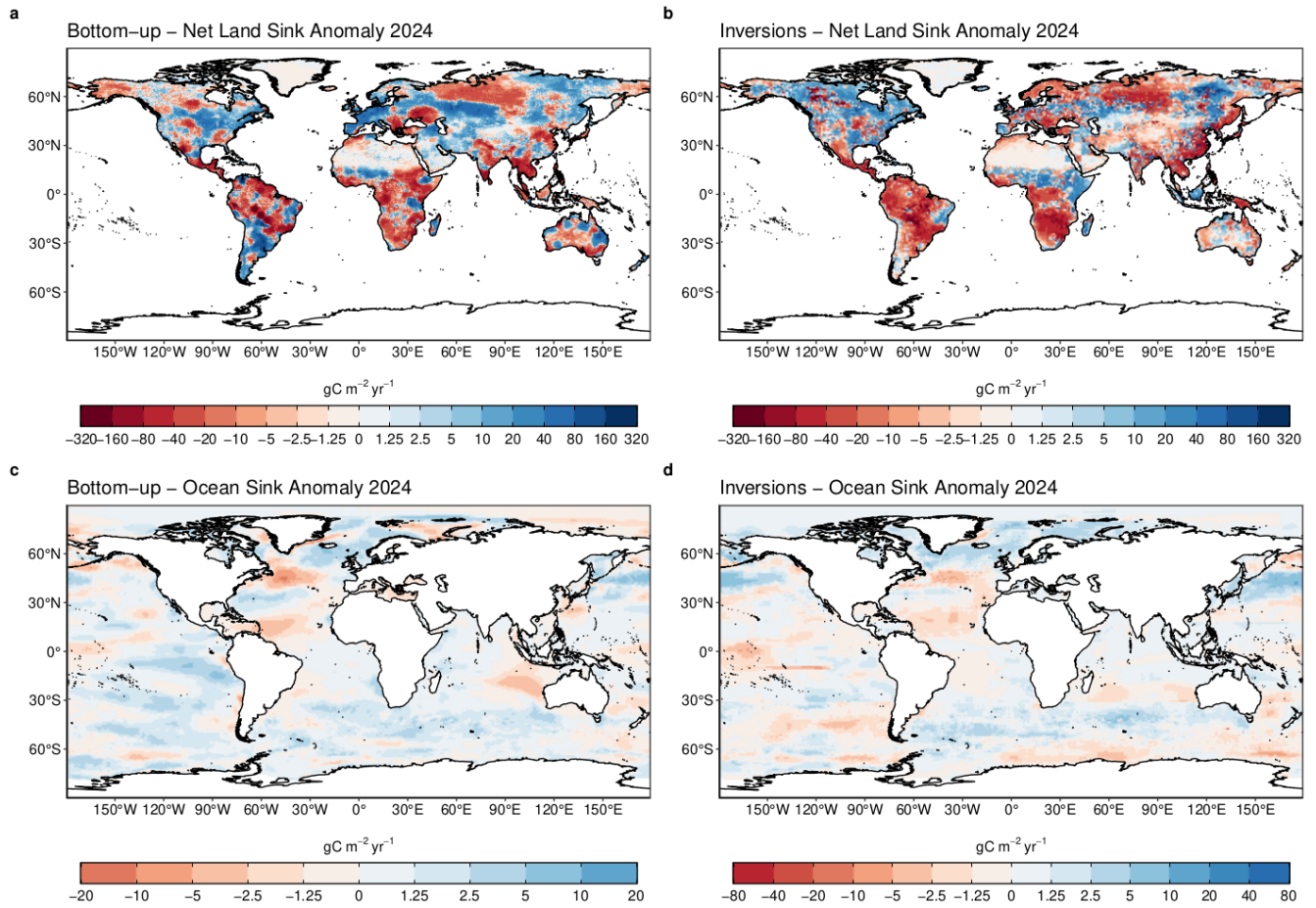


4294

4295 **Figure 9:** Annual atmospheric CO₂ growth rates based on observations from the surface network (by NOAA
 4296 (National Oceanic and Atmospheric Administration) and SIO (Scripps Institution of Oceanography), as well as
 4297 using the Growth Rate from Satellite Observations (GRESO) approach using OCO-2 based XCO₂ observations
 4298 in ppm yr⁻¹ with uncertainties. To obtain G_{ATM}, the surface observation-based growth rate in units of ppm yr⁻¹ is
 4299 converted to units of GtC yr⁻¹ by multiplying by a conversion factor (CF) of 2.124 GtC per ppm, assuming
 4300 instantaneous mixing of CO₂ throughout the atmosphere. The purple lines are the atmospheric growth rates (in
 4301 GtC yr⁻¹) calculated as the sum of the fluxes derived by the atmospheric inversions. Note that the right hand axis
 4302 shows the growth rate in GtC yr⁻¹, with intervals of the conversion factor.

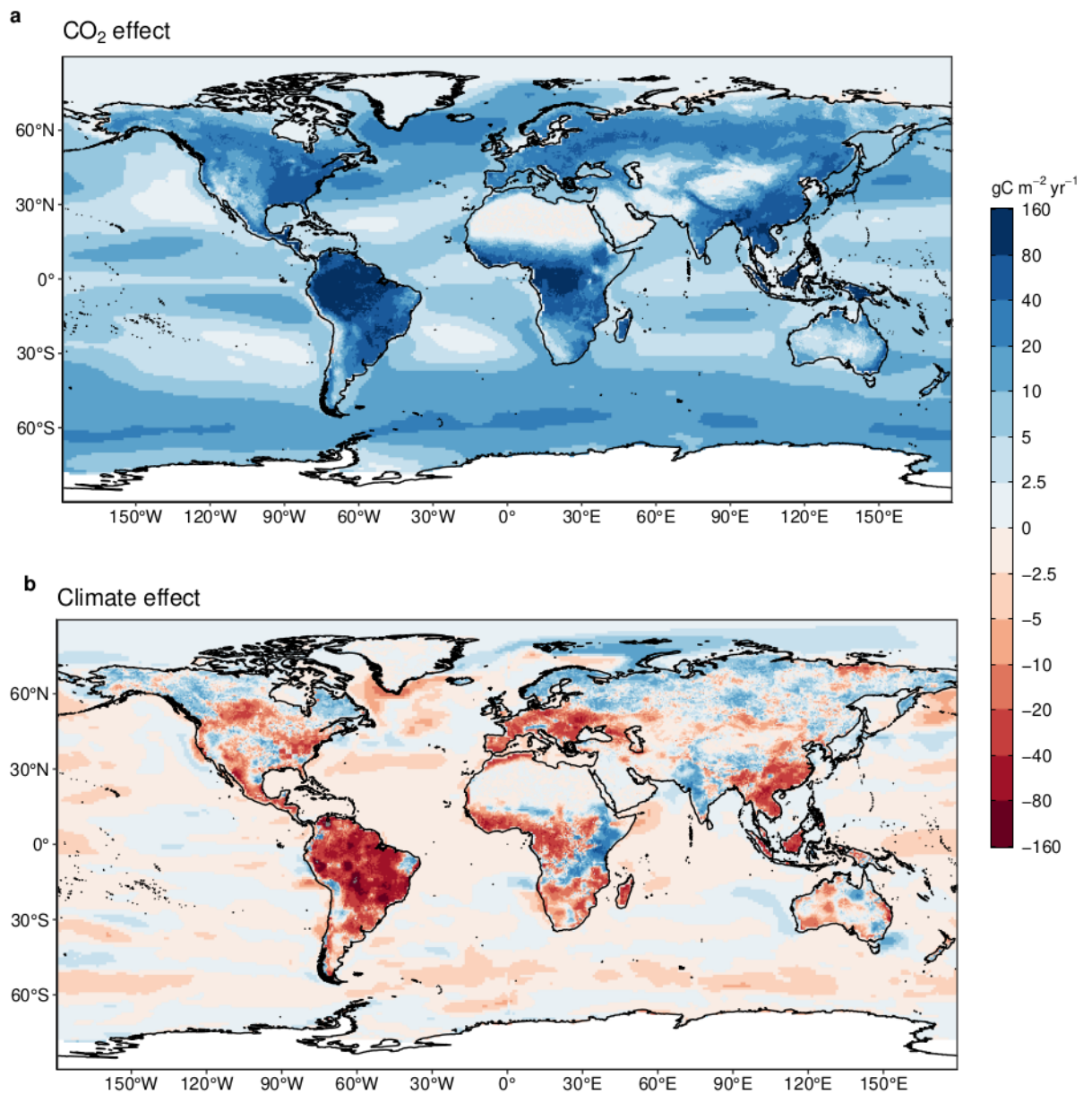


4303 **Figure 10.** (a) The land CO₂ sink (S_{LAND}) estimated by individual DGVMs (thin green lines). The DGVM multi-
 4304 model mean is shown as the thick green line. The S_{LAND} budget estimate (black with $\pm 1\sigma$ uncertainty), is the
 4305 DGVM multi-model mean adjusted for the RSS bias (i.e. reduced by 19%). (b) Comparison of the
 4306 anthropogenic atmosphere-ocean CO₂ flux showing the budget values of S_{OCEAN} (black; with the uncertainty in
 4307 grey shading), individual ocean models (royal blue), and the ocean fCO_2 -products (cyan). Adjustments were
 4308 applied to S_{OCEAN} (black) for the known underestimation in GOBMs and the warm layer/cool skin effect for
 4309 fCO_2 -products. Individual model lines as well as GOBM and fCO_2 -product ensemble means (thick cyan and
 4310 royal blue lines) do not include these adjustments, with the exception of 2 fCO_2 -products (UExp-FNN-U and
 4311 JMA-MLR) that include temperature corrections as part of their air-sea CO₂ flux calculation (see section 2.5).
 4312 Two fCO_2 -products (Jena-MLS, LDEO-HPD) extend back to 1959. All fCO_2 -products were adjusted for the pre-
 4313 industrial ocean source of CO₂ from river input to the ocean, by subtracting a source of 0.65 GtC yr⁻¹ to make
 4314 them comparable to S_{OCEAN} (see Section 2.5). The bar-plot in the lower right illustrates the number of monthly
 4315 gridded values in the SOCAT v2025 dataset (Bakker et al., 2025a). Grey bars indicate the number of grid cells
 4316 in SOCAT v2024, and coloured bars indicate the newly added grid cells in v2025.



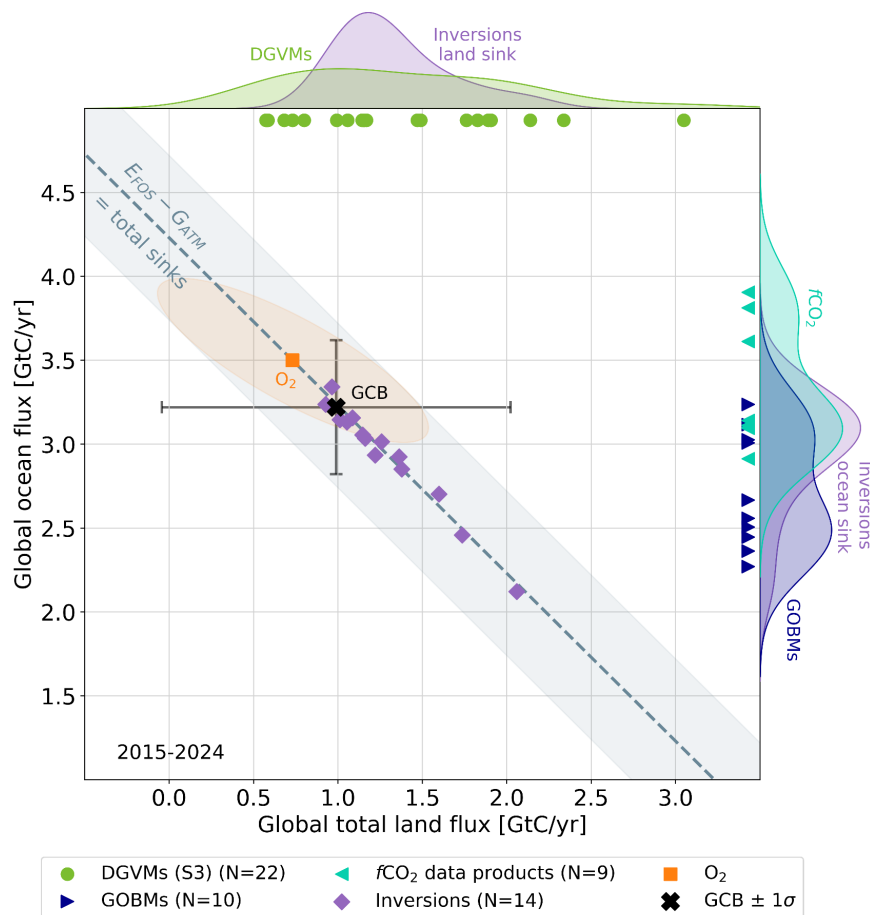
4317

4318 **Figure 11.** Anomalies in land and ocean sinks for 2024. Maps show the 2024 fluxes relative to the 2015-2024
 4319 decadal mean. Units are $\text{gC m}^{-2} \text{yr}^{-1}$. (a) The bottom-up anomaly in the net land flux combines both the anomaly
 4320 in S_{LAND} from DGVMs and in E_{LUC} from bookkeeping models, although the E_{LUC} contribution to the anomaly is
 4321 minimal. Panel (b) shows the mean anomaly in the net land flux across 14 inversions. Panel (c) shows the mean
 4322 anomaly from GOBMs and f_{CO_2} product ensemble means. The mean anomaly for GOBMs and f_{CO_2} products is
 4323 first calculated, and then the mean of the two products is shown. Panel (d) shows the mean anomaly in ocean
 4324 fluxes across 14 inversions.



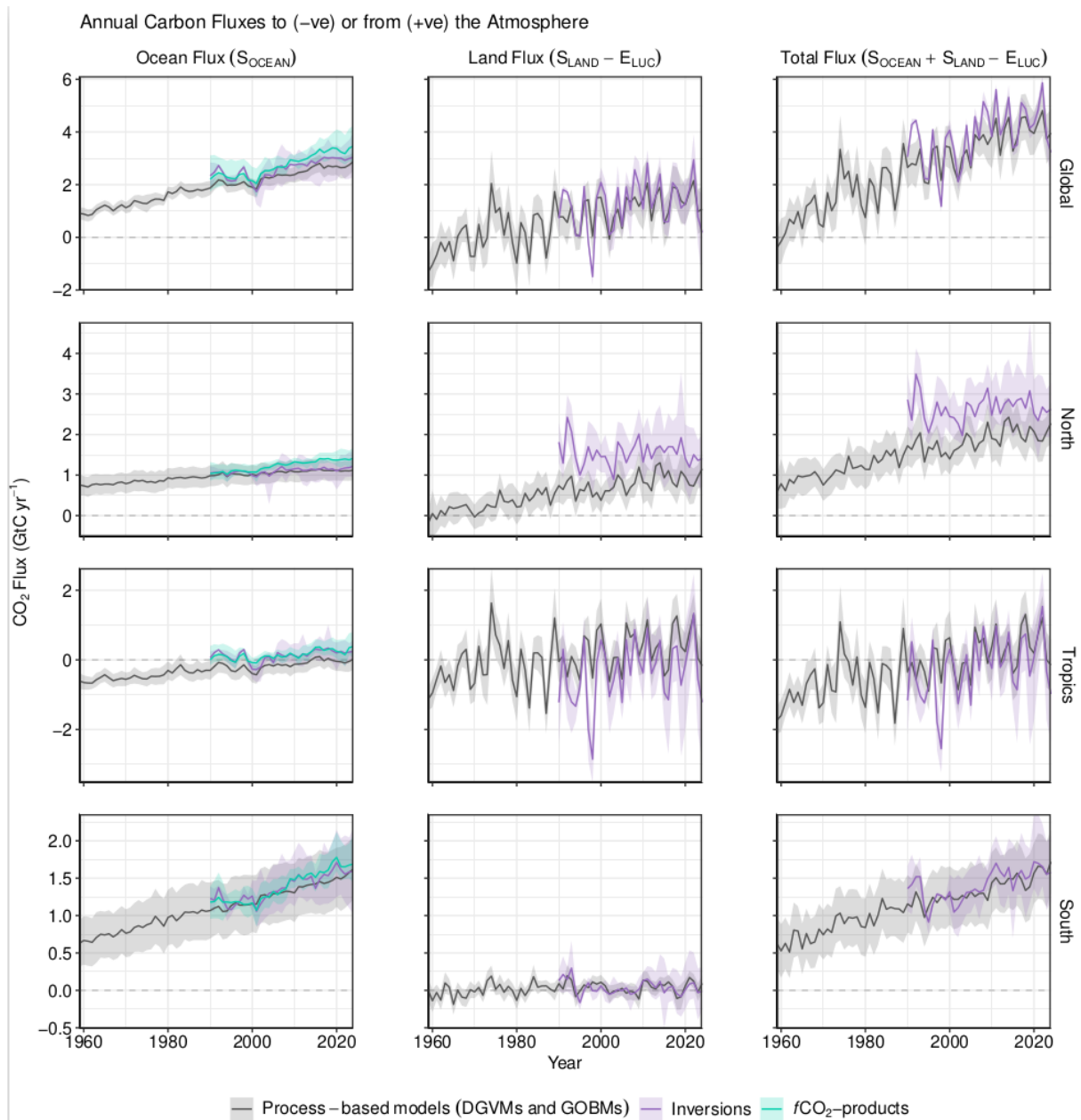
4325

4326 **Figure 12.** Attribution of the atmosphere-ocean (S_{OCEAN}) and atmosphere-land (S_{LAND}) CO₂ fluxes to (a)
 4327 increasing atmospheric CO₂ concentrations and (b) changes in climate, averaged over the previous decade 2015-
 4328 2024. All data shown is from the processed-based GOBMs and DGVMs. Note that the sum of ocean CO₂ and
 4329 climate effects shown here will not equal the ocean sink shown in Figure 6, which includes the $f\text{CO}_2$ -products.
 4330 No adjustments were applied to the DGVMs or GOBMs. See Supplement S.3.2 and S.4.1 for attribution
 4331 methodology. Units are in gC m⁻² yr⁻¹ (note the non-linear colour scale). Positive values (blue) are CO₂ sinks,
 4332 negative values (red) are CO₂ sources.



4333

4334 **Figure 13.** The 2015-2024 decadal mean global net atmosphere-ocean and net atmosphere-land fluxes derived
 4335 from the ocean models and fCO_2 products (y-axis, right and left pointing blue triangles respectively), and from
 4336 the DGVMs (x-axis, green symbols), and the same fluxes estimated from the atmospheric inversions (purple
 4337 symbols). The shaded distributions show the densities of the ensembles of individual estimates. The black
 4338 central cross ('GCB') is the mean ($\pm 1\sigma$) of S_{OCEAN} and $(S_{LAND} - E_{LUC})$ as assessed in this budget. The grey
 4339 diagonal line represents the constraint on the global land + ocean net flux, i.e. global fossil fuel emissions minus
 4340 the atmospheric growth rate from this budget ($E_{FOS} - G_{ATM}$). The orange square represents the same global net
 4341 atmosphere-ocean and atmosphere-land fluxes as estimated from the atmospheric O₂ constraint (the ellipse
 4342 drawn around the central atmospheric O₂ estimate is a contour representing the 1σ uncertainty of the land and
 4343 ocean fluxes as a joint probability distribution). Positive values are CO₂ sinks. Note that the inverse estimates
 4344 have been scaled for a minor difference between E_{FOS} and GridFEDv2025.1 (Jones et al., 2025). The 'GCB'
 4345 central mean estimate includes the S_{LAND} and S_{OCEAN} global adjustments. The inversions and fCO_2 products
 4346 include the river adjustment (see Section 2). No further adjustments were applied to the individual bottom-up
 4347 estimates.



4348

4349

4350

4351

4352

4353

4354

4355

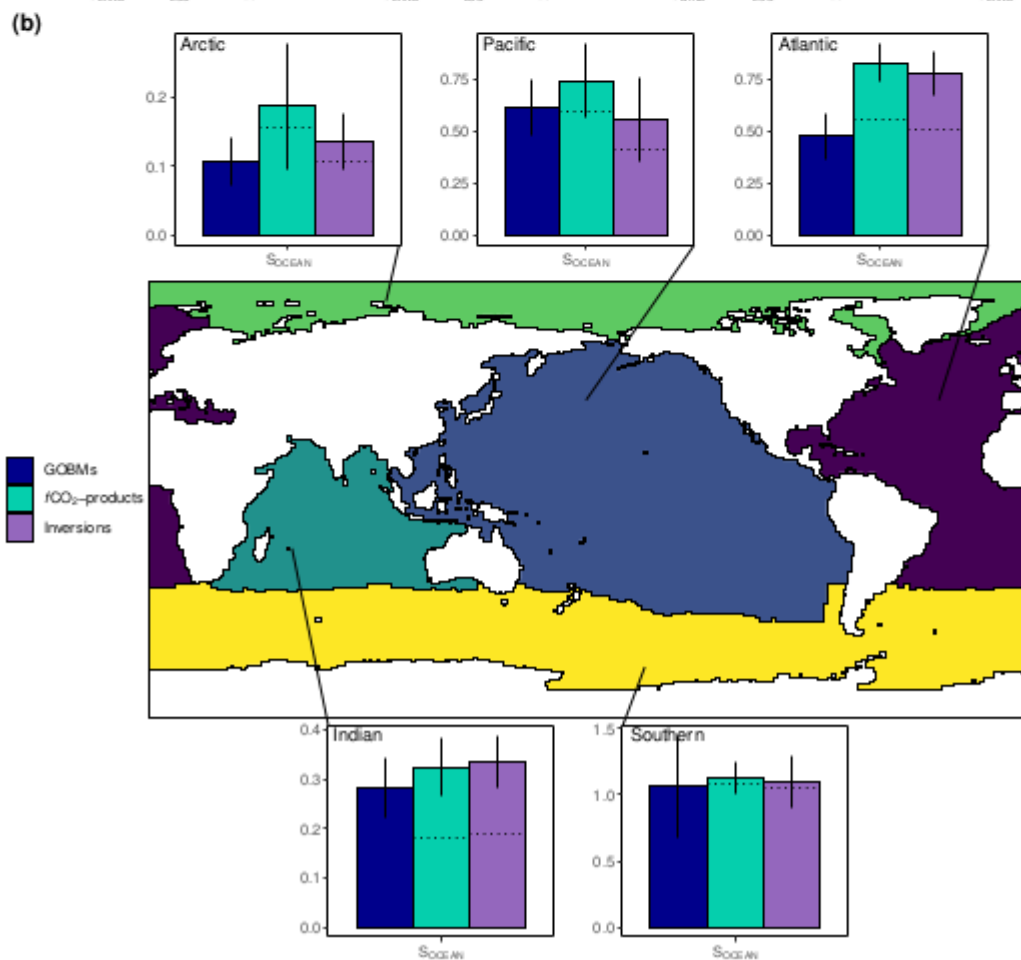
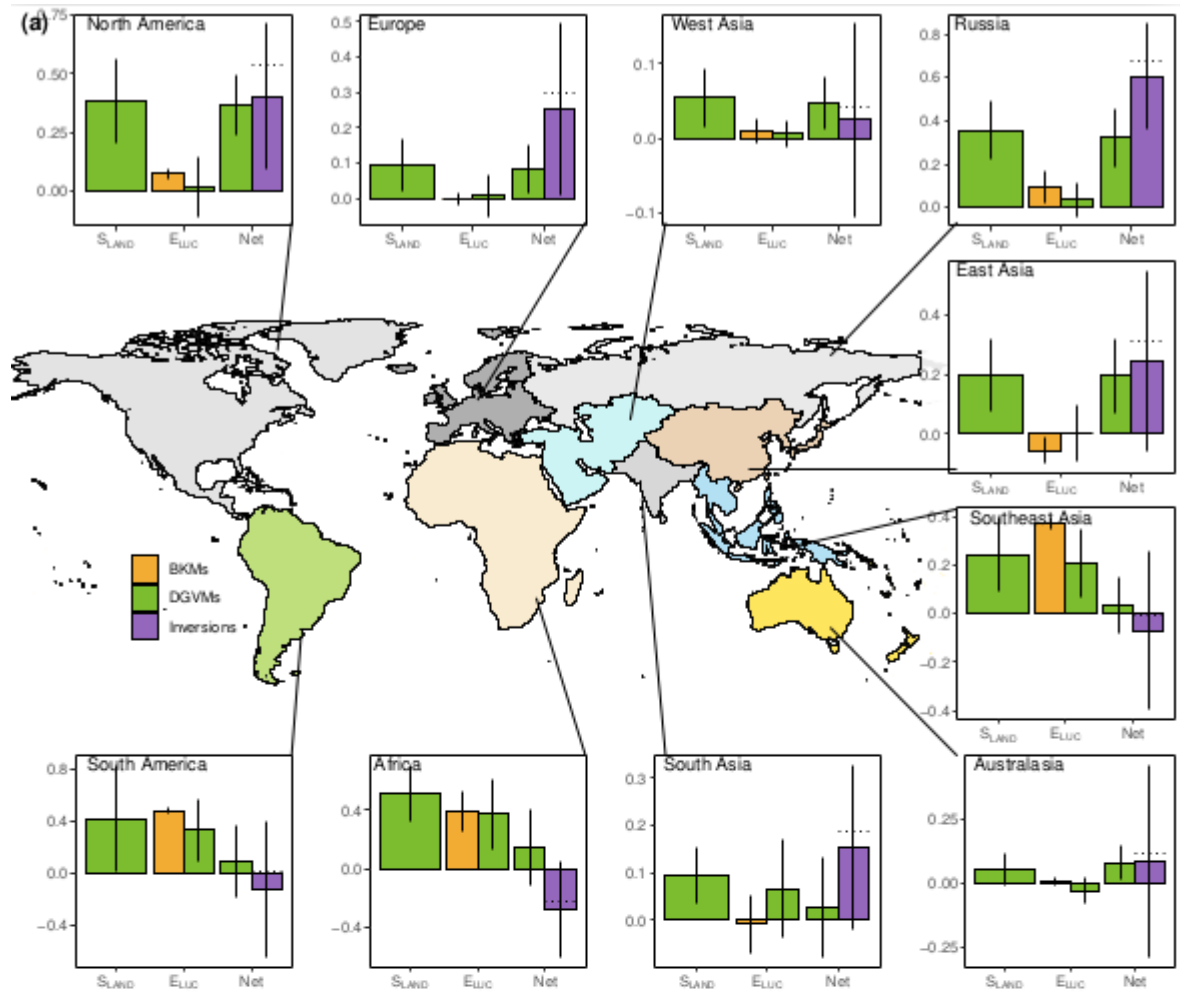
4356

4357

4358

Figure 14. CO₂ fluxes between the atmosphere and the Earth's surface separated between land and oceans, globally and in three latitude bands. The ocean flux is S_{OCEAN} and the land flux is the net atmosphere-land fluxes from the DGVMs. The latitude bands are (top row) global, (2nd row) north ($>30^{\circ}\text{N}$), (3rd row) tropics (30°S - 30°N), and (bottom row) south ($<30^{\circ}\text{S}$), and over ocean (left column), land (middle column), and total (right column). Estimates are shown for: process-based models (DGVMs for land, GOBMs for oceans); inversion systems (land and ocean); and $f\text{CO}_2$ -products (ocean only). Positive values are CO₂ sinks. Mean estimates from the combination of the process models for the land and oceans are shown (black line) with $\pm 1 \sigma$ of the model ensemble (grey shading). For the total uncertainty in the process-based estimate of the total sink, uncertainties are summed in quadrature. Mean estimates from the atmospheric inversions are shown (purple lines) with their full spread (purple shading). Mean estimates from the $f\text{CO}_2$ -products are shown for the ocean domain (light blue

4359 lines) with full model spread (light blue shading). The global S_{OCEAN} (upper left) and the sum of S_{OCEAN} in all
4360 three regions represents the anthropogenic atmosphere-to-ocean flux based on the assumption that the pre-
4361 industrial ocean sink was 0 GtC yr^{-1} when riverine fluxes are not considered. This assumption does not hold at
4362 the regional level, where pre-industrial fluxes can be significantly different from zero. Hence, the regional
4363 panels for S_{OCEAN} represent a combination of natural and anthropogenic fluxes.



4365 **Figure 15.** Decadal mean (a) land and (b) ocean fluxes for RECCAP-2 regions over 2015-
4366 2024. For land fluxes, S_{LAND} is estimated by the DGVMs (green bars), with the error bar as
4367 $\pm 1\sigma$ spread among models. A positive S_{LAND} is a net transfer of carbon from the atmosphere to
4368 the land. E_{LUC} fluxes are shown for both DGVMs (green) and bookkeeping models (orange),
4369 again with the uncertainty calculated as the $\pm 1\sigma$ spread. Note, a positive E_{LUC} flux indicates a
4370 loss of carbon from the land. For the DGVMs, S_{LAND} and E_{LUC} are adjusted for RSS bias. The
4371 net land flux is shown for both DGVMs (green) and atmospheric inversions (purple),
4372 including the full model spread for inversions. The ocean sink (S_{OCEAN}) is estimated by
4373 GOBMs (royal blue), $f\text{CO}_2$ -products (cyan), and atmospheric inversions (purple). No
4374 adjustments were applied to GOBMs and $f\text{CO}_2$ -products at regional scale. Uncertainty is
4375 estimated as the $\pm 1\sigma$ spread for GOBMs, and the full model spread for the other two datasets.
4376 The dotted lines show the $f\text{CO}_2$ -products and inversion results without river flux adjustment.
4377 Positive values are CO_2 sinks.